Tridentate NacNac Ligand Supported Main-Group and Transition Metal compounds: Pendent Picolyl Powers Peculiar Chemistry

by

Vishal Kumar Sharma

10CC19A26042

A thesis submitted to the
Academy of Scientific & Innovative Research
For the Award of the Degree of
DOCTOR OF PHILOSOPHY
in
SCIENCE

Under the supervision of

Dr. Sakya Singha Sen

CSIR-National Chemical Laboratory, Pune

Academy of Scientific and Innovative Research
AcSIR Headquarters, CSIR-HRDC campus
Sector 19, Kamla Nehru Nagar,
Ghaziabad, U.P.–201 002, India

January 2025

Certificate

This is to certify that the work incorporated in this Ph.D. thesis entitled, "*Tridentate NacNac Ligand Supported Main-Group and Transition Metal compounds: Pendent Picolyl Powers Peculiar Chemistry*", submitted by *Vishal Kumar Sharma* to the Academy of Scientific and Innovative Research (AcSIR), in partial fulfillment of the requirements for the award of the Degree of *Doctor of Philosophy in Science*, embodies original research work carried out by the student. We, further certify that this work has not been submitted to any other University or Institution in part or full for the award of any degree or diploma. Research material(s) obtained from other source(s) and used in this research work has/have been duly acknowledged in the thesis. Image(s), illustration(s), figure(s), table(s), etc., used in the thesis from other source(s), have also been duly cited and acknowledged.

Vishal Sharma

(Signature of Student)
Vishal Kumar Sharma
Date: 21-01-2025

Sakya Singha Sen

(Signature of Supervisor)
Dr. Sakya Singha Sen
Date: 21-01-2025

STATEMENTS OF ACADEMIC INTEGRITY

I, Vishal Kumar Sharma, a Ph.D. student of the Academy of Scientific and Innovative Research (AcSIR) with Registration No. 10CC19A26042 hereby undertake that, the thesis entitled "Tridentate NacNac Ligand Supported Main-Group and Transition Metal compounds: Pendent Picolyl Powers Peculiar Chemistry" has been prepared by me and that the document reports original work carried out by me and is free of any plagiarism in compliance with the UGC Regulations on *"Promotion of Academic Integrity and Prevention of Plagiarism in Higher Educational Institutions (2018)"* and the CSIR Guidelines for "*Ethics in Research and in Governance (2020)*".

Vishal Sharma

Signature of the Student
Date : 21-01-2025
Place : CSIR-NCL, Pune

It is hereby certified that the work done by the student, under my supervision, is plagiarism-free in accordance with the UGC Regulations on *"Promotion of Academic Integrity and Prevention of Plagiarism in Higher Educational Institutions (2018)"* and the CSIR Guidelines for "*Ethics in Research and in Governance (2020)*".

NA

Signature of the Co-supervisor (if any)
Name :
Date :
Place :

Sakya Singha Sen

Signature of the Supervisor
Name : Dr. Sakya Singha Sen
Date : 21-01-2025
Place : CSIR-NCL, Pune

"To my esteemed Gurus and Mentors, whose wisdom, guidance, and unwavering support have illuminated my path. With deepest gratitude, I dedicate this endeavour to you."

ACKNOWLEDGEMENTS

A Ph.D. journey is a profound exploration, not only of knowledge but also of self. It is a unique experience that takes you along an uncharted path, ultimately leading to the fulfillment of your aspirations. This journey is rarely traveled alone; the support, encouragement, and inspiration of others are indispensable. I am deeply indebted to those whose kindness, guidance, and encouragement have been pivotal in completing this journey. Success in research is never achieved in isolation-it is made possible by the invaluable contributions of mentors, the support of friends, and the goodwill of well-wishers. With heartfelt gratitude, I take this opportunity to acknowledge and express my sincere thanks to everyone who has directly or indirectly supported me, making the research work presented in this thesis a reality.

First and foremost, I want to express my profound gratitude to ***Dr. Sakya S. Sen*** *for extending to me the opportunity to pursue my Ph.D. under his guidance. His ideas, accessibility, and encouragement to explore uncharted territories have not only enriched my learning experience but also empowered me to pursue bold ideas, many of which have culminated in this thesis. His critical insights and a completely different perspective on things, especially chemistry along with invaluable guidance have trained me on essential aspects such as extracting key insights from scientific literature, critical thinking, identifying gaps, writing research papers, and delving into more intricate skills like tailoring research presentations to suit different types of audiences. I attribute the successful completion of my doctoral journey to his unwavering support and motivation through the highs and lows of my Ph.D. I consider myself incredibly fortunate and privileged to have been under his mentorship and to be a part of his research group. I could not have asked for a better supervisor.*

This journey (Ph.D.) cannot be successful without the suggestions given by my Doctoral Advisory Committee (DAC) members during the DAC meetings. I express my sincere thanks to the Doctoral Advisory Committee members, ***Dr. Benudhar Punji, Dr. Pradip Maity,*** *and* ***Dr. Sailaja Krishnamurty,*** *for their contribution in stimulating suggestions and encouragement during my Ph.D.*

*I am grateful to **Prof. Ashish Lele** (Director, CSIR-NCL), **Prof. A. K. Nangia** (Former Director, CSIR-NCL), **Dr. Vijay V. Bokade** (Head, Catalysis and Inorganic Chemistry Division), **Dr. Shubhangi B. Umbarkar** and **Dr. C. S. Gopinath** (Former Head, Catalysis and Inorganic Chemistry Division), for giving me this opportunity and providing all necessary infrastructure and facilities to carry out my research work. I would like to acknowledge all the support from Catalysis and Inorganic Chemistry Division office staff. I am also highly thankful to the **Council of Scientific & Industrial Research (CSIR)**, New Delhi, and the **Academy of Scientific and Innovative Research (AcSIR)**, Ghaziabad, for the financial assistance and coursework facilities, respectively. My sincere thanks to **Purushothaman Sir, the Library staff** especially **Gati Sir, the Student academic office staff, DIRC** and all **other scientists of NCL** for their motivation, constant encouragement, and support.*

*I am highly grateful to our collaborators **Dr. Kumar Vanka** (CSIR-NCL, Pune) and his doctoral students, **Soumya Ranjan Dash** and **Dr. Vipin Raj K** for their essential support in DFT calculations, **Dr. Rajesh Gonnade** (CSIR-NCL, Pune) and his group members, **Dr. Christy, Bhupender, Parth, Akaram** and for single-crystal X-ray diffraction measurements, analysis, and for valuable suggestions and help at different parts of my research journey. I am deeply grateful for the assistance provided by the Spectroscopy, Analytical, and the Mass group which have helped me advance my research smoothly. I extend my sincere gratitude to the support staff from the NMR division, especially **Mr. Vaibhav** and **Ms. Neeta** for their unwavering support and assistance. I would also extend my gratitude to **Mr. Ganesh Sevi, Ms. Megha Mali** and **Ms. Mrudula Kulkarni** from HRMS.*

I sincerely acknowledge my teachers from Dept. of Chemistry, NIT Jamshedpur (M.Sc.), and University College of Science, Udaipur (B. Sc.) for their teaching skills and inspiration which have brought me to this stage.

*I consider myself highly privileged to work and spend most of my day with the Sen Lab's wonderful and motivated young research team of colleagues. My experience studying through our group meetings has been fantastic. It is my pleasure to thank my lab-mates, **Dr. Ajith, Biplab**, **Kajal, Debjit, Amrutha**, **Pratiksha**, **Devaraj and Arpan** for their kind support, help and suggestions during my research work. I would like to express my deepest gratitude to my*

*former labmates, **Dr. V. S. V. S. N. Swamy**, and **Dr. Milan Bisai**, and **Dr. Gargi Kundu**, for instructing me in sensitive chemistry and for being very good seniors. I am especially grateful to **Dr. Sanjukta Pahar**, **Dr. Rohit Kumar** and **Dr. Kritika Gour** who has been there always for motivating me during the hard times and their support has been phenomenal throughout our time together here. I will remember all the experiences with my lab mates throughout out my life.*

*I am thankful to **Dr. Ashish, Chandan, Neha, Arindam, Dipak, Anjali, Vrushali** and **Anurag** for being very helping and joyful lab neighbours. I am lucky to have so many friends in and away from CSIR-NCL, whose company never allowed me to feel bored during the entire course of my work. I sincerely thank all of my NCL friends **Dr. Rahul Jagtap, Dr. Sachin, Dr. Nirshad**, **Dr. Surya**, **Dr. Rohit Senior, Dr. Sairam, Dr. Akash, Dr. Someshwar, Dr. Ravi Kumar, Dr. Anirban, Dr. Shibam, Dr. Pawan Dongapure, Dr. Himanshu Bajpai, Dr. Monika, Dr. Sailaja, Dr. Ruchi, Dr. Indrajeet, Dr. Kranti, Dr. Tanuja, Dr. Rajanigandha, Dr. Samadhan, Dr. Shivshankar, Kailash, Amit Naglekar, Ashish Jagtap, Jairam, Sangram, Kiran, Dinesh, Sameer, Anand, Sadhana, Vijaykumar, Rajkumar, Rahul Choudhury, Tubai, Chandrakant, Sonia, Monica, Ashwini, Vishal, Subhashree, Sanket, Mayur, Pooja, Jyotsana, Anuradha, Jyoti Tekawadia, Jayesh, Kundan, Anouska, Akhil, Pranali, Sidharth, Sonu, Nittan, Umasaran, Sowmomita, Manoj, Virendra, Sudha, Chandani, Subhranshu, Poonam, Akshay, Nilu, Himanshu, Priyam, Smrithi, Gayatri, Jyoti, Rinu, Geetika, Zeel, Simran** and many others for their irreplaceable cooperation.*

*I am also grateful to **Dr. Nasrina Di, Dr. Nilanjana, Ruksana, Sandeep, Kumar Gourav, and Vijay** from IISER Pune for their unwavering support and assistance whenever I needed it.*

*I would like to express my special gratitude to **Dr. Lavanya K** who has been a great friend, and has helped me immensely in the final stages of my PhD. I am also grateful to **Dr. Pawan** (Chota Pawan) and **Prashant Bhaiya** for making the stay at NCL memorable.*

*I want to take a heartfelt moment to thanks the bundle of happiness **Honey,** for embracing me so warmly into her family **Sumit** and **Sushank**. Every time they visited me at NCL, made me feel truly special and cherished. Your love, kindness, and untiring support mean everything to*

*me. Also, I would like to thanks **Aarti vahini** for giving us special treats of some delicious Marathi cuisines and letting us do wander with her beloved husband.*

*One of the things that has had the most profound effect on my life is the **IB Group**! This group comprises of **Bharath, Swapnil, Manish, Pawan, Prem, Dharmendra** and **ViksHit** (no significance of order as they have equal contributions of course!) This particular set of friends is a completely different breed that has transformed my perspective on life. They are the ones who loved, cared, stood by me and supported me during both highs and lows. If not for these guys, then my PhD journey would not have been all that colourful and the time spent with them was one of the best phases of my life. Their steadfast presence is beyond words, and I could easily dedicate an entire chapter solely to express my acknowledgment of their unwavering support.*

*My family is always a source of inspiration and great moral support for me in pursuing my education. I owe a lot to my beloved parents, who encouraged and helped me at every stage of my personal and academic life, and longed to see this achievement come true. My sincere thanks to my beloved family members, my father '**Shanti Lal Sharma**', my mother '**Sushila Sharma'**, my brother '**Vikas Sharma'**, my sister '**Manju Sharma**' and jijaji **'Jagdish Sharma'**. And finally, I would love to express a deep sense of gratitude for the two important ladies of my family, '**Chandi Bai** and **Sukhi Devi**' for nurturing me and fostering the values for life in me. I am glad to announce that today whatever I am, it is only because of my parents, and I can never even think of paying it back. I am very much indebted to my whole family, who supported me in every possible way to see the completion of this research work. Thank you, **Shilpi, Rakesh, Kushal, Somvir, Prashant** and **Vinod** for being my bestest of friends even when I am unable to call or talk often.*

*Finally, I would like to take a moment to thank **Pukaar** and the entire family, especially **Bhuvnesh, Moni, Rishabh, Praveen, Khusbu, Pulkit,** and **Divya,** for the wonderful adventures we've shared and for the many more to come whenever we meet.*

Above all, I extend my gratitude to the Almighty God for giving me the wisdom, health, and strength to undertake this research work and hardships and enabling me to complete it.

Vishal Sharma

Contents of the Thesis

Chapter 2:

Chapter 3:

Chapter 4:

Chapter 5:

Abbreviations

Units and standard terms

BDE	Bond Dissociation Energy
°C	Degree Centigrade
DFT	Density Functional Theory
mg	Milligram
h	Hour
Hz	Hertz
mL	Millilitre
min.	Minute
mmol	Millimole
NPA	Natural Population Analysis
NBO	Natural Bond Order
ppm	Parts per million
%	Percentage
M.P.	Melting Point
B. P.	Boiling Point
Calcd.	Calculated
CCDC	Cambridge Crystallographic Data Centre
CIF	Crystallographic Information file

Chemical Notations

Ar	Aryl
MeCN	Acetonitrile
$CDCl_3$	Deuterated chloroform
C_6D_6	Deuterated benzene
DMSO-d_6	Deuterated dimethyl sulfoxide
Toluene-d_8	Deuterated toluene
CD_3CN	Deuterated acetonitrile
DCM	Dichloromethane
DMSO	Dimethyl sulfoxide
EtOH	Ethanol
Me	Methyl
Et	Ethyl
Dipp	Di-isopropyl phenyl
*i*Pr	Isopropyl
*t*Bu	Tertiary butyl
HBpin	Pinacolborane
THF	Tetrahydrofuran
Et_2O	Di-ethyl ether
TMSCN	Trimethylsilyl cyanide
*n*BuLi	*n*-butyllithium

Other Notations

δ	Chemical shift
J	Coupling constant in NMR
Equiv.	Equivalents
HRMS	High Resolution Mass Spectrometry
NMR	Nuclear Magnetic Resonance
RT	Room temperature
UV	Ultraviolet
SC-XRD	Single Crystal X-Ray Diffraction

General remarks

- All chemicals were purchased from commercial sources and used as received.
- All reactions were carried out under an inert atmosphere following standard procedures using Schlenk techniques and glovebox.
- Deuterated solvents for NMR spectroscopic analyses were used as received. All ^{1}H NMR and ^{13}C NMR analyses were obtained using Bruker or JEOL 200 MHz, 400 MHz, or 500 MHz spectrometers. Coupling constants were measured in Hertz. All chemical shifts are quoted in ppm, relative to TMS, using the residual solvent peak as a reference standard.
- HRMS spectra were recorded at UHPLC-MS (Q-exactive-Orbitrap Mass Spectrometer) using electron spray ionization [(ESI^{+}, +/− 5kV), solvent medium: acetonitrile and methanol] technique, and mass values are expressed as *m/z*. GC-HRMS (EI) was recorded in Agilent 7200 Accurate-mass-Q-TOF.
- The solvent used were purified by an MBRAUN solvent purification system MBSPS-800 and further dried over activated molecular sieves prior to use.
- The preparation of sensitive NMR samples was carried out in a Glove box or under an inert atmosphere of argon applying standard Schlenk technique.
- Column chromatography was performed on silica gel (100-200 mesh size).
- LC-MS were obtained using a Q Exactive Thermo Scientific and an Agilent Technologies 6120.
- Chemical nomenclature (IUPAC) and structures were generated using ChemDraw Professional 20.1.

Synopsis Report

AcSIR	**Synopsis of the Thesis to be submitted to the Academy of Scientific and Innovative Research for Award of the Degree of Doctor of Philosophy in Sciences/ Engineering**
Name of the Candidate	Vishal Kumar Sharma
Degree Enrollment No. &Date	PhD in Chemical Sciences; 10CC19A26042; August 2019
Laboratory	CSIR-National Chemical Laboratory
Title of the Thesis	Tridentate NacNac Ligand Supported Main-Group and Transition Metal compounds: Pendent Picolyl Powers Peculiar Chemistry
Research Supervisor/ Co-supervisor	Dr. Sakya S. Sen

Introduction

In recent years a major theme of organometallic chemistry has been the design and development of metal catalysts to mimic the precious noble metal catalysts by more economical and environmentally viable alternatives. As we all know transition metal complexes form the heart of catalysis but the mostly used metals are late transition metals, which are less abundant and their byproducts are hazardous in nature. Hence, nowadays people are trying to find the alternative of late transition metals.

Recent years have been witnessed that early transition metals and main group metal complexes are used as the alternative of late transition metal complexes because most of these metals are cheap in price compared to late transition metals and their byproducts are less hazardous in nature. Especially alkaline earth metals are earth-abundant and have worldwide accessibility but these metals follow Schlenk equilibrium i.e. these metals favour homoleptic complexes over heteroleptic complexes. Stabilizing early transition metals in low oxidation states also

requires specific steric as well as electronic support. Hence to overcome this issue we have to design a ligand which can stabilize metal complexes electronically as well as sterically.

In last two decades a substantial amount of research has been done to understand the designing of ligand system, there are few commonly used ligands (figure 1). Among these *β*-diketiminate ligand scaffold commonly known as nacnac has emerged as a versatile ligand to stabilize different metal centres or low valent main group elements[1] because of its electronic and steric properties can be altered by changing the substituents.

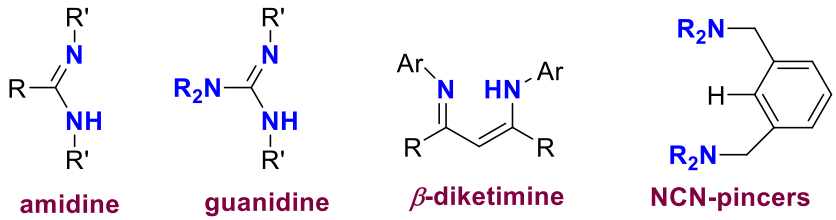

Figure 1: Monoanionic ligands.

The field of nacnac as ligand has started getting attention after the discovery of nacnac stabilized Al(I) by Roesky[2] followed by the reports on alkaline earth metal complexes by Jones, Harder and Hill.[3] Few milestones in the chemistry of nacnac are shown in figure 2.

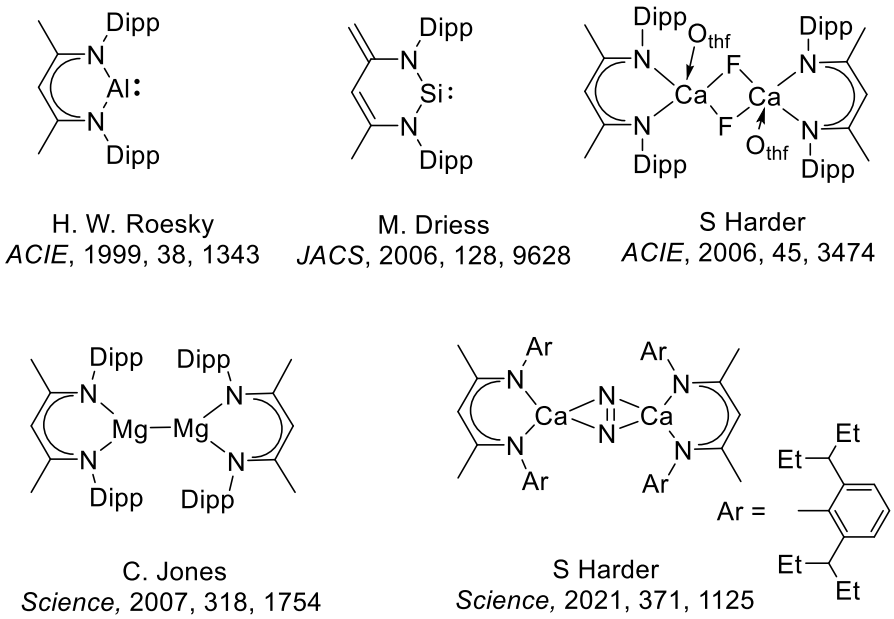

Figure 2: Milestone discoveries in the chemistry of nacnac.

Despite the enrich chemistry of nacnac ligand there is a need to find a suitable ligand which can stabilizes the metal complexes without aggregation. Modification in nacnac is required. In recent years our group has studied the modified tridentate nacnac ligand moiety (figure 3) with an extra donor nitrogen site to provide better stabilization towards the metal centre and could able to isolate mononuclear heteroleptic complexes of low valent main group elements.

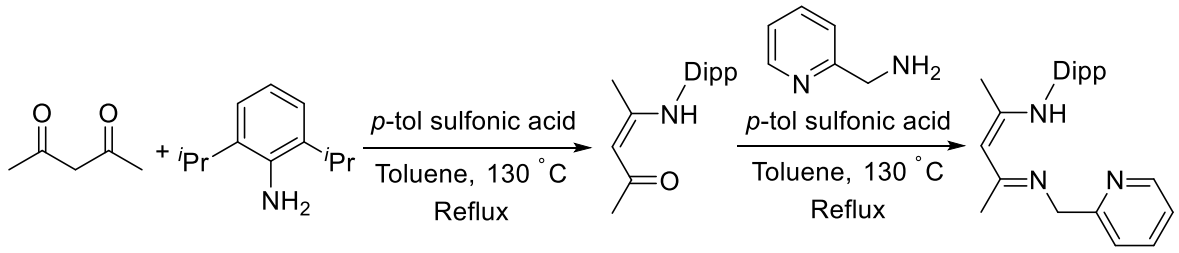

Figure 3: Modified tridentate nacnac ligand.

We have studied the chemistry of low-valent group 13 and 14 elements using modified tridentate nacnac ligand.[4] So to explore more about the chemistry of low valent transition metal and alkaline earth metals, here we have utilised tridentate nacnac supported ligand scaffold to stabilize T-shaped nickel radical and further extends its reactivity towards small molecule activation. Also, we have explored it to stabilize monomeric complexes of magnesium and its application towards E-H bond activation.

Statement of the problem

All the challenges make us think about how we can tackle the problems associated with the stabilization of main group elements with the use of a proper ligand which will lead us to use the respective compounds in small molecule activation and industrially important catalysis.

Methodology

The compounds targeted in my work are expected to be highly air and moisture-sensitive and will be handled under an inert atmosphere. Standard techniques for the synthesis and characterization of air and moisture-sensitive compounds are well-established. Experiments at very low or high temperatures, under high pressure, or in high vacuum can be carried out at convenience. Besides the standard laboratory equipment glove boxes for work in an inert gas

environment (<5 ppm O_2 and H_2O), equipped with –35 °C freezers) and Schlenk lines are available. All new complexes are characterized thoroughly by state-of-the-art spectroscopic analyses as well as by single-crystal X-ray diffraction studies.

Results and their interpretation

As discussed earlier, in our work, we have successfully shown, how the ligand moiety can play an important role in stabilizing low valent main group and transition metal complexes. For this, the thesis is divided into five chapters. Among these, the first chapter is a general introduction (please see the introduction section). Details of the chapters are as follows:

Chapter 2: Tridentate Nacnac Tames T-Shaped Nickel Radical

The chemistry of small molecule activation mediated by the transition metal center is of paramount importance in numerous stoichiometric and catalytic transformations. Recently, coordinatively unsaturated metal centers have received enormous attention owing to their unusual structure and reactivities[5]. A similar strategy may be possible with T-shaped d^9 species, but it remains mainly unexplored because the synthesis of a compound having rigid T-shaped geometry is difficult. Earlier attempts utilising *β*-diketiminate, N-heterocyclic carbene, and large phosphine ligands frequently resulted in Y-shaped structures[6]. A key to exploiting the metalloradical reactivity is to prepare a suitable ligand that can stabilize the metalloradical species. In recent times pincer based ligands are reported to synthesize T-shaped metalloradicals but the area is not well explored.[7,8]

Due to our recent success with the chemistry of modified tridentate nacnac ligand.[4] In the present work we report on the synthesis and characterization of T-shaped Nickel (I) radical complex, which is very rare. Further the reactivity towards small molecule activation is explored. (Scheme 1)

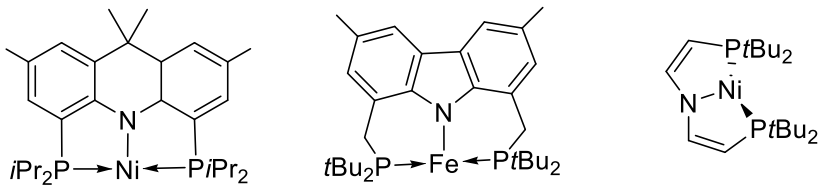

Figure 4. Previously reported T-shaped metalloradicals.

What is surprising is the base exchange reaction of 6-SIDipp·$ZnEt_2$ with 5-IDipp/5-SIDipp, (5-IDipp = 1,3-bis(2,6-diisopropylphenyl)-imidazol-2-ylidene; 5-SIDipp = 1,3-bis(2,6-diisopropylphenyl)-imidazolin-2-ylidene) leading to the smooth formation of zinc adducts with 5-NHCs.

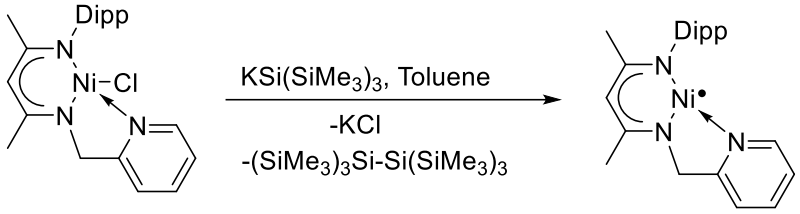

Scheme 1. Synthesis of tridentate nacnac supported T-shaped nickel radical and its reactivity.

In Summary:

- The presented results demonstrate a convenient method for synthesizing T-shaped nickel metalloradical.
- We were able to trap nickel radical using TEMPO as a trapping reagent.
- We investigated the reactivities of nickel(I) radical towards dichalcogenides (Ph_2E_2, E= S, Se) to get homolytic E-E bond cleavage, we also observed an unusual C-C bond coupling along with the bond cleavage.
- The nickel radical could also activate hydrogen to generate monomeric nickel hydride complex.

Chapter 3: Metal-Ligand Cooperation in Magnesium-Mediated Water Activation

Metal−ligand cooperation (MLC) is a versatile approach for activating chemical bonds through the aromatization/dearomatization of pincer-type complexes[1-5] This method is characterized by the fact that the metal center's oxidation state remains unchanged during the bond activation, as the process involves both the metal and the ligand. The advantage lies in the ability of redox-

innocent main-group metals to activate chemical bonds favorably without altering their oxidation state. Traditionally, this MLC process has been dominated by expensive transition metals, and the application of main-group metals in this context is still nascent[6-11] but there has been progress, such as N−H and H−H bond activation, hydrogenation of alkenes, and semi-hydrogenation of alkynes by main-group species as well as zinc through the MLC process. Given our recent interest in magnesium chemistry,[12-16] the aim is to design more such magnesium complexes using different ligand systems and extend the application to more challenging reactions such as water activation using the MLC activation process. Using the tridentate nacnac ligand systems as above we could able to synthesize monomeric magnesium complexes. (Scheme 2)

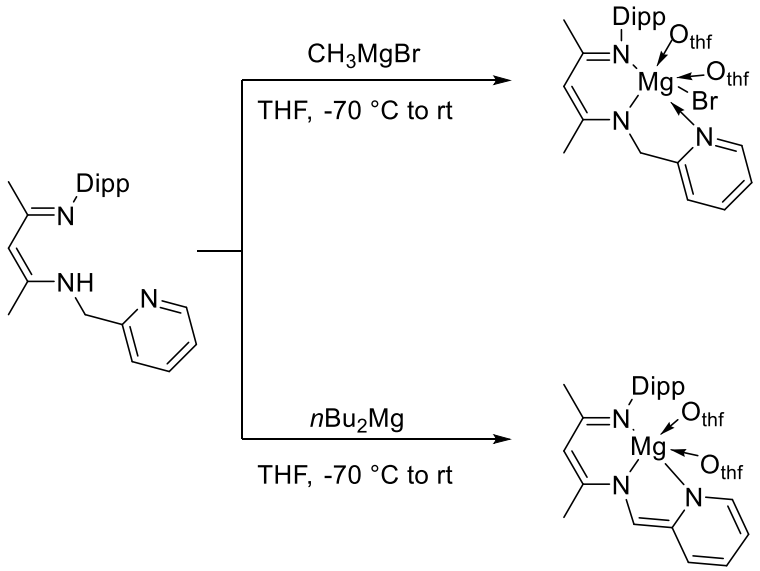

Scheme 2: Synthesis of monomeric magnesium complexes.

After having dearomatized magnesium complex, we further explored the reactivity of it towards the activation of water. Since activating water through homolytic cleavage is a formidable task because of the thermodynamic stability of H_2O, attributed to the high bond dissociation energy (BDE = 118 kcal/mol) of the O–H bonds. (Scheme 3)

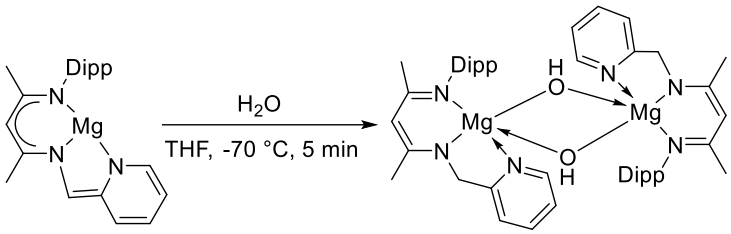

Scheme 3: magnesium mediated water activation.

To confirm the activation of water, the same reaction was repeated with D2O in THF (Scheme 4) and 2H NMR was recorded. The 2H NMR spectra show peaks at 4.61 ppm and 11.21 ppm corresponding to CD (methylene sidearm) and OD respectively.

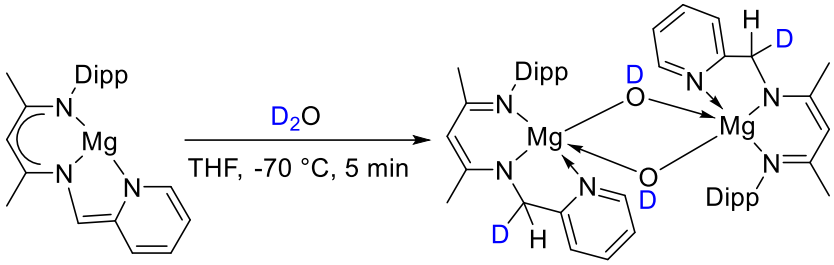

Scheme 4: Deuterium labeling experiment.

In Summary:

- We have synthesized the dearomatized complex of Magnesium using modified nacnac scaffold as a ligand
- We synthesized heteroleptic monomeric magnesium bromide complex
- We could able to show the very first example of water activation via metal ligand cooperation by magnesium

<u>Chapter 4</u>: Magnesium-Mediated C-H bond Activation

Sustainable development became a need of the time to have the future secure. Sustainability is attained when the needs of the present can be fulfilled without bargaining those of the future. In recent years, sustainability has appeared as a dominant theme in organic transformations. Sustainability can be induced in a process by the use of mild conditions, catalytic reactions and limiting step-count and waste typically results in cost savings and cycle-time reduction. In recent times C-H bond activation has emerged as a sustainable approach to get C-C bond

coupling. In comparison to the more traditional cross-coupling reactions, C−H activation removes the requirement for pre-functionalization of both partners. The use of precious metal catalyst, high temperature and stoichiometric metal-based oxidants are required for unactivated C-H bond activation. In search of more sustainable approach the more abundant main group can be investigated as an alternative to the precious metal catalysts, a much less studied approach in this area. As Hauser bases are known to activate C-H bond. In 2015, Mashima and Harder reported alkaline earth metals as Mg and Ca complexes respectively to activate C-H bond. (Figure 5) Very recently, Eva Hevia reported main group elements such as Mg, Li, Zn mediated C-H bond activation. These developments towards sustainable C-H bond activation using main group elements motivated us to use our tridentate nacnac based magnesium complexes to activate various C-H bonds.

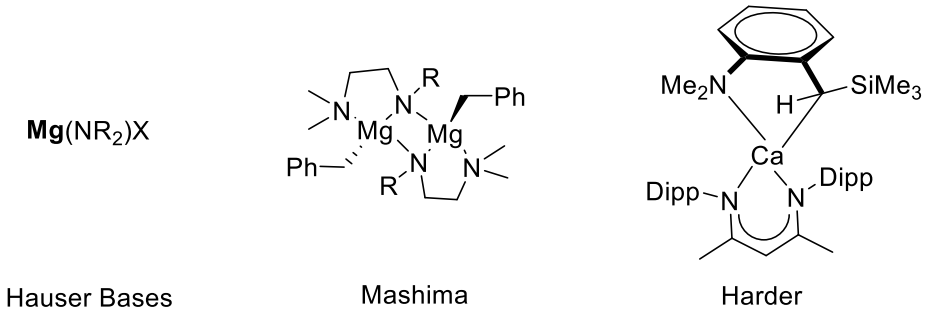

Figure 5. Previously reported main group mediated C-H bond activation.

To explore the reactivity, we have reacted the dearomatized Mg complex with phenylacetylene which resulted in a rearomatized Mg alkyl complex via C-H bond activation of the alkyne. (Scheme 5) We also treated the Mg complex with trimethylsilyl diazomethane, which also yielded a Mg rearomatized complex after the C-H bond activation. In diazomethane case the migration of $SiMe_3$ group from carbon to nitrogen resulted into the formation of CN triple bond and an unusual magnesium cyanide complex.(Scheme 5)

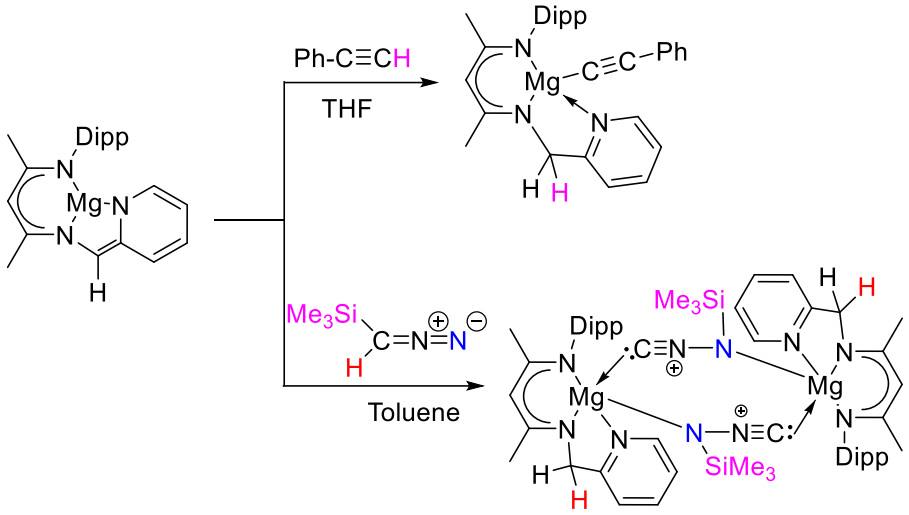

Scheme 5: C-H bond activation.

Having monomeric magnesium bromide in hand we tried to yield magnesium hydride reacting it with k-selectride, but we ended up with inter molecular reduction of pyridine. (Scheme 6)

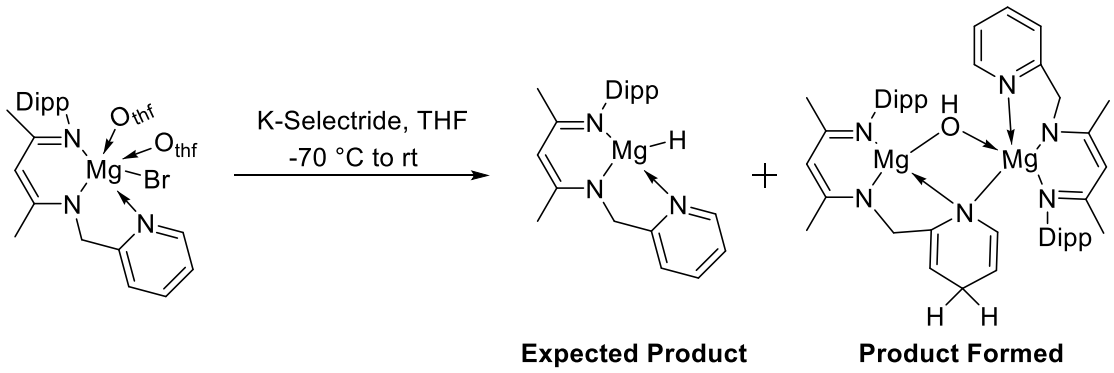

Scheme 6: Reaction with k-selectride.

In Summary:

- Explored the C–H bond activation of trimethylsilyldiazomethane and phenylacetylene
- The SiMe3 migration led to a cyanide magnesium complex
- The efforts to prepare magnesium hydride eventually ended up getting inter molecular pyridine reduction via inter molecular C–H bond activation
- We are currently exploring further C-H bond activation and also tying to isolate the monomeric magnesium hydride complex.

<u>Chapter 5</u>: Tridentate Nacnac supported chemistry of Aluminum and Gallium

The symmetrical β-diketiminato ligand can provide adequate thermodynamic and/or kinetic effort to stabilize a large variety of transition metals and main group elements. The nacnac supported group 13 elements have enjoyed an extensive devotion due to their usefulness as a synthon. Whereas a tridentate pendent picolyl functionalized nacnac framework is comparatively less well-explored system which has been used for the synthesis of iron, chromium, yttrium, and scandium complexes along with only few reports on main group recently reported from our group. Motivated by the recent results in main group chemistry we were keen to explore the ligand system to yield main group hydride, since we were not able to do it so. When we tried earlier to synthesize aluminium hydride with alane. We ended up with C-C coupled six membered binuclear aluminium hydride system. (Scheme 8) To understand the system further we tried the same reaction with different reaction conditions. (Scheme 8) The reaction in diethyl ether yielded monomeric aluminium hydride the desired product and were also able to isolate the intermediate from which the six membered binuclear aluminium complex is forming as an end product.

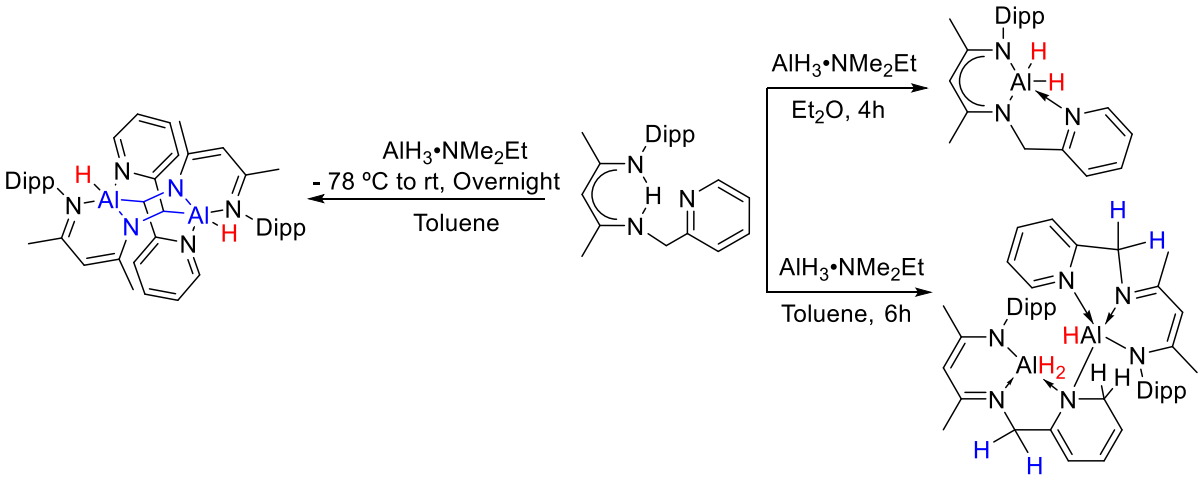

Scheme 6: Solvent effect on the reaction.

Next when we used benzyl potassium rather than using the traditional bases used to abstract the proton from the ligand, and followed by the addition of MCl_3 (M= Al, Ga). We were able to isolate the corresponding metal halides. (Scheme 9)

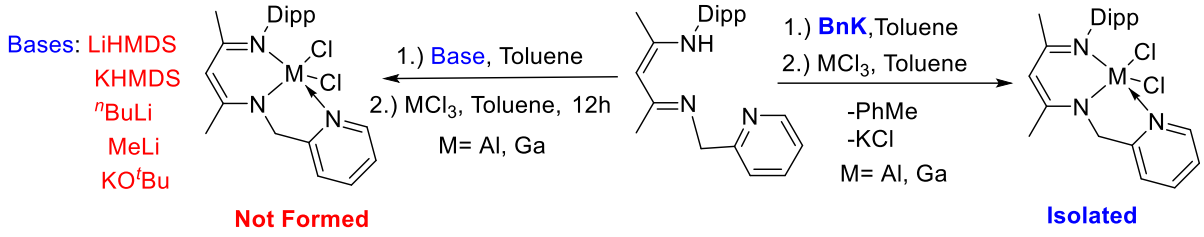

Scheme 6: Synthesis of metal halides of Ga, Al.

In Summary:

- Isolation monomeric aluminum hydride complex
- Demonstrated the intermolecular hydroamination of pyridine
- Developed a new direct method for synthesis of aluminum chloride.
- Currently further reactivity studies of metal halides and hydrides are going on.

References:

1. H. W. Roesky, S. Singh, V. Jancik, V. Chandrasekhar, *Acc. Chem. Res.* 2004, **37**, 969-981.
2. H. Wessel, H. S. Park, P. Müller, H. W. Roesky, I. Usón, *Angew. Chem. Int. Ed.* 1999, **38**, 813–815.
3. S. P. Sarish, S. Nembenna, S. Nagendran, H. W. Roesky, *Acc. Chem. Res.*, 2011, **44**, 3, 157–170.
4. (a) S. Pahar, V. Sharma, S. Tothadi, S. S. Sen, *Dalton Trans.*, 2021, **50**, 16678 – 16684; (b) S. Pahar, V. S. V. S. N. Swamy, T. Das, R. G. Gonnade, K. Vanka, S. S. Sen, *Chem. Commun.*, 2020, **56**, 11871–11874; (c) S. Pahar, V. Sharma, B. Mahata, C. P. George, H. Sharma, K. Vanka, S. S. Sen, *Inorg. Chem.*, 2022, **61**, 17370–17377.
5. C. Yoo, Y. Lee, *Angew. Chem. Int. Ed.*, 2017, **56**, 9502−9506; *Angew. Chem.*, 2017, **129**, 9630–9634.
6. J. C. Ott, H. Wadepohl, L. H. Gade, *Angew. Chem. Int. Ed.*, 2020, **59**, 9448–9452; *Angew. Chem.*, 2020, **132**, 9535–9539.
7. C. Gunanathan, D. Milstein, *Acc. Chem. Res.*, 2011, **44**, 588−602.
8. C. Gunanathan, D. Milstein, *Chem. Rev.*, 2014, **114**, 12024−12087.

9. J. R. Khusnutdinova, D. Milstein, *Angew. Chem. Int. Ed.*, 2015, **54**, 12236−12273.
10. A. Mukherjee, D. Milstein, *ACS Catal.*, 2018, **8**, 11435−11469.
11. T. W. Myers, L. A. Berben, *J. Am. Chem. Soc.*, 2013, **135**, 9988−9990.
12. T. W. Myers, L. A. Berben, *Chem. Sci.*, 2014, **5**, 2771−2777.
13. T. Simler, L. Karmazin, C. Bailly, P. Braunstein, A. A. Danopoulos, *Organometallics*, 2016, **35**, 903−912.
14. M. Rauch, S. Kar, A. Kumar, L. Avram, L. J. W. Shimon, D. Milstein, *J. Am. Chem. Soc.*, 2020, **142**, 14513−14521.
15. Y. Liang, J. Luo, Y. Diskin-Posner, D. Milstein, *J. Am. Chem. Soc.*, 2023, **145**, 9164–9175.
16. Y. Liang, U. K. Das, J. Luo, Y. Posner-Diskin, L. Avram, D. Milstein, *J. Am. Chem. Soc.*, 2022, **144**, 19115–19126.
17. (a) R. Kumar, V. Sharma, S. Banerjee, K. Vanka, S. S. Sen, *Chem. Commun.*, 2023, **59**, 2255–2258; (b) S. Yadav, R. Dixit, M. K. Bisai, K. Vanka, S. S. Sen, *Organometallics*, 2018, **37**, 4576–4584.
18. R. E. Mulvey, *Organometallics*, 2006, **25**, 1060–1075.
19. N. R. Judge, A. Logallo, E. Hevia, *Chem. Sci.*, 2023,**14**, 11617-11628.

Publications

1. Semester-IV (June-2021): Milan Kumar Bisai, **Vishal Sharma**, Rajesh G. Gonnade* and Sakya S. Sen*, *Organometallics*., **40**, 2133 - 2138 (2021).

2. Semester-V (October-2021): Sanjukta Pahar, **Vishal Sharma**, Srinu Tothadi and Sakya S. Sen*, *Dalton Trans.*, **50**, 16678 - 16684 (2021).

3. Semester-VI (March-2022): Rohit Kumar, **Vishal Sharma**, Shailja Jain, Himanshu Sharma, Kumar Vanka and Sakya S. Sen*, *ChemCatChem*., **14**, e202101788 (2022)

4. Semester-VI (July-2022): Rohit Kumar, Sayan Dutta, **Vishal Sharma**, Praval P. Singh, Rajesh G. Gonnade*, Debasis Koley* and Sakya S. Sen*, *Chem. Eur. J.*, **28**, e202201896 (2022)

5. Semester-VII (October-2022): Sanjukta Pahar, **Vishal Sharma**, Biplab mahata, Christy P. George, Himanshu Sharma, Kumar Vanka and Sakya S. Sen*, *Inorg. Chem.*, **61**, 17370 - 17377 (2022)

6. Semester-VIII (January-2023): Rohit Kumar, **Vishal Sharma**, Subhrashis Banerjee, Kumar Vanka and Sakya S. Sen*, *Chem. Commun.*, **59**, 2255 - 2258 (2023)

7. Semester-X (January-2024): Sanjukta Pahar, † **Vishal Sharma**, † K. Vipin Raj, Mayur P. Sangole, Christy P. George, Kirandeep Singh, Kumar Vanka, Rajesh G. Gonnade and Sakya S. Sen, *Chem. Eur. J.*, **30**, e202303957 (2024). († = equal contribution from both the authors)- Thesis Related.

Signature of Student

Vishal Sharma

Signature of Guide

Dr Sakya S. Sen

Chapter-1

Introduction

Abstract

This chapter briefly explains about the importance of a ligand in organometallic chemistry to stabilize metal centre. The development of nacnac ligand and its chemistry around main group as well as transition metal complexes is also discussed. Further, a brief overview of modified tridentate nacnac ligand and its recent advancements are also discussed. At last, the purposes and findings of this contribution are discussed.

1: Introduction

1.1 Ligand

Ligand systems are fundamental to organometallic chemistry[1], and the pioneering work of Werner in coordination chemistry played a crucial role in shaping the modern understanding of metal-ligand interactions.[2] Werner's groundbreaking discoveries in the early 20th century provided insights into the structure and bonding of coordination compounds thus establishing the foundational principles of modern inorganic chemistry.[2b] His research elucidated how metals bind to ligands, which significantly influenced the development of both organometallic and bioinorganic chemistry.[3] In recognition of his contributions, Werner was awarded the Nobel Prize in Chemistry in 1913, marking a milestone in the study of coordination compounds.

1.1.1 Importance of Ligand Systems

Ligands are crucial in organometallic chemistry, playing a key role in determining the structure, reactivity, and catalytic efficiency of metal complexes.[3] As molecules or ions that bind to metal centres, ligands influence both the electronic properties and the steric environment of the metal, thereby controlling vital aspects of reactivity such as bond activation, coordination geometry and reaction selectivity.[4]

Ligands can be broadly classified into two categories: actor ligands and spectator ligands. Actor ligands are directly involved in chemical reactions, often by associating, dissociating, or interacting with the metal centre, making them particularly important in catalytic processes. In contrast, spectator ligands do not undergo changes during the reaction but play an essential role in controlling metal's properties to optimize its performance in specific applications. The impact of ligands extends beyond simple metal stabilization. Electron-rich ligands, such as phosphines and N-heterocyclic carbenes (NHCs), can enhance the electron density at the metal centre, promoting oxidative addition and facilitating key catalytic cycles.[5] The ground breaking scientific achievements may have constituted the initial spur to this growth: (i) the first utilization of NHC complexes by Herrmann and co-workers in catalysis[6a] and (ii) the preparation of the Grubbs' second-generation catalyst and related catalysts,[6b] which undoubtedly

contributed to the award of the Nobel Prize for Chemistry 2005. On the other hand, electron-withdrawing ligands, such as carbonyl (CO) or halides, can stabilize high oxidation states or influence reductive elimination steps.[7] Steric effects are equally important: bulky ligands can create selective environments, steering catalytic pathways to favour desired products while minimizing side reactions.[8]

Ligand design has evolved to meet the demands of modern chemistry, including the development of chelating and pincer ligands that enhance catalyst stability and performance.[9] These ligands are crucial in industrial processes, such as olefin polymerization using Ziegler-Natta catalyst[10,11] and cross-coupling reactions like the Suzuki-Miyaura coupling,[11d] which are vital for pharmaceutical and material synthesis. In recent years, the critical role of ligands in stabilizing transition metal complexes has driven organometallic chemists to explore alternatives to transition metals, given their limited abundance and high costs. Compounds with low-valent main group elements have emerged as auspicious candidates for substituting transition metals in various organic transformations and small molecule activation processes.[12] These elements offers advantages such as greater availability, lower costs, and distinctive reactivity profiles. However, their utilization requires overcoming the inherent instability of low-valent main group compounds, which is heavily dependent on innovative ligand design, enabling the exploration of unique electronic and steric environments.[13] Recent efforts have focused on designing ligands that provide robust steric protection, facilitate electron delocalization, or incorporate donor-acceptor interactions to support low-valent states.[14] Such ligand frameworks not only stabilize reactive intermediates but also unlock new catalytic pathways and reactivity patterns previously inaccessible to traditional transition metal systems.[15] This paradigm shift expands the scope of main group chemistry, offering sustainable and efficient alternatives for challenging chemical transformations.

1.1.2 Few Commonly Used Ligand Systems

Ligand systems commonly employed in organometallic chemistry often exhibit bidentate or tridentate chelating coordination modes, with tridentate ligands being predominantly referred to as pincer ligands. The versatility of pincer ligands facilitates

the design of compounds with altered electronic properties and reactivity. Their intrinsic adaptability, coupled with the capacity to stably coordinate otherwise labile groups, enhances their applicability across a wide range of chemical transformations.[9] Specifically, N, N-chelating ligands have become highly prevalent in the field of coordination chemistry. Their remarkable compliance in terms of steric and electronic characteristics, attached with their capability to act as bidentate ligand, makes them highly effective for coordinating with transition metals,[16] lanthanides,[17] and main-group elements.[18] While the study of transition metal complexes featuring N,N-chelating ligands has long been an established area with widespread applications in catalysis,[19] there has been a rising focus on exploring their role in main-group element chemistry over the past few decades.[20] Few N, N-chelating monoanionic ligands are amidinate, guanidinates, *β*-diketiminate, and NCN pincers are shown in Scheme 1.1.

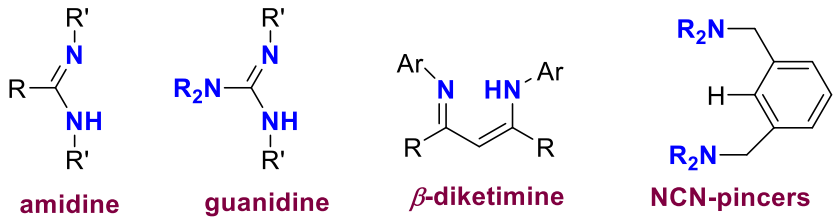

Scheme 1.1 A few examples of ligands commonly used in organometallic complexes.

1.2 *β*-diketimine as a Ligand System

Starting with the *β*-diketonato or acetylacetonato ligand, generally referred as acac (**A**), this ligand system plays a crucial role in coordination chemistry.[21] Its versatility arises from the keto-enol tautomerism present in the parent diketone. Replacing one oxygen atom of the diketone with an imine group (NR) resulted in the *β*-enaminoketonato ligand system **B**.[22] This substitution to NR group allows, the nitrogen atom's substituent to be modified, which in turn adjusts the electronic and steric characteristics of the *β*-enaminoketonato ligand. Furthermore, the *β*-diketiminato ligand, often known as nacnac (**C**) due to its nitrogen-based substitution of acac, deserves mention. Unlike the *β*-enaminoketonato ligand, nacnac replaces both the keto group with imine fun ctionalities, significantly enhancing the ability to fine-tune the electronic and steric

properties of the chelating ligand system (Scheme 1.2). The electronic and steric characteristics of these ligands can be readily modified by varying the substituents on the nitrogen atom at the α-position or by altering those on the alkyl backbone at the β and γ positions.

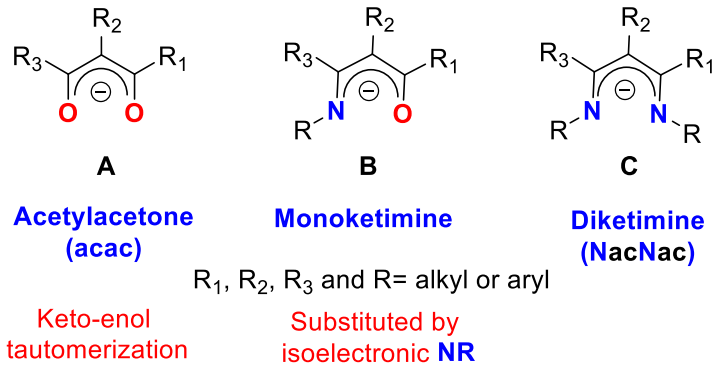

Scheme 1.2 Isoelectronic monoanionic ligands: acetylacetonato (**A**), *β*-enaminoketonato (**B**) and *β*-diketiminato (**C**).

The synthesis of the parent *β*-diketimine ligands can be accomplished mainly by using two different pathways shown in Scheme 1.3. The pathway (i) shows the condensation reaction starting from the corresponding *β*-diketone and the desired amine NH_2R.[23] For the formation of aryl substituted *β*-diketimine, one ketone reacts selectively with ethylene glycol to give the corresponding ketal, which can undergo the condensation reaction with the primary amine as shown in pathway (ii).[24]

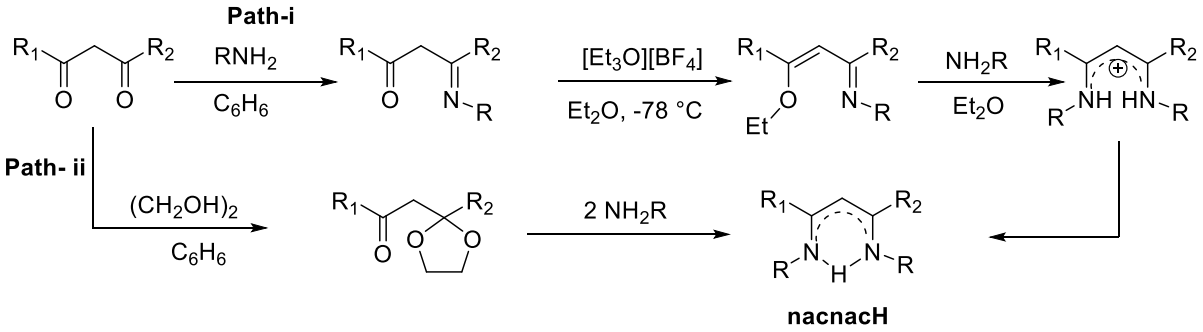

Scheme 1.3 Synthetic procedures for nacnacH ligands.

Since the first synthesis of the Dipp substituted ligand $[\{N(Dipp)C(Me)\}_2CH]^-$ in 1997,[25] this derivate probably developed to one of the most studied nacnac ligand systems in current research topics. Due to this fact, a more facile synthetic approach with good yields of about 80

% was developed, especially for ligands carrying aromatic imine substituents (Scheme 1.4). Additionally, for the implementation of amplified steric bulkiness at the backbone of the nacnac ligands, ^{t}Bu groups were introduced, starting from pivaloyl chloride and the corresponding primary amine and followed lithiation reactions for coupling.[26]

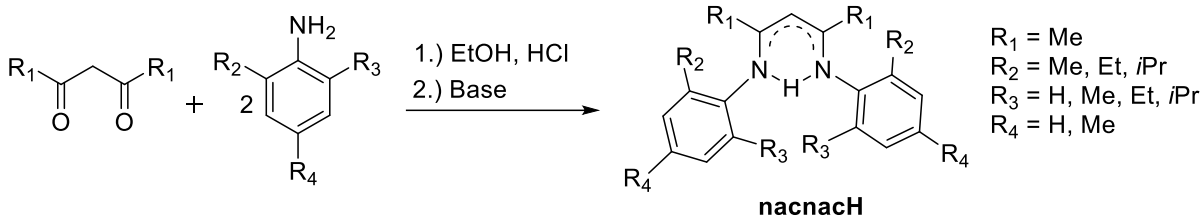

Scheme 1.4 Synthetic procedure for aryl substituted symmetric nacnacH ligands.

Scheme1.5 illustrates various bonding forms of the deprotonated monoanionic nacnac ligand, all of which have been structurally confirmed through solid-state analysis. The most typical and anticipated configuration is depicted in mode **(i)**, where the six-membered metalla-heterocycle exhibits a planar structure, and coordination is achieved through the two imine nitrogen atoms in a terminal chelating arrangement. Modes **(ii)** and **(iii)** represent variations of this coordination motif but differ in the conformation of the metalla-heterocycle, which adopts a boat-like shape.[27] Motif **(iv)** illustrates a dimeric arrangement in which the metal ions are chelated similarly to the previous modes, but two nitrogen atoms also act as bridging donors, connecting the adjacent metal centers.[28] Modes **(v)** and **(vi)** offers intriguing alternative coordination patterns. In **(v)**, the ligand no longer behaves as a chelate. Instead, it adopts an open-chain conformation, with each terminal nitrogen atom coordinating a separate metal ion, effectively bridging the two centers.[29] Mode **(vi)**, although uncommon, involves coordination via the methylene bridge. In these rare cases, the metal ion preferentially binds to the carbanionic centre of the ligand rather than the typical nitrogen donors, particularly in the solid-state structure.[30]

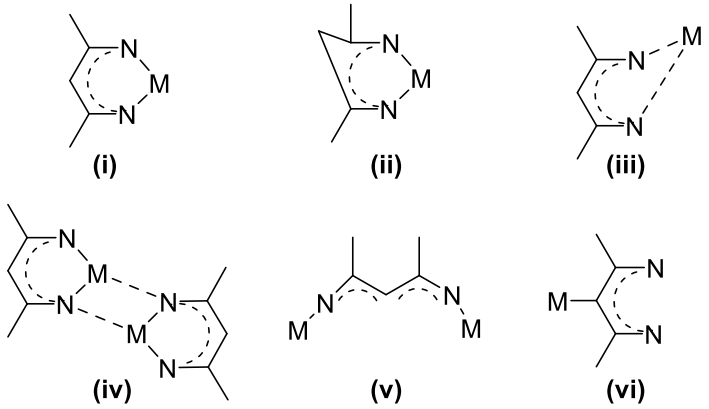

Scheme 1.5 Various binding modes of nacnac ligand.

1.2.1 History at A Glance

Since Parks and Holm first defined *β*-diketimine-based nickel (II) complexes in 1968,[31] the use of nacnac ligands has expanded significantly. Over the past two decades, these ligands have played a critical role in numerous advancements, particularly in the coordination chemistry of main-group elements and low valent first row transition metal complexes. Followed by the discovery of Parks and Holm, the first lithium nacnac complexes were reported in 1994 by the group of Lappert and coworker.[28] The introduction of the dipp (diisopropylphenyl) substituted nacnac ligand significantly advanced the stabilization of heterolytic metal complexes, largely due to the additional steric hindrance provided by the isopropyl groups.[32] A significant advancement in the main group chemistry of nacnac ligands occurred in 1999, when Roesky reported the synthesis of a nacnac-supported Al(I) compound.[33] This milestone spurred extensive research into the chemistry of nacnac-based main group compounds and heavier group 13 and 14 analogs of carbenes were also successfully synthesized in following years.[34] Subsequently, Driess achieved the synthesis of nacnac supported silylene where the CH_3 attached to backbone got deprotonated to make the ligand di-anionic (Scheme 1.6).[35] In this context, *β*-diketimines served as a gateway to the synthesis of diverse and significant main-group element complexes.

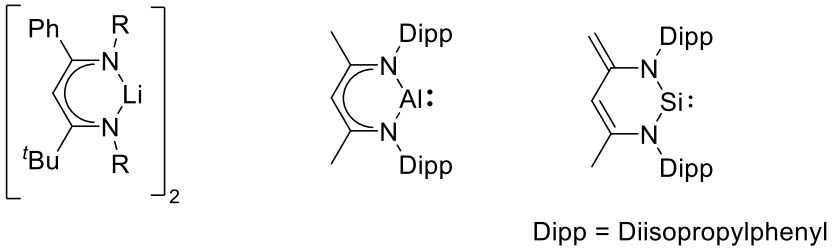

Scheme 1.6 Nacnac ligand supported early discoveries in main group elements.

Especially in alkaline earth metal coordination chemistry, nacnac ligands are responsible for several milestones in the last two decades, whereas the chemistry of alkaline earth metals was limited to mostly homoleptic complexes because of the Schlenk equilibrium. However, in 2001 Roesky successfully synthesized a heteroleptic magnesium iodide complex stabilized by a nacnac ligand, effectively circumventing the limitations of the Schlenk equilibrium.[36] This was followed in 2004 by Chisholm's synthesis of a nacnac-stabilized calcium amide complex.[37] These foundational discoveries paved the way for two major milestones: the development of a soluble calcium hydride complex by Harder and the first reported Mg(I) species by Jones.[38,39] Additionally, Roesky and colleagues achieved another milestone with the synthesis of the first soluble monomeric calcium fluoride complex (Scheme 1.7).[40]

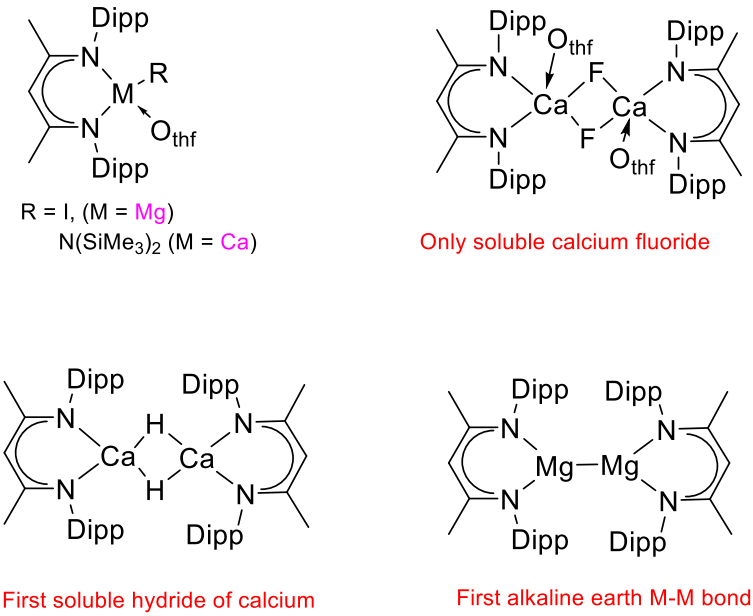

Scheme 1.7 Nacnac ligand supported milestone discoveries in alkaline earth metals.

Unlike conventional reducing agents such as potassium mirrors or KC_8, electron-rich Mg(I) complexes offer the advantage of being soluble in hydrocarbon solvents, making them highly effective, user-friendly, and selective reducing agents for various applications. Since their introduction, these complexes have been instrumental in enabling the isolation of a wide range of novel compounds that were previously unattainable with traditional reducing agents.[41] In recent times modification has also been made to nacnac ligand making it more suitable to synthesize low valent monomeric alkaline earth metal complexes. An impressive demonstration of the stabilizing properties of nacnac ligands was provided in 2018 by the research teams of Harder and Hill, who successfully isolated cationic Lewis-base-free β-diketiminate complexes of magnesium and calcium (Scheme 1.8).[42]

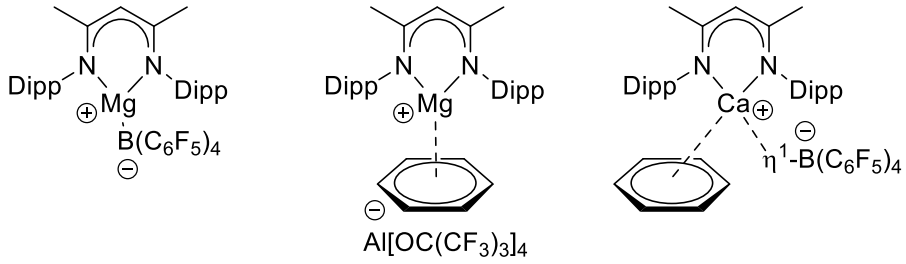

Scheme 1.8 Cationic complexes of magnesium and calcium.

1.3 Methylpyridinato-*β*-diketiminate Ligand System

A less extensively studied ligand system features a nacnac framework functionalized with a picolyl group (**LH**). The pyridine moiety attached to one of the nitrogen atoms not only introduces additional steric shielding but also enhances electronic stabilization of the metal centre. Moreover, the picolyl arm offers a flexible, labile coordination site that can dynamically interact with the metal centre, thereby facilitating an adaptable environment around the reactive site and potentially influencing catalytic activity.

1.3.1 Synthesis of Tridentate NacNac Ligand

Ligand (**LH**) was synthesized via a modified synthetic process.[43] Initially, 2-((2,6-diisopropylphenyl) imido)-2-penten-4-one was obtained via the condensation of acetylacetone with 2,6-diisopropylaniline, using a catalytic amount of *p*-toluenesulfonic acid. This was recrystalized as pure product in hot hexane, then reacted with 2-picolylamine

in toluene, again in the presence of *p*-toluenesulfonic acid as a catalyst. The reaction mixture was refluxed for 18 hours using a Dean-Stark apparatus to yield the ligand precursor LH with a 61% yield (Scheme 1.9). The product was purified by crystallization from diethyl ether, and the crystals were washed with cold pentane to get pure product.

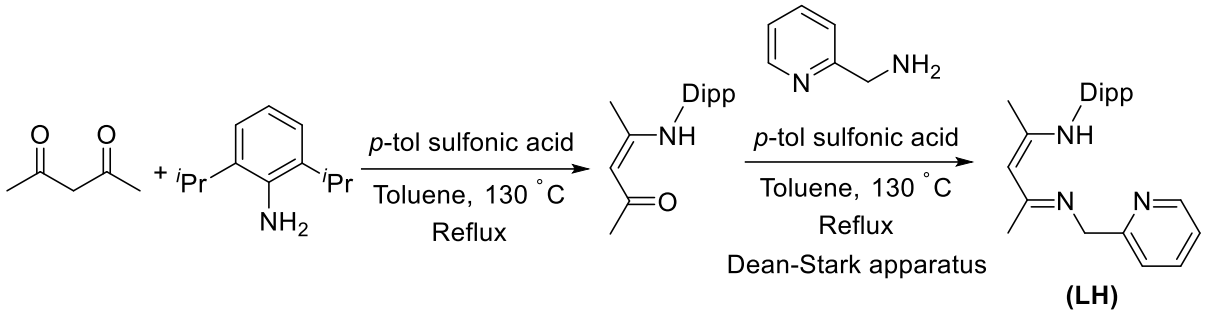

Scheme 1.9 Synthetic protocol for methylpyridinato *β*-diketiminate ligand (LH).

1.3.2 Prior Literature Precedence

This tridentate nacnac ligand was initially employed in the synthesis of coordination complexes with iron, chromium, scandium, and yttrium, marking its foundational application in transition metal and rare earth chemistry (Scheme 1.10).[44,45]

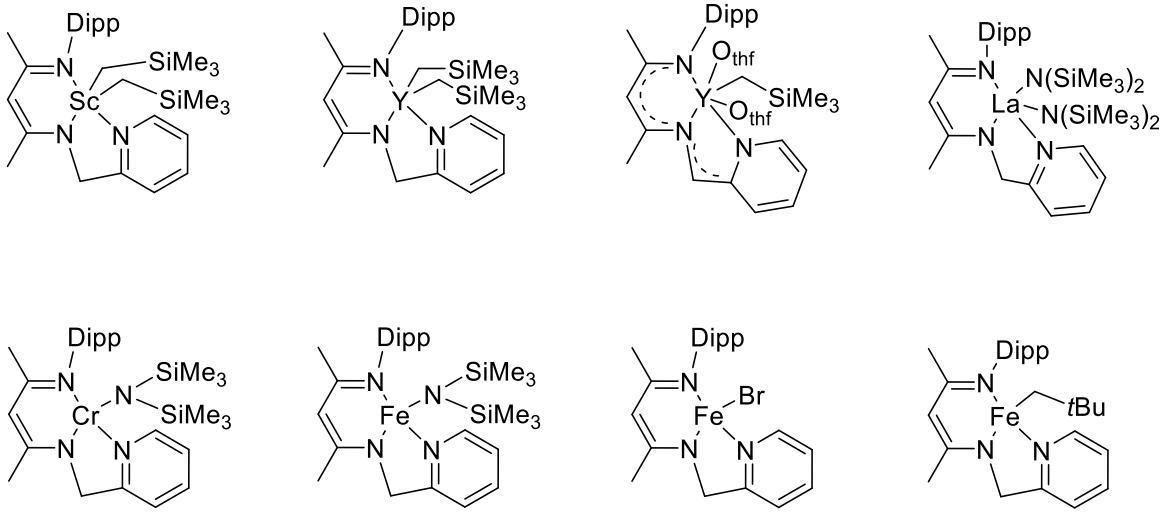

Scheme 1.10 Lanthenides and Transition metal complexes of **LH**.

Additional motivation arises from a recent study on pyridine-functionalized silane, which revealed extraordinary binding characteristics with Rh and Ir.[46] Recently, we have

demonstrated homoleptic magnesium and calcium complexes using this ligand and established their utility as catalysts for the hydroboration of aldehydes and ketones.[47] Additionally we have also utilised this ligand system to synthesize tetrylenes. The attempts to synthesize germylium ylidene was not successful. Instead, the picolyl functionality in LH facilitated several unusual and alternative reactivities, including smooth ring contraction via C–N bond cleavage, efficient dehydrocoupling, transmetallation, and the formation of a six-membered Al-heterocycle. Such reactivities are not typically observed in traditional nacnac-based systems. This study underscores how minor modifications in ligand design can lead to remarkably novel and unanticipated chemical outcomes.[48]

Subsequently, we investigated the potential of this ligand system for stabilizing nickel chloride, cationic nickel species, and nickel hydride complexes. Furthermore, the catalytic application of nickel hydride was explored in the hydroboration of various unsaturated bonds.[49] These studies highlight the versatility of the tridentate nacnac framework in the context of main group and nickel chemistry, as illustrated in Scheme 1.11.

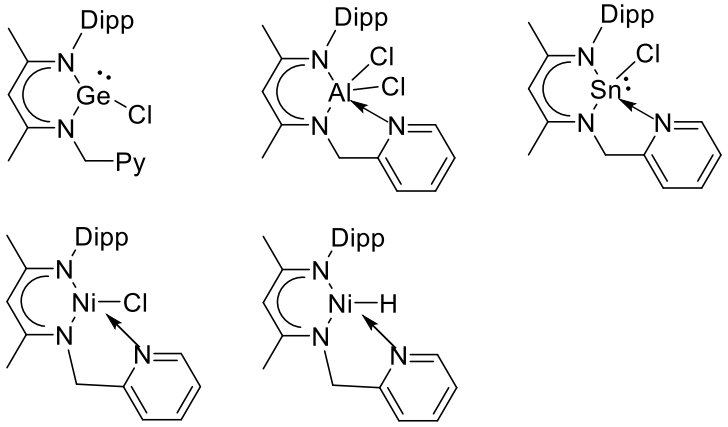

Scheme 1.11 Previously reported complexes of **LH** from our group.

1.4 Aim and Outline of The Thesis

There are five chapters in the thesis. While this chapter describes the advances of nacnac and modified tridentate ligand toward stabilization of low valent main group as well as transition metal complexes. The other four chapters will showcase our contribution towards further exploration of modified tridentate nacnac ligand. The thesis aims to increase our

knowledge of the structural characteristics, reactivity, and synthesis of organo-magnesium and Ni(I) complexes. The work on the thesis was primarily focused on the following points:

1) Designing novel T-shaped Ni(I) radical species.

2) Preparation of the hydrocarbon soluble monomeric/heteroleptic organo-magnesium complexes and study their reactivity towards water activation.

3) The application of these soluble dearomatized magnesium complex towards C-H bond activation and C-C cross coupling reaction.

4) Preparation of group 13 halides and demonstration of solvent effect on the stability of tridentate nacnac supported alane complex.

Chapter 2 discusses the synthesis and characterization of a tridentate nacnac ligand-stabilized T-shaped Ni(I) metalloradical, including its radical trapping using TEMPO as a trapping agent. The reactivity of the complex toward small molecule activation is also investigated. Structural and bonding arrangements of all complexes were elucidated through single-crystal X-ray diffraction (XRD) analysis. Density Functional Theory (DFT) studies further corroborate the presence of a single unpaired electron localized on the nickel centre, confirming its metalloradical nature.

Chapter 3 contains the synthesis of monomeric magnesium bromide complex and dearomatized magnesium complex using Grignard reagent and dibutylmagnesium respectively. Among them dearomatized magnesium complex has been utilised to activate O–H bond of water, which was confirmed by deuterium-labelling experiments. The synthesis of magnesium hydride is also attempted eventually leading to inter molecular pyridine reduction.

Chapter 4 covers the utilization of dearomatized magnesium complex towards C–H bond of terminal alkynes and diazoalkane. The magnesium alkynylide complexes of magnesium was structurally characterized using single crystal XRD and NMR spectroscopy. The magnesium alkynylide complexes were further explored towards the C–C cross coupling using Pd as a catalyst.

Chapter 5 details the synthesis of tridentate nacnac ligand-supported aluminum and gallium halides using a novel synthetic protocol that had not been previously achieved using other bases. The solvent effect on the stability of tridentate nacnac-stabilized aluminum hydride was investigated, leading to the successful isolation of a monomeric aluminum hydride complex.

Density Functional Theory (DFT) calculations were performed to elucidate the reaction mechanism and confirm the formation of the final aluminum hydride dimer through the identified intermediate species.

1.5 References

1. (a) D. H. Busch, *Chem. Rev.*, 1993, **93**, 3, 847–860; (b) A. H.-Jungemann, N. FeliuIoanna, M. H. A. Alkilany, I. Chakraborty, A. Masood, M. F. Casula, A. Kostopoulou, E. Oh, K. Susumu, M. H. Stewart Igor, L. M. E. Stratakis, W. J. Parak, A. G. Kanaras, *Chem. Rev.*, 2019, **119**, 8, 4819–4880; (c) M. Yamanaka, K. Mikami, *Organometallics,* 2005, ***24***, 19, 4579–4587.
2. (a) E. C. Constablea, C. E. Housecrofta, *Chem. Soc. Rev.,* 2013, **42**, 1429–1439; (b) C. S. Diercks, M. J. Kalmutzki, N. J. Diercks, O. M. Yaghi, *ACS Cent. Sci.,* 2018, **4**, 11, 1457–1464.
3. S. S. Stahl, *J. Am. Chem. Soc.,* 2010, **132**, 24, 8524–8525.
4. (a) C. A. Tolman, *Chem. Rev.,* 1977, **77**, 3, 313–348; (b) D. J. Stacchiola, *Acc. Chem. Res.,* 2015, **48**, 7, 2151–2158; (c) E. F. Murphy, R. Murugavel, H. W. Roesky, *Chem. Rev.,* 1997, **97**, 8, 3425–3468.
5. (a) M. Poyatos, J. A. Mata, E. Peris, *Chem. Rev.,* 2009, **109**, 8, 3677–3707; (b) E. Peris, R. H. Crabtree, *Coord. Chem. Rev.*, 2004, **248**, 2239–2246; (c) T. W. Lyons, M. S. Sanford, *Chem. Rev.,* 2010, **110**, 2, 1147–1169.
6. (a) W. A. Herrmann, M. Elison, J. Fischer, C. Kocher, G. R. J. Artus, *Angew. Chem., Int. Ed. Engl.,* 1995, **34**, 2371; (b) R. H. Grubbs, *Angew Chem., Int. Ed.*, 2006, **45**, 37602.
7. (a) M. Yamanaka, K. Mikami, *Organometallics,* 2005, ***24***, 19, 4579–4587; (b) C. Gauss, D. Veghini, O. Orama, H. Berke, *Journal of Organometallic Chemistry,* 1997, **541**, 19–38.
8. (a) E. Peris, R. H. Crabtree, *Chem. Soc. Rev.*, 2018, **47**, 1959–1968; (b) C. H. Suresh, *Inorg. Chem.,* 2006, **45**, 13, 4982–4986.
9. E. Peris, R. H. Crabtree, *Chem. Soc. Rev.,* 2018, **47**, 1959–1968.
10. E. h. Karl Ziegler, E. Holzkamp, H. Breil, H. Martin, *Angew. Chem.,* 1955, **67**, 541–547.

11. (a) Z. Chen, E. Vorobyeva, S. Mitchell, E. Fako, M. A. Ortuño, N. López, S. M. Collins, P. A. Midgley, S. Richard, G. Vilé, J. P.-Ramírez, *Nature Nanotech.,* 2018, **13**, 702–707; (b) J. H. Kirchhoff, M. R. Netherton, I. D. Hills, G. C. Fu, *J. Am. Chem. Soc.*, 2002, **124**, 46, 13662–13663; (c) A. Molnár, *Chem. Rev.,* 2011, **111**, 2251–2320; (d) N. Miyaura, A. Suzuki, *Chem. Rev.,* 1995, **95**, 7, 2457–2483; (e) N. Miyaura, K. Yamada, A. Suzuki, *Tetrahedron Letters,* 1979, **36**, 3437–3440.
12. (a) P. P. Power, *Nature*, 2010, 463, 171; (b) C. Weetman, S. Inoue, *ChemCatChem,* 2018, **10**, 4213–4228.
13. (a) S. Aldridge, C. Jones, *Chem. Soc. Rev.,* 2016, **45**, 763–764; (b) C. Jones, *Coord. Chem. Rev.,* 2010, **254**, 1273–1289; (c) T. J. Hadlington, M. Driess, C. Jones, *Chem. Soc. Rev.,* 2018, **47**, 4176–4197.
14. P. P. Power, *Chem. Rev.,* 2003, **103**, 3, 789–810.
15. D. W. Stephan, G. Erker, *Angew. Chem. Int. Ed.,* 2010, **49**, 46–76.
16. (a) J.-Y. Zhang, Y. Ma, A.-L. Cheng, Q. Yue, Q. Sun, E.-Q. Gao, *Dalton Trans.,* 2011, **40**, 7219–7227; (b) R. L. Webster, *Dalton Trans.* 2017, **46**, 4483–4498.
17. (a) L. F. Sánchez-Barba, D. L. Hughes, S. M. Humphrey, M. Bochmann, *Organometallics,* 2005, **24**, 3792–3799; (b) Y. Yao, Z. Zhang, H. Peng, Y. Zhang, Q. Shen, J. Lin, *Inorg. Chem.,* 2006, **45**, 2175–2183; (c) M. V. Yakovenko, A. V. Cherkasov, G. K. Fukin, D. Cui, A. A. Trifonov, *Eur. J. Inorg. Chem.,* 2010, **2010**, 3290–3298; (d) P. Liu, H. Chen, Y. Zhang, M. Xue, Y. Yao, Q. Shen, *Dalton Trans.,* 2014, **43**, 5586–5594.
18. (a) R. T. Boeré, M. L. Cole, P. C. Junk, *New J. Chem.,* 2005, **29**, 128–134; (b) C. Jones, P. C. Junk, M. Kloth, K. M. Proctor, A. Stasch, *Polyhedron,* 2006, **25**, 1592–1600; (c) S. Harder, *Chem. Commun.,* 2012, **48**, 11165–11177; (d) M. E. Desat, S. Gärtner, R. Kretschmer, *Chem. Commun.,* 2017, **53**, 1510–1513.
19. M. E. Desat, R. Kretschmer, *Inorg. Chem.* **2019**, *58*, 16302–16311.
20. H. Nagashima, H. Kondo, T. Hayashida, Y. Yamaguchi, M. Gondo, S. Masuda, K. Miyazaki, K. Matsubara, K. Kirchner, *Coord. Chem. Rev.,* 2003, **245**, 177–190.
21. (a) S. Harder, *Chem. Rev.,* 2010, **110,** 3852–3876; (b) S. Harder, *Early main group metal catalysis*. *Concepts and reactions*, *Wiley-VCH,* Weinheim, Germany, 2020.
22. R. C. Mehrotra, R. Bohra, D. P. Gaur, Metal *ß*-Diketonates and Allied Derivatives, Academic Press, New York, 1978.

23. (a) M. Calligaris, L. Randaccio, Comprehensive Coordination Chemistry, Vol. 2, chapter 20.21, Pergamon, Oxford, U.K., 1987; (b) J. E. Parks, R. H. Holm, *Inorg. Chem.,* 1968, **7**, 1408–1416.
24. (a) S. G. McGeachin, *Can. J. Chem.*, 1968, **46**, 1903–1912; (b) L. C. Dorman, *Tetrahedron Lett.,* 1966, **7**, 459–464.
25. J. Feldman, S. J. McLain, A. Parthasarathy, W. J. Marshall, J. C. Calabrese, S. D. Arthur, *Organometallics,* 1997, **16**, 1514–1516.
26. P. H. M. Budzelaar, A. B. van Oort, A. G. Orpen, *Eur. J. Inorg. Chem.,* 1998, **1998**, 1485–1494.
27. (a) P. B. Hitchcock, M. F. Lappert, S. Tian, *J. Chem. Soc., Dalton Trans.,* 1997, 1945–1952; (b) M. F. Lappert, D. S. Liu, *J. Organomet. Chem.,* 1995, **500**, 203–217; (c) P. B. Hitchcock, M. F. Lappert, D. S. Liu, *J. Chem. Soc., Chem. Commun.,* 1994, 2637–2638.
28. (a) B.-J. Deelman, M. F. Lappert, H. K. Lee, T. C. W. Mak, W. P. Leung, P. R. Wei, *Organometallics,* 1997, **16**, 1247–1252; (b) P. B. Hitchcock, M. F. Lappert, D.-S. Liu, *J. Chem. Soc., Chem. Commun.,* 1994, 1699–1700.
29. W. Clegg, S. J. Coles, E. K. Cope, F. S. Mair, *Angew. Chem. Int. Ed.,* 1998, **37**, 796–798.
30. B. Räke, F. Zülch, Y. Ding, J. Prust, H. W. Roesky, M. Noltemeyer, H.-G. Schmidt, *Z. Anorg. Allg. Chem.* 2001, **627**, 836–840.
31. J. E. Parks, R. H. Holm, *Inorg. Chem.,* 1968, **7**, 1408–1416.
32. J. Feldman, S. J. McLain, Anju Parthasarathy, W. J. Marshall, J. C. Calabrese, S. D. Arthur, *Organometallics,* 1997, **16**, 1514–1516.
33. (a) H. W. Roesky, *Angew. Chem. Int. Ed.,* 1999, **38**, 1343; (b) C. Cui, H. W. Roesky, H.-G. Schmidt, M. Noltemeyer, H. Hao, F. Cimpoesu, *Angew. Chem., 2000*, **112**, 4274–4276.
34. (a) N. J. Hardman, B. E. Eichler, P. P. Power, *Chem. Commun.*, 2000, 1991–1992; (b) M. S. Hill, P. B. Hitchcock, *Chem. Commun.,* 2004, 1818–1819; (c) Y. Cheng, P. B. Hitchcock, M. F. Lappert, M. Zhou, *Chem. Commun.,* 2005, 752–753; (d) M. S. Hill, P. B. Hitchcock, R. Pongtavornpinyo, *Dalton Trans.,* 2005, 273–277; (e) M. S. Hill, R. Pongtavornpinyo, P. B. Hitchcock, *Chem. Commun.,* 2006, 3720–3722.
35. M. Driess, S. Yao, M. Brym, C. van Wüllen, D. Lentz, *J. Am. Chem. Soc.,* 2006, **128**, 9628 –9629.

36. M. H. Chisholm, J. C. Gallucci, K. Phomphrai, *Inorg. Chem.* 2004, **43**, 21, 6717–6725.
37. J. Prust, K. Most, I. MuÈller, E. Alexopoulos, A. Stasch, I. Uson, H. W. Roesky, *Z. Anorg. Allg. Chem.,* 2001, **627**, 2032–2037.
38. S. Harder, J. Brettar, *Angew. Chem. Int. Ed.,* 2006, **45**, 3474 –3478.
39. S. P. Green, C. Jones, A. Stasch, *Science,* 2007, **318**, 5857, 1754–1757.
40. S. Nembenna, H. W. Roesky, S. Nagendran, A. Hofmeister, J. Magull, P.-J. Wilbrandt, M. Hahn, *Angew. Chem. Int. Ed.,* 2007, **46**, 2512–2514.
41. C. Jones, *Nat. Rev. Chem.,* 2017, **1**, 877.
42. (a) L. Garcia, M. D. Anker, M. F. Mahon, L. Maron, M. S. Hill, *Dalton Trans.,* 2018, **47**, 12684–12693; (b) J. Pahl, S. Brand, H. Elsen, S. Harder, *Chem. Commun.,* 2018, **54**, 8685–8688.
43. F. Kaiser, R. M. Reich, E. Rivard and F. E. Kühn, *Organometallics,* 2018, **37**, 136−144.
44. (a) L. Bourget-Marle, M. F. Lappert, J. R. Severn, *Chem. Rev.,* 2002, **102**, 3031–3066. (b) C. Camp, J. Arnold, *Dalton Trans.,* 2016, **45**, 14462–14498.
45. X. Xu, Y. Chen, G. Zou, J. Sun, *Dalton Trans.,* 2010, **39**, 3952–3958.
46. W. D. Morris, P. T. Wolczanski, J. Sutter, K. Meyer, T. R. Cundari, B. Lobkovsky, *Inorg. Chem.,* 2014, **53**, 14, 7467–7484.
47. S. Yadav, R. Dixit, M. K. Bisai, K. Vanka, S. S. Sen, *Organometallics,* 2018, **37**, 4576–4584.
48. S. Pahar, V. S. V. S. N. Swamy, T. Das, R. G. Gonnade, K. Vanka, S. S. Sen, *Chem. Commun.,* 2020, **56**, 11871–11874.
49. S. Pahar. V. Sharma, B. Mahata, C. P. George, H. Sharma, K. Vanka, S. S. Sen, *Inorg. Chem.* 2022, **61**, 17370–11377.

Chapter-2

Tridentate NacNac Tames T-Shaped Nickel(I) Radical

Abstract: This chapter describes the synthesis of a thermally stable nickel(I) complex with a T-shaped structure **2.1** by reacting a nickel(II) chloride complex containing a tridentate *β*-diketiminato ligand with a pyridine group [2,6-*i*Pr_2-$C_6H_3NC(Me)CHC(Me)NH(CH_2py)]Ni(II)Cl$] with $KSi(SiMe_3)_3$. Interestingly, this reaction did not require the use of any strong reducing agent. The compound's metalloradical nature was confirmed through electron paramagnetic resonance (EPR) studies and its reaction with TEMPO, resulting in the formation of a three-membered nickeloxaziridine complex **2.2**. When compound **2.1** was reacted with disulfide and diselenide, the S–S and Se–Se bonds were cleaved, and a coupled product was formed through carbon atom of the pyridine-imine group. The nickel(I) radical activates H_2 at room temperature and atmospheric pressure to give a monomeric nickel hydride, **2.7**.

2.1 Introduction

Transition metal complexes with partially filled *d* orbitals have garnered considerable attention due to their unique reactivity and electronic structure.[1] The presence of three-coordinate nickel complexes, in particular, has intrigued researchers because they are rare,[2] and have biological relevance as they resemble the proximal nickel site of acetylcoenzyme A synthase.[3c,d] These complexes typically adopt a trigonal planar (D_3h) geometry to minimize steric repulsion among the ligands (Scheme 2.1). However, the enforced T-shaped geometry suggests direct access to one of the *d*-orbitals, specifically dz^2 or dx^2-y^2, depending on its orientation, pointing towards the available coordination site. Enforcing a strictly T-shaped coordination mode presents challenges, as three-coordinate complexes tend to favour trigonal-planar coordination geometries due to reduced inter-ligand steric repulsion.[3]

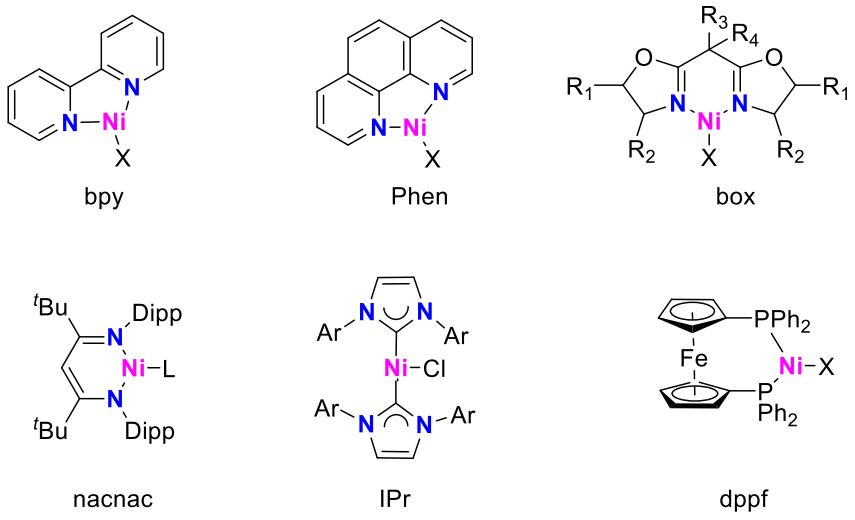

Scheme 2.1 Selected T-shaped Ni complexes based on pincer ligands

Strictly T-shaped nickel(I) complexes are exceedingly rare, with only two examples reported by Lee and Schneider group.[4] Gade and his colleagues also published seminal work in this area,

isolating a remarkable T-shaped iron complex (Scheme 2.2).[5] To isolate the metalloradicals, it is crucial to prepare a structurally rigid supporting ligand. Recent studies on T-shaped first-row transition metal complexes have capitalized on pincer ligands, which offer significant advantages. The prearranged, meridional coordination mode of these ligands supports the active centre, while the substituents on the peripheral donor atoms effectively shield the coordination sphere.[6]

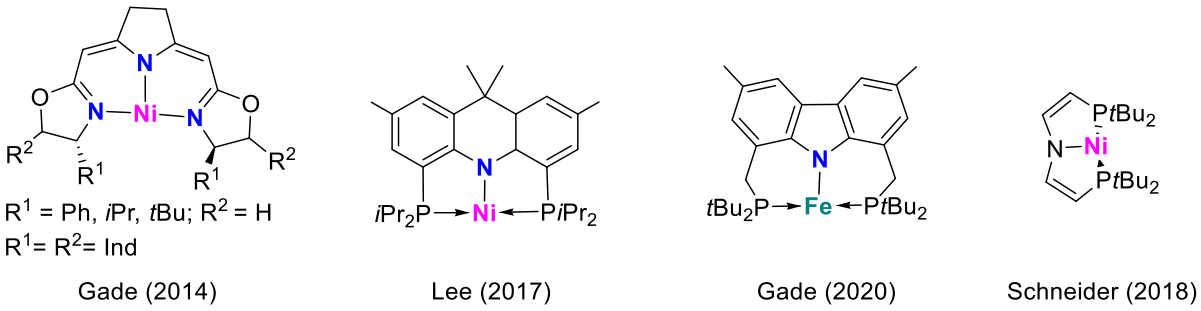

Scheme 2.2. T-shaped Ni and Fe complexes based on pincer ligands.

Holland and his colleagues reported a three-coordinate *β*-diketiminate-nickel(I) complex with a carbonyl ligand, but its structure does not strictly adhere to the T-shape.[7] The same holds true for Limberg's *β*-diketiminate-nickel(I) dinitrogen complex.[8] More recently, our research group and others have utilized a modified nacnac ligand, wherein one of the N-aryl moiety is replaced with a methyl-pyridine side arm. We and others have reported the synthesis of a range of complexes, encompassing main-group, transition metal, and lanthanide species, employing this tridentate nacnac ligand [2,6-*i*Pr$_2$-C$_6$H$_3$NC(Me)CHC(Me)NH(CH$_2$py)].[9] Through our investigations, we have demonstrated that this ligand stabilizes a monomeric Ni(II) hydride species by virtue of the additional donation from the coordinating picolyl moiety.[10] In this chapter, we present the preparation of the first T-shaped Ni(I) radical using a non-pincer ligand

2.1. The presence of the metal-centred radical was confirmed through the isolation of the TEMPO adduct **2.2**. Remarkably, **2.1** undergoes unusual C-C bond formation via coupling upon reaction with Ph_2S_2 and Ph_2Se_2. The activation of dihydrogen is also observed resulting in the previously reported monomeric nickel hydride.[10]

2.2 Results and Discussions

2.2.1 Synthesis of T-shaped Nickel Radical

The synthesis of nickel(I) radical is a one pot reaction. Generally, nickel(I) and Iron(I) complexes are obtained by reduction of corresponding halides.[4,5] We have employed $KSi(SiMe_3)_3$ as a reducing agent. Power and coworkers also reported the same by using $KSi(SiMe_3)_3$ for the formation of Bi-Bi bond from bismuth halides.[11] The reaction of nickel(II) chloride [2,6-*i*Pr_2-C_6H_3NC(Me)CHC(Me)NH(CH_2py)]Ni(II)Cl] with $KSi(SiMe_3)_3$ led to a T-shaped nickel(I) radical species **2.1** in high yield (Scheme 2.3). The red crystals of **2.1** were obtained from toluene/hexane (1:8) solution at – 36 °C within a week suitable for single crystal analysis. The crystals of **2.1** are stable in the glove-box for almost 30 days without any decomposition whereas some of the Ni(I) radicals are unstable even in the glove-box.[12a]

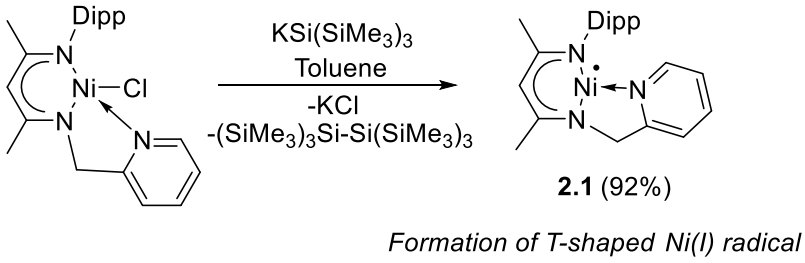

Formation of T-shaped Ni(I) radical

Scheme 2.3. Synthesis of T-shaped nickel(I) radical complex

The molecular structure of complex **2.1** is shown in Figure 2.1, which shows that the central nickel atom has adopted the T-shaped geometry with the L–Ni–L angles of 174.21°, 85.96°, and 98.57°, similar to those reported by Lee and coworkers.[4] Paramagnetic species **2.1** is NMR inactive which negates the anticipation of dimer formation in solution state as well. The molecular ion peak was detected with the highest relative intensity at m/z 406.1783. The cyclic voltammogram of compound **2.1** shows a reversible redox behavior with redox peak at –1.35/1.32 V ($Ni^{I}\rightarrow Ni^{0}/Ni^{0}\rightarrow Ni^{I}$) and Quasi reversible peak at -1.94/1.86 V ($Ni^{II}\rightarrow Ni^{I}/Ni^{I}\rightarrow Ni^{II}$) vs Fc/Fc+.[13]

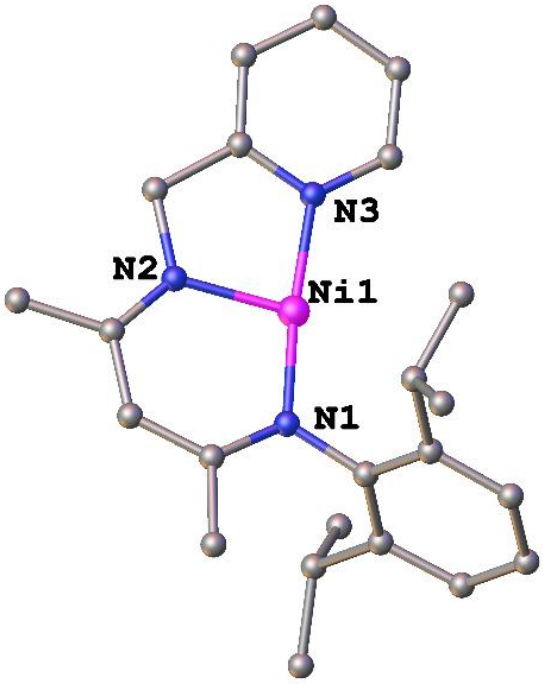

Figure 2.1. The molecular structure of **2.1** with anisotropic displacement parameters depicted at the 50% probability level. Hydrogen atoms are not shown for clarity. Selected bond lengths (Å) and bond angles (°): Ni1–N1 1.866(3), Ni1–N2 1.902(3), Ni1–N3 1.910(3); N1–Ni1–N2 98.94(13), N1–Ni1–N3 173.41(13), N2–Ni1–N3 85.91(14).

2.2.2 Trapping of T-shaped Ni(I) Radical Species

To confirm the presence of radical on nickel, we have treated **2.1** with TEMPO (2,2,6,6-tetramethylpiperidine-1-oxyl radical), which led to the formation of diamagnetic nickel-oxaziridine derivative, **2.2** with N–Ni–O three-membered ring in η^2-coordination mode (Scheme 2.4). The formation of the three-membered ring occurs with concomitant cleavage of the $Ni–N_{pyridyl}$ bond. Yellow colored single crystals of **2.2** suitable for X-ray diffraction studies were grown from the saturated solution of hexane/toluene at -30 °C in a freezer.

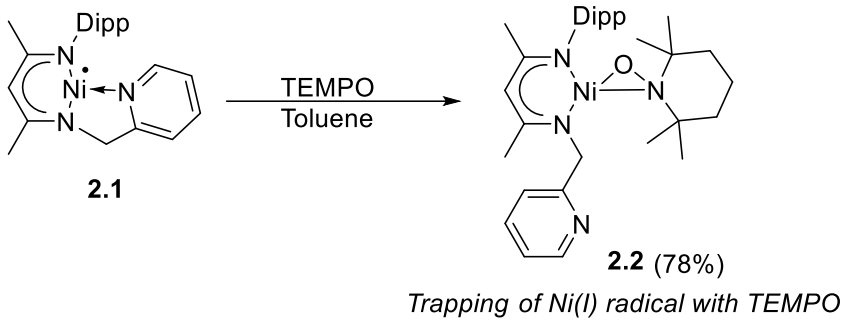

Scheme 2.4. Trapping of T-shaped nickel(I) radical with TEMPO

The molecular structure of **2.2** is shown in Figure 2.2 along with the important bond lengths and angles in the legends. The $Ni–N_{TEMPO}$ and Ni–O bond distances are 1.960(5) and 1.830(4) Å, respectively, which are comparable to the related Ni-TEMPO complexes.[12] The ^{1}H and ^{13}C NMR spectra in $CDCl_3$ show the expected number of resonances and multiplicity for a diamagnetic complex presenting the TEMPO-bonded nickel center(See FigureA2).

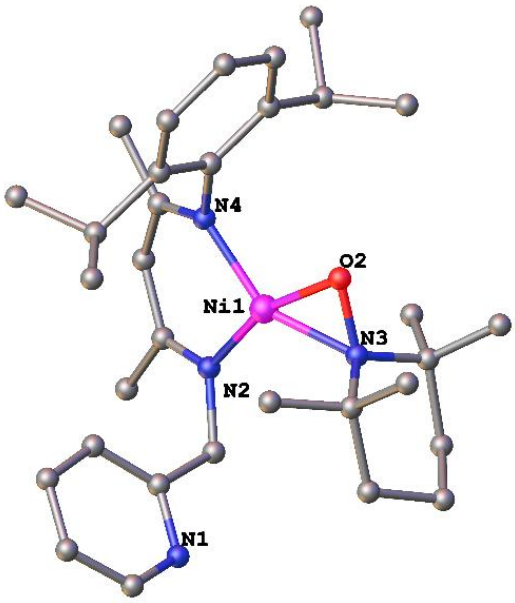

Figure 2.2. The molecular structure of **2.2** with anisotropic displacement parameters depicted at the 50% probability level. Hydrogen atoms are not shown for clarity. Selected bond lengths (Å) and bond angles (°): Ni1–O1 1.830(4), Ni1–N4 1.878(5), Ni1–N2 1.878(5), Ni1–N3 1.960(5), O1–N3 1.403(6); O1–Ni1–N4 102.73(19), O1–Ni1–N2 160.9(2), N4–Ni1–N2 95.8(2), O1–Ni1–N3 43.30(18), N4–Ni1–N3 145.9(2), N2–Ni1–N3 117.8(2), N3–O1–Ni1 73.3(3).

Further, to confirm the radical nature of **2.1**, we have also performed the EPR experiment in the solid state at 298 K. The Ni centre in the complex features a T-shaped geometry with s=1/2. Interestingly, X-band EPR spectra showed a rhombic/quasi-rhombic signal[7b] with g_x=2.205, g_y=2.142, and g_z=2.115, which is in well agreement with such Ni(I) (s=1/2 spin state) T-shaped complexes.[4] The simulated spectrum merged with the experimental spectrum is given below in Figure 2.3.

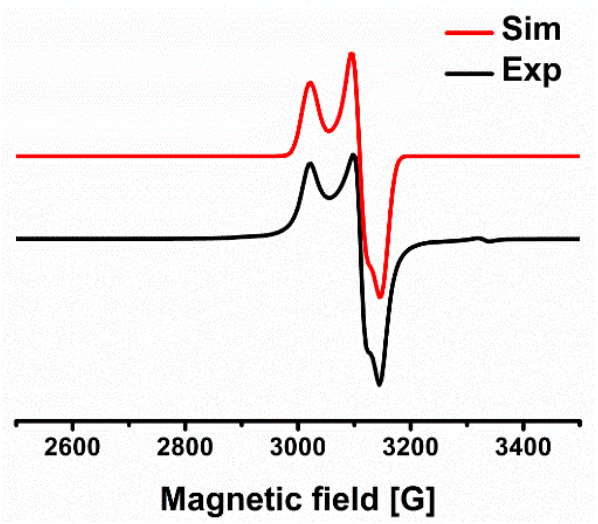

Figure 2.3. Experimental (black line) and simulated (red line) X-band EPR spectrum of **2.1** in toluene at 100 K. [Simulation parameters: g_x = 2.205, g_y = 2.142, g_z = 2.115, w_x = 28, w_y = 22, w_z = 24].

SQUID-VSM measurement was performed to understand the magnetic behaviour of compound **2.1** which showed a weak antiferromagnetic interaction. The calculated effective magnetic moment using the equation, $2.828\sqrt{\chi_M T} = \mu_{eff}$ gives value nearly 6 BM (Bohr Magneton), which further confirms the affluence of a single electron on the nickel center.

2.2.3 Reactivity of Nickel(I) with Dichalcogenides

2.2.3.1 Reaction With Disulfide

The addition of 0.5 equivalents of diphenyl disulfide (Ph_2S_2) to a toluene solution of **2.1** resulted in the cleavage of the S–S bond homolytically and led to the construction of the Ni–S bond in **2.3**. The addition of one equivalent of Ph_2S_2 led to the formation of **2.3** along with C–C coupled product (**2.5**) formed via coupling of the imine carbons

(Scheme 2.5). A precedent for such C–C coupling has been reported by Wolczanski and coworkers, who described C–C bond formation via coupling of the imine carbons.[9c] The solid state structures of **2.3** and **2.5** are shown in Figure 2.4. The molecular structure of **2.3** shows a diamagnetic Ni center with a Ni–S bond length of 2.2330(3) Å, whereas the dimeric product **2.5** shows the Ni–S and C–C bond lengths 2.207(18) and 1.572(13) Å, respectively.

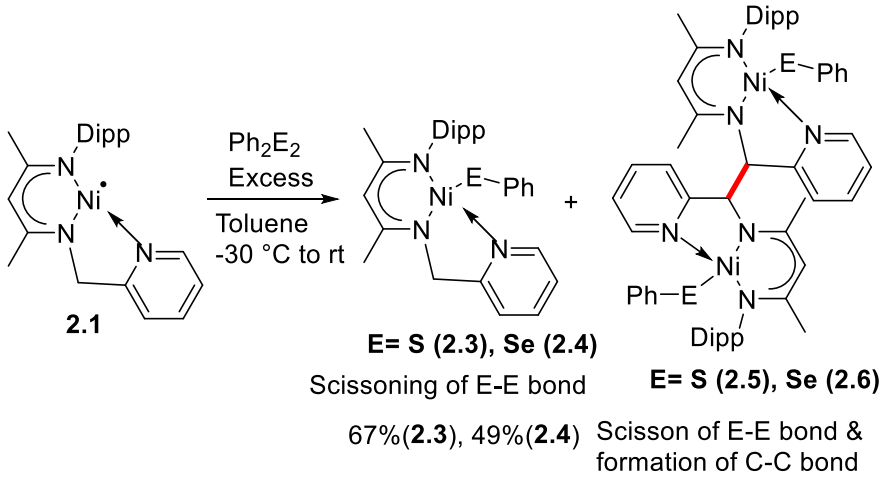

Scheme 2.5. Activation of dichalcogenides.

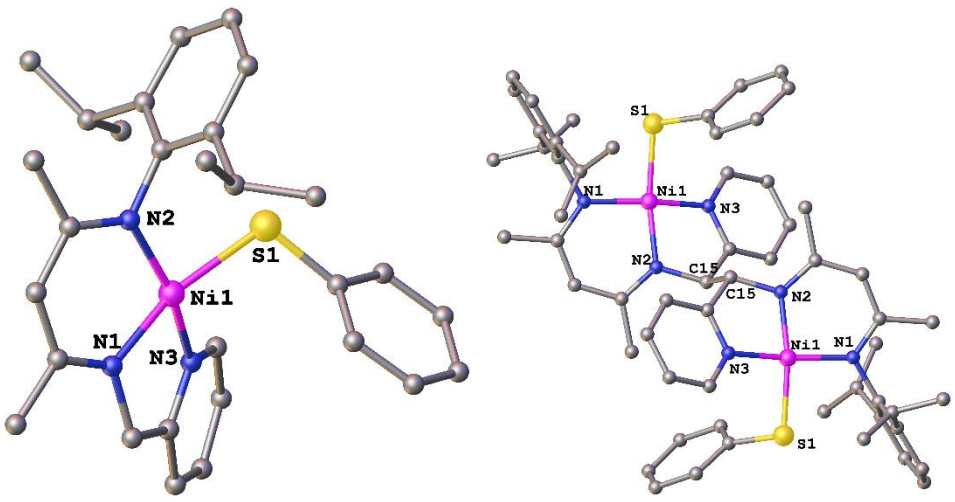

Figure 2.4. The molecular structure of **2.3** (left) and **2.5** (right) with anisotropic displacement parameters depicted at the 50% probability level. Hydrogen atoms are not shown for clarity. Selected bond lengths (Å) and bond angles (°) for **2.3**: Ni1–N1 1.8789(9), Ni1–N2 1.8923(9), Ni1–N3 1.9063(10), Ni1–S1 2.2330(3); N1–Ni1–N2 94.39(4), N1–Ni1–N3 83.81(4), N2–Ni1–N3 163.60(4), N1–Ni1–S1 164.36(3), N2–Ni1–S1 93.04(3), N3–Ni1–S1 92.83(3), C1–S1–Ni1 106.76(4). Selected bond lengths (Å) and bond angles (°) for **2.5:** Ni1–N1 1.910(6), Ni1–N2 1.876(5), Ni1–N3 1.922(5), Ni1–S1 2.207(18), C6–C6 1.572(13); N2–Ni1–N1 94.6(18), N2–Ni1–N3 82.7(2), N1–Ni1–N3 165.2(2), N2–Ni1–S1 167.6(16), N1–Ni1–S1 92.11(14), N3–Ni1–S1 93.3(17).

2.2.3.2 Reaction With Diselenide

Likewise, the reaction with Ph_2Se_2 led to the formation of monomer **2.4** along with the formation of the C–C coupled dimeric product **2.6** at the CH_2 position of the picolyl group (Scheme 2.5). Both **2.4** and **2.6** were crystalized in the same reaction flask at -30 °C (Figure 2.5). The Ni–Se bond length of compounds **2.4** and **2.6** are 2.3446(4) and 2.342(14) Å respectively. The C–C bond length of C–C coupled product **2.6** is 1.580(11) Å. The Ni–S and Ni–Se bond lengths are in good agreement with the previously reported Ni–E (E= S, Se) bonds by Roesky and coworkers i.e. 2.2030(12) and 2.3582(4) Å respectively.[14]

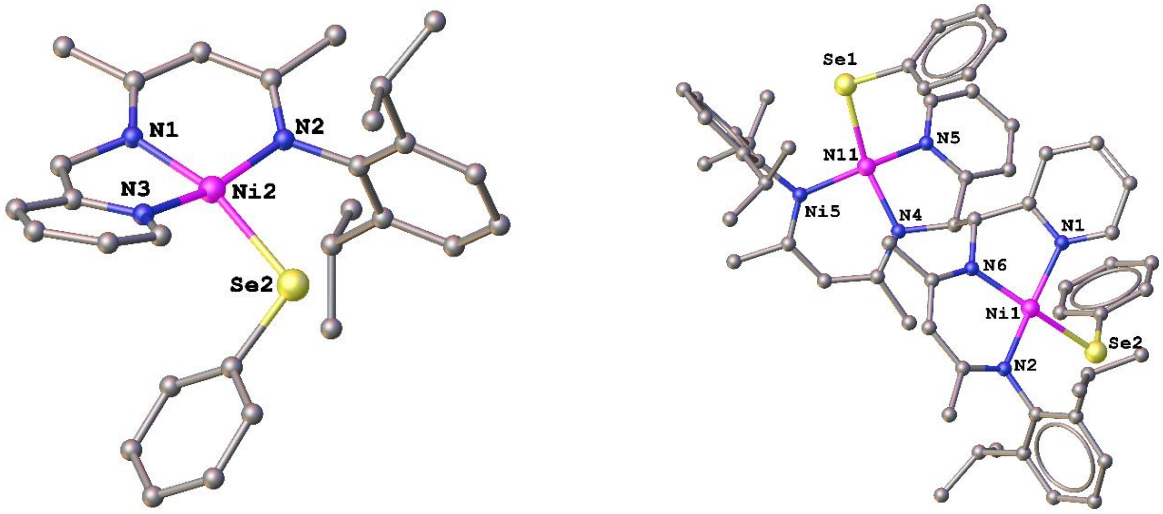

Figure 2.5 The molecular structure of **2.4** (left) and **2.6** (right) with anisotropic displacement parameters depicted at the 50% probability level. Hydrogen atoms are not shown for clarity. Selected bond lengths (Å) and bond angles (°) for **2.4**: Ni1–N1 1.8758(18), Ni1–N2 1.8910(18), Ni1–N3 1.9043(19), Se1–C1 1.916(2), Se1–Ni1 2.3446(4); C1–Se1–Ni1 105.72(7), N1–Ni1–N2 94.47(8), N1–Ni1–N3 84.00(8), N2–Ni1–N3 162.99(8), N1–Ni1–Se1 162.13(6), N2–Ni1–Se1 93.11(6), N3–Ni1–Se1 93.32(6). Selected bond lengths (Å) and bond angles (°) for **2.6**: Ni1–N1 1.932(6), Ni1–N2 1.921(6), Ni1–N3 1.886(6), Ni1–Se1 2.342(14), C4–C34 1.580(11), Ni2–N4 1.893(6), Ni2–N5 1.895(7), Ni2–N6 1.915(7), Se2–Ni2 2.3570(15); N3–Ni1–N1 83.2(3), N3–Ni1–N2 95.3(3), N2–Ni1–N1 162.5(3), N1–Ni1–Se1 92.9(2), N2–Ni1–Se1 93.6(19), N4–Ni2–N5 83.5(3), N4–Ni2–N6 94.3(3), N5–Ni2–N6 162.5(3), N4–Ni2–Se2 160.0(2), N5–Ni2–Se2 93.0(2), N6–Ni2–Se2 94.7(2).

2.2.4 Activation of Hydrogen

The bubbling hydrogen gas to the toluene solution of compound **2.1** resulted in an immediate color change from red to orangish yellow. Inspection of the ^{1}H NMR indicates the rupture of

the H-H σ-bond and the formation of monomeric nickel(II) hydride **2.7** (Scheme 2.6). The formation of compound **2.7** was confirmed through a comparison of ^{1}H NMR and unit cell values with previously reported literature.[10]

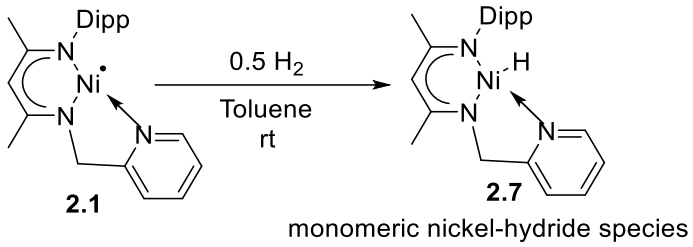

Scheme 2.6. Activation of dihydrogen by a Ni radical.

2.3 Computational Studies

To gain insight into the electronic structure of **2.1**, density functional theory calculations were conducted at the PBE-D3/TZVP level of theory. The spin density plot of **2.1** (Figure 2.6) reveals that the majority of the unpaired electron spin is localized around the vacant coordination site of the nickel center, providing evidence for the observed metalloradical character of the nickel. Analysis of the Kohn-Sham frontier orbitals indicates that the SOMO primarily resides on nickel's $d_{x^2-y^2}$ orbital,[13,15] with significant contributions from the nitrogen atoms, while the LUMO is localized on the pyridine ring (Figure 2.6). Additionally, we have also plotted the spin density, SOMO, and LUMO of **2.1** at the B3LYP-D3/def2-TZVP level of theory and they match the results obtained at the PBE-D3/TZVP level of theory.

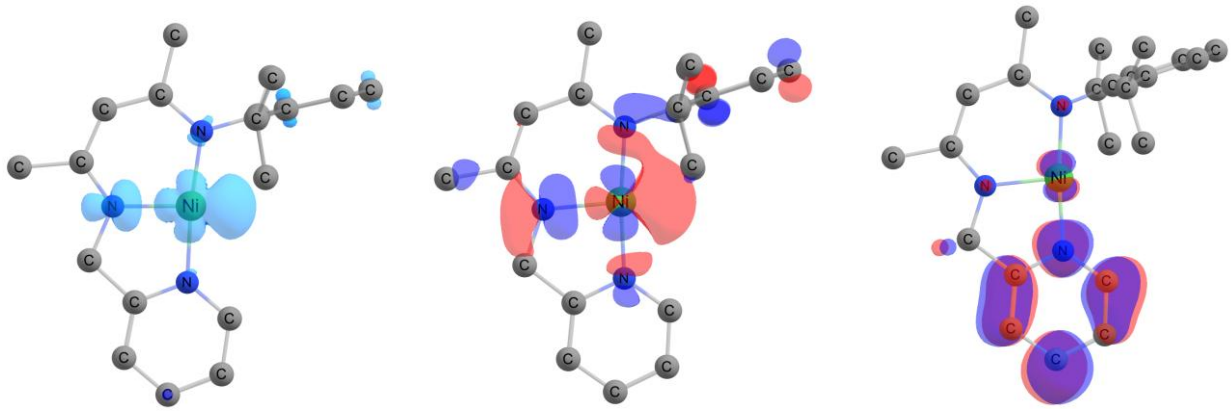

a b c

Figure 2.6 (a) The spin density plot, (b) the SOMO, and (c) the LUMO of **2.1**. The isovalue of the spin density plot is 0.004, while for the SOMO and LUMO, the isovalue is 0.04.

2.4 Conclusion

In conclusion, a T-shaped thermally stable nickel(I) complex (**2.1**) was synthesized by combining a nickel(II) chloride complex [2,6-*i*Pr$_2$-C$_6$H$_3$NC(Me)CHC(Me)NH(CH$_2$py)]Ni(II)Cl] and KSi(SiMe$_3$)$_3$. The presence of the radical center on Ni was verified by the formation of an unusual three-membered nickeloxaziridine complex (**2.2**) upon reaction with TEMPO as well as from the rhombic/quasi-rhombic signal in X-band EPR spectrum. DFT studies confirmed a T-shaped nickel(I) center with a half-filled $d_{x^2-y^2}$ orbital as the SOMO. Homolytic cleavage of σ-bonds of dihydrogen, disulphide and diselenide by **2.1** at ambient conditions was investigated. The activation of dihydrogen by **2.1** produces a monomeric nickel hydride (**2.7**) and underscores the effectiveness of utilizing a metalloradical in dihydrogen activation.

2.5 References

1. a) M. J. Ingleson, H. Fan, M. Pink, J. Tomaszewski and K. G. Caulton, *J. Am. Chem. Soc.*, 2006, **128**, 1804−1805; b) M. J. Ingleson, M. Pink and K. G. Caulton, *J. Am. Chem. Soc.*, 2006, **128**, 4248−4249; c) M. J. Ingleson, M. Pink, H. Fan and K. G. Caulton, *J. Am. Chem. Soc.* 2008, **130**, 4262−4276.

2. a) G. A. Dawson, Q. Lin, M. C. Neary and T. Diao, *J. Am. Chem. Soc.,* 2023, **145,** 20551−20561; b) C. L. Wagner, G. Herrera, Q. Lin, C. T. Hu and T. Diao, *J. Am. Chem. Soc.*, 2021, **143**, 5295−5300; c) A. Bismuto, P. Müller, P. Finkelstein, N. Trapp, G. Jeschke and B. Morandi, *J. Am. Chem. Soc.*, 2021, **143**, 10642−10648.

3. a) S. Alvarez, *Coord. Chem. Rev.*, 1999, **193–195**, 13–41; b) C. C. Cummins, *Prog. Inorg. Chem.*, 1998, **47**, 685–836; c) Structural review: C. L. Drennan, T. I. Doukov and S. W. Ragsdale, *J. Biol. Inorg. Chem.*, 2004, **9**, 511–515; d) Mechanistic review: E. L. Hegg, *Acc. Chem. Res.*, 2004, **37**, 775–783.

4. a) C. Yoo and Y. Lee, *Angew. Chem. Int. Ed.*, 2017, **56**, 9502–9506; *Angew.Chem.*, 2017, **129**, 9630–9634; b) F. Schneck, J. Ahrens, M. Finger, A. C.Stuckl, C. Wurtele, D. Schwarzer and S. Schneider, *Nat. Commun.*, 2018, **9**,1161 (1-8); c) C. Rettenmeier, H. Wadepohl and L. H. Gade, *Chem. Eur. J.*, 2014, **20**, 9657–9665; d) J. C. Ott, H. Wadepohl and L. H. Gade, *Angew. Chem. Int. Ed.*, 2020, **59**, 9448–9452; *Angew. Chem.*, 2020, **132**, 9535–9539.

5. a) J. C. Ott, D. Bürgy, H. Guan and L. H. Gade, *Acc. Chem. Res.*, 2022, **55**, 857−868; b) C.-Y. Lin and P. P. Power, *Chem. Soc. Rev.*, 2017, **46**, 5347–5399.

6. a) N. A. Eckert, A. Dinescu, T. R. Cundari and P. L. Holland, *Inorg. Chem.*, 2005, **44**, 7702–7704; b) C. A. Laskowski, D. J. Bungum, S. M. Baldwin, S. A. Del Ciello, V. M. Iluc and G. L. Hillhouse, *J. Am. Chem. Soc.*, 2013, **135**, 18272−18275; c) R. Beck, M. Shoshani, J. Krasinkiewicz, J. A. Hatnean and S. Johnson, *Dalton Trans.*, 2013, **42**, 1461−1475.

7. S. Pfirrmann, C. Limberg, C. Herwig, R. Stößer and B. A. Ziemer, *Angew. Chem. Int. Ed.*, 2009, **48**, 3357–3361; *Angew. Chem.*, 2009, **121**, 3407−3411; b) P. Zimmermann, A. F. R. Kilpatrick, D. Ar, S. Demeshko, B. Cula, C. Limberg, *Chem. Commun.* 2021, **57**, 875–878.

8. a) S. Yadav, R. Dixit, M. K. Bisai, K. Vanka and S. S. Sen, *Organometallics* 2018, **37**, 4576–4584; b) S. Pahar, V. S. V. S. N. Swamy, T. Das, R. G. Gonnade, K. Vanka and S. S. Sen, *Chem. Commun.*, 2020, **56**, 11871–11874; c) W. D. Morris, P. T. Wolczanski, J. Sutter, K. Meyer, T. R. Cundari and E. B. Lobkovsky, *Inorg. Chem.*, 2014, **53**, 7467−7484; d) X. Xu, Y. Chen, G. Zou and J. Sun, *Dalton Trans.*, 2010, **39**, 3952–3958.

9. S. Pahar, V. Sharma, B. Mahata, C. P. George, H. Sharma, K. Vanka and S. S. Sen, *Inorg. Chem.*, 2022, **61**, 17370–17377.

10. S. Pahar, V. Sharma, S. Tothadi and S. S. Sen, *Dalton Trans.*, 2021, **50**, 16678–16684.

11. a) S. Pelties, D. Herrmann, B. de Bruin, F. Hartl and R. Wolf, *Chem. Commun.*, 2014, **50**, 7014–7016; b) U. Chakraborty, F. Urban, B. Mühldorf, C. Rebreyend, B. de Bruin, N. van Velzen, S. Harder and R. Wolf, *Organometallics* 2016, **35**, 1624−1631; c) D. Isrow and B. Captain, *Inorg. Chem.*, 2011, **50**, 5864–5866.

12. J. B. Diccianni, J. Katigbak, C. Hu and T. Diao, *J. Am. Chem. Soc.*, 2019, **141**, 1788–1796.

13. M. J. Ingleson, B. C. Fullmer, D. T. Buschhorn, H. Fan, M. Pink, J. C. Huffman and K. G. Caulton, *Inorg. Chem.*, 2008, **47**, 407–409.

14. C. Zovko, F. Krätschmer, S. Schmidt, T. P. Seifert, M. T. Gamer and P. W. Roesky, *ChemPlusChem.*, 2022, **87**, e2022002.

15. C. Yoo, S. Oh, J. Kima and Y. Lee, *Chem. Sci.*, 2014, **5**, 3853–3858.

16. a) W. H. Harman and J. C. Peters, *J. Am. Chem. Soc.*, 2012, **134**, 5080–5082; b) Y. Wang, A. Kostenko, S. Yao and M. Driess, *J. Am. Chem. Soc.*, 2017, **139**, 13499–13506; c) Y. Cai, S. Jiang, T. Rajeshkumar, L. Maron and X. Xu, *J. Am. Chem. Soc.*, 2022, **144**, 16647–16655.

17. a) G. Zeng and S. Sakaki, *Inorg. Chem.*, 2013, **52**, 2844−2853; b) P. Ríos, J. Borge, F. Fernández de Córdova, G. Sciortino, A. Lledós and A. Rodríguez, *Chem. Sci.*, 2021, **12**, 2540-2548; c) K. Boonpalit, C. Uthayopas and P. Surawatanawong, *Organometallics* 2022, **41**, 259–269.

Chapter-3

Metal-Ligand Cooperation in Magnesium-Mediated Water Activation

Abstract: This chapter details the synthesis and reactivity of heteroleptic monomeric magnesium complexes. Earlier attempts to synthesize heteroleptic magnesium complexes using a tridentate nacnac ligand featuring a pendant picolyl group, via reactions with KHMDS and MgI_2, yielded a homoleptic, hexa-coordinated magnesium species. In contrast, the reaction of the same ligand with CH_3MgBr successfully afforded the heteroleptic magnesium bromide complex (**3.1**). Furthermore, treatment with Bu_2Mg produced a unique dearomatized magnesium species (**3.2**). Theoretical investigations revealed a non-bonding orbital on magnesium in **3.2**, rendering it susceptible to nucleophilic attack. Supporting this prediction, **3.2** was reacted with H_2O and D_2O to cleave the O−H and O–D bond via magnesium-ligand cooperative mechanisms, forming magnesium hydroxide species (**3.3** and **3.4**). Efforts to generate a magnesium hydride complex from **3.1** resulted in the de-aromatization of the pyridine ring, leading to the formation of a magnesium hydroxide species (**3.5**), likely due to trace water contamination. Additionally, the reaction of **3.1** with a lithiated diazo compound, $LiC(SiMe_3)N_2$, yielded a dimeric magnesium complex (**3.6**) featuring a Mg_2N_2 four-membered ring. These results highlight the versatility of the nacnac ligand system in stabilizing diverse magnesium coordination environments and promoting cooperative reactivity.

3.1 Introduction

Transition metal catalysts have profoundly expanded the reactivity landscape of organic compounds by enabling a wide array of reaction mechanisms, including oxidative addition, reductive elimination, and β-hydride elimination.[1] In these transformations the ligand remains unchanged during the course of reaction. In contrast many enzymes, bond activation proceeds through a distinct mechanism involving a precisely tuned ligand environment that synergistically interacts with the metal centre. This cooperation facilitates bond activation, resulting in chemical modifications to both the ligand and the metal centre (Scheme 3.1). For instance, in [FeFe], [NiFe], and [Fe]-only hydrogenases, H_2 activation occurs via a cooperative mechanism between the ligand and the metal, leading to the heterolytic cleavage of H_2 across the metal–ligand bond.[2-3]

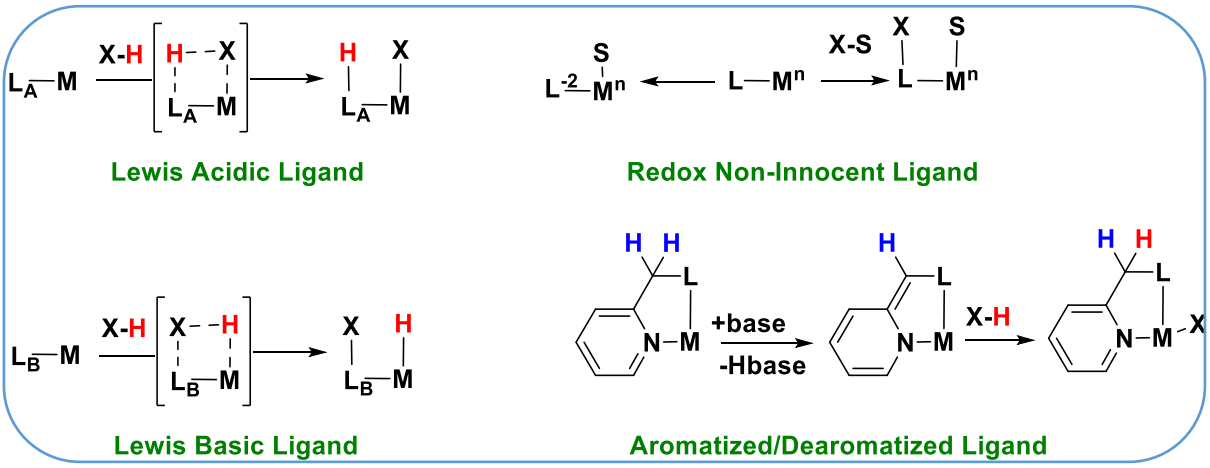

Scheme 3.1. Types of the metal-ligand cooperation.

The identification of these systems has spurred innovative strategies in ligand design and broadened the range of catalytic processes, including the development of several recent reactions with environmental and energy-related benefits.[4] Metal-ligand cooperation (MLC) being a versatile approach for activating chemical bonds through the aromatization/dearomatization of pincer-type complexes.[4-7] This method is advantageous because the metal center's oxidation state remains unchanged during the bond activation. Traditionally, this MLC process has been dominated by transition metals, and the application of main-group metals in this context is still nascent[7-14] but there has been progress, such as N−H and H−H bond activation, hydrogenation of alkenes, and semi-hydrogenation of alkynes by main-group species as well as zinc through the MLC process.[12-14]

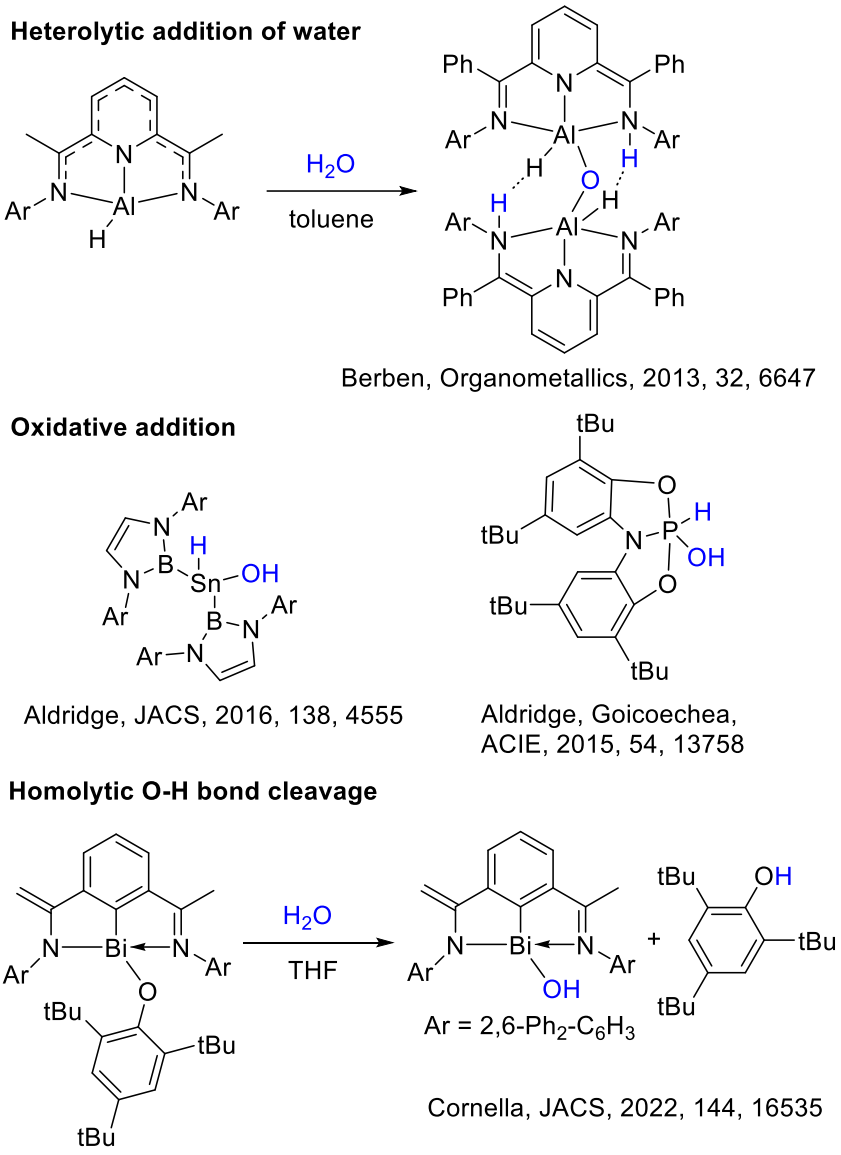

Scheme 3.2. Selected examples of splitting of O-H bond of water by *p*-block elements.

The recent results from the groups of Milstein with magnesium is quite encouraging as magnesium is the 7th most abundant element in the Earth's crust. So, the aim is to design similar magnesium complexes using different ligand systems and extend the application to more challenging reactions using the MLC activation process such as splitting of O-H bonds of water. Current methodologies for water activation involving main group elements are exceedingly uncommon (Scheme 3.2).[15-22] Notable example of O-H bond addition across a metal-ligand bond include the work by Berben and colleagues with aluminum.[22]

In this chapter, we report the synthesis of two new magnesium complexes: a heteroleptic magnesium bromide complex (**3.1**) and a second complex featuring a dearomatized picolyl

moiety (**3.2**). The dearomatized magnesium complex (**3.2**) is utilized for the heterolytic cleavage of O−H/D bonds through a magnesium-ligand cooperative mechanism. Efforts were also made to stabilize a magnesium hydride complex, which resulted in the de-aromatization of the pyridine ring and the subsequent formation of a magnesium hydroxide species (**3.5**), potentially attributable to trace amounts of water. The reactivity of the heterolaptic magnesium bromide (**3.1**) towards diazo compound is also explored.

3.2 Results and Discussions

3.2.1 Synthesis of Magnesium Bromide Complex

The reaction of ligand with methyl magnesium bromide in THF smoothly yielded the heteroleptic magnesium complex **3.1** (Scheme 3.3). The crystals of **3.1** suitable for SCXRD obtained from the saturated THF solution at – 4 °C after two days. The molecular structure of **3.1** is shown in Figure 3.1. The length of the Mg1−N1 bond is 2.234(13) Å, which is longer than those of other two Mg−N bonds (2.147(12) and 2.106(12) Å), confirming the coordination bond with pyridine nitrogen. The ^{1}H NMR spectrum of **3.1** displays a resonance at 9.73 ppm, attributed to the *ortho*-hydrogen of the pyridine ring, and another at 4.93 ppm corresponding to the CH_2 group of the picolyl moiety (See Figure A17). High-resolution mass spectrometry (HRMS) confirmed the molecular ion peak at m/z 452.1495 (See Figure A19), consistent with the calculated mass for the complex.

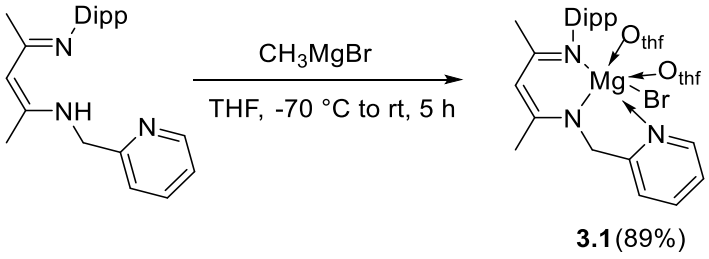

Scheme 3.3. Synthesis of heteroleptic magnesium complex **3.1**.

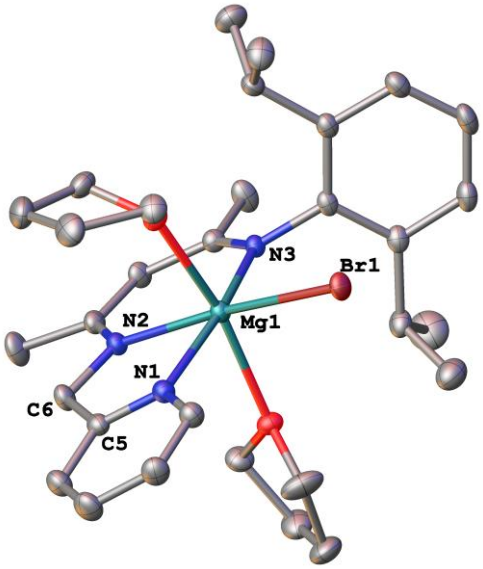

Figure 3.1. The molecular structure of **3.1** with anisotropic displacement parameters depicted at the 50% probability level. Hydrogen atoms are not shown for clarity. Selected bond lengths (Å) and bond angles (°): Br1–Mg1 2.5712(5), Mg1–N3 2.1470(12), Mg1–N2 2.1061(12), Mg1–N1 2.2340(13), C5–C6 1.504(2); N3–Mg1–N2 89.48(5), N1–Mg1–N3 166.76(5), N1–Mg1–N2 77.66(5).

3.2.2 Synthesis of Dearomatized Magnesium Complex

The analogous reaction with nBu$_2$Mg resulted in immediate color change from yellow to dark magenta and the formation of a dearomatized magnesium compound (**3.2**) via deprotonation from the picolyl backbone (Scheme 3.4). The successful dearomatization can be confirmed by the appearance of new peaks in the ^{1}H NMR spectrum, specifically at 6.16, 6.41, and 6.82 ppm, corresponding to the dearomatized pyridine moiety, and at 5.42 ppm, attributed to the methine proton of the picolyl arm (See Figure A20).

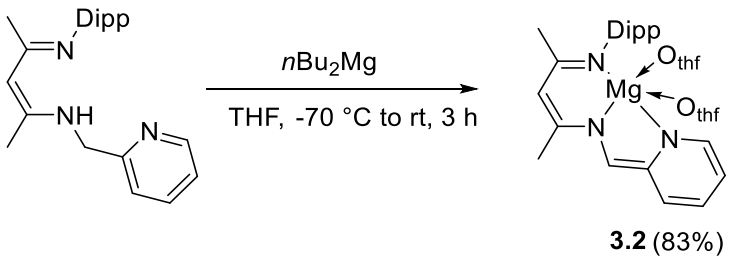

Scheme 3.4. Synthesis of dearomatized magnesium complex **3.2**.

The crystals suitable for SC-XRD of **3.2** was obtained in THF at -36 °C within a week. The molecular structure of **3.2** is shown in Figure 3.2. The magnesium atom is five-coordinate and adopts a distorted TBP geometry. As expected, the length of the Mg1−N2 bond (2.107(18) Å) is considerably shorter than that of the Mg1−N1 bond (2.234(13) Å) in **3.1** suggesting the covalent nature of the Mg−N bond along with Mg1−N1 = 2.08(18) Å and Mg1−N3= 2.09(18) Å. The bond length between C5−C6 = 1.376(3) Å in **3.2** is shorter than that of **3.1** (C5−C6 = 1.504(2) Å), which also supports the deprotonation taking place from the picolyl moiety resulting in the double bond formation, and dearomatized structure. High-resolution mass spectrometry (HRMS) confirmed the molecular ion peak at m/z 372.2401, consistent with the calculated mass for the complex (See Figure A22).

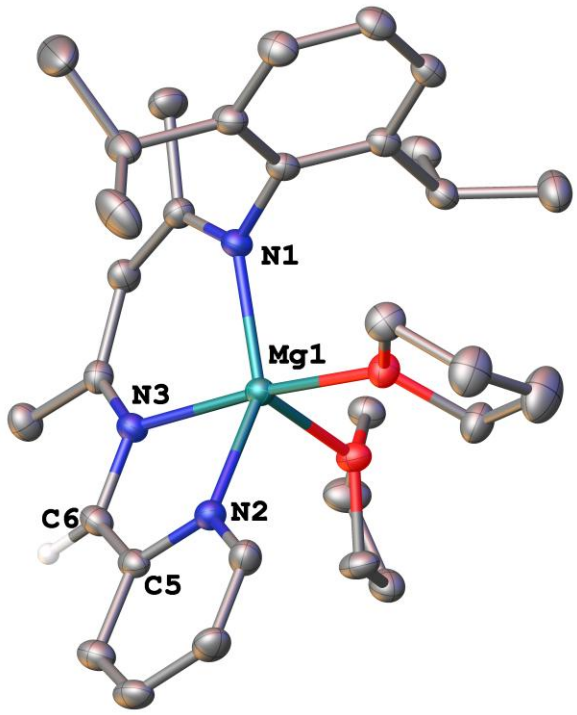

Figure 3.2. The molecular structure of **3.2** with anisotropic displacement parameters depicted at the 50% probability level. Hydrogen atoms are not shown for clarity (except on the picolyl arm). Selected bond lengths (Å) and bond angles (°): Mg1–N1 2.0811(18), Mg1–N2 2.1073(18), Mg1–N3 2.0914(18), C5–C6 1.374(3); N1–Mg1–N3 89.07(7), N1–Mg1–N2 146.11(7), N2–Mg1–N3 80.00(7).

3.2.3 Theoretical Illumination of Dearomatized Magnesium

Frontier orbital analysis revealed that the HOMO and LUMO of **3.2** are delocalized on the backbone *β*-diketiminate methyl pyridinato ligand (excluding the Dipp moiety), whereas the MO corresponding to the vacant non-bonding (LP*) orbital of Mg, the site for the attack of incoming nucleophiles, was obtained at LUMO+1 (Figure 3.3). The MEP reveals a significant positive potential (+80.0 kcal/mol) localized at the magnesium center, which lies within the plane of the Mg-bound *β* -diketiminate methyl pyridinato ligand. Notably, two additional regions of positive potential are observed above and below this plane, with values of +34.4 kcal/mol and +33.3 kcal/mol, respectively.

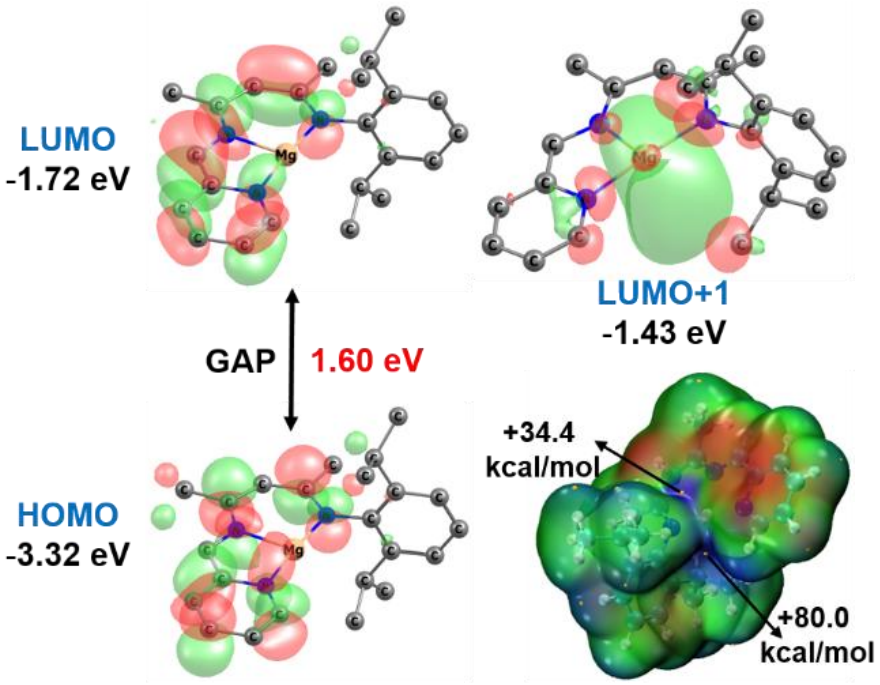

Figure 3.3. Frontier orbitals of compound **3.2** along with molecular electrostatic potential (MEP) plot (RGB color scale, isovalue = 0.001 au). In MEP blue highlights the positive/electron deficient region and red shows electron rich region.

3.2.4 MLC Mediated O-H Bond Splitting of Water

With the dearomatized magnesium compound (**3.2**) in hand, we have performed the reaction of **3.2** with H_2O at -70 °C in THF (Scheme 3.5), resulted in immediate color change from magenta to reddish orange. The orange crystals of **3.3** were obtained from

the THF solution at -36 °C. The molecular structure of **3.3** is shown in Figure 3.4. To confirm the activation of water by **3.2**, the same reaction was performed using D_2O in THF (Scheme 3.5) and ^2H NMR was recorded. The ^2H NMR spectrum of **3.4** shows peaks at 4.61 ppm and 11.21 ppm corresponding to CD (methylene sidearm) and OD respectively for **3.4** (See Figure A25).

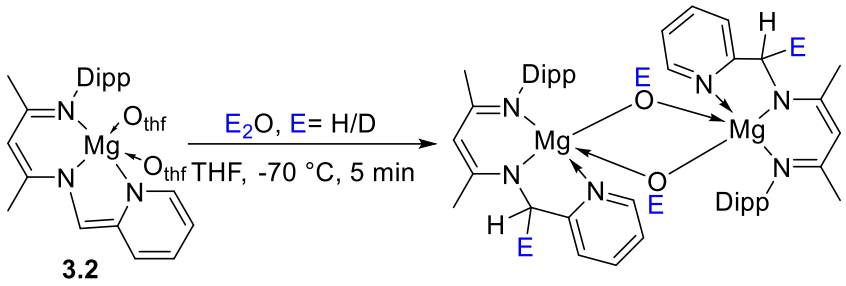

Scheme 3.5. Splitting of the O-H and O-D bond of water and D_2O by the dearomatized magnesium compound (**3.2**).

While well-defined magnesium hydroxide compounds are known, thanks to the works of Parkin, Bochmann, Roesky, and others, they were prepared by either serendipitously or hydrolysis of Mg-amide bond.[23-25] No magnesium hydroxide was prepared via elegant MLC so far. The single-crystal X-ray diffraction structure of **3.3** is shown in Figure 3.4, which reveals a centro-symmetric dimer. The two nitrogen−magnesium bonds are similar, Mg1–N1 2.128(2) Å, Mg1–N3 2.090(2) Å, while the Mg1–N2 is considerably longer of 2.192(2) Å, reflecting the conversion from the covalent bond to dative bond. Similarly, the C−C bond length at the backbone increases to 1.503(3) Å, confirming the formation of a single bond after protonation from water.

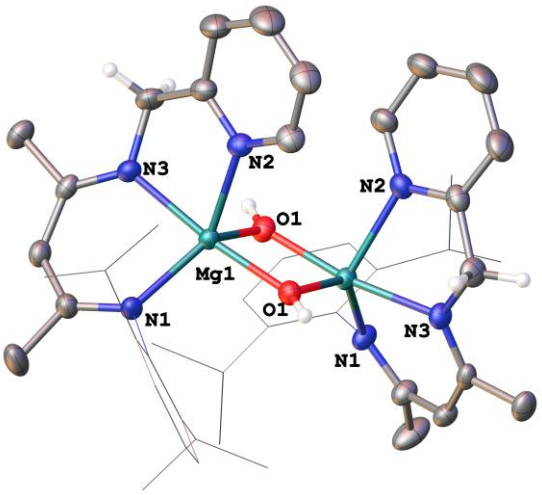

Figure 3.4. The molecular structure of **3.3** with anisotropic displacement parameters depicted at the 50% probability level. Hydrogen atoms are not shown for clarity. Selected bond lengths (Å) and bond angles (°): Mg1–N1 2.128(2), Mg1–N2 2.142(2), Mg1–N3 2.090(2), Mg1–O1 1.9813(17), C12–C13 1.503(3); N1–Mg1–N2 126.22(8), N1–Mg1–N3 85.52(8), N2–Mg1–N3 76.30(8), O1–Mg1–N1 98.48(8), O1–Mg1–N2 95.06(8), O1–Mg1–N3 171.19(18).

3.2.5 Theoretical Illumination for Mechanistic Investigation

DFT calculations revealed that the binding of water molecule at the Mg centre (**3.2**) is thermodynamically favourable by 7.6 kcal/mol (ΔG). The cleavage of O–H bond of the water molecule was found to be readily feasible with a requirement of only +5.8 kcal/mol kinetic barrier via metal-ligand cooperation (Scheme 3.6). The activation of O–H bond leads to a water activated product (ΔG = -17.1 kcal/mol), which upon dimerization leads to a highly exergonic compound **3.3** (ΔG = -44.6 kcal/mol) (Scheme 3.6).

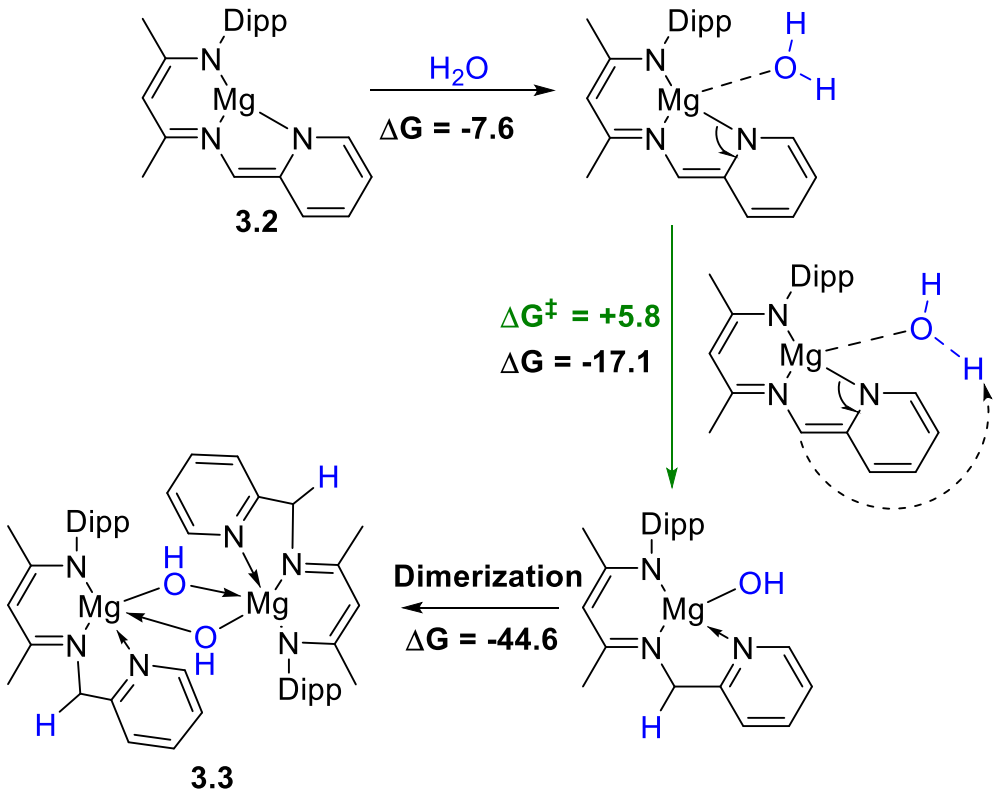

Scheme 3.6. Pathway for the activation of water molecule leading to the formation of **3.3**, computed at PBE-D3/def2TZVP level of theory.

3.2.6 Attempt for Magnesium Hydride

Our attempts to make magnesium species from **3.1** remained unsuccessful. The reaction of **3.1** with potassium tri-sec-butylborohydride (K-Selectride) led to the reduction of the pyridine ring and formation of **3.5**. We assume the magnesium hydride was formed at the first step, which subsequently reduces the pyridine ring (Scheme 3.7b). The adventitious amount of water present in the reaction mixture reacts with the magnesium center and afforded a four-membered Mg_2NO ring (**3.5**) (Scheme 3.7a). Though we were able to obtain few crystals of **3.5**, it was always obtained as yellow oily deposit containing significant amounts of impurities which does not permit for a full spectroscopic characterisation. The molecular structure of **3.5** is shown in Figure 3.5 which shows a four membered ring and a dearomatized pyridine ring. The nitrogen-magnesium bond distances, Mg1–N6 2.230(15) Å and Mg2–N6 2.1982(15) Å, exhibit a notable difference. This suggests that the Mg1–N6 interaction is predominantly coordinate in nature, whereas the Mg2–N6 bond displays characteristics of a covalent bond.

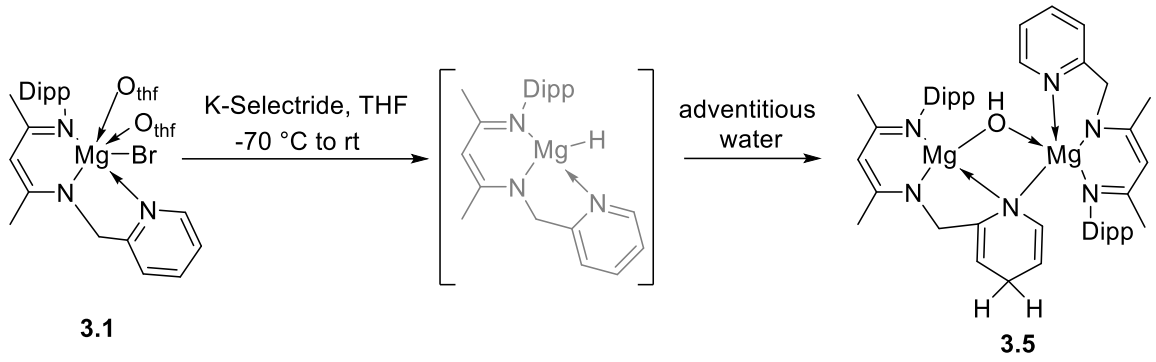

3.1 3.5

Scheme 3.7a Attempt to synthesize magnesium hydride from **3.1** led to donor-acceptor stabilized monomeric magnesium hydroxide (**3.5**).

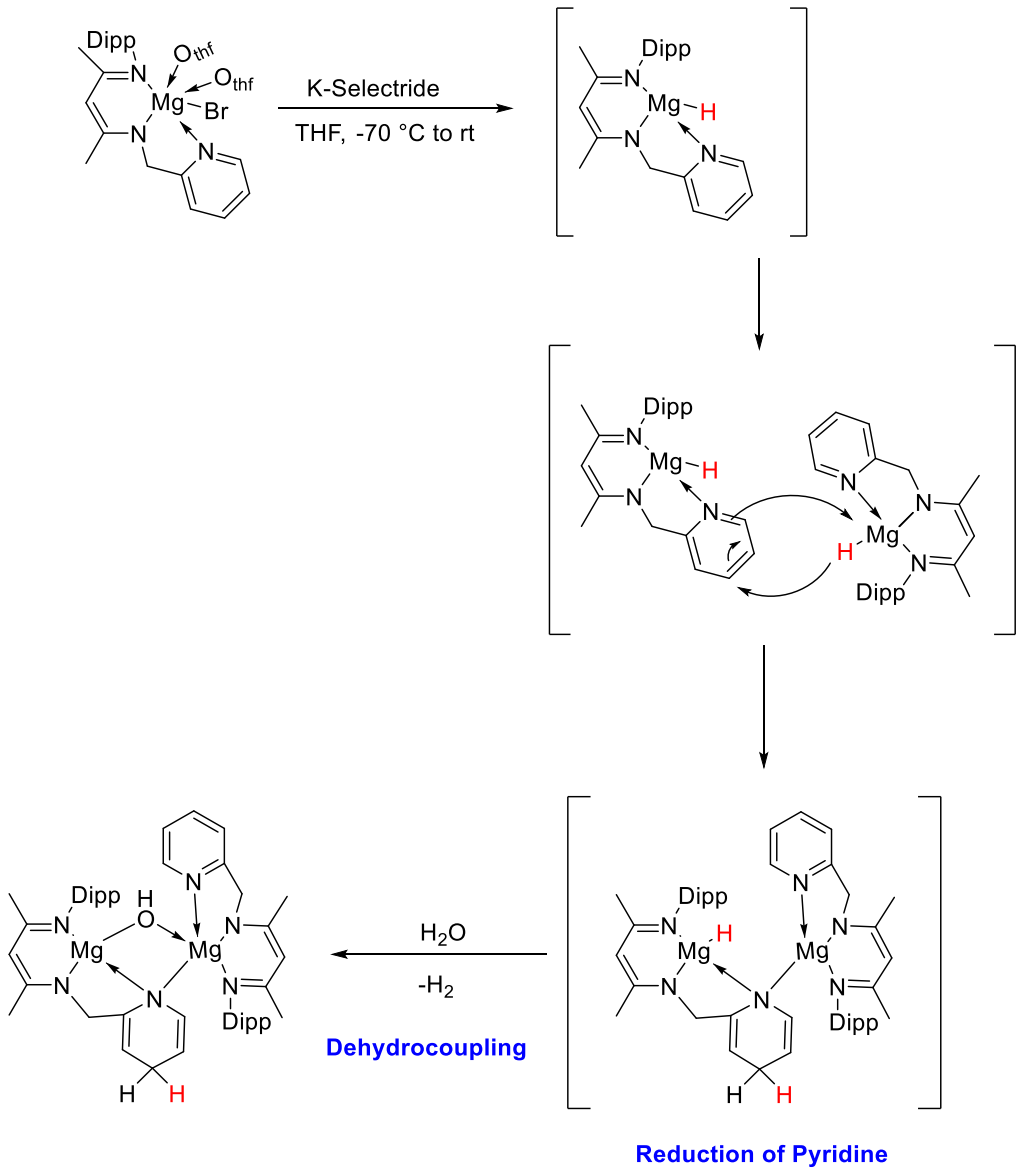

Scheme 3.7b Tentative pathway for the synthesis of donor-acceptor stabilized monomeric magnesium hydroxide (**3.5**).

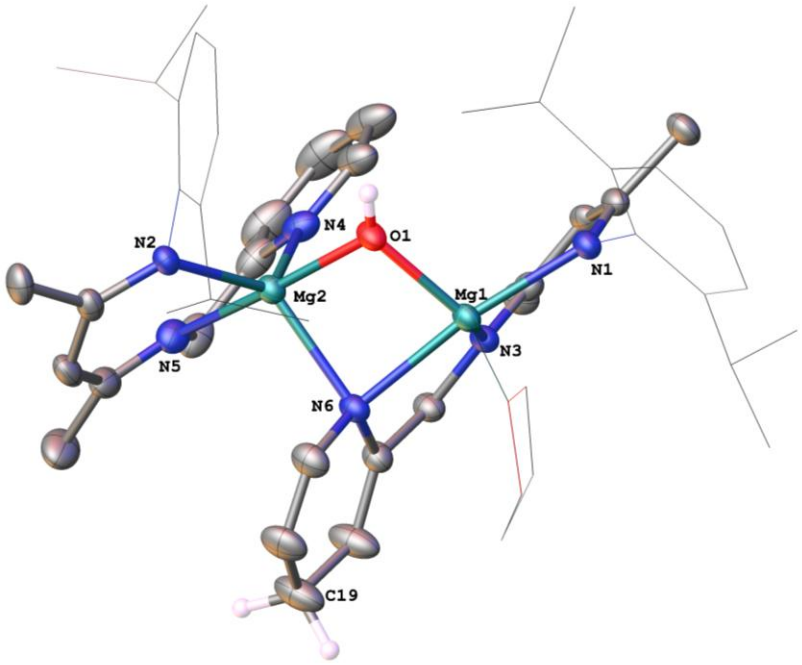

Figure 3.5 The molecular structure of **3.5** with anisotropic displacement parameters depicted at the 50% probability level. Hydrogen atoms (except on the pyridine ring) are not shown for clarity. Selected bond lengths (Å) and bond angles (°): Mg1–N1 2.128(15), Mg1–N3 2.079(15), Mg1–N6 2.230(15), Mg1–O1 1.951(14), Mg2–O1 1.972(14), Mg2–N4 2.182(16), Mg2–N5 2.082(16), Mg2–N2 2.119(15), Mg2–N6 2.197(16); N1–Mg1–N6 165.38(6), N6–Mg1–N3 78.63(6), Mg1–O1–Mg2 39.51(4), Mg1–N6–Mg2 46.27(4), O1–Mg2–N6 83.15(6).

3.2.7 Reaction of Magnesium Bromide Complex with Diazo Compound

The reaction of **3.1** with lithiated trimethylsilyldiazomethane $LiC(SiMe_3)N_2$, led to the formation of a dimeric magnesium **3.6** (Scheme 3.8). The molecular structure of **3.6** shown in Figure 3.6. The solid state structure shows a bridged dimeric magnesium compound having a four membered ring Mg_2N_2. The structural analysis reveals a significant disparity in the nitrogen-magnesium bond lengths, with Mg1–N3 2.195(4) Å and Mg1–N4 2.093(3) Å. This variation indicates a predominantly covalent character for the bridged Mg1–N4 bond. Additionally, the N5–C24 bond length of 1.117(5) Å indicates the formation of C≡N triple bond and is in good agreement with the C≡N bond lengths reported by Jones and co-workers

in {[HC(C(Me)N-2,6-*i*Pr$_2$C$_6$H$_3$)$_2$]Mg[μ-CN)]}$_3$,[26] suggesting the transformation of the diazo group into a cyanide functional group. The NMR and mass spectrometry data for compound 3.6 could not be obtained due to its low solubility and limited stability. However, the IR spectrum recorded in ATR mode displays a characteristic absorption band at 2129 cm^{-1}, corresponding to the C≡N triple bond.

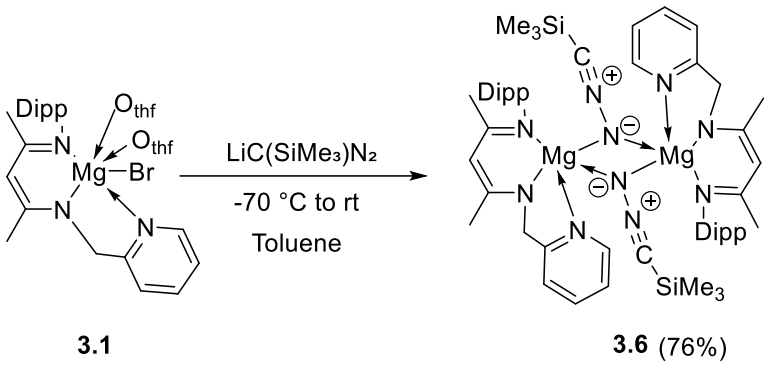

3.1 **3.6** (76%)

Scheme 3.8 Reaction of **3.1** with LiC(SiMe$_3$)N$_2$.

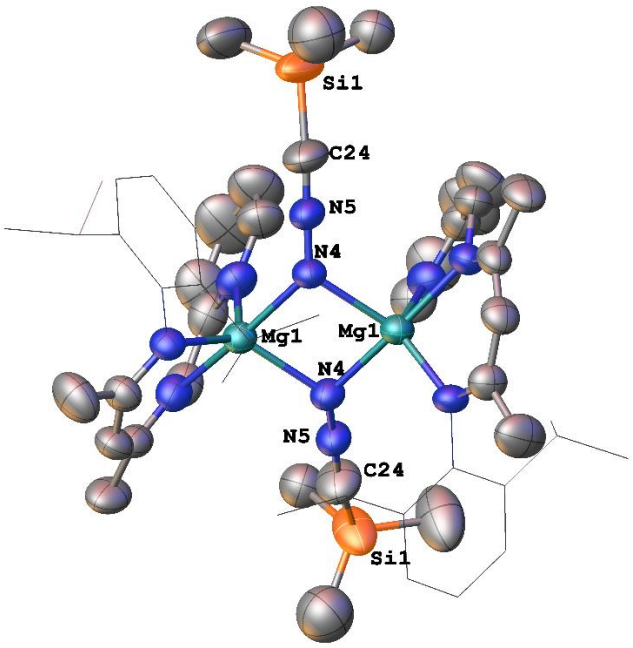

Figure 3.6 The molecular structure of **3.6** with anisotropic displacement parameters depicted at the 50% probability level. Hydrogen atoms (except on the pyridine ring) are not shown for clarity. Selected bond lengths (Å) and bond angles (°): Mg1–N1 2.087(3), Mg1–N2 2.066(3), Mg1–N3 2.195(3), Mg1–N4 2.093(15), N4–N5 1.225(4), C24–N5 1.117(5); N1–Mg1–N2 86.55(12), N2–Mg1–N4 99.86(12), N1–Mg1–N4 131.71(13), C24–N5–N4 178.7(5).

3.3 Conclusion

In summary, two novel magnesium compounds **3.1** and **3.2** supported by tridentate nacnac ligand was readily synthesized and crystallographically characterized, and its electronic structure was studied by DFT calculations. Remarkably, it has been experimentally revealed for the first time that O–H bond of H_2O can be activated by magnesium-ligand cooperation involving an aromatization/dearomatization pathway, previously unknown for alkaline earth metals. The attempt to synthesize monomeric magnesium hydride led to **3.5** *via* intramolecular reduction of the pyridine moiety followed by the addition of adventitious amount of water present in the reaction mixture.

3.4 References

1. J. F. Hartwig, *J. Am. Chem. Soc.,* 2016, **138**, 2–24; (b) R. H. Grubbs, *Angew. Chem. Int. Ed.,* 2006, **45**, 3760–3765; (c) A. Suzuki, *Angew. Chem. Int. Ed.,* 2011, **50**, 6722–6737.
2. a) J. C. Gordon, G. J. Kubas, *Organometallics* 2010, **29**, 4682; b) J. I. vander Vlugt, *Eur. J. Inorg. Chem.,* 2012, 363; c) V. T. Annibale, D. Song, *RSC Adv.* 2013, **3**, 11432; d) D. L. DuBois, *Inorg. Chem.,* 2014, **53**, 3935.
3. B. Zhao, Z. Han, K. Ding, *Angew. Chem. Int. Ed.,* 2013, **52**, 4744; *Angew. Chem.,* 2013, **125**, 4844.
4. R. H. Crabtree, *New J. Chem.,* 2011, **35**, 18; b) J. R. Khusnutdinova, D. Milstein, *Angew. Chem. Int. Ed.,* 2015, **54**, 12236 – 12273.
5. C. Gunanathan, D. Milstein, *Acc. Chem. Res.,* 2011, **44**, 588−602.
6. C. Gunanathan, D. Milstein, *Chem. Rev.,* 2014, **114**, 12024−12087.
7. A. Mukherjee, D. Milstein, *ACS Catal.,* 2018, **8**, 11435−11469.
8. Y. Liang, I. Efremenko, Y. Diskin-Posner, L. Avram, D. Milstein, *Angew. Chem. Int. Ed.,* 2024, **63**, e202401702.
9. T. W. Myers, L. A. Berben, *J. Am. Chem. Soc.*, 2013, **135**, 9988−9990.
10. T. W. Myers, L. A. Berben, *Chem. Sci.*, 2014, **5**, 2771−2777.
11. T. Simler, L. Karmazin, C. Bailly, P. Braunstein, A. A. Danopoulos, *Organometallics* 2016, **35**, 903−912.

12. M. Rauch, S. Kar, A. Kumar, L. Avram, L. J. W. Shimon, D. Milstein, *J. Am. Chem. Soc.*, 2020, **142**, 14513−14521.
13. Y. Liang, J. Luo, Y. Diskin-Posner, D. Milstein, *J. Am. Chem. Soc.,* 2023, **145**, 9164–9175.
14. Y. Liang, U. K. Das, J. Luo, Y. Posner-Diskin, L. Avram, D. Milstein, *J. Am. Chem. Soc.*, 2022, **144**, 19115–19126.
15. T. P. Robinson, D. M. De Rosa, S. Aldridge, J. M. Goicoechea, *Angew. Chem. Int. Ed.,* 2015, **54**, 13758–13763.
16. A. V. Protchenko, J. I. Bates, L. M. A. Saleh, M. P. Blake, A. D. Schwarz, E. L. Kolychev, A. L. Thompson, C. Jones, P. Mountford, S. Aldridge, *J. Am. Chem. Soc.,* 2016, **138**, 4555−4564.
17. X. Yang, E. J. Reijerse, K. Bhattacharyya, M. Leutzsch, M. Kochius, N. Nöthling, J. Busch, A. Schnegg, A. A. Auer, J. Cornella, *J. Am. Chem. Soc.*, 2022, **144**, 16535–16544.
18. F. Krischer, V. S. V. S.N. Swamy, K. S. Feichtner, R. J. Ward, V. H. Gessner, *Angew. Chem. Int. Ed.,* 2024, **63**, e202403766.
19. S. Sinhababu, R. P. Singh, M. R. Radzhabov, J. Kumawat, D. H. Ess, N. P. Mankad, *Nat. Commun.,* 2024, **15**, 1315.
20. R. S. Ghadwal, R. Azhakar, H. W. Roesky, K. Popper, B. Dittrich, S. Klein, G. Frenking, *J. Am. Chem. Soc.*, 2011, **133**, 17552–17555.
21. Z. Mo, T. Szilvási, Y.-P. Zhou, S. Yao, M. Driess, *Angew. Chem., Int. Ed.,* 2017, **56**, 3699-3702.
22. T. W. Myers, L. A. Berben, *Organometallics* 2013, **32**, 6647−6649.
23. P. Ghosh, G. Parkin, *Inorg. Chem.*, 1996, **35**, 1429–1430.
24. L. F. Sánchez-Barba, D. L. Hughes, S. M. Humphrey, M. Bochmann, *Organometallics* 2006, **25**, 1012–1020.
25. S. Nembenna, S. Singh, S. S. Sen, H. W. Roesky, H. Ott, D. Stalke, *ZAAC*, 2011, **637**, 201–205.
26. Ma, M.; Stasch, A.; Jones, C. Magnesium(I) Dimers as Reagents for the Reductive Coupling of Isonitriles and Nitriles. *Chem. - Eur. J.,* 2012, 18, 10669−10676.

Chapter-4

Magnesium-Mediated C–H Bond Activation of Alkynes and a Diazoalkane

Abstract: The reaction of **3.2** with terminal alkynes, such as phenylacetylene and 4-fluorophenylacetylene facilitates selective C–H bond cleavage, resulting in the formation of novel monomeric magnesium alkynyl complexes **4.1** and **4.2**, respectively. Additionally, **3.2** undergoes C–H bond activation with trimethylsilyldiazomethane (Me_3SiCHN_2), yielding a novel magnesium complex (**4.3**) featuring a bridging isocyanide moiety. This transformation involves a migration of the $SiMe_3$ group from the carbon to the nitrogen atom. Furthermore, these magnesium alkynylides undergo palladium-catalysed cross-coupling reactions with aryl halides, producing the corresponding C–C coupled products.

4.1 Introduction

The ubiquitous presence of C–H bonds in organic molecules makes them highly appealing targets for functionalization, enabling the construction of valuable molecular scaffolds. As a result, C–H activation has transcended its status as a subject of fundamental scientific interest and has emerged as a powerful and versatile tool in modern organic synthesis.[1-3] The capability of homogeneous catalysts to enable selective functionalization of stable C–H bonds under mild conditions, without relying on harsh reaction parameters or highly reactive reagents, has driven significant advancements in this field in recent years.[4-7] However, the field of catalytic C–H activation has been predominantly driven by homogeneous catalysts based on noble transition metals, including Rh, Ru, Pd, Ir, and Pt. These metals are rare, expensive, and often toxic, posing challenges to the sustainability of these methodologies.[9]

Recent efforts have increasingly focused on developing catalysts derived from inexpensive and earth abundant metals. Main group metals such as Mg, Ca, and Zn have garnered substantial attention due to their affordability, wide availability, low toxicity, and their prevalence in biological systems, demonstrating their potential for broad applicability in this domain.[10] This progress, as highlighted in Power's review, *"Main-group compounds as transition metals,"* has reshaped our understanding of the versatility and utility of these elements, further establishing their relevance in sustainable catalytic systems.[11] Deprotonative metalation using Hauser bases, $Mg(NR_2)X$ or $Mg(NR_2)_2$, and turbo-Hauser bases, $Mg(NR_2)X{\cdot}LiCl$ or $Mg(NR_2)_2{\cdot}LiCl$ (R = alkyl, most commonly *i*Pr or R_2N = TMP; X = Cl, Br) have been used in chemoselective functionalization of a large variety of arenes and heteroarenes even in the presence of sensible functional groups.[12] The use of magnesium-based compounds as stoichiometric reagents for C–H functionalization reactions is well known (Scheme 4.1).[13-14]

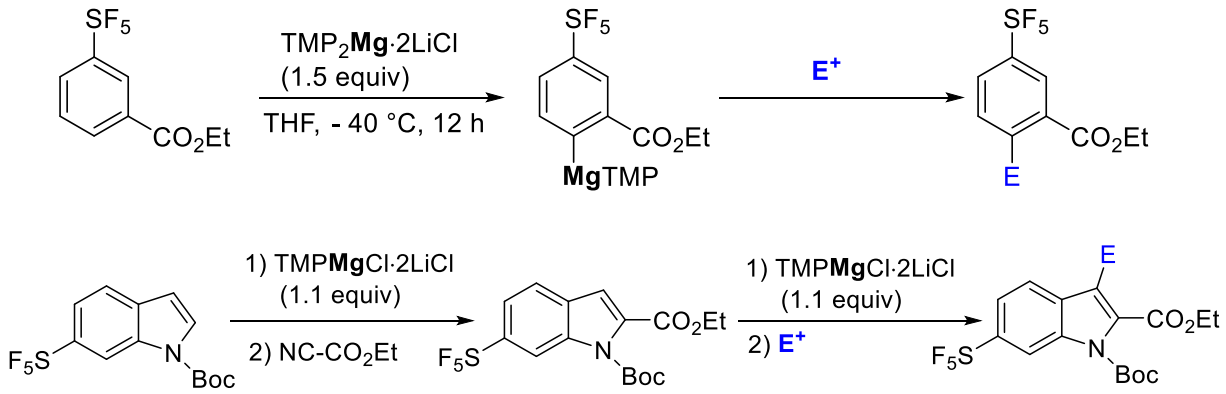

Scheme 4.1 Selected examples of magnesium-based C-H functionalization reactions.

In 2012, Kanai and co-workers made a significant breakthrough by developing a magnesium-catalyzed enantioselective benzylic C–H bond functionalization of *iso*-indolinones, an important structural motif found in numerous natural products and biologically active compounds.[15] This work highlighted the potential of magnesium in catalyzing challenging transformations. Building on such advancements, Mashima, and their team synthesized a dimeric organomagnesium complex that demonstrated high efficiency as a precatalyst for the sequential isomerization of terminal alkynes into allenes, followed by their conversion into internal alkynes.[16] Despite these promising developments, magnesium-mediated C–H bond activation remains predominantly base-driven, with only a limited number of examples involving direct C–H bond cleavage using magnesium.

Magnesium alkynylide species, though hypothesized as critical intermediates in various catalytic transformations, are rarely isolated, and their structural characterization is even less common. A comprehensive analysis of structurally validated magnesium alkynylide species (Scheme 4.2) reveals the notable absence of monomeric magnesium alkynylide compounds in the literature, underscoring the challenges in isolating and characterizing such entities.[17,18-23]

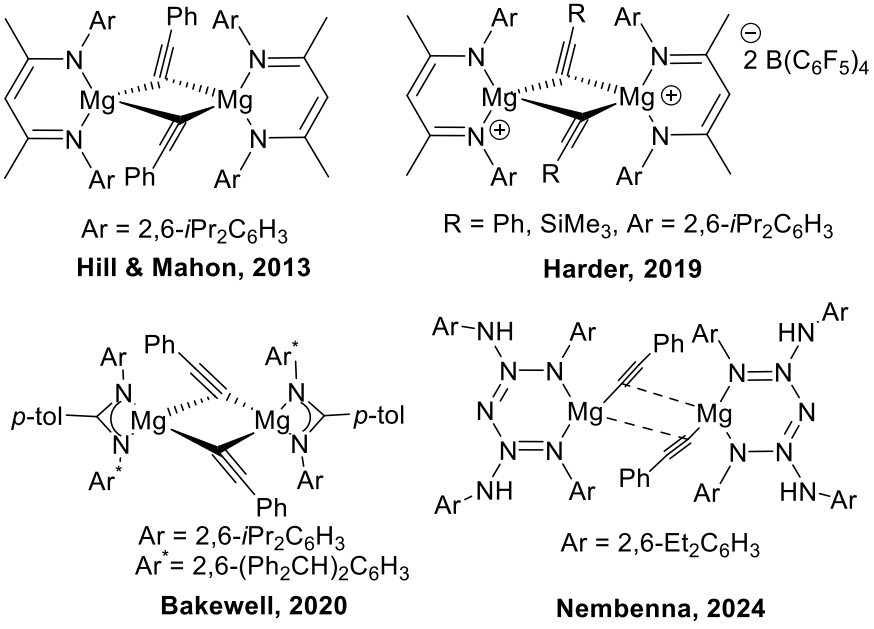

Scheme 4.2 Selected examples of magnesium alkynylide species.

4.2 Results and Discussions

4.2.1 Activation of C−H Bond of Alkynes

Reaction of **3.2** with terminal alkynes such as PhC≡CH and *p*-fluorophenylacetylene led to magnesium alkynylide complexes **4.1** and **4.2** respectively (Scheme 4.3) via MLC mediated C−H bond cleavage. The colorless crystals of **4.1** and **4.2** were obtained from the toluene solution at –4 °C. The molecular structures of **4.1** and **4.2** are shown in Figure 4.1 and 4.2 respectively.

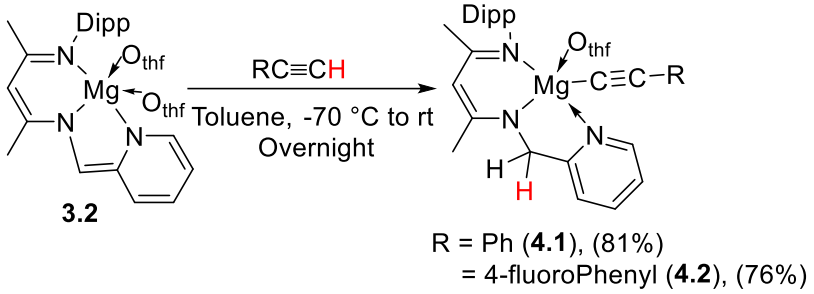

Scheme 4.3 Synthesis of magnesium alkynylide complexes by a magnesium species (**3.2**).

Well defined magnesium alkynylide compounds are very rare[21,22]. To the best of our knowledge, this is the first example of well-defined magnesium alkynylides via sophisticated MLC. The solid-state structure of **4.1** and **4.2** shows Mg−$N_{pyridine}$ bond length of 2.198(5) Å and 2.180(3) Å respectively, which is longer than that of **3.2** confirms the conversion of covalent bond to dative bond. The bond distances between Mg−C_{alkyne}, 2.175(6) Å and 2.160(4) Å for **4.1** and **4.2** respectively shows a bond of covalent character which is in agreement with the previously reported magnesium alkynylide complex [{LMgCCPh}$_2$; L={(ArHN)(ArN)−C=N−C=(NAr)(NHAr); Ar= 2,6-Et_2-C_6H_3 }] 2.153(4) Å by Nembenna.[22b]

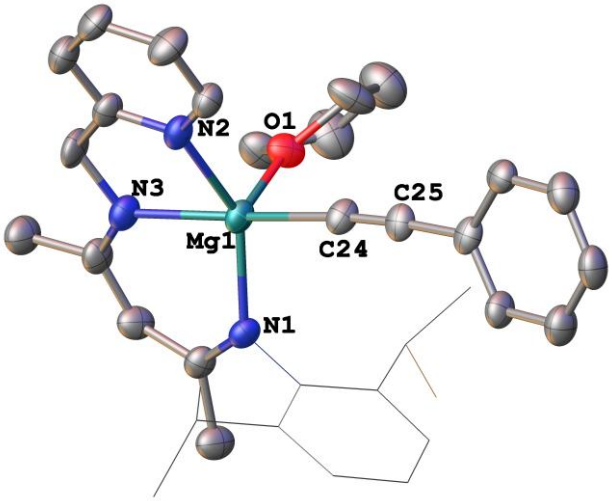

Figure 4.1 The molecular structure of **4.1** with anisotropic displacement parameters depicted at the 50% probability level. Hydrogen atoms are not shown for clarity. Selected bond lengths (Å) and bond angles (°): Mg1–N1 2.126(5), Mg1–N2 2.198(5), Mg1–N3 2.126(5), Mg1–C24 2.175(6), C24–C25 1.212(7); N1–Mg1–N3 86.46(18), N1–Mg1–N2 146.6(2), N2–Mg1–N3 75.95(18), N3–Mg1–C24 165.80(2).

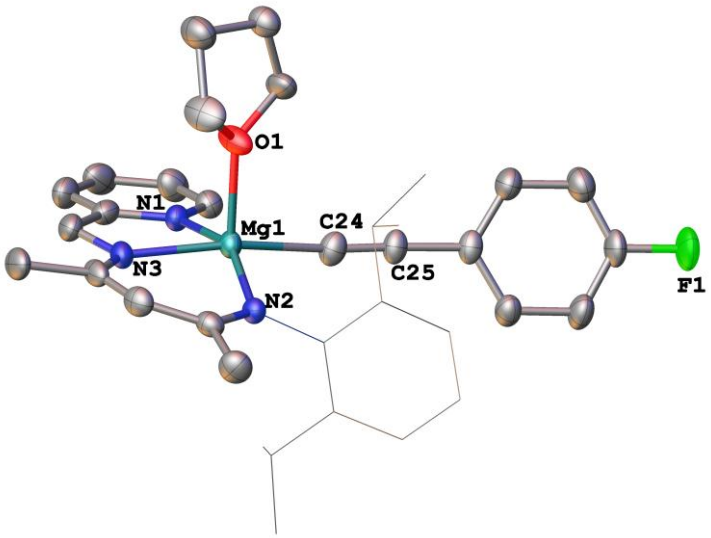

Figure 4.2 The molecular structure of **4.2** with anisotropic displacement parameters depicted at the 50% probability level. Hydrogen atoms are not shown for clarity. Selected bond lengths (Å) and bond angles (°): Mg1–N1 2.185(3), Mg1–N2 2.119(3), Mg1–N3 2.111(3), Mg1–C24 2.160(4), C24–C25 1.216(5); N1–Mg1–N3 76.56(12), N1–Mg1–N2 153.99(12), N2–Mg1–N3 88.17(12), N3–Mg1–C24 164.45(14).

4.2.2 Activation of C−H Bond of Diazoalkane

Very recently, Maron and Xu reported the synthesis of zinc diazoalkyl complex, which was obtained from the C–H activation of Me_3SiCHN_2 by a zinc hydride.[24] We have reported the same with NHC.[25] Addition of 1 equivalent of Me_3SiCHN_2 to the THF solution of **3.2** led to immediate color change to orange, which is a characteristic of protonation of the dearomatized picolyl backbone. **4.3** was obtained through C–H activation of Me_3SiCHN_2 via MLC with concomitant migration of the $SiMe_3$ group from the carbon to the nitrogen atom (Scheme 4.4).[26-28]

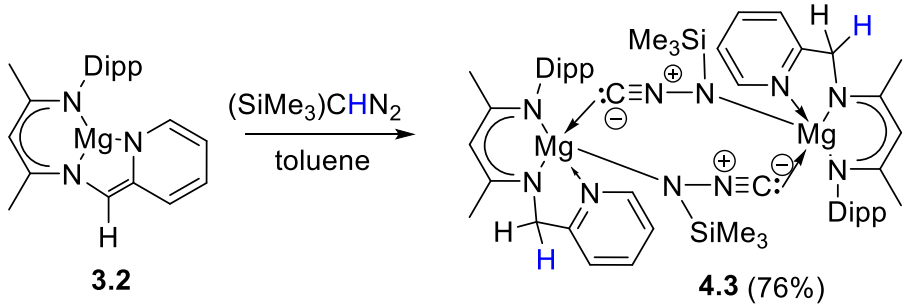

Scheme 4.4. Splitting of the C–H bond of Me_3SiCHN_2 by magnesium species (**3.2**).

Figure 4.1 depicts the molecular structure of **4.3**, which is a centrosymmetric dimer. There are three Mg–N covalent bonds of more or less same lengths 2.0992(13), 2.0864(13), and 2.1130(13) Å, while the Mg–N1 bond length is substantially longer (2.2497(15) Å). The Mg–C bond of 2.2480(16) Å, which is slightly shorter than the magnesium-tertbutyl isonitrile adduct, $\{Mg[CH(SiMe_3)_2](\mu\text{-Br})(CN\textit{t}Bu)\}_2$ (2.12 Å) reported by Lappert.[29] The N5–C27 bond length of 1.163(19) Å indicates the formation of C≡N triple bond and is in good agreement with the C≡N bond lengths reported by Jones and co-workers in $\{[HC(C(Me)N\text{-}2,6\text{-}\textit{i}Pr_2C_6H_3)_2]Mg[\mu\text{-}CN)]\}_3$.[30]

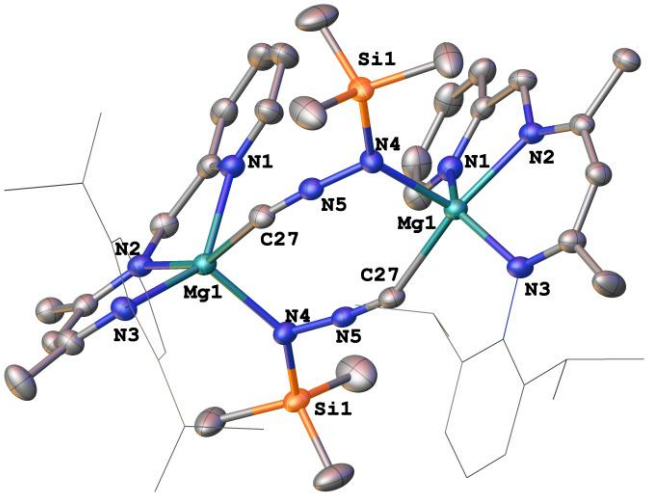

Figure 4.3. The molecular structure of **4.3** with anisotropic displacement parameters depicted at the 50% probability level. Hydrogen atoms are not shown for clarity. Selected bond lengths (Å) and bond angles (°): Mg1–N3 2.0992(13), Mg1–N2 2.0864(13), Mg1–N1 2.2497(15), Mg1–N4 2.1130(13), Mg1–C27 2.2482(17), N5–C27 1.163(2), N4–N5 1.3415(15); N1–Mg1–N2 85.57(5), N2–Mg1–N4 104.18(5), N3–Mg1–N4 116.28(5), N3–Mg1–C27 97.01(8), N2–Mg1–C27 157.08(6), N1–Mg1–N3 140.13(5).

4.2.3 Mechanistic Investigation of Compound 4.3

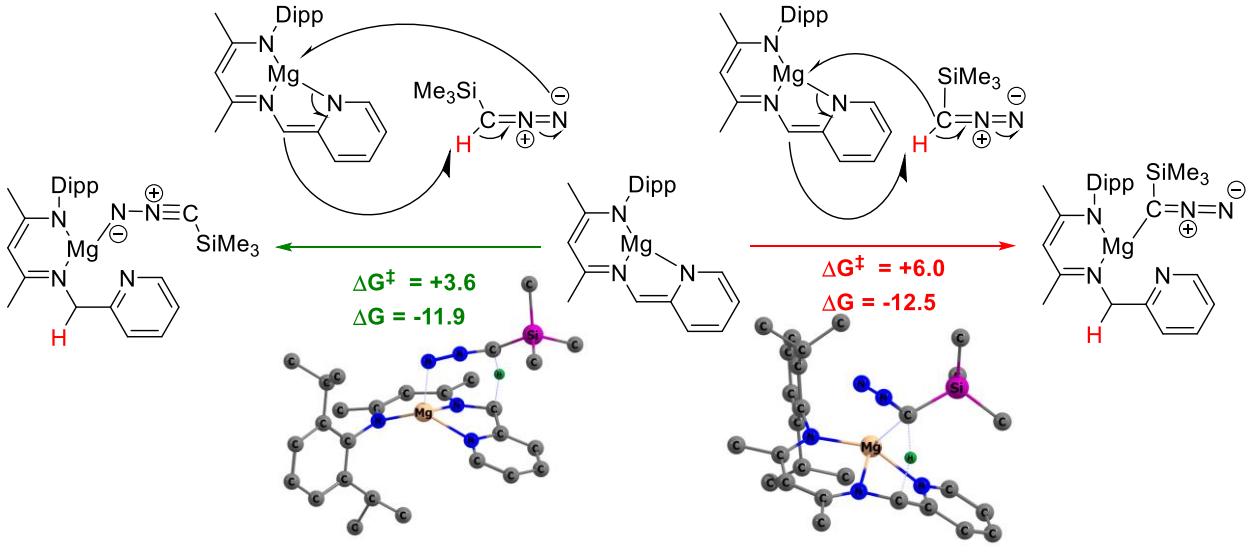

Figure 4.4 Pathways for the C-H bond activation of Me_3SiCHN_2 by **3.2**, computed at the PBE-D3/def2TZVP level of theory. Peripheral hydrogen atoms have been removed for clarity.

DFT calculations revealed that the C-H bond activation required for initiating the reaction between **3.2** and Me_3SiCHN_2 is highly facile, with a kinetic barrier of only +3.6 kcal/mol. ($\Delta G^{\ddagger}$). Two different possibilities for the C-H bond activation *via* the metal-ligand cooperation are shown in Figure 4.4. Notably, the transition state where the nitrogen of Me_3SiCHN_2 coordinates with Mg is 2.4 kcal/mol ($\Delta G^{\ddagger}$) more favourable than the transition state where the carbon of Me_3SiCHN_2 interacts with Mg.

Following C-H bond activation, $SiMe_3$ migration from carbon to nitrogen (coordinated to the Mg centre) occurs (ΔG = -2.1 kcal/mol), followed by dimerization (**Figure 4.5**), ultimately yielding the highly exergonic product **4.3** (ΔG = -34.2 kcal/mol). While a four-membered transition state for the migration was identified with a prohibitively high kinetic barrier of +54.1 kcal/mol -rendering it unlikely at the reaction temperature - an alternative pathway involving Me_3SiCHN_2 as a $SiMe_3$ shuttling agent could enable migration *via* a six-membered transition state. Despite extensive efforts, we were unable to locate this six-membered transition state computationally. Nevertheless, the overall reaction between Me_3SiCHN_2 and **3.2**, culminating in the dimerization product (**4.3**), remains highly favourable thermodynamically (overall ΔG = -48.2 kcal/mol).

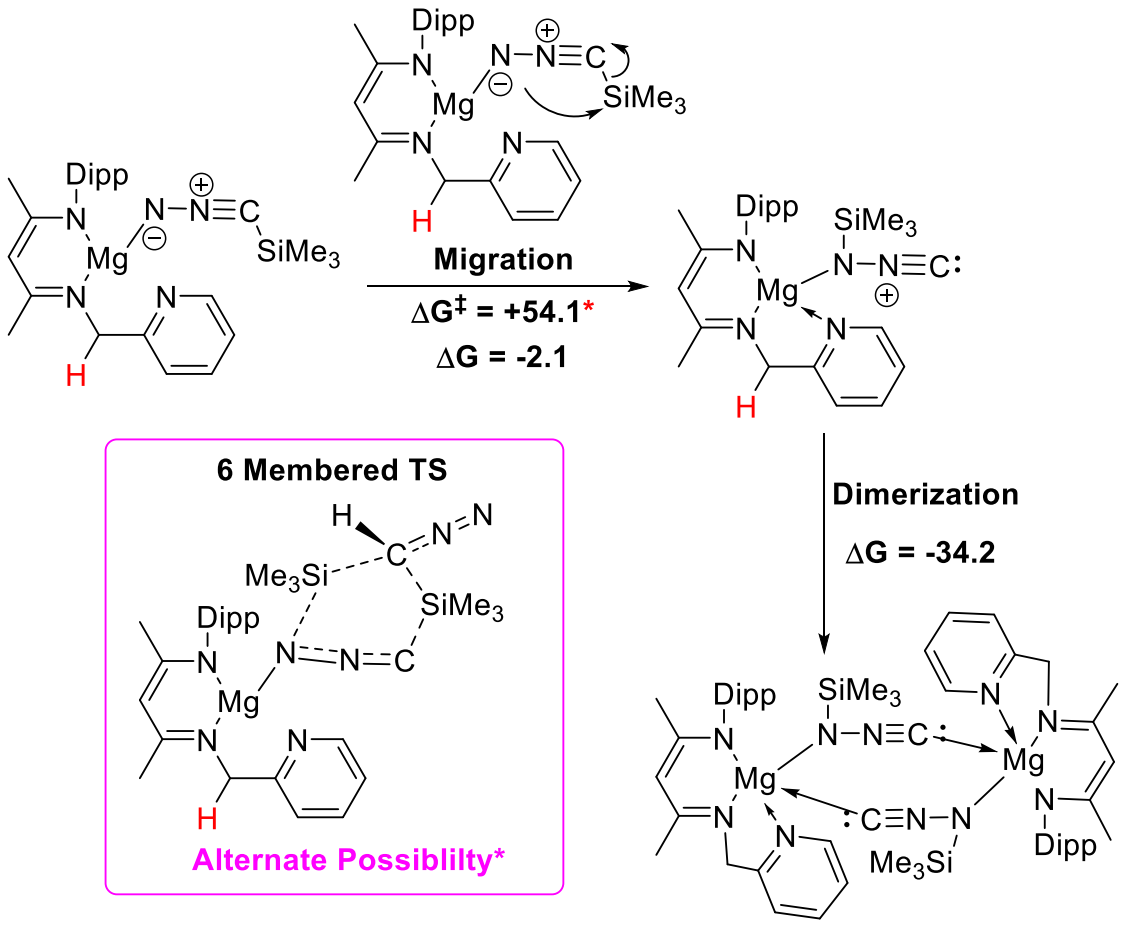

Figure 4.5 Pathways for subsequent migration and dimerization, computed at the PBE-D3/def2TZVP level of theory.

4.2.4 Theoretical Illumination of Compound 4.3

The unique formation of compound **4.3** prompted us to investigate its electronic structure. From Wiberg bond indices (WBI) analysis of **4.3**, it was observed that the Mg-C (WBI = 0.146) and Mg-N (WBI = 0.072) bonds, of the bridging site, have very low covalent character (Figure 4.6). These findings are also corroborated by bond critical point (BCP) analysis, where both the electron density (ρ_r) as well as the Laplacian of electron density ($\nabla^2\rho_r$) were found to be +ve and also associated with a very low electron localization function (ELF) value. Notably, a high contribution from electrostatic interactions (58%) was obtained from the energy decomposition analysis (EDA) of **4.3**, considering a monomeric unit of Mg-N(SiMe$_3$)NC. The contribution from orbital interaction was found to be only about 28%, whereas the contribution from

dispersion interaction was 13%. This suggests that the electrostatic interactions are the driving force for the formation of **4.3**.

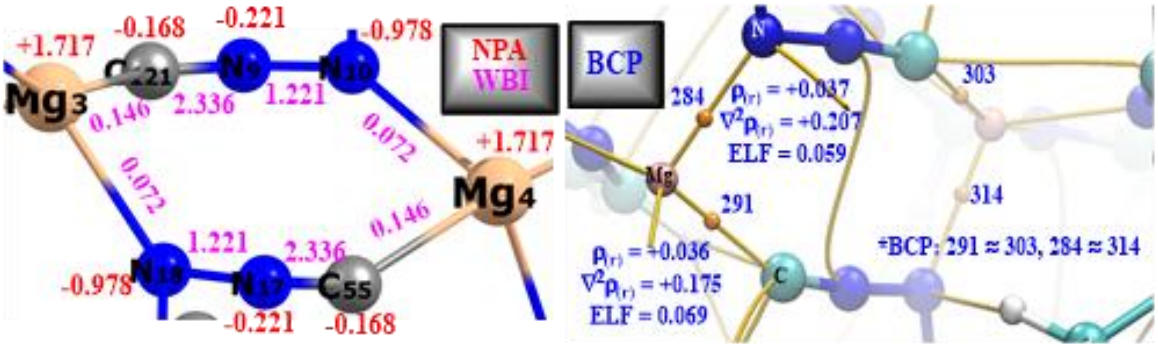

Figure 4.6. WBI, NPA and BCP analysis of **4.3** (Only the bridging site is shown for clarity).

Natural bond orbital (NBO) analysis also could not locate any bonding NBO corresponding to the bridging Mg-N or Mg-C, although it revealed that both of these interactions are facilitated by electron density transfer from lone pair of N and C to non-bonding vacant orbital (LP*) of Mg (Figure 4.7). Interestingly, the charge transfer interaction between C and Mg was found to be much stronger in comparison to the N-Mg interaction. The charge transfer from C to Mg, considering the fragmentation *via* two units of Mg-N($SiMe_3$)NC, was also observed from extended transition state-natural orbital for chemical valence (ETS-NOCV) analysis.

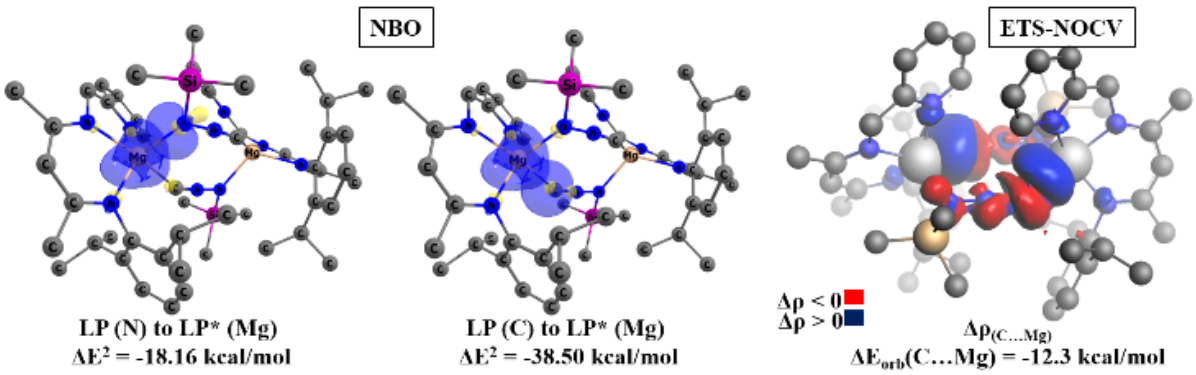

Figure 4.7. NBO and ETS-NOCV analysis of **4.3**. For ETS-NOCV plot, red region represents outflow of electron density (charge depletion) and blue region represents inflow of electron density (charge accumulation).

4.2.5 Palladium Catalysed C–C Cross Coupling

With the successful synthesis of magnesium alkynylide compounds, we turned our attention to explore their potential in C–C cross-coupling reactions. The unique reactivity of magnesium alkynylides, which contain highly nucleophilic and reactive alkynyl groups, presents an intriguing opportunity to design novel coupling strategies. When **4.1** was reacted with 4-iodotoluene in presence of catalytic amounts of $[Pd(PPh_3)_2Cl_2]$, it yielded C–C coupled product **4.4** (Scheme 4.6), which was separated using column chromatography and characterized by NMR and mass spectroscopy. Efforts to broaden the substrate scope for this reaction are ongoing.

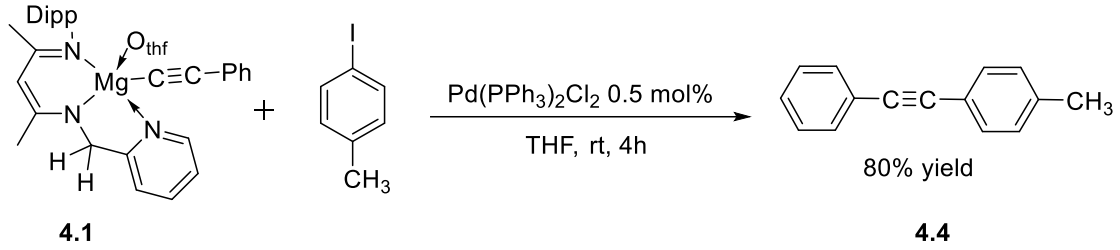

Scheme 4.6 C–C hetero-coupling using magnesium alkynylide complex **4.1** as feedstock.

4.3 Conclusion

In conclusion, we expanded the reactivity profile of the dearomatized magnesium complex **3.2**, focusing on C–H bond activation in alkynes and diazoalkanes. This work led to the isolation of the first structurally characterized monomeric magnesium alkynylide complexes (**4.1** and **4.2**). Additionally, we showcased the utility of these magnesium alkynylide complexes as precursors for C–C cross-coupling reactions.

4.4 References

1. S. Murahashi, J. Am. Chem. Soc., 1995, 77, 6403–6404.
2. J. Chatt, J. M. Davidson, *J. Chem. Soc.*, 1965, 843–855.
3. A. H. Janowicz, R. G. Bergman, *J. Am. Chem. Soc.*, 1982, **104**, 352–354.
4. C. S. Yeung, V. M. Dong, *Chem. Rev.,* 2011, **111**, 1215–1292; b) S. Murai, *Proc. Jpn. Acad., Ser.,* 2011, **87**, 230–241; c) N. Kuhl, M. N. Hopkinson, J. Wencel-Delord, F.

Glorius, *Angew. Chem., Int. Ed.,* 2012, **51**, 10236–10254; d) K. M. Engle, J. Yu, *J. Org. Chem.*, 2013, **78**, 8927–8955; e) S. A. Girard, T. Knauber, C. Li, *Angew. Chem., Int. Ed.*, 2014, **53**, 74–100.

5. J. Schranck, A. Tlili, M. Beller, *Angew. Chem., Int.Ed.,* 2014, **53**, 9426–9428; b) C. Liu, J. Yuan, M. Gao, S. Tang, W. Li, R. Shi, A. Lei, *Chem. Rev.,* 2015, **115**, 12138–12204; c) T. M. Shaikh, F. Hong, *J. Organomet. Chem.,* 2016, **801**, 139–156.
6. M. Gulías, J. L. Mascareñas, *Angew. Chem. Int. Ed.*, 2016, **55**, 11000–11001.
7. H. M. L. Davies, D. Morton, *J. Org. Chem.*, 2016, **81**, 343–350; b) B. Zhao, Z. Shi, Y. Yuan, *Chem. Rec.,* 2016, **16**, 886–896.
8. D. Y. -K. Chen, S. W. Youn, *Chem. Eur. J.*, 2012, **18**, 9452–9474.
9. M. Lersch, M. Tilset, *Chem. Rev.*, 2005, **105**, 2471–2526.
10. M. S. Holzwarth, B. Plietker, *ChemCatChem*., 2013, **5**, 1650–1679; b) S. Harder, *Chem. Rev.,* 2010, **110**, 3852–3876.
11. M. R. Crimmin, M. Arrowsmith, A. G. M. Barrett, I. J. Casely, M. S. Hill, P. A. Procopiou, *J. Am. Chem. Soc.*, 2009, **131**, 9670–9685.
12. C. R. Hauser, H. G. Walker, *J. Am. Chem. Soc.,* 1947, **69**, 295–297.
13. A. Frischmuth, A. Unsinn, K. Groll, H. Stadtmüller, P. Knochel, *Chem. Eur. J.*, 2012, **18**, 10234–10238; b) T. Satoh, *Heterocycles*, 2012, **85**, 1–33.
14. S. Murarka, I. Deb, C. Zhang, D. Seidel, *J. Am. Chem. Soc.,* 2009, **131**, 13226–13227; b) L. Chen, L. Zhang, J. Lv, J. Cheng, S. Luo, *Chem. Eur. J.,* 2009, **18**, 8891–8895; c) S. J. Kwon, D. Y. Kim, *Chem. Rec.*, 2016, **16**, 1191–1203.
15. Y. Suzuki, M. Kanai, S. Matsunaga, *Chem. Eur. J.*, 2012, **18**, 7654–7657.
16. R. Rochat, K. Yamamoto, M. J. Lopez, H. Nagae, H. Tsurugi, K. Mashima, *Chem. Eur. J.,* 2015, **21**, 8112–8120.
17. L. F. Sánchez-Barba, D. L. Hughes, S. M. Humphrey, M. Bochmann, *Organometallics*, 2006, **25**, 1012–1020
18. A. Xia, M. J. Heeg, C. H. Winter, *Organometallics,* 2003, **22**, 1793–1795.
19. J. Pahl, T. E. Stennett, M. Volland, D. M. Guldi, S. Harder, *Chem. Eur. J.,* 2019, **25**, 2025-2034.
20. M. Arrowsmith, M. R. Crimmin, M. S. Hill, S. L. Lomas, D. J. MacDougall, M. F. Mohan, *Organometallics,* 2013, **32**, 4961−4972.
21. 21. R. J. Schwamm, M. P. Coles, *Organometallics,* 2013, **32**, 5277–5280.

22. 22. M. Arrowsmith, M. R. Crimmin, M. S. Hill, S. L. Lomas, M. S. Heng, P. B. Hitchcock, G. Kociok-Köhn, *Dalton Trans.,* 2014, **43**, 14249–1425.
23. S. Mukhopadhyay, S. Rajput, R. K. Sahoo, S. Nembenna, *Eur. J. Org. Chem.,* 2024, **27**, e202400702.
24. S. Jiang, Y. Cai, T. Rajeshkumar, I. D. Rosal, L. Maron, X. Xu, *Angew. Chem., Int. Ed.,* 2023, **62**, e202307244.
25. K. Balayan, H. Sharma, K. Vanka, R. G. Gonnade, S. S. Sen, *Chem. Sci.,* 2024, **15**, 18387–18394.
26. W. J. Evans, E. Montalvo, T. M. Champagne, J. W. Ziller, A. G. DiPasquale, A. L. Rheingold, *J. Am. Chem. Soc.,* 2008, **130**, 16−17.
27. A. Jana, I. Objartel, H. W. Roesky, D. Stalke, *Inorg. Chem.,* 2009, **48**, 7645−7649.
28. W. Ren, D. Gu, *Inorg. Chem.*, 2016, **55**, 11962−11970.
29. C. F. Caro, P. B. Hitchcock, M. F. Lappert, M. Layh, *Chem. Commun.,* 1998, 1297−1298.
30. M. Ma, A. Stasch, C. Jones, *Chem. Eur. J.,* 2012, **18**, 10669−10676.

Chapter-5

Tridentate NacNac Supported Chemistry of Aluminium and Gallium

Abstract: In our earlier study, we demonstrated that the reaction of a tridentate nacnac ligand featuring a pendant picolyl group with alane [$AlH_3 \cdot NMe_2Et$] yielded a binuclear aluminum hydride system **V** characterized by a six-membered C–C coupled framework. In this chapter, we explore the influence of reaction conditions on this system, revealing that the reaction of the same ligand with [$AlH_3 \cdot NMe_2Et$] under modified conditions results in the formation of distinct aluminum hydride species, **5.1** and **5.2**. Additionally, the reaction of the ligand with benzyl potassium, followed by the introduction of metal halides ECl_3 (E = Al, Ga), leads to the high-yield synthesis of metal halide complexes **5.3** and **5.4**, respectively. These products, which could not be obtained using alternative base systems, underscore the importance of reaction conditions and reagents in tuning the reactivity of this ligand system.

5.1 Introduction

Among the main-group metals, aluminum stands out as one of the most abundant elements in the Earth's crust. Its low toxicity, cost-effectiveness, and environmental compatibility make it particularly appealing[1,2]. The significance of aluminum in organic chemistry was first demonstrated in the ground-breaking Friedel-Crafts reaction[3]. Aluminum predominantly exists in the +3 oxidation state due to its thermodynamic stability, which is more favourable compared to the +2 and +1 oxidation states.

Aluminum hydrides are considered as fuel storage materials with reasonable prospects in a hydrogen-based alternate energy-supply concept.[4,5] In applied science, chemical vapor deposition technology leverages the thermodynamic characteristics of molecular aluminum hydrides to fabricate composite materials.[6-8] The chemistry of aluminum hydrides has progressed considerably since Stecher and Wiberg's first synthesis of AlH_3 in 1942.[9] A significant breakthrough occurred in 1960 when Hawthorne synthesized a series of amine adducts of alane, catalysing substantial developments in the coordination chemistry of heavier group 13 hydrides[10,11]. A range of hydridoalanes has been designed, with their reactivity frequently modulated through steric hindrance at the aluminium centre and the incorporation of strongly electron-donating groups bonded to the aluminium atom.[10,11]. These advances have been complemented by extensive characterization of aluminium hydrides through single-crystal X-ray diffraction, leading to the elucidation of a wide array of structural motifs[12-16].

Despite its potential as a viable alternative to transition metal catalysts, research into aluminium among group 13 elements saw limited progress until the seminal work by Yang, Parameswaran, and Roesky.[17] The utilization of aluminium hydrides like **I**[18] (Scheme 5.1), featuring highly specialized ligands, enables the formation of diverse, isolatable, and well-defined model complexes. Consequently, the inclusion of an ancillary ligand is necessary, while preserving two reactive functional groups at the metal centre for subsequent chemical transformations.

The *β*-diketimino moiety has proven to be a pivotal ligand in developing a diverse range of main-group compounds. Its role in stabilizing aluminum dihydrides has been extensively studied[12]. Notably, compound **II** (Scheme 5.1) exemplifies this utility, facilitating the activation of non-polar element–element bonds, as evidenced by its reactions with elemental sulphur or selenium[12d]. Inoue and coworkers investigated various aluminum hydrides featuring diverse

bulky ligand groups and highlighted the critical role of exploring aluminum hydrides with varying degrees of steric hindrance and strong electron-donating substituents at the aluminum centre **III** (Scheme 5.1). This approach was shown to play a significant role in tuning reactivity for applications in organic synthesis[19,20] Recently, our group investigated the synthesis of aluminium hydride complexes employing an imidazolidine-2-iminato (NHI) ligand and a modified tridentate nacnac ligand incorporating a picolyl arm. The use of the NHI ligand resulted in the formation of a dimeric alane complex **IV**, while the modified nacnac ligand led to the generation of an unusual C–C coupled six-membered aluminium hydride dimer complex **V** (Scheme 5.1).[21,22]

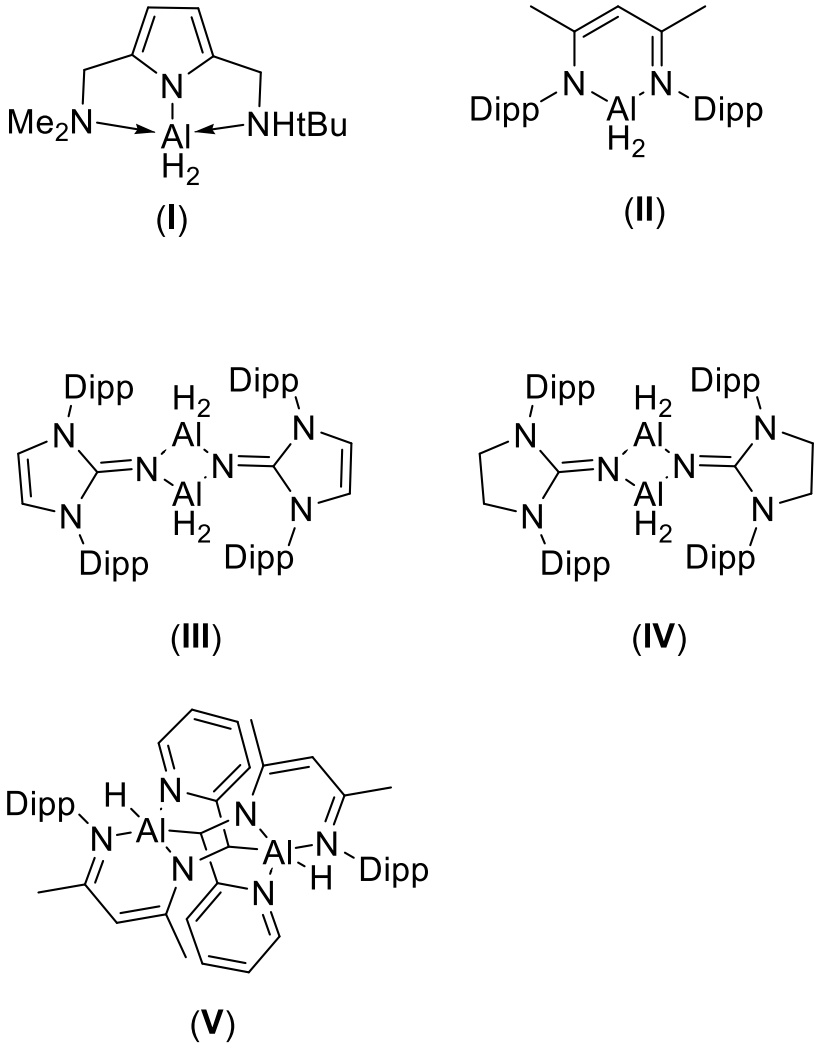

Scheme 5.1 Selected examples of aluminum hydride compounds.

In this chapter, we investigated the influence of solvent on stabilizing a monomeric aluminum hydride complex utilizing a modified tridentate nacnac ligand.

5.2 Results and Discussions

5.2.1 Synthesis and characterization of 5.1

The reaction of ligand with alane [$AlH_3 \cdot NMe_2Et$] in diethyl ether smoothly yielded the heteroleptic aluminum hydride complex **5.1** (Scheme 5.2). Which was isolated and the crystals of **5.1** suitable for SCXRD obtained from the saturated DEE solution at – 4 °C after 2 days. The molecular structure of **5.1** is shown in Figure 5.1. The molecular structure of **5.1** shows Al–N bond lengths 1.945(8), 2.009(9), and 2.106(9) Å, which are in great agreement with the reported alane.[17]

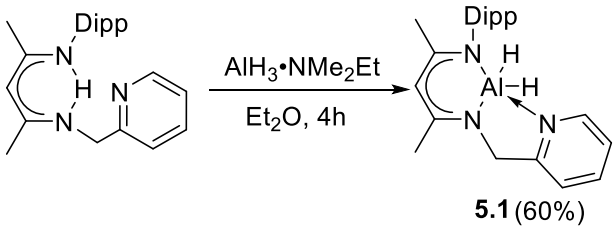

Scheme 5.2 Synthesis of monomeric aluminium hydride complex **5.1**.

The isolation of a tridentate nacnac-supported monomeric aluminium hydride can be achieved by simply altering the reaction solvent from toluene to diethyl ether. The ^{1}H NMR spectrum of compound **5.1** exhibits two distinct septets at 2.76 ppm and 3.52 ppm, corresponding to the isopropyl group. Additionally, the methylene sidearm protons appear as two separate doublets at 4.81 ppm and 4.96 ppm, indicating inequivalent chemical environments for the CH_2 protons (See Figure A36).

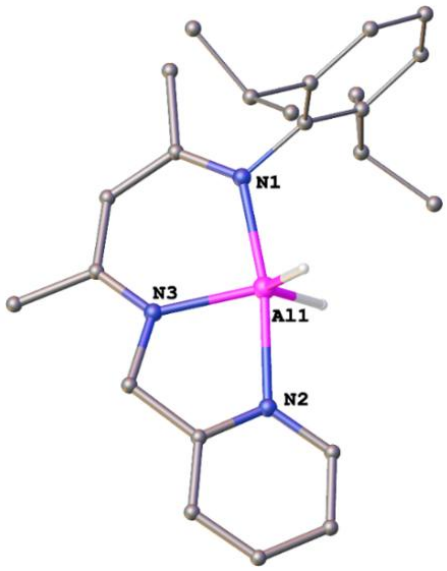

Figure 5.1 The molecular structure of **5.1** with anisotropic displacement parameters depicted at the 50% probability level. Hydrogen atoms (except those attached to aluminium) are not shown for clarity. Selected bond lengths (Å) and bond angles (°): Al1–N1 2.009(9), Al1–N2 2.106(9), Al1–N3 1.945(8); N1–Al1–N3 90.86(4), N1–Al1–N2 170.06(4), N2–Al1–N3 79.53(3).

5.2.2 Synthesis and characterization of 5.2

After isolating the mononuclear aluminium hydride **5.1**, we intended to elucidate the mechanism underlying the formation of **V**. To achieve this, we conducted the same reaction with a shorter reaction time to capture potential intermediates. After 6 hours of reaction, we successfully isolated compound **5.2** (Scheme 5.3). Single crystals suitable for X-ray diffraction analysis were obtained by growing crystals from a supersaturated solution of toluene at –36 °C within 24 hours. The molecular structure of **5.2**, depicted in Figure 5.2, reveals that it arises from an intermolecular hydroalumination of the C–N bond of another alane moiety, ultimately leading to the formation of a binuclear aluminium hydride complex featuring a reduced pyridine ring. The Al1–N6 bond length of 2.096(9) Å is notably longer than the Al2–N6 bond length of 1.915(9) Å, indicating the predominantly covalent character of the Al1–N6 interaction. Additionally, the C–N6 bond length of 1.496(4) Å within the pyridine moiety provides evidence for intermolecular hydroalumination of the pyridine ring. The ^{1}H NMR spectra show a doublet at 3.90 ppm for the *o*-CH_2 of the reduced pyridine ring (Figure A38).

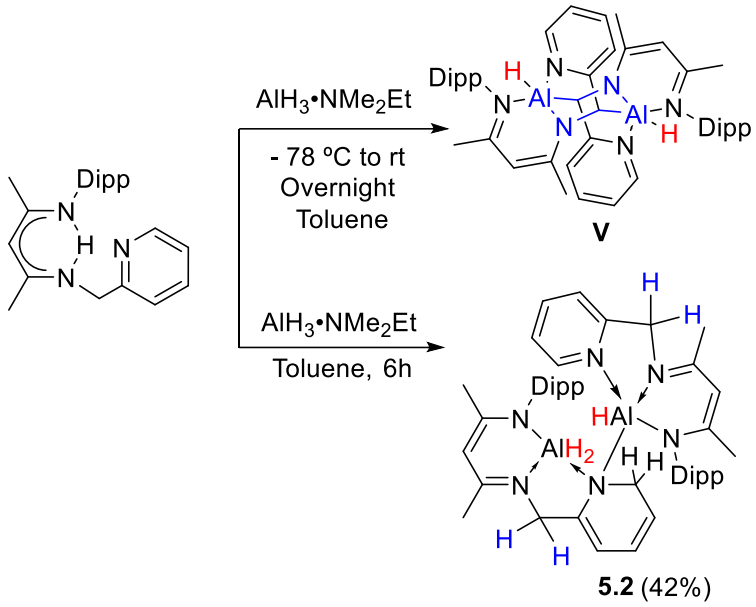

Scheme 5.3 Isolation of intermediate complex **5.2** *via* time control experiment.

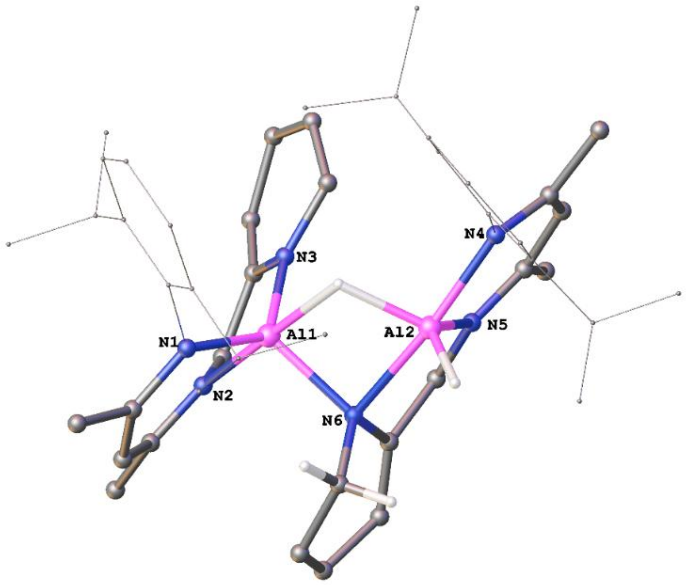

Figure 5.2 The molecular structure of **5.2** with anisotropic displacement parameters depicted at the 50% probability level. Hydrogen atoms (except those attached to aluminium and *o*-CH_2 of reduced pyridine) are not shown for clarity. Selected bond lengths (Å) and bond angles (°): Al1–N1 1.909(9), Al1–N2 1.922(9), Al1–N3 1.872(8), Al1–N6 1.963(9), Al2–N6 2.096(8), Al2–N5 1.915(9), Al2–N4 1.983(9); N1–Al1–N3 132.16(4), N1–Al1–N2 92.02(4), N2–Al1–N3 84.38(4), N6–Al1–Al2 47.51(2), N6–Al2–N4 172.77(3), N4–Al2–N5 92.94(3), N6–Al2–N5 83.55(4).

5.2.3 Thermodynamics of the mechanistic pathway

The chemical transformation leading to the formation of **V** from the ligand manifests a notably exergonic nature, evidenced by a Gibbs free energy change (ΔG) of **-74.6 kcal/mol**. Moreover, the reaction pathway involves the identification of two distinct intermediates, each exhibiting favourable thermodynamic feasibility. The ΔG for the formation of the first intermediate (**Int-1**) from the reactants is calculated to be **-52.7 kcal/mol**, while the subsequent formation of the second intermediate (**Int-2**) from the first displays a lower energy demand at **-4.2 kcal/mol** . Subsequently, the generation of **V** from the second intermediate is also exergonic, as indicated by a ΔG value of **-17.7 kcal/mol** (Figure 5.3).

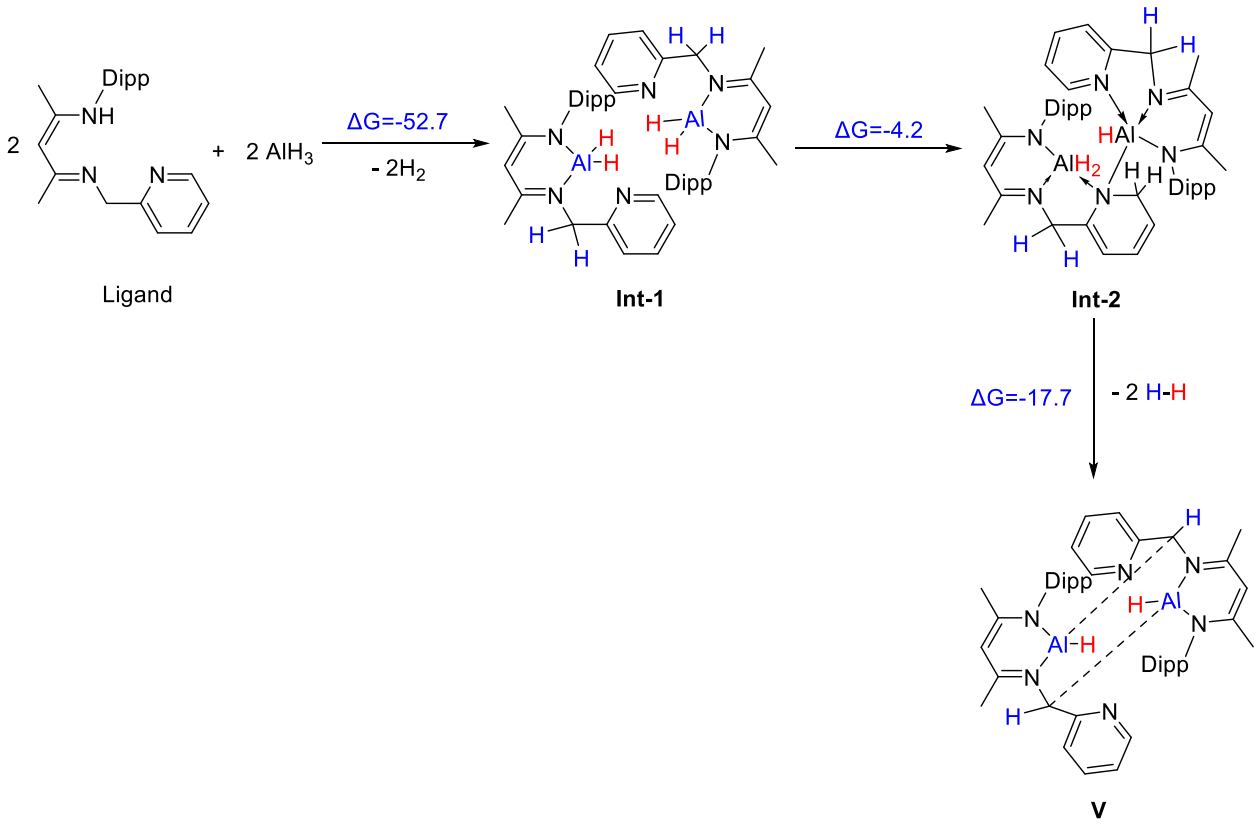

Figure 5.3 Thermodynamics of the mechanistic pathway computed at the PBE-D3/TZVP (Solvent=Toluene) level of theory. All the free energy values are in kcal/mol.

5.2.4 Synthesis and characterization of 5.3 and 5.4

After successfully isolating the monomeric aluminium hydride complex, we aimed to synthesize tridentate nacnac-supported aluminium and gallium halide complexes. The reaction of the ligand with benzyl potassium, followed by the addition of the metal halide ECl_3 (E = Al, Ga) in toluene, yielded the heteroleptic metal halides **5.3** and **5.4** smoothly (Scheme 5.4). Notably, the synthesis of these tridentate nacnac-supported metal halides was not successful with other bases, such as MeLi, KO*t*Bu, KHMDS, or LiHMDS. The crystals of **5.3** and **5.4** suitable for single-crystal X-ray diffraction were obtained from a saturated toluene solution at –4 °C after one week. The formation of aluminium chloride complex **5.3** was confirmed by comparing its unit cell and NMR spectroscopy data with those reported earlier for a similar complex synthesized via transmetallation with germylene chloride.[22] The molecular structure of gallium chloride complex **5.4** is shown in Figure 5.4.

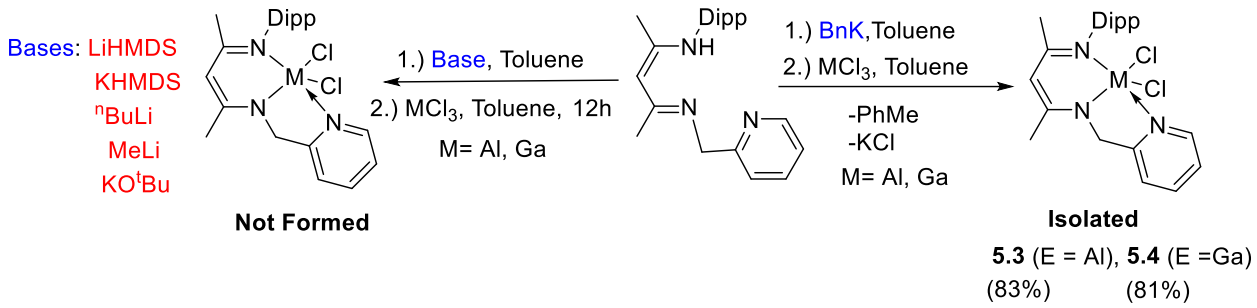

Scheme 5.4 Synthesis of metal halide complexes **5.3** and **5.4**.

The solid-state structure of **5.4** reveals a Ga1–N1 bond length of 2.147(11) Å, which is longer than the Ga1–N2 and Ga1–N3 bond lengths of 1.961(11) Å and 2.013(4) Å, respectively confirming the coordinate character of Ga–$N_{pyridine}$ bond. The ^{1}H NMR spectrum exhibit a characteristic resonance at 3.22 ppm, corresponding to the CH proton of the isopropyl group, as well as signals at 5.15 ppm and 4.89 ppm, attributed to the backbone CH proton and the methylene (CH_2) group, respectively (See Figure A41).

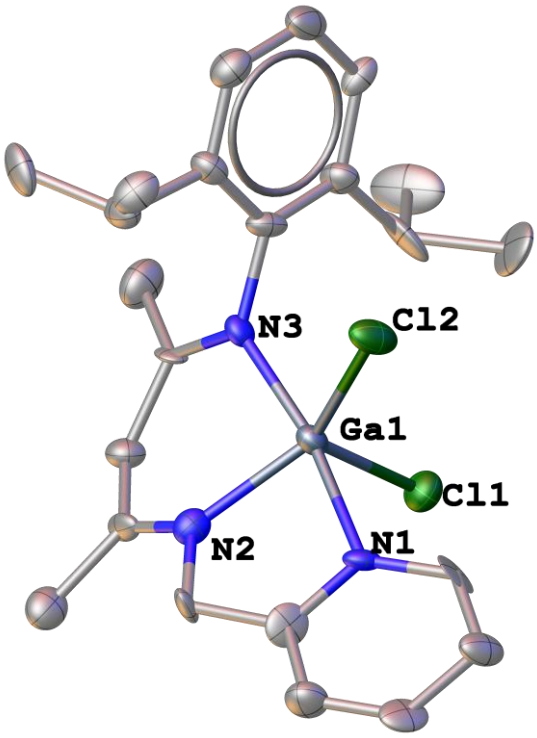

Figure 5.4 The molecular structure of **5.4** with anisotropic displacement parameters depicted at the 50% probability level. Hydrogen atoms are not shown for clarity. Selected bond lengths (Å) and bond angles (°): Ga1–N1 2.147(11), Ga1–N2 1.967(11), Ga1–N3 2.013(4), Ga1–Cl1 2.218(4), Ga1–Cl2 1.240(4); N1–Ga1–N3 168.8(4), N1–Ga1–N2 79.0(4), N2–Ga1–N3 92.2(4).

5.3 Conclusions

In summary, the influence of solvent on the stability of tridentate nacnac-supported aluminium hydride was investigated, leading to the successful isolation and characterization of the monomeric aluminium hydride complex, **5.1**. Additionally, the intermediate aluminium hydride complex, **5.2**, was also isolated. Furthermore, a novel synthetic method was developed for the preparation of complexes **5.3** and **5.4**, which could not be achieved using standard salt elimination reaction.

5.4 References

1. P. P. Power, *Nature,* 2010, **463**, 171–177; (b) S. Harder, *Chem. Rev.,* 2010, **110**, 3852–3876.
2. G. I. Nikonov, *ACS Catal.*, 2017, **7**, 7257–7266.
3. N. O. Calloway, *Chem. Rev.,* 1935, **17**, 327–392; (b) M. Rueping, B. J. Nachtsheim, *Beilstein J. Org. Chem.,* 2010, **6**, DOI: 10.3762/bjoc.6.6.; (c) M. M. Heravi, V. Zadsirjan, P. Saedi, T. Momeni, *RSC Adv.,* 2018, **8**, 40061–40163.
4. S.-I. Orimo, Y. Nakamori, J. R. Eliseo, A. Züttel, C. M. Jensen, *Chem. Rev.,* 2007, **107**, 4111–4132.
5. R. Zidan, B. L. Garcia-Diaz, C. S. Fewox, A. C. Stowe, J. R. Gray, A. G. Harter, *Chem. Commun.,* 2009, 3717–3719.
6. M. D. Francis, D. E. Hibbs, M. B. Hursthouse, C. Jones, N. A. Smithies, *J. Chem. Soc., Dalton Trans.,* 1998, 3249–3254.
7. R. J. Baker, M. L. Cole, C. Jones, M. F. Mahon, *J. Chem. Soc., Dalton Trans.,* 2002, 1992–1996.
8. S. Singh, H. W. Roesky, *J. Fluorine Chem.,* 2007, **128**, 369–372.
9. O. Stecher, E. Wiberg, *Ber. deut. chem.* Gesellschaft (A and B Series), 1942, **75**, 2003–2012.
10. J. K. Ruff, M. F. Hawthorne, *J. Am. Chem. Soc.,* 1960, **82**, 2141–2144.
11. (a) A. J. Downs, C. R. Pulham, *Chem. Soc. Rev.,* 1994, 175; (b) M. G. Gardiner, C. L. Raston, *Coord. Chem. Rev.,* 1997, **166**, 1–34; (c) C. Jones, G. A. Koutsantonis, C. L. Raston, *Polyhedron,* 1993, **12**, 1829; (d) S. Aldridge, A. J. Downs, *Chem. Rev.,* 2001, **101**, 3305; (e) C. L. Raston, *J. Organomet. Chem.,* 1994, **475**, 15.
12. For synthesis and reactions of β-diketiminate stabilized dihydrides see: (a) N. Kuhn, S. Fuchs, M. Steimann, *Z. Anorg. Allg. Chem.,* 2000, **626**, 1387–1392; (b) C. Cui, H. W. Roesky, H. Hao, H.-G. Schmidt, M. Noltemeyer, *Angew. Chem., Int. Ed.,* 2000, **39**, 1815–1817; (c) B. Twamley, N. J. Hardman, P. P. Power*, Acta Crystallogr., Sect. E: Struct. Rep. Online.,* 2001, **57**, 1227; (d) H. Zhu, Z. Yang, J. Magull, H. W. Roesky, H.-G. Schmidt, M. Noltemeyer, *Organometallics,* 2005, **24**, 6420–6425; (e) S. Singh, H.-J. Ahn, A. Stasch, V. Jancik, H. W. Roesky, A. Pal, M. Biadene, R. Herbst-Irmer, M. Noltemeyer, H.-G. Schmidt, *Inorg. Chem.,* 2006, **45**, 1853–1860; (f) S. González-

Gallardo, V. Jancik, R. Cea-Olivares, R. A. Toscano, M. Moya-Cabrera, *Angew. Chem., Int. Ed.,* 2007, **46**, 2895 –2898; (g) W. Uhl, B. Jana, *Chem. Eur. J*., 2008, **14**, 3067–3071; (h) C. Chen Hui, Y. Ying, Z. Hong Ping, *Sci. China Chem.,* 2010, **53**, 1970; (i) S. Harder, J. Spielmann, *Chem. Commun.,* 2011, **47**, 11945 –11947; (j) X. Ma, Z. Yang, X. Wang, H. W. Roesky, F. Wu, H. Zhu, *Inorg. Chem.,* 2011, **50**, 2010–2014; (k) Z. Yang, P. Hao, Z. Liu, X. Ma, H. W. Roesky, K. Sun, J. Li, *Organometallics,* 2012, **31**, 6500 –6503; (l) I. M. Riddlestone, S. Edmonds, P. A. Kaufman, J. Urbano, J. I. Bates, M. J. Kelly, A. L. Thompson, R. Taylor, S. Aldridge, *J. Am. Chem. Soc.,* 2012, **134**, 2551–2554; (m) P. Hao, Z. Yang, X. Ma, X. Wang, Z. Liu, H. W. Roesky, K. Sun, J. Li, M. Zhong, *Dalton Trans.,* 2012, 13520–13524; (n) I. M. Riddlestone, J. Urbano, N. Phillips, M. J. Kelly, D. Vidovic, J. I. Bates, R. Taylor, S. Aldridge, *Dalton Trans.,* 2013, **42**, 249–258; (o) S. González-Gallardo, A. S. Cruz-Zavala, V. Jancik, F. Cortés-Guzmán, M. Moya-Cabrera, *Inorg. Chem.,* 2013, 52, 2793–2795.

13. For synthesis and reactions of guanidinate and amidinate stabilized dihydrides see: (a) M. L. Cole, C. Jones, P. C. Junk, M. Kloth, A. Stasch, *Chem. Eur. J.,* 2005, **11**, 4482-4491; (b) S. J. Bonyhady, D. Collis, G. Frenking, N. Holzmann, C. Jones, A. Stasch, *Nat. Chem.,* 2010, **2**, 865–869.
14. (a) H. V. R. Dias, W. Jin, R. E. Ratcliff, *Inorg. Chem.,* 1995, **34**, 6100-6105; (b) A. E. Nako, S. J. Gates, A. J. P. White, M. R. Crimmin, *Dalton Trans.,* 2013, **42**, 15199–15206; (c) S. Yow, S. J. Gates, A. J. P. White, M. R. Crimmin, *Angew. Chem., Int. Ed.,* 2012, **51**, 12559–12563.
15. (a) G. C. Welch, W. E. Piers, M. Parvez, R. McDonald, *Organometallics,* 2004, **23**, 1811–1818; (b) J. D. Masuda, D. M. Walsh, P. Wei, D. W. Stephan, *Organometallics,* 2004, **23**, 1819–1824.
16. (a) R. J. Wehmschulte, J. J. Ellison, K. Ruhlandt-Senge, P. P. Power, *Inorg. Chem.,* 1994, **33**, 6300-6306; (b) C. Eaborn, S. M. El-Hamruni, M. S. Hill, P. B. Hitchcock, M. Hopman, A. Le Gouie, J. D. Smith, *J. Organomet. Chem.,* 2000, **597**, 3-9; (c) S. Bensiek, M. Bangel, B. Neumann, H.-G. Stammler, P. Jutzi, *Organometallics,* 2000, **19**, 1292–1298; (d) D. T. Carey, F. S. Mair, R. G. Pritchard, J. E. Warren, R. J. Woods, *Dalton Trans.,* 2003, 3792-3798; (e) J. L. Atwood, S. M. Lawrence, C. L. Raston, *J. Chem. Soc., Chem. Commun.,* 1994, 73.

17. Z. Yang, M. Zhong, X. Ma, S. De, C. Anusha, P. Parameswaran, H. W. Roesky, *Angew. Chem., Int. Ed.,* 2015, **54**, 10225–10229.
18. Y. L. Lien, Y. C. Chang, N. T. Chuang, A. Datta, S. J. Chen, C. H. Hu, W. Y. Huang, C. H. Lin, J. H. Huang, *Inorg. Chem.,* 2010, **49**, 136-143.
19. (a) P. Andrews, C. M. Latham, M. Magre, D. Wilcox, S. Woodward, *Chem. Commun.,* 2013, **49**, 1488-1490; (b) M. Lautens, P. Chiu, S. Ma, T. Rovis, *J. Am. Chem. Soc.,* 1995, **117**, 532-533.
20. D. Franz, E. Irran, S. Inoue, *Dalton Trans.,* 2014, **43**, 4451–4461.
21. S. Pahar, G. Kundu, C. P. George, R. G. Gonnade, S. S. Sen, *Organometallics,* 2023, **42**, 276−282.
22. S. Pahar, V. S. V. S. N. Swamy, T. Das, R. G. Gonnade, K. Vanka, S. S. Sen, *Chem. Commun.,* 2020, **56**, 11871 – 11874.

Appendix: Experimental details, crystallographic data and spectral details

6.1 General Experiment Details

6.2 Chapter 2 experimental details

6.2.1 Synthesis and characterization of compound **2.1**

6.2.2 Synthesis and characterization of compounds **2.2**

6.2.3 Synthesis and characterization of compounds **2.3** and **2.5**.

6.2.4 Synthesis and characterization of compounds **2.4** and **2.6**.

6.2.5 Synthesis of compounds **2.7.**

6.2.6 Crystallographic data for the structural analysis of compounds **2.1-2.6**

6.2.7 EPR studies.

6.2.8 Cyclic Voltametric analysis.

6.2.9 Magnetism data analysis.

6.2.10 Details of theoretical calculations.

6.3: Chapter 3 experimental details

6.3.1 Synthesis and characterization of compound **3.1**.

6.3.2 Synthesis and characterization of compounds **3.2**.

6.3.3 Synthesis and characterization of compounds **3.3** and **3.4**

6.3.4 Synthesis and characterization of compounds **3.5**.

6.3.5 Synthesis and characterization of compounds **3.6**.

6.3.6 Crystallographic data for the structural analysis of compounds **3.1**-**3.3** and **3.5, 3.6**.

6.4: Chapter 4 experimental details

6.4.1 Synthesis and characterization of compound **4.1** and **4.2**.

6.4.2 Synthesis and characterization of compounds **4.3**.

6.4.3 Synthesis and characterization of compounds **4.4**.

6.4.4 Crystallographic data for the structural analysis of compounds **4.1**-**4.3**.

6.5: Chapter 5 experimental details

6.5.1 Synthesis and characterization of compound **5.1**.

6.5.2 Synthesis and characterization of compounds **5.2**.

6.5.3 Synthesis and characterization of compounds **5.3**.

6.5.4 Synthesis and characterization of compounds **5.4**

6.5.5 Crystallographic data for the structural analysis of compounds **5.1**, **5.2** and **5.4**.

6.1: General experiment details

All manipulations and experiments including NMR sample preparation were carried out under an inert atmosphere of argon applying standard Schlenk techniques or in a Glove-box. The solvents used were purified by an MBRAUN solvent purification system as MB SPS-800. All chemicals purchased from Sigma Aldrich and TCI Chemicals were used without further purification. Ligand **LH** was prepared according to the literature procedure. [S1] The ^{1}H, ^{2}H, and ^{13}C NMR spectra were recorded in C_6D_6 and $CDCl_3$ using a Bruker Avance DPX 400 or a Bruker Avance DRX 500 spectrometer and were referenced to external $SiMe_4$. The HRMS and LC-mass spectra were obtained using a Q Exactive Thermo Scientific and an Agilent Technologies 6120. Melting points were measured in a sealed glass tube on a Stuart SMP-30 melting point apparatus and were uncorrected. The IR data were recorded using a Bruker Alpha II FTIR Spectrophotometer.

6.2: Chapter 2 experimental details

6.2.1. Synthetic procedure and characterization data of (2.1): The toluene solution of $KSi(SiMe_3)_3$ (0.469 g, 1.08 mmol) was slowly added to a stirred solution of **1** (0.457 g, 1.03 mmol) in toluene (10 mL) at –78 °C over a period of 10 min. The pale-yellow color of the solution was changed to intense red with the addition. The solution was warmed to room temperature and stirred for 6 h. All volatiles were removed under reduced pressure and extracted with a mixture of hexane (10 mL) and toluene (3 mL). The solvent was reduced to 5 mL and stored at –30 °C in a freezer to obtain the red crystals of **2.1** suitable for X-ray analysis. Yield: 0.387 g (92 %). Mp: 196.5 °C. HRMS: Calcd: 406.1799, found: [m/z] 406.1783. NMR: No NMR resonance has been observed due to the paramagnetic behaviour of compound **2.1**.

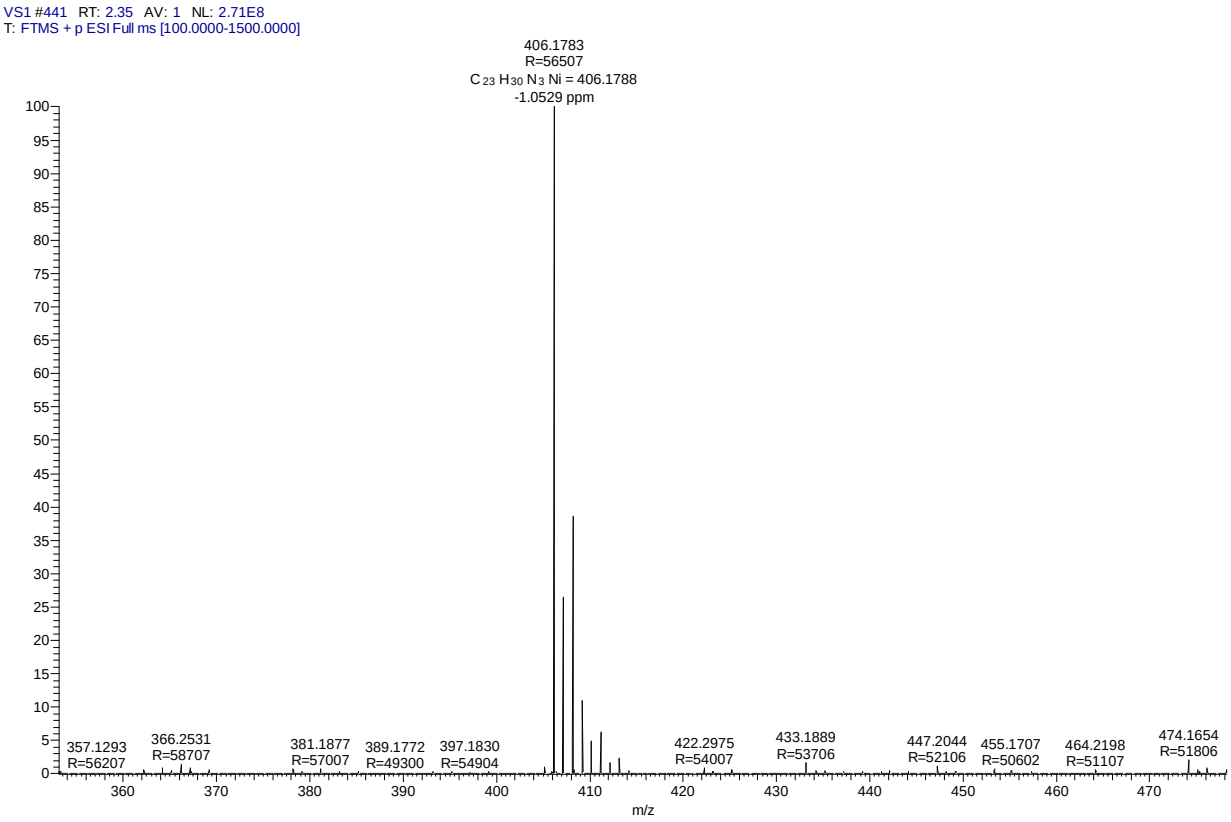

Figure A1. HRMS of **2.1**

6.2.2. Synthesis and characterization of compound 2.2: Toluene (20 mL) was added to a mixture of **1** (0.450 g, 1 mmol), $KSi(SiMe_3)_3$ (0.453 g, 1.05 mmol) and TEMPO (0.167 g, 1.05 mmol) at –78 °C. The solution turned red at low temperature and slowly warmed to room temperature. The reaction was further stirred for another 4 h until the color of the solution changed to yellowish brown. All volatiles were removed under reduced pressure and extracted with a mixture of hexane (10 mL) and toluene (3 mL). The solution was reduced to 5 mL and stored at –30 °C in a freezer to obtain the yellow crystals of **2.2** suitable for X-ray analysis. Yield: 0.440 g (78%). Mp: 211.3 °C. NMR: ^{1}H NMR (500 MHz, $CDCl_3$, 298K): δ 8.89 (d, J = 5.8 Hz, 1H), 7.60 (t, J = 7.6 Hz, 1H), 7.13 (d, J = 7.4 Hz, 2H), 7.03 (d, J = 7.5 Hz, 3H), 4.89 (s, 1H), 4.73 (s, 2H), 3.96 – 3.82 (m, 2H), 2.11 (s, 3H), 1.65 (d, J = 6.8 Hz, 6H), 1.48 (s, 3H), 1.27 (s, 12H), 1.18 (d, J = 6.9 Hz, 6H), 0.89 (s, 6H) ppm. ^{13}C NMR (101 MHz, $CDCl_3$, 298K) δ 162.2 (s), 160.8 (s), 157.8 (s), 151.7 (s), 142.0 (s), 137.2 (s), 125.2 (s), 122.8 (s), 122.1 (s), 118.4 (s), 98.5 (s), 61.7 (s), 31.7 (s), 28.7 (s), 24.6 (s), 24.4 (s), 24.1 (s), 22.7 (s), 21.5 (s), 14.1 (s) ppm. HRMS: Calcd: 562.3182, found [M-1]: 561.3091.

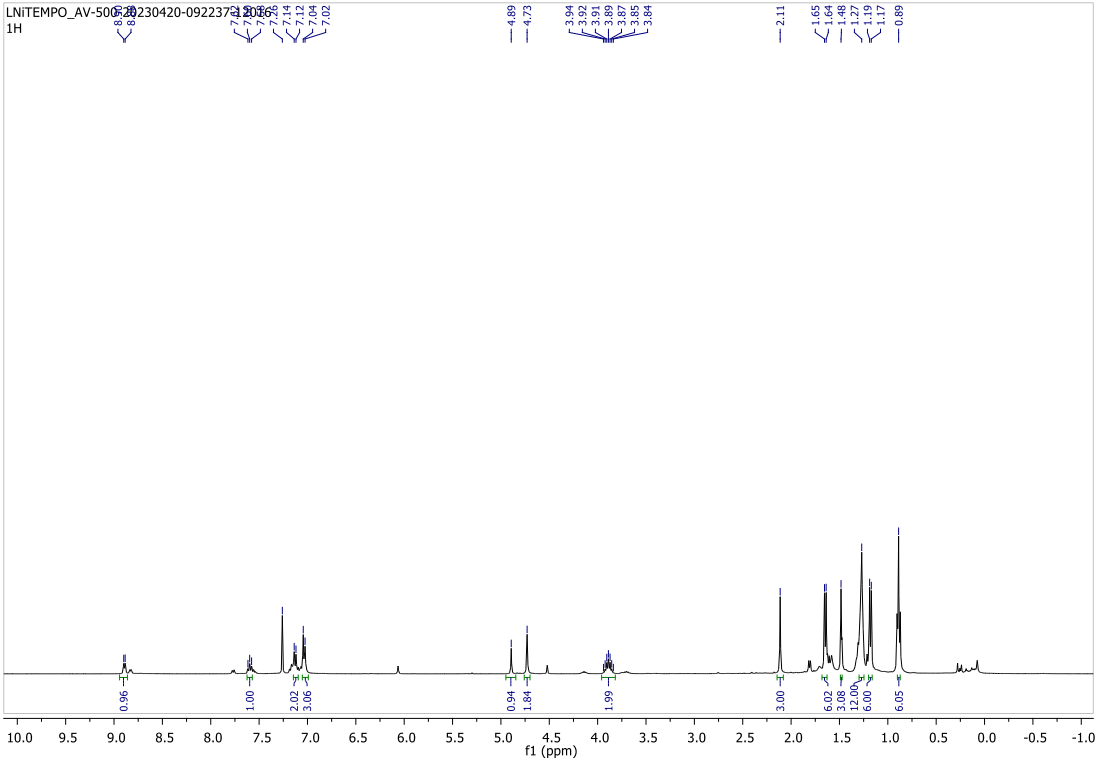

Figure A2. ^{1}H NMR of **2.2**

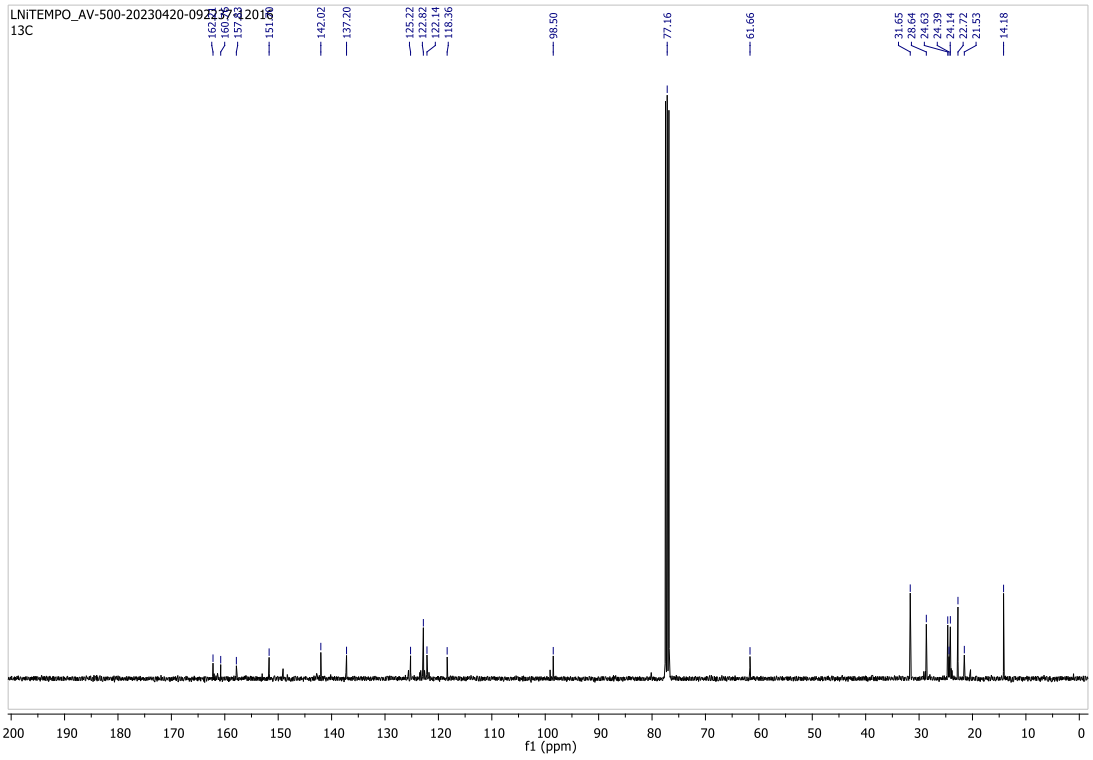

Figure A3. ^{13}C NMR of **2.2**

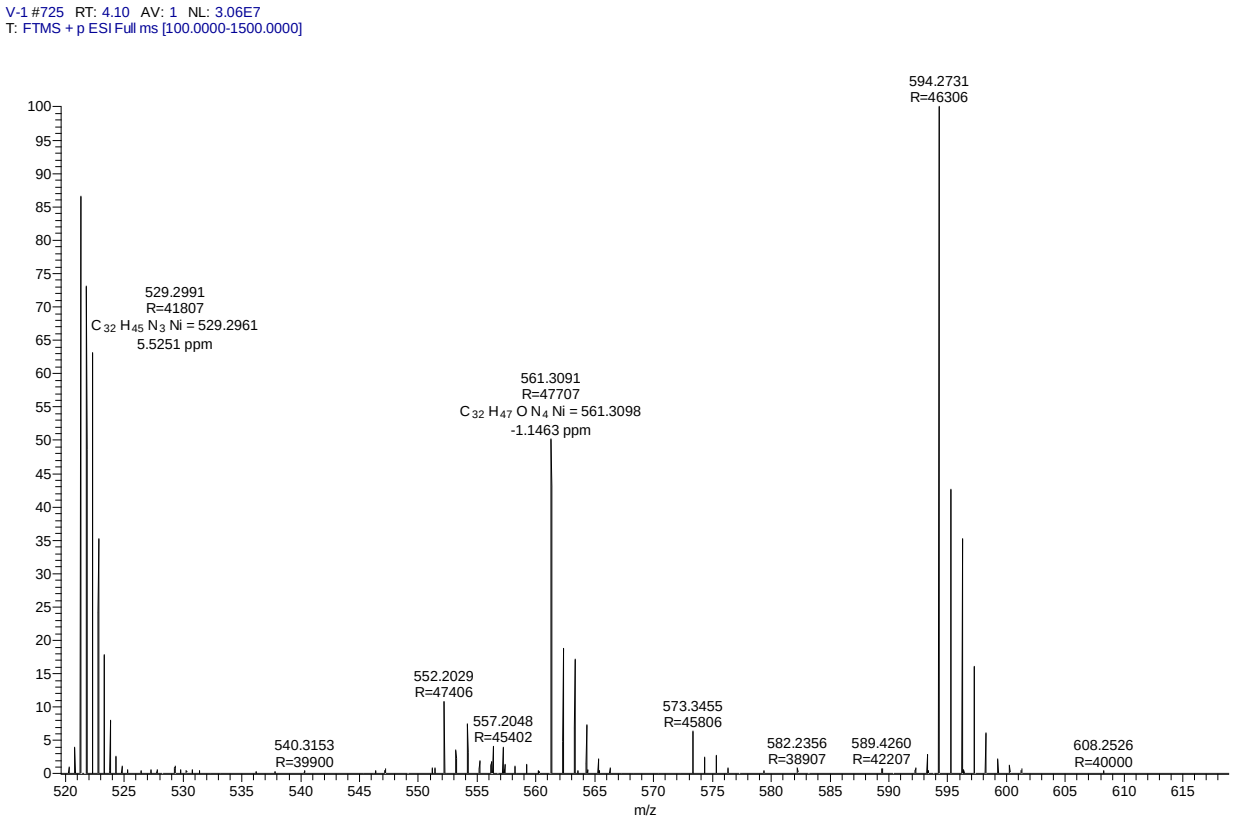

Figure A4. HRMS of **2.2**

6.2.3: Synthesis and characterization of compounds 2.3 and 2.5: The toluene solution of Ph_2S_2 (0.120 g, 0.56 mmol) was slowly added to a stirred solution of **2.1** (0.457 g, 1 mmol) in toluene (10 mL) at –78 °C over a period of 5 min. The solution was warmed to room temperature and stirred for 12 h. All volatiles were removed under reduced pressure and extracted with a mixture of hexane (10 mL) and toluene (5 mL). The solvent was reduced to 5 mL and stored at –30 °C in a freezer to obtain the red crystals of **2.3** suitable for X-ray analysis. Yield of **2.3**: 0.360 g (67 %). The excess amount of Ph_2S_2 leads to the formation of a mixture of **2.3** and **2.5**. The suitable crystals for X-ray analysis of compound **2.5** were isolated and mounted from a mixture of **2.3** and **2.5** of a toluene and hexane mixture. NMR for compound **2.3**: ^{1}H NMR (400 MHz, $CDCl_3$, 298K) δ 9.12 (d, J = 5.8 Hz, 1H), 8.13 (d, J = 7.2 Hz, 2H), 7.34 (t, J = 8.3 Hz, 1H), 7.17 – 7.13 (m, 1H), 7.07 (d, J = 7.3 Hz, 2H), 6.93 (d, J = 7.8 Hz, 1H), 6.75 (t, J = 7.5 Hz, 2H), 6.69 – 6.64 (m, 2H), 4.91 (s, 1H), 4.81 (s, 2H), 3.95 (hept, J = 6.9 Hz, 1H), 2.15 (s, 3H), 1.57 (d, J = 6.8 Hz, 6H), 1.54 (s, 3H), 1.18 (d, J = 6.9 Hz, 6H) ppm. ^{13}C NMR (101 MHz, $CDCl_3$, 298K) δ 162.4 (s), 160.3 (s), 158.0 (s), 153.1 (s), 149.3 (s), 142.7 (s), 136.2 (s), 132.6 (s), 126.7 (s), 125.6 (s), 122.9 (s), 122.3 (s), 121.4 (s), 118.0 (s), 97.4 (s), 61.2

(s), 28.7 (s), 24.8 (s), 24.4 (s), 21.5 (s) ppm. HRMS for compound **2.3**: Calcd: 515.1905, Found [M-1]: 514.1816.

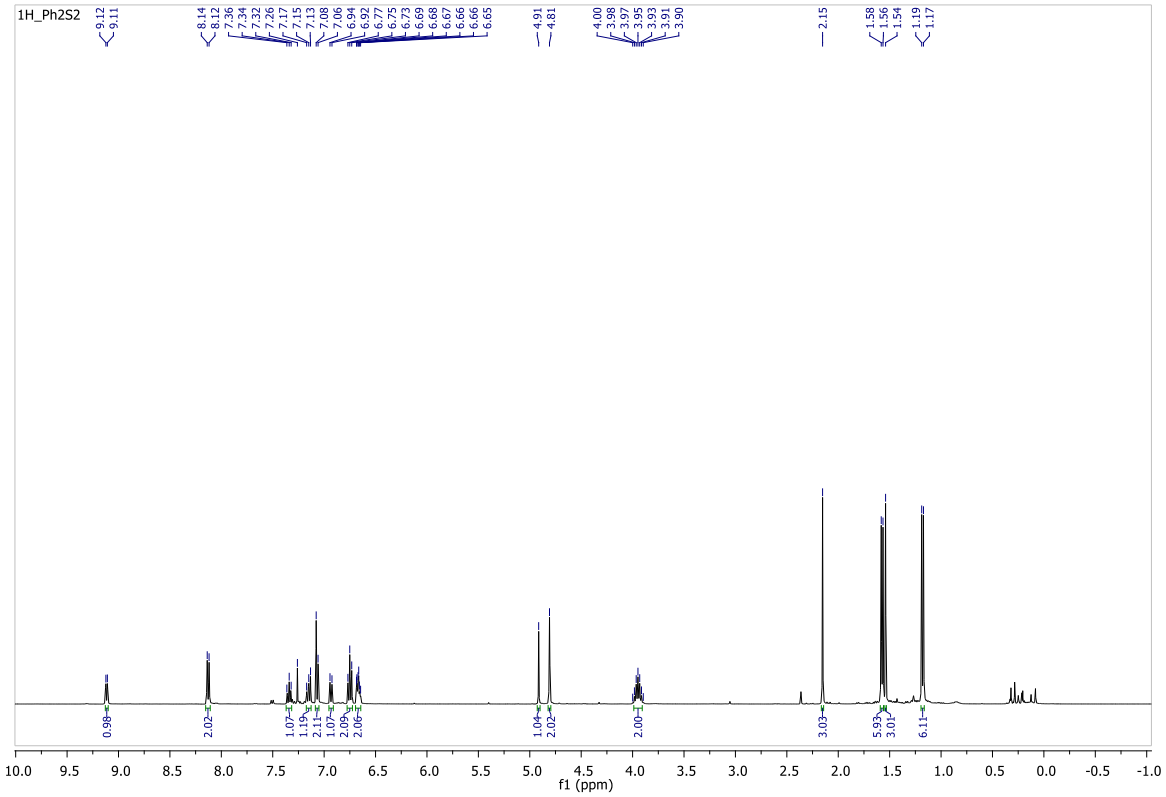

Figure A5. ^{1}H NMR of **2.3**

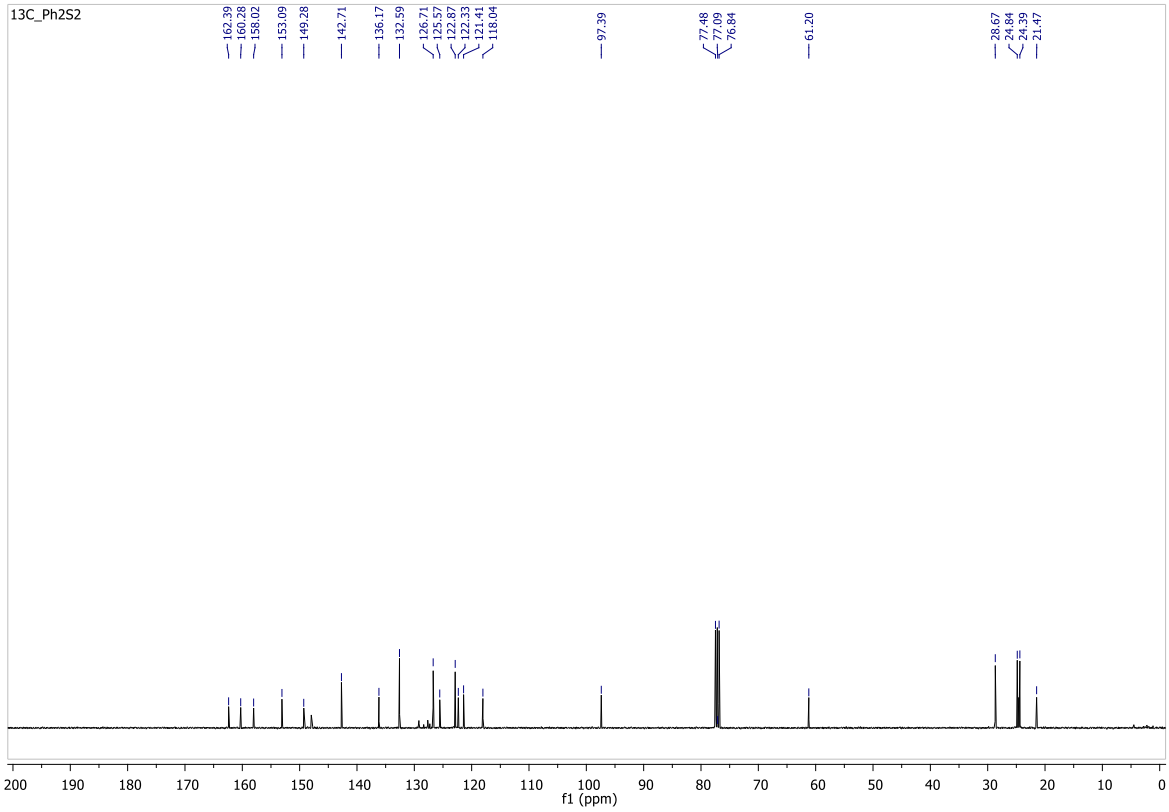

Figure A6. ^{13}C NMR of **2.3**

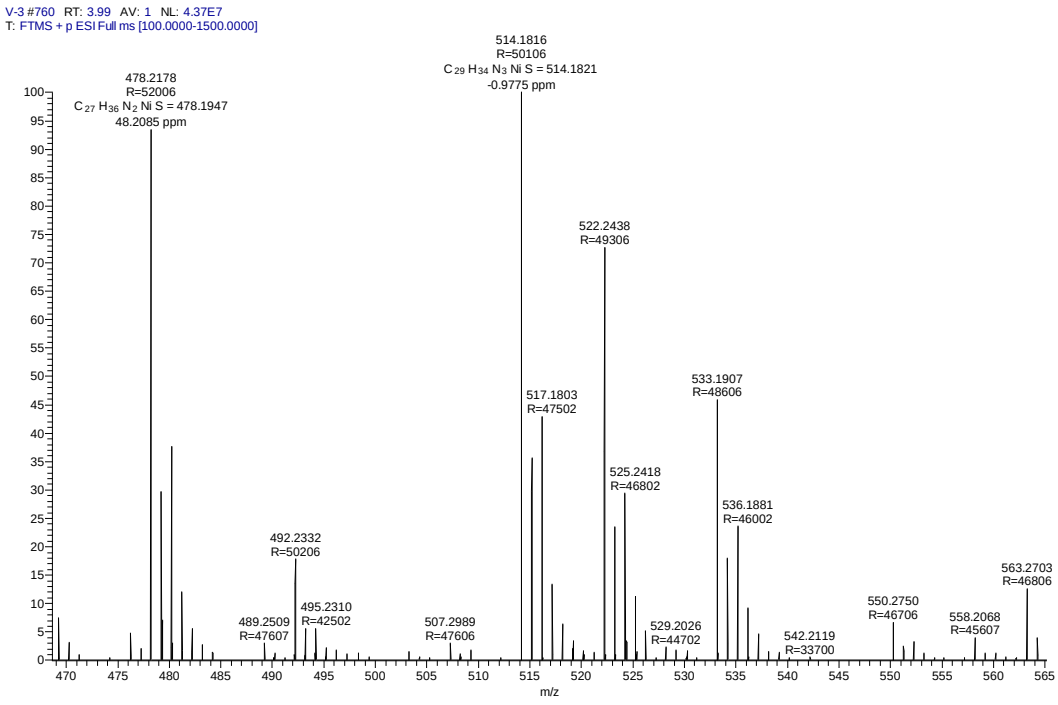

Figure A7. HRMS of **2.3**

NMR for compound **2.5**: We isolated a single crystal of **2.5** to mount and characterized it crystallographically. We didn't get any clean NMR to integrate with its proper values, due to the low-solubility of the solid mixture of both the two compounds (**2.3** and **2.5**) in most of the organic solvents. HRMS: Compound **2.5** is easily fragmented into compound **2.3**, hence we didn't observe the HRMS for compound **2.5**. However, we have measured the IR for compound **2.5**.

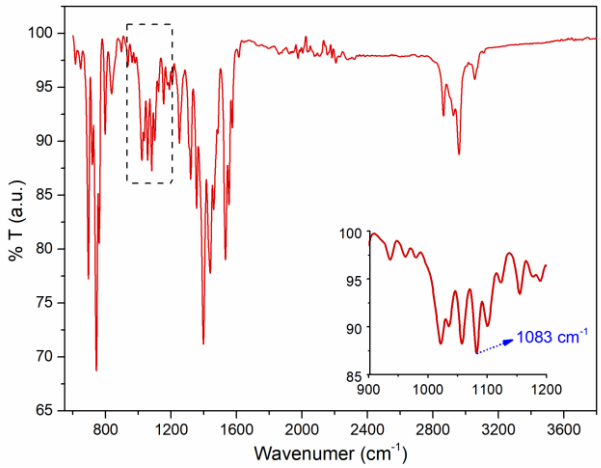

Figure A8. FTIR (ATR) for compound **2.5**.

6.2.4: Synthesis and characterization of compounds 2.4 and 2.6: The toluene solution of Ph_2Se_2 (0.370 g, 1.2 mmol, Toluene 10 mL) was slowly added to a stirred toluene solution of **2.1** (0.450 g, 1.10 mmol) at –78 °C over a period of 5 min. The solution was warmed to room temperature and stirred for 8 h. All volatiles were removed under reduced pressure and extracted with a mixture of hexane (10 mL) and toluene (5 mL). The solvent was reduced to 5 mL and stored at –30 °C in a freezer to obtain the mixture of two types of crystals of **2.4** and **2.6** suitable for X-ray analysis. Yield of a mixture of compound **2.4** and **2.6:** 0.309 g (49 %). NMR for the mixture of compounds **2.4** and **2.6:** ^{1}H NMR (400 MHz, $CDCl_3$, 298K): δ 9.14 (d, J = 5.5 Hz, 0.33H), 8.89 (d, J = 6.0 Hz, 1H), 7.97 (s, 0.71H), 7.74 (d, J = 6.9 Hz, 0.79H), 7.59 (s, 2H), 7.44 (d, J = 11.7 Hz, 1H), 7.12 (d, J = 7.2 Hz, 2H), 7.09 (s, 0.5H), 7.03 (d, J = 7.4 Hz, 3H), 6.90 (d, J = 7.7 Hz, 0.45H), 6.69 (dd, J = 17.1, 7.3 Hz, 1H), 6.49 (t, J = 6.4 Hz, 0.36H), 4.89 (s, 1H), 4.85 (s, 1H), 4.72 (s, 2H), 4.09 – 4.02 (m, 1H), 3.88 (dd, J = 13.7, 6.9 Hz, 2H), 2.14 (s, 1H), 2.11 (s, 3H), 1.67 (s, 2H), 1.63 (s, 6H), 1.52 (s, 1H), 1.48 (s, 3H), 1.19 (s, 3H), 1.17 (s, 3H) ppm. ^{13}C NMR (101 MHz, $CDCl_3$, 298K) δ 162.3 (s), 160.8 (s), 157.9 (s), 151.8 (s), 142.1 (s), 137.2 (s), 136.6 (s), 131.7 (s), 130.1 (s), 129.3 (s), 127.9 (s), 125.3 (s), 122.9 (s),

122.2 (s), 118.4 (s), 98.6 (s), 61.7 (s), 28.7 (s), 24.7 (s), 24.5 (s), 24.2 (s), 21.6 (s) ppm. ^{77}Se NMR (76 MHz, $CDCl_3$, 298K) δ 652.55, 462.63, 317.41 ppm. HRMS: Calcd: 563.1350, Found [M-1]: 562.1254 (due to the fragmentation of compound **2.6**, we have only observed the molecular ion peak for monomeric compound **2.4**).

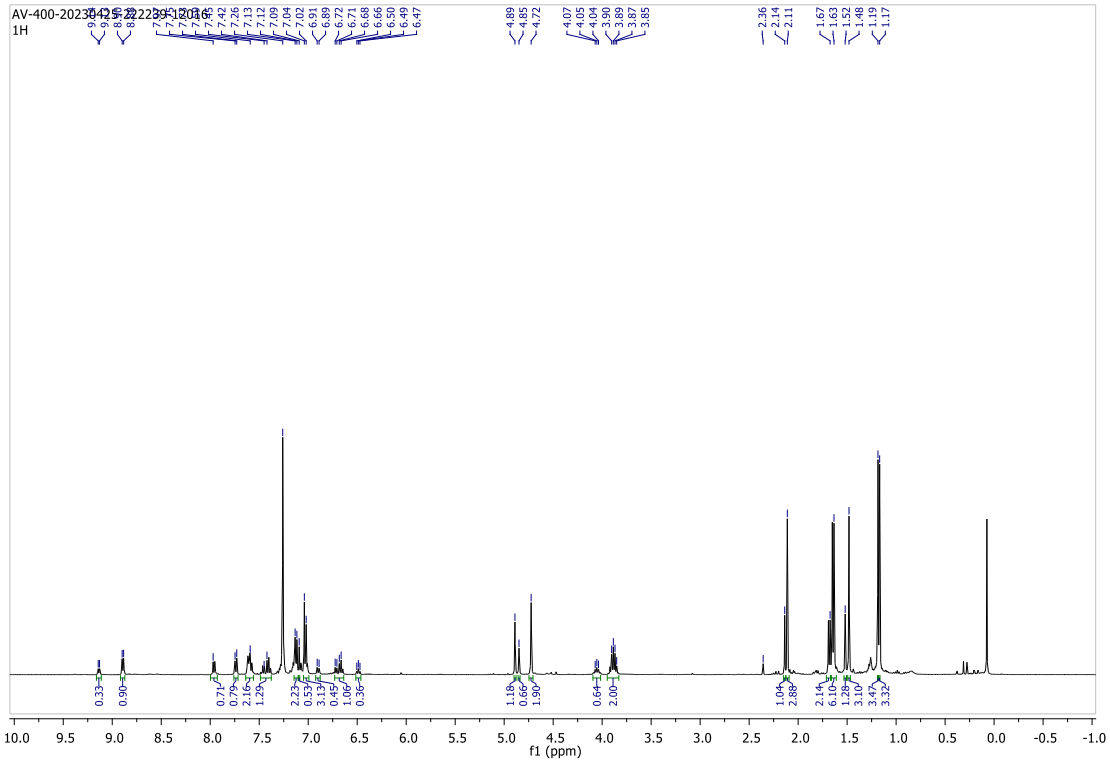

Figure A9. ^{1}H NMR of a mixture of compounds **2.4** and **2.6**

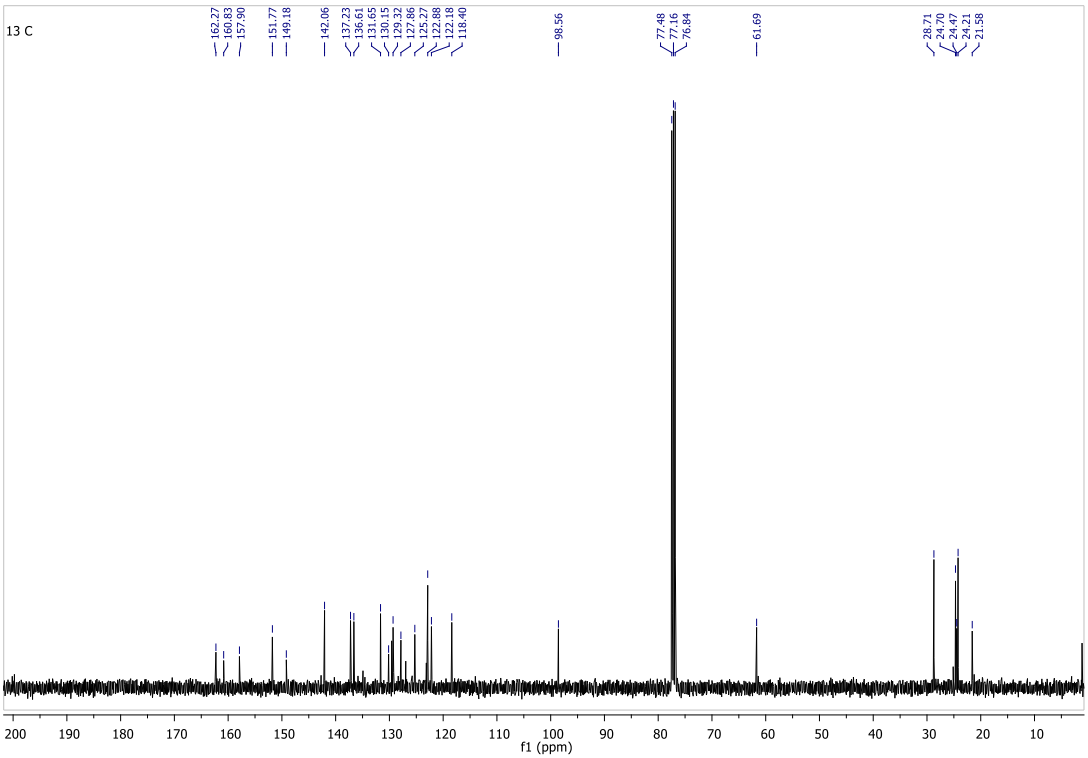

Figure A10. ^{13}C NMR of mixture of compound **2.4** and **2.6**

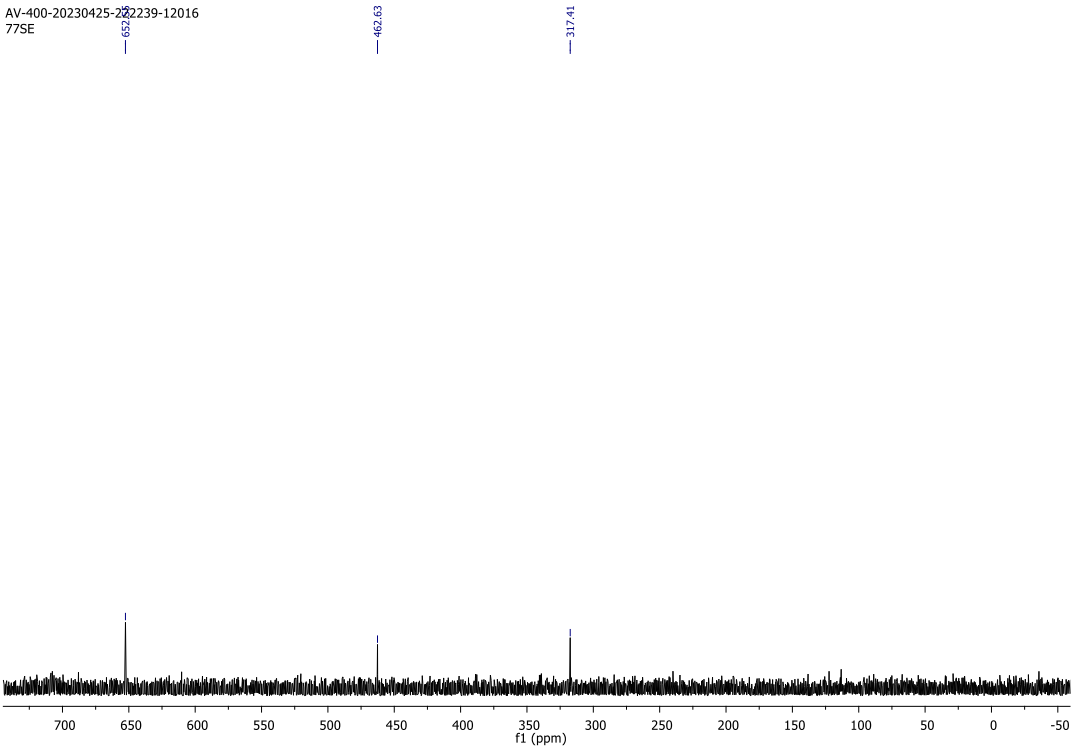

Figure A11. ^{77}Se NMR of mixture of compound **2.4** and **2.6**

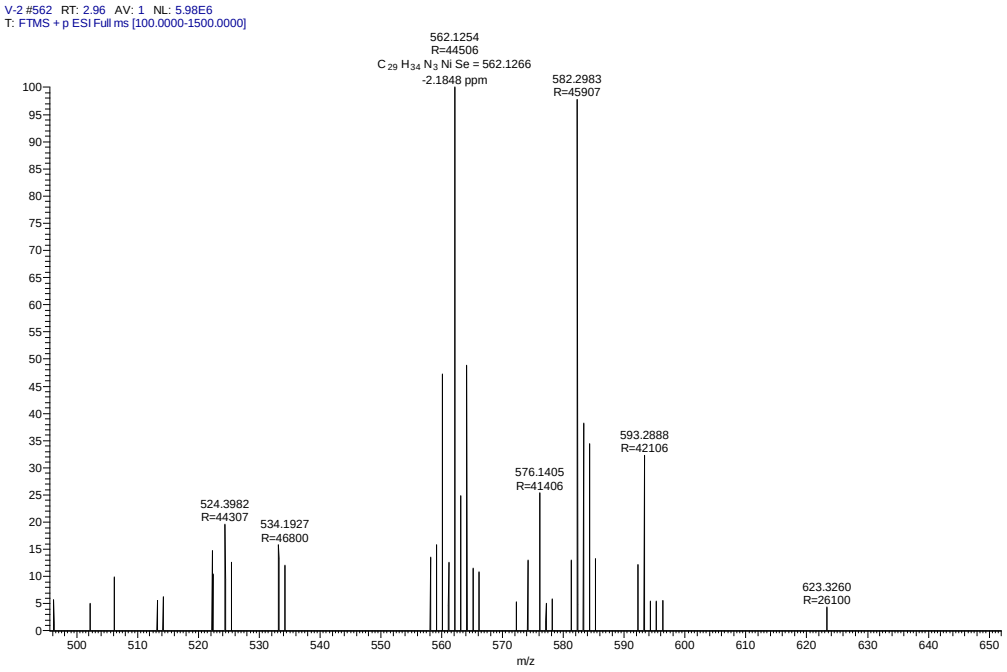

Figure A12. HRMS of **2.4**

6.2.5: Synthesis of 2.7: The 10 mL toluene solution of compound **2.1** (0.1 g, 0.24 mmol) was stirred in the presence of dihydrogen for 3 h at room temperature. The reaction mixture was dried under reduced pressure. The ^{1}H NMR spectrum of the crude gives a characteristic peak at –22.73 ppm and confirms the formation of the previously reported same nickel hydride complex **2.7**.[S1]

6.2.6: Crystallographic data for the structural analysis of compounds 2.1-2.6

Crystal data of compound 2.1: $C_{23}H_{30}N_3Ni$**,** M = 407.19, CCDC: 2271416, Red, block, 0.31 x 0.19 x 0.12 mm^3, triclinic, space group '*P-1'*, *a = 8.339(7)Å, b = 15.952(13)Å, c = 17.977(17)Å*, α = 115.99(3)°, β = 90.74(3)°, γ = 96.15(3)°, Volume = 2132(3)Å^3, Z = 2, *T* = 161(2) K, D_{calc} (g cm^{-3}) = 0.459, *F*(*000*) = 280, μ (mm^{-1}) = 1.807, 132211 reflections collected, 11012 unique reflections (R_{int}= 0.0725), 8139 observed ($I > 2\sigma$ (I)) reflections, multi-scan absorption correction, T_{min} = 0.649, T_{max} = 0.745, 499 refined parameters, *S* = 1.091, *R*1 = 0.0728, *wR*2 = 0.1387 (all data *R* = 0.1070, *wR*2 = 0.1523), maximum and minimum residual electron densities; $\Delta\rho_{max}$ = 0.84, $\Delta\rho_{min}$= -0.88 (eÅ^{-3}).

Crystal data of compound 2.2: $C_{39}H_{56}N_4NiO$**,** M = 655.57, CCDC: 2271420, Yellow,, block, 0.22 × 0.18 × 0.11 mm^3, monoclinic, space group '$P2_1/c$', *a = 11.3431(16)Å, b = 14.1925(17)Å, c = 21.929(3)Å*, α = 90°, β = 90.498(5)°, γ = 90°, Volume = 3530.1(8)Å^3, Z = 4, *T* = 100(2) K, D_{calc} (g cm^{-3}) = 1.234, *F*(*000*) = 1416, μ (mm^{-1}) = 0.585, 33710 reflections

collected, 6232 unique reflections (R_{int}= 0.0875), 3847 observed ($I > 2\sigma(I)$) reflections, multi-scan absorption correction, T_{min} = 0.297, T_{max} = 0.500, 417 refined parameters, S = 1.043, $R1$ = 0.0875, $wR2$ = 0.1950 (all data R = 0.1479, $wR2$ = 0.2278), maximum and minimum residual electron densities; $\Delta\rho_{max}$ = 1.20, $\Delta\rho_{min}$= -0.94(eÅ^{-3}).

Crystal data of compound 2.3: $C_{36}H_{43}N_3NiS$**,** M = 608.48, CCDC: 2271418, Red, rod, 0.37 × 0.31 × 0.26 mm^3, monoclinic, space group '$P2_1/n$', *a = 12.4124(11)Å, b = 17.1945(15)Å, c = 16.1810(13)Å,* α =90°, β =111.237(3)°, γ = 90°, Volume = 3218.9(5)Å^3, Z = 4, T = 100(2) K, D_{calc} (g cm^{-3}) = 1.256, $F(000)$ = 1296, μ (mm^{-1}) = 0.696, 213787 reflections collected, 8291 unique reflections (R_{int}= 0.0552), 7745 observed ($I > 2\sigma(I)$) reflections, multi-scan absorption correction, T_{min} = 0.783, T_{max} = 0.840, 377 refined parameters, S = 1.058, $R1$ = 0.0277, $wR2$ = 0.0712 (all data R = 0.0302, $wR2$ = 0.0735), maximum and minimum residual electron densities; $\Delta\rho_{max}$ = 0.41, $\Delta\rho_{min}$= -0.24 (eÅ^{-3}).

Crystal data of compound 2.4: $C_{36}H_{43}N_3NiSe$**,** M = 655.38, CCDC: 2271417, Red, plate, 0.38 × 0.35 × 0.27 mm^3, monoclinic, space group '$P2_1/n$', *a = 12.3444(14)Å, b = 17.2388(17)Å, c = 16.2008(19)Å,* α =90°, β = 110.170(4)°, γ = 90°, Volume = 3236.1(6)Å^3, Z = 4, T = 100(2) K, D_{calc} (g cm^{-3}) = 1.345, $F(000)$ = 1368, μ (mm^{-1}) = 1.753, 149316 reflections collected, 5719 unique reflections (R_{int}= 0.0804), 5009 observed ($I > 2\sigma(I)$) reflections, multi-scan absorption correction, T_{min} = 0.813, T_{max} = 0.862, 377 refined parameters, S = 1.075, $R1$ = 0.0313, $wR2$ = 0.0752 (all data R = 0.0382, $wR2$ = 0.0789), maximum and minimum residual electron densities; $\Delta\rho_{max}$ = 0.41, $\Delta\rho_{min}$= -0.42 (eÅ^{-3}).

Crystal data of compound 2.5: $C_{58}H_{68}N_6Ni_2S_2$**,** M = 1026.65, CCDC: 2271467, Colorless, block, 0.26 × 0.21 × 0.14 mm^3, trigonal, space group 'R-*3*', *a = 36.777(3)Å, b = 36.777(3)Å, c = 15.7171(13)Å,* α = 90°, β = 90°, γ = 120°, Volume = 18410(3)Å^3, Z = 9, T = 100(2) K, D_{calc} (g cm^{-3}) = 0.837, $F(000)$ = 4914.0, μ (mm^{-1}) = 0.539, 86520 reflections collected, 7233 unique reflections (R_{int}= 0.250), 3161 observed ($I > 2\sigma(I)$) reflections, multi-scan absorption correction, T_{min} = 0.447, T_{max} = 0., 729 refined parameters, S = 0.983, $R1$ = 0.0887, $wR2$ = 0.1895 (all data R = 0.1733, $wR2$ = 0.2279), maximum and minimum residual electron densities; $\Delta\rho_{max}$ = 0.53, $\Delta\rho_{min}$= -0.47 (eÅ^{-3}).

Crystal data of compound 2.6: $C_{58}H_{68}Se_2N_6Ni_2$**,** M = 1124.49, CCDC: 2271463, Colorless, block, 0.18 × 0.11 × 0.07 mm^3, triclinic, space group 'P-*1*', *a = 17.423(2)Å, b = 20.120(3)Å, c = 21.121(3)Å,* α =65.071(4)°, β = 77.623(5)°, γ = 73.220(4)°, Volume = 6391.5(16)Å^3, Z =

4, T = 298(2) K, D_{calc} (g cm^{-3}) = 1.169, $F(000)$ = 2328, μ (mm^{-1}) = 1.764, 22756 reflections collected, 10169 unique reflections (R_{int}= 0.0797), 1359 observed ($I > 2\sigma(I)$) reflections, multi-scan absorption correction, T_{min} = 0.585, T_{max} = 0.655, 588 refined parameters, S = 1.006, $R1$ = 0.0798, $wR2$ = 0.1898 (all data R = 0.1634, $wR2$ = 0.2420), maximum and minimum residual electron densities; $\Delta\rho_{max}$ = 0.64, $\Delta\rho_{min}$= -1.25 (eÅ^{-3}).

6.2.7: EPR Spectrum studies

X-band EPR spectra of compound **2.1** were recorded on a Bruker BiospinEMX^{micro} 1444 spectrometer. Spectra were collected with the following experimental parameters: microwave frequency, 9.32 GHz; microwave power, 1.99 mW; receiver gain, 1.00×10^2; modulation frequency, 100 kHz; modulation amplitude, 10 G; temperature, 298K. Spectral acquisitions were made using Bruker WinEPR software and simulated using Bruker SIMFONIA software.

6.2.8: Cyclic Voltametric analysis

Electrochemical experiments were carried out using a Biologic SP-300 potentiostat. A glassy carbon (0.19625 cm^2) was used as the working electrode, a graphite rod (Alfa Aesar) as the counter electrode, and a non-aqueous Ag/AgCl as the reference electrode in a three-electrode configuration. The sample (5 mM) was dissolved in THF, and the sample solution was then supplemented with a 0.1 M concentration of supporting electrolyte [^{n}Bu$_4$N][PF$_6$].

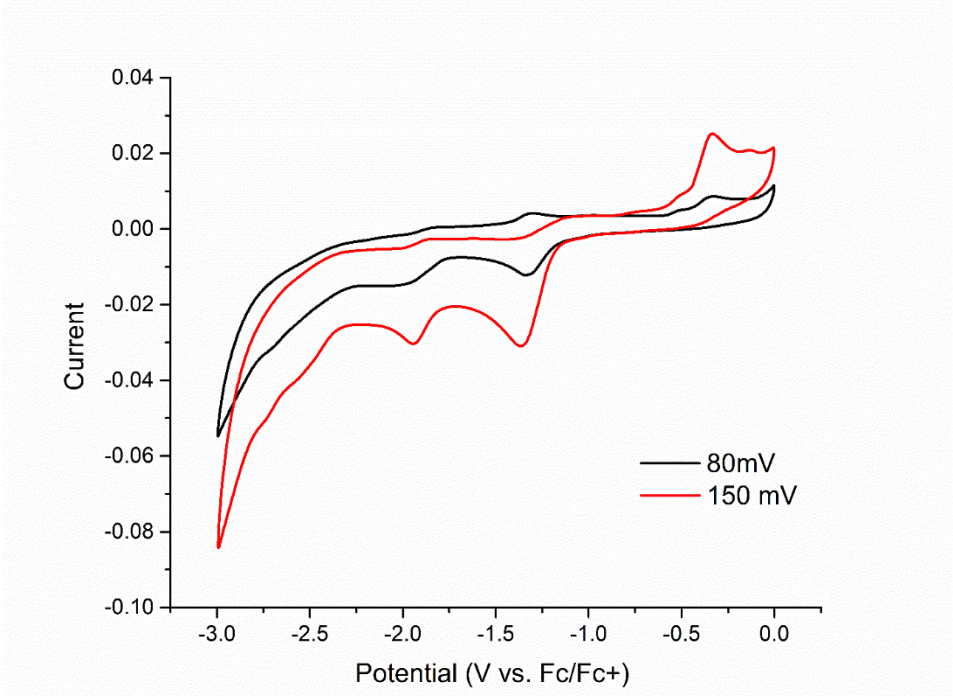

Figure A13. CV of compound **2.1**

6.2.9 Magnetism data analysis

The magnetic properties were measured by loading the samples in the Quantum-Design Magnetic Property Measurement System (MPMS). The magnetization of the samples was recorded in Field cooled (FC) conditions using SQUID mode as a function of temperature in the 5K-300K range. During the M-T measurement, a magnetic field of 100 Oe was applied. Prior to the measurement, MPMS was calibrated using a standard sample (Palladium) at 298K and 1 Tesla magnetic field. At the time of calibration, it was ensured that the experimentally obtained magnetization of the Pd sample matched closely with its theoretical value and the obtained error is less than 0.2%.

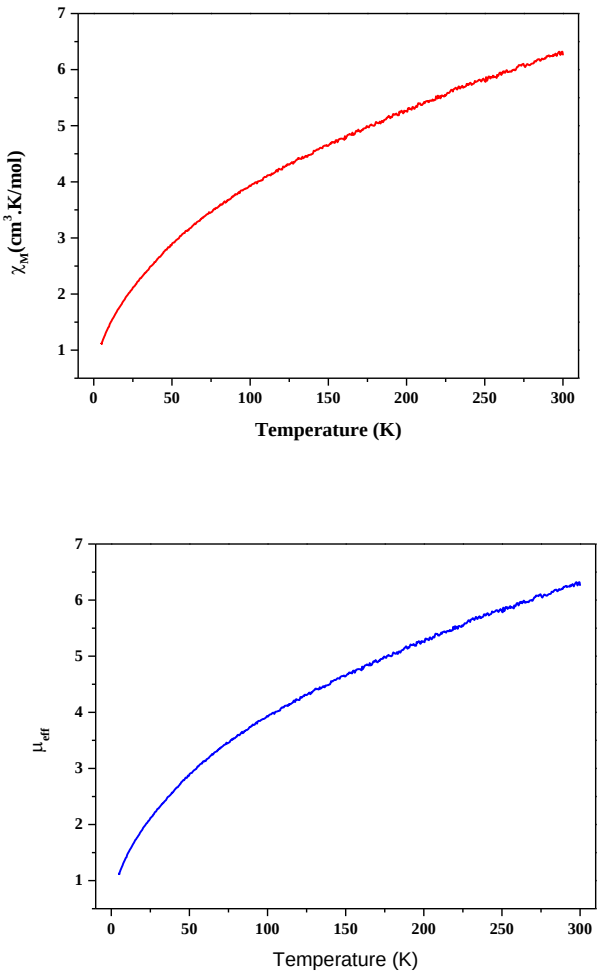

Figure A14. SQUID data of compound **2.1**

Figure A14 shows the direct current (dc) magnetic data of **2.1**, expressed as χ_M.T against temperature, where χ_M is the molar magnetic susceptibility. The continuous decreasing behavior of χ_M.T upon cooling indicates weak intermolecular antiferromagnetic interactions.[S6] In order to get further insights, the effective magnetic moment ($\mu_{eff,}$) of the sample was calculated (inset **2.1**) using $2.828\sqrt{\chi_M T} = \mu_{eff} = \sqrt{n(n+2)}$, where n is the number of unpaired d electrons. A nearly 6 BM (Bohr Magneton) value of μ_{eff} at 300 K corresponds to 5 unpaired electrons in the sample.

6.2.10: Computational Details

All the calculations in this study have been performed with density functional theory (DFT) using the Turbomole 7.5 suite of programs.[S7] The PBE functional,[S8] along with D3 dispersion correction,[S9] has been employed. The TZVP basis set has been used.[S10] For an accurate and efficient treatment of the electronic Coulomb term in the DFT calculations, the resolution of identity (RI)[S11] and the multipole accelerated resolution of identity (marij) approximations[S12] have been employed. Solvent corrections were incorporated in the optimization calculations using the COSMO model,[S13] with toluene (ε = 2.374) as the solvent. The reported values are ΔG values, with zero-point energy corrections. Internal energy and entropic contributions were included through frequency calculations on the optimized minima, with the temperature taken to be 298.15 K. Harmonic frequency calculations were performed for all stationary points to confirm them as local minima or transition state structures.

Furthermore, to obtain the accurate spin density, SOMO, and LUMO the geometry optimization of **2.1** in this study was performed using density functional theory (DFT) with the aid of the Gaussian 09 suite of programs.[S14] We have done calculations at the PBE-D3/TZVP level of theory and the B3LYP-D3/def2-TZVP level of theory.[S15,S16] Additionally, an implicit solvent model (PCM) with toluene as the solvent was employed with both calculations.[S17]

(a) Spin density plot, SOMO, and LUMO of **2.1** at B3LYP-D3/def2-TZVP level of theory

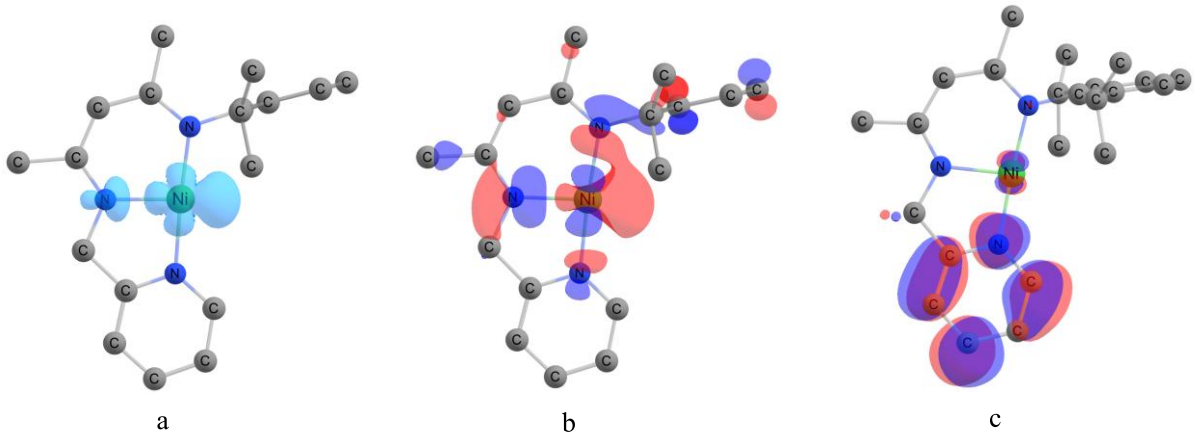

Figure A15. (a) The spin density plot, (b) the SOMO, and (c) the LUMO of **2.1**. The isovalue of the spin density plot is 0.004, while for the SOMO and LUMO, the iso value is 0.04.

(b) Thermodynamics for the formation of **2.5** from **2.1**

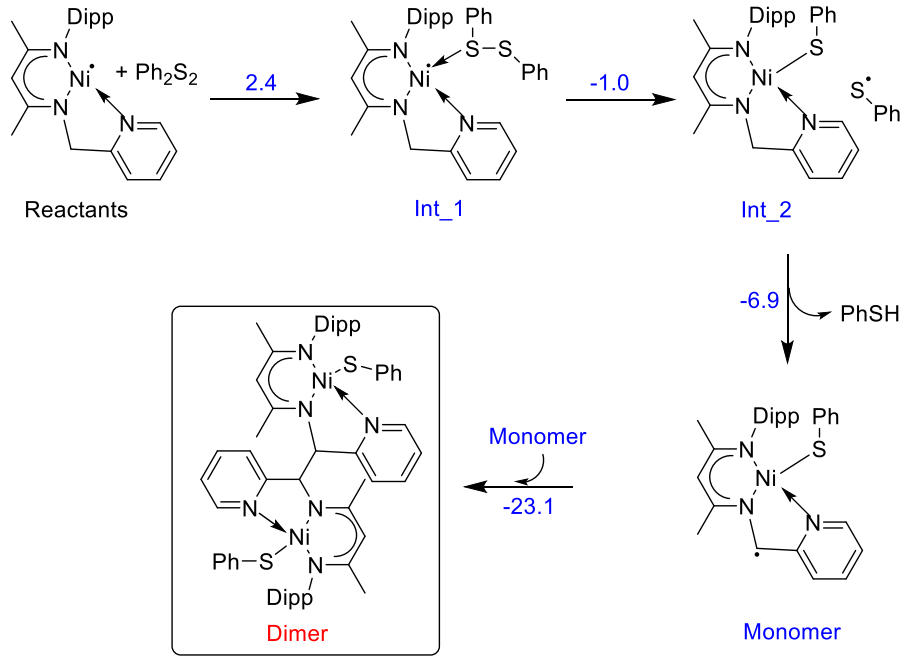

Figure A16. The thermodynamics for the formation of **2.5** (dimer) from **2.1** using Ph_2S_2. ΔG values are in kcal/mol.

6.3: Chapter 3 experimental details

6.3.1 Synthesis and characterization of compound 3.1: CH_3MgBr (0.4 ml, 1.13 mmol, 3.0 M diethyl ether) was slowly added to a stirred solution of ligand **LH** (0.360 g, 1.03 mmol) in THF (15 ml) at –78 °C over a period of 10 min. The yellow color solution was changed to an intense pink color after the addition. The solution was stirred at low temperature for 30 min

and then it was allowed to warm to room temperature and stirred for another 5 h. The color of the solution was changed to magenta. All volatiles were removed under reduced pressure and extracted with THF (10 ml). The solvent was reduced to 5 mL and stored at –4 °C in a freezer to obtain the colorless crystals of **3.1** suitable for X-ray analysis. Yield: 0.550 g (89 %). Mp: 87.5 °C.

^{1}H NMR (400 MHz, $CDCl_3$, 298K): δ 9.72 (d, *J*=5.3 Hz, 1 H, Py), 7.93 (t, *J*=7.6 Hz, 1 H, Py), 7.41 - 7.50 (m, 2 H, Ph), 7.29-7.35 (m, 1 H, Ph), 7.25 (s, 1 H, Py), 4.93 (s, 2 H, CH_2), 4.90 (s, 1 H, CH), 3.18 (m, J=13.7, 6.8 Hz, 2 H, CH_{Dipp}), 2.32 (s, 3 H, CH_3), 1.81 (s, 3 H, CH_3), 1.40 (s, 6 H, $CH_{3(Dipp)}$), 1.31 (d, *J*=6.9 Hz, 6 H, $CH_{3(Dipp)}$) ppm.

^{13}C NMR (101 MHz, $CDCl_3$, 298K) δ 168.1 (s), 166.7 (s), 160.2 (s), 150.9 (s), 148.0 (s), 141.6 (s), 138.1 (s), 124.1 (s), 122.8 (s), 121.9 (s), 121.8 (s), 93.8 (s), 76.7 (s), 68.6 (s), 53.6 (s), 27.9 (s), 25.4 (s), 25.1 (s), 24.2 (s), 24.2 (s), 23.2 (s) ppm.

HRMS: Calcd: 452.1546, found [m+1]: 452.1495.

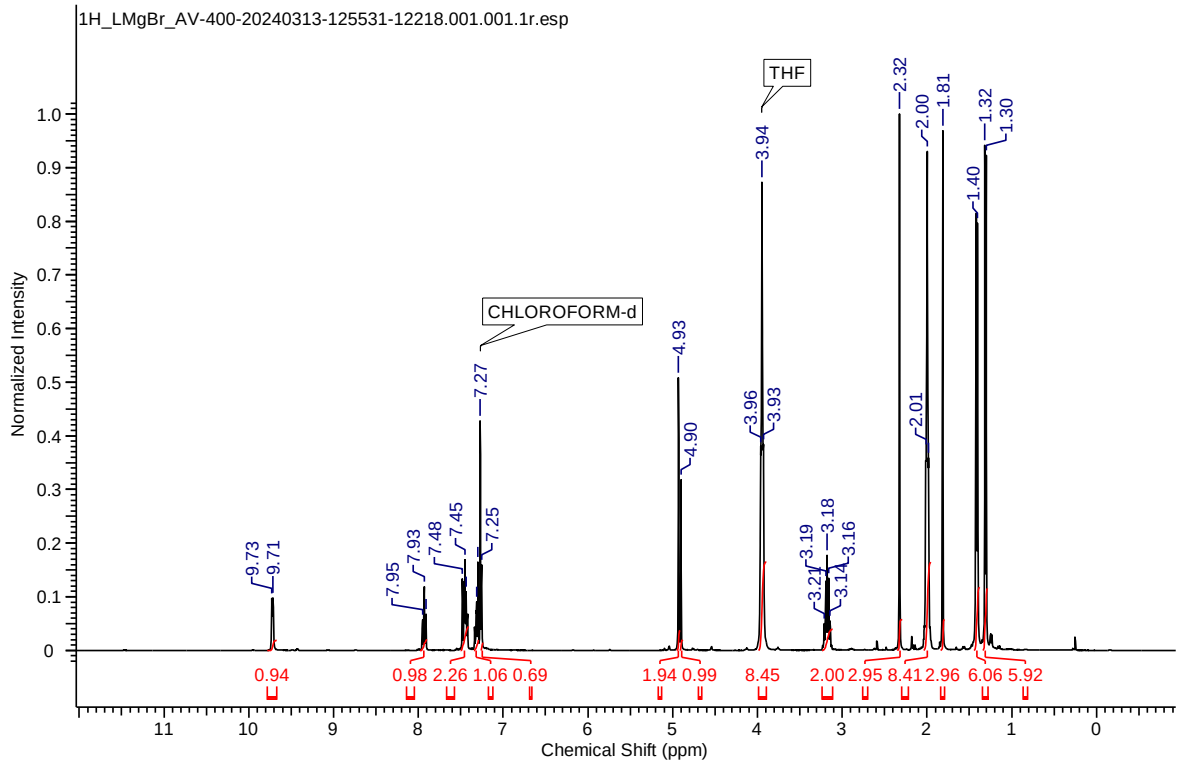

Figure A17. The ^{1}H NMR of **3.1**

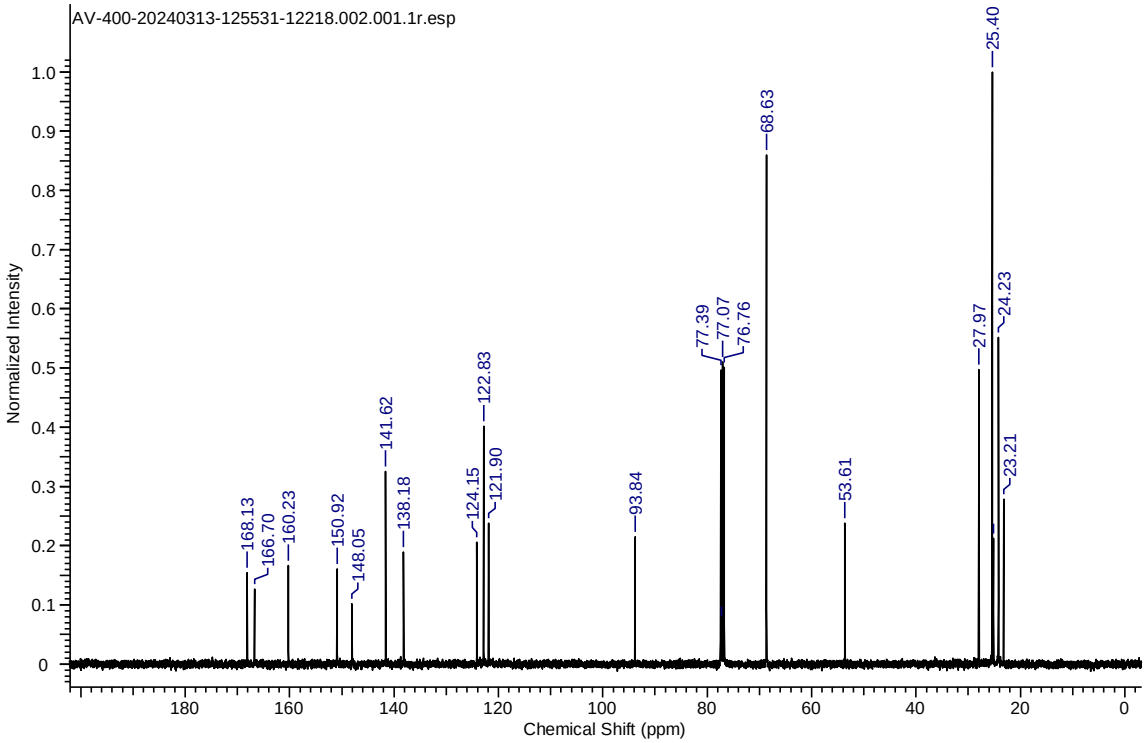

Figure A18. The ^{13}C NMR of **3.1**

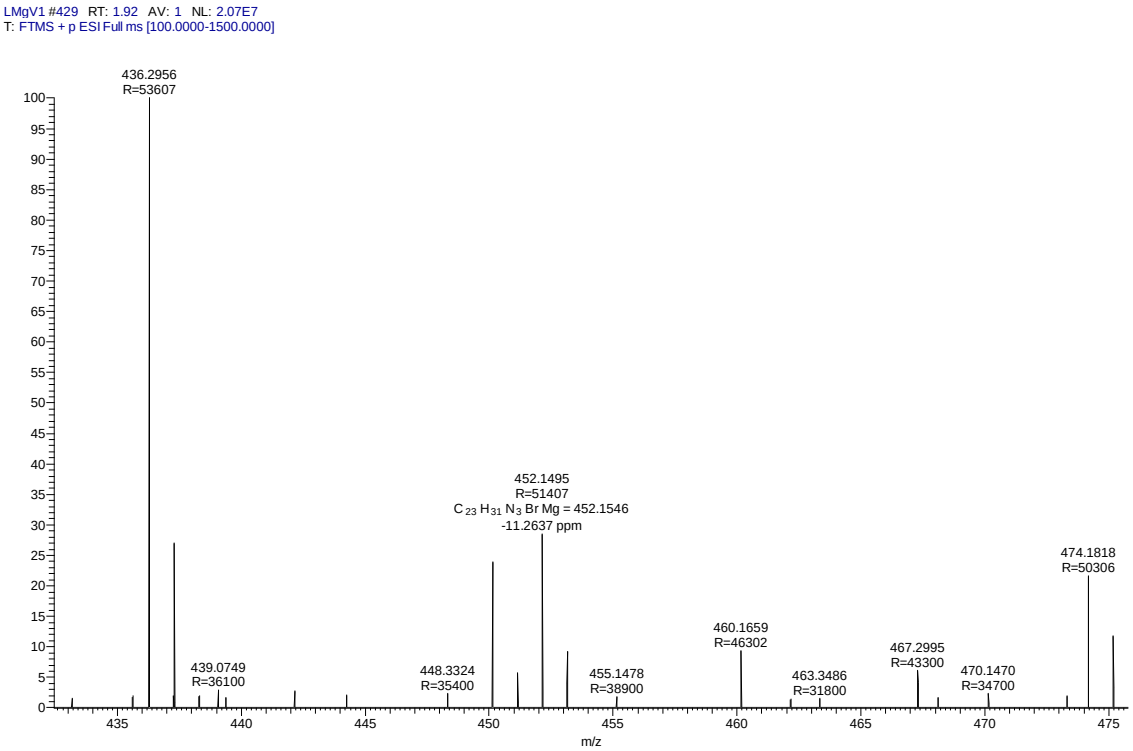

Figure A19. The HRMS of **3.1**

6.3.2 Synthesis and characterization of compound 3.2: *n*-dibutylmagnesium (1.5 ml, 1.5 mmol, 1.0 M in heptane) was slowly added to a stirred solution of **LH** (0.457 g, 1.30 mmol) in

THF (15 ml) at –78 °C over a period of 15 min, the solution color was changed from yellow to dark magenta after the addition. The solution was warmed to room temperature and stirred for 3 h. All volatiles were removed under reduced pressure and extracted with mixture of THF (5 ml) and hexane (10 ml). The solvent was reduced to 3-5 mL, and stored at –4 °C in a freezer to obtain the red color crystals of **3.2** in a week suitable for X-ray analysis. Yield: 0.570 g (83%). Mp: 209.4 °C.

1H NMR (500 MHz, C_6D_6, 298K): δ 7.26 (s, 1 H, Ph), 6.83 (d, J=5.9 Hz, 1 H, Ph), 6.48-6.57 (m, 1 H, Ph), 6.40 (d, J=9.0 Hz, 1 H, Pyde), 6.16 (s, 1 H, Pyde), 5.42 (t, J=5.9 Hz, 1 H, Pyde), 5.04 (s, 1 H, Pyde), 3.51-3.56 (m, 2 H, CH_{Dipp}), 2.21 (s, 3 H, CH_3), 1.96 (s, 3 H, CH_3), 1.31 (d, J=6.9 Hz, 6 H, $CH_{3(Dipp))}$, 1.19 (d, J=6.9 Hz, 6 H, $CH_{3(Dipp))}$ ppm.

13C NMR (101 MHz, C_6D_6, 298K) δ 155.3 (s), 150.5 (s), 148.7 (s), 145.7 (s), 144 (s), 129.3 (s), 123.4 (s), 123 (s), 118.7 (s), 100.9 (s), 98.8 (s), 96.4 (s), 68.8 (s), 27.5 (s), 25.2 (s), 24.2 (s), 23.9 (s), 20.8 (s) ppm.

HRMS: Calcd: 372.2285, found [m+1]: 372.2401.

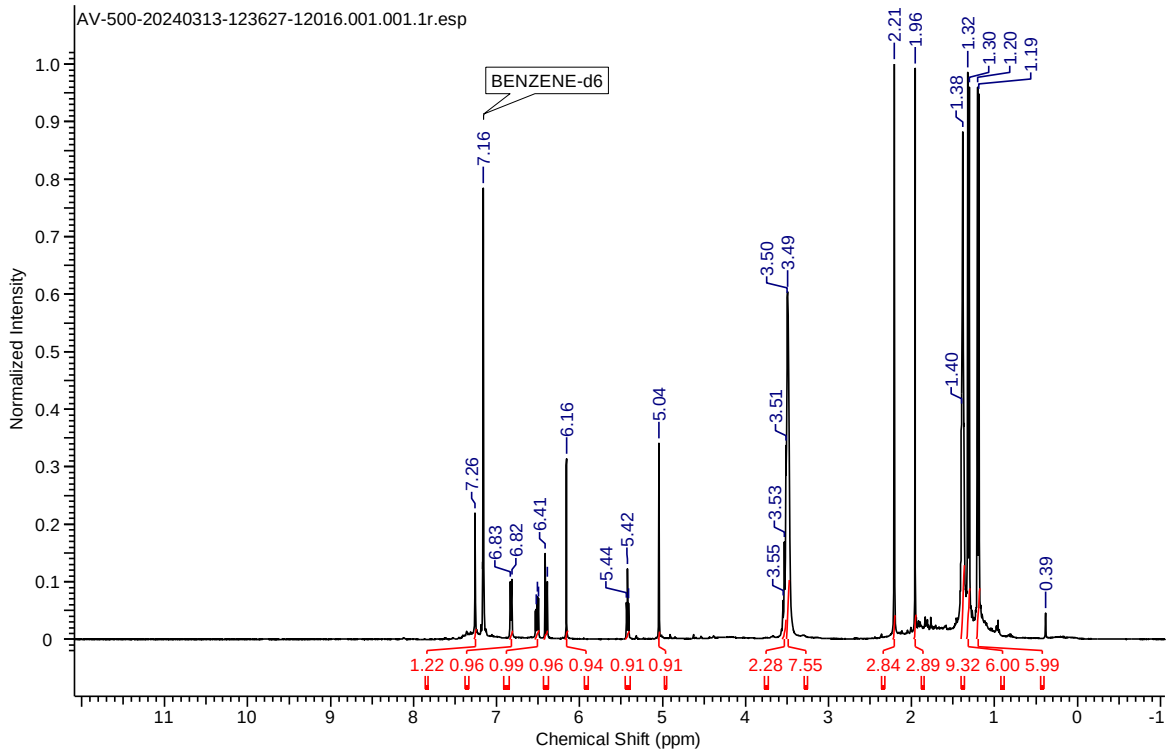

Figure A20. The ^{1}H NMR of **3.2**

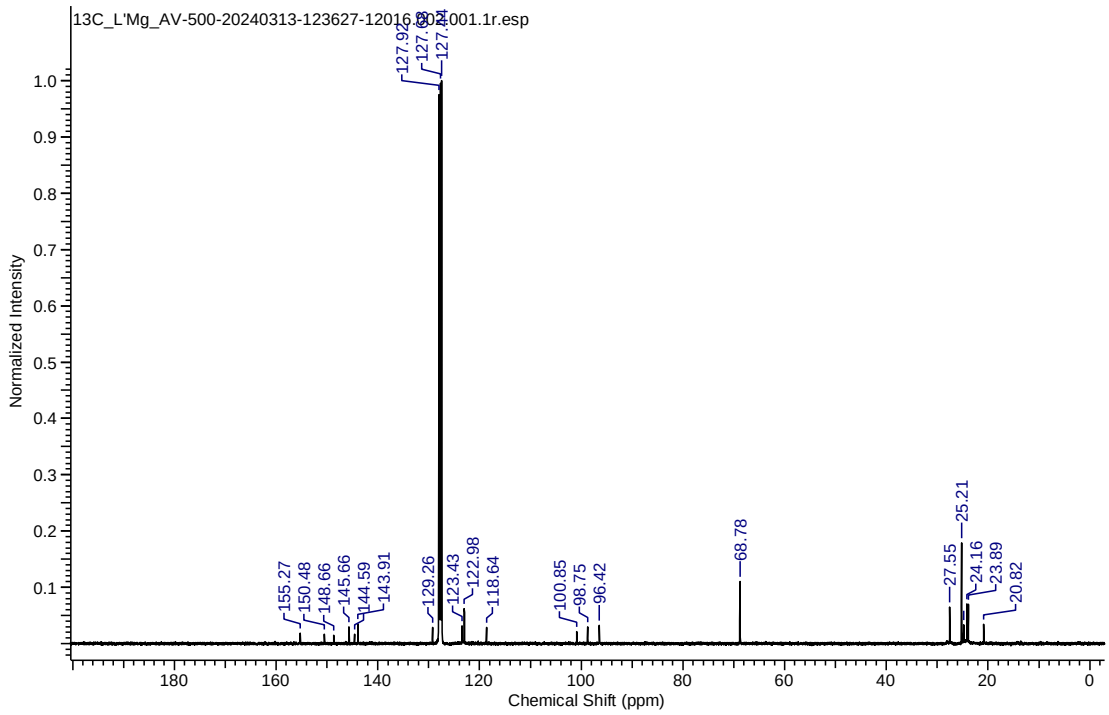

Figure A21. The ^{13}C NMR of **3.2**

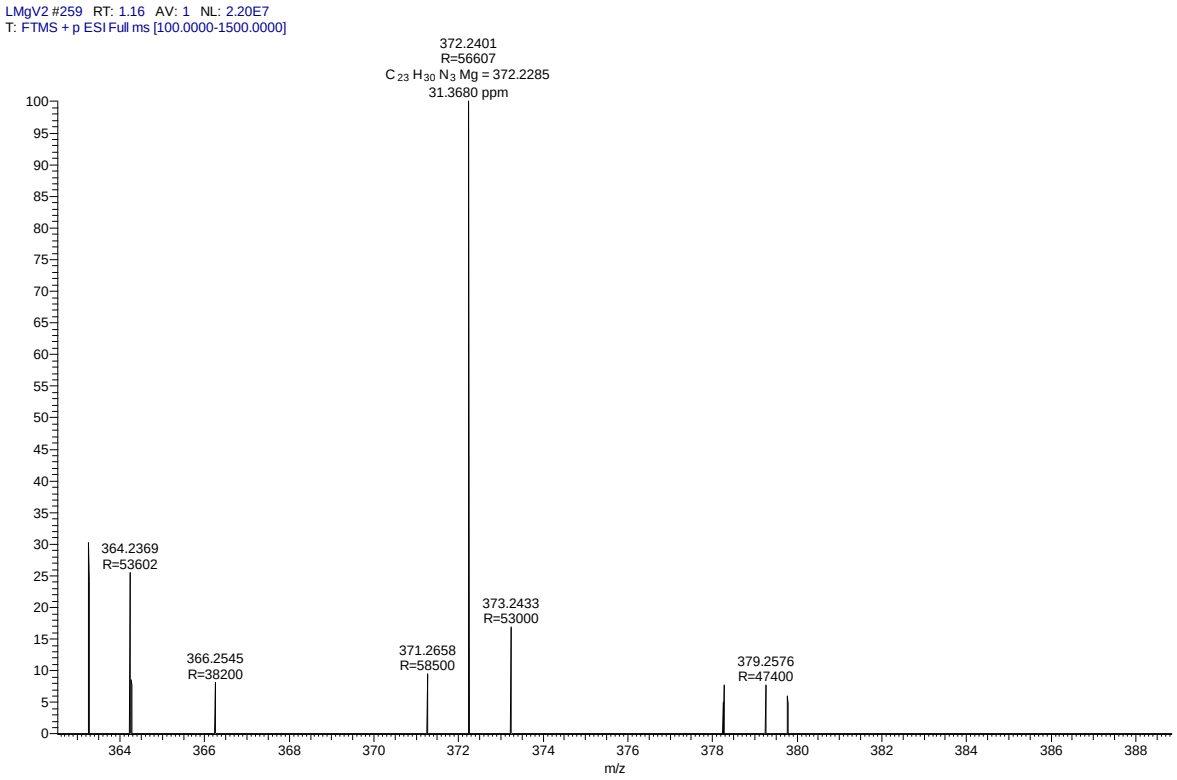

Figure A22. The HRMS of **3.2**.

6.3.3 Synthesis and characterization of compound 3.3 and 3.4: Double distilled degassed water (11 µL, 0.6 mmol) was added drop by drop to a stirred THF solution of compound **3.2**

(300 mg, 0.58 mmol) at –70 °C. The reaction colour changed immediately from deep red to orange. The reaction was stirred for 5 min at -70 °C and the reaction mixture was dried at low temperature keeping the cooling bath. Orange solid was obtained as the final product, which was recrystallized in thf/hexane mixture to get the red colour crystals of **3.3** for X-ray analysis. Yield: 0.320 g (69.80 %) Mp: 168.2 °C.

^{1}H NMR (400 MHz, $CDCl_3$, 298K): δ 8.53 (d, *J*=4.8 Hz, 1 H, Py), 7.61 - 7.68 (m, 1 H, Py), 7.08-7.18 (m, 3 H, Ph), 7.02 (s, 1 H, Py), 4.78 (s, 1 H, CH), 4.59 (s, 2 H, CH_2), 2.86-2.98 (m, 2 H, CH_{Dipp}), 1.99 (s, 3 H, CH_3), 1.69 (s, 3 H, CH_3), 1.18 (d, *J*=7.0 Hz, 6 H, $CH_{3(Dipp)}$), 1.09 (d, *J*=6.9 Hz, 6 H, $CH_{3(Dipp)}$) ppm.

^{13}C NMR (101 MHz, $CDCl_3$, 298K) *δ* 166.5 (s) 160.1 (s) 155.2 (s) 149.3 (s) 146.7 (s) 137.9 (s) 136.8 (s) 122.7 (s) 122.7 (s) 121.9 (s) 120.4 (s) 94.4 (s) 77.3 (s) 77.2 (s) 77.0 (s) 76.7 (s) 68.0 (s) 48.8 (s) 28.1 (s) 25.6 (s) 23.8 (s) 22.9 (s) 21.7 (s) 19.2 (s) ppm.

IR (cm^{-1}): 3672, 2956, 1656, 1625, 1589, 1552, 1503, 1432, 1361, 1332, 1302, 1225, 1180, 1086, 789, 747 cm^{-1}.

HRMS: Calcd: 229.1060, found [m+1]: 229.0920.

The reaction of **3.2** with D_2O yielded into **3.4** which gives significant peaks in ^{2}H NMR.

^{2}H NMR (400 MHz, $CDCl_3$, 25 °C): 4.61 (S, 1D, $CHD_{methylene}$), 11.21(S, 1D, OD) ppm.

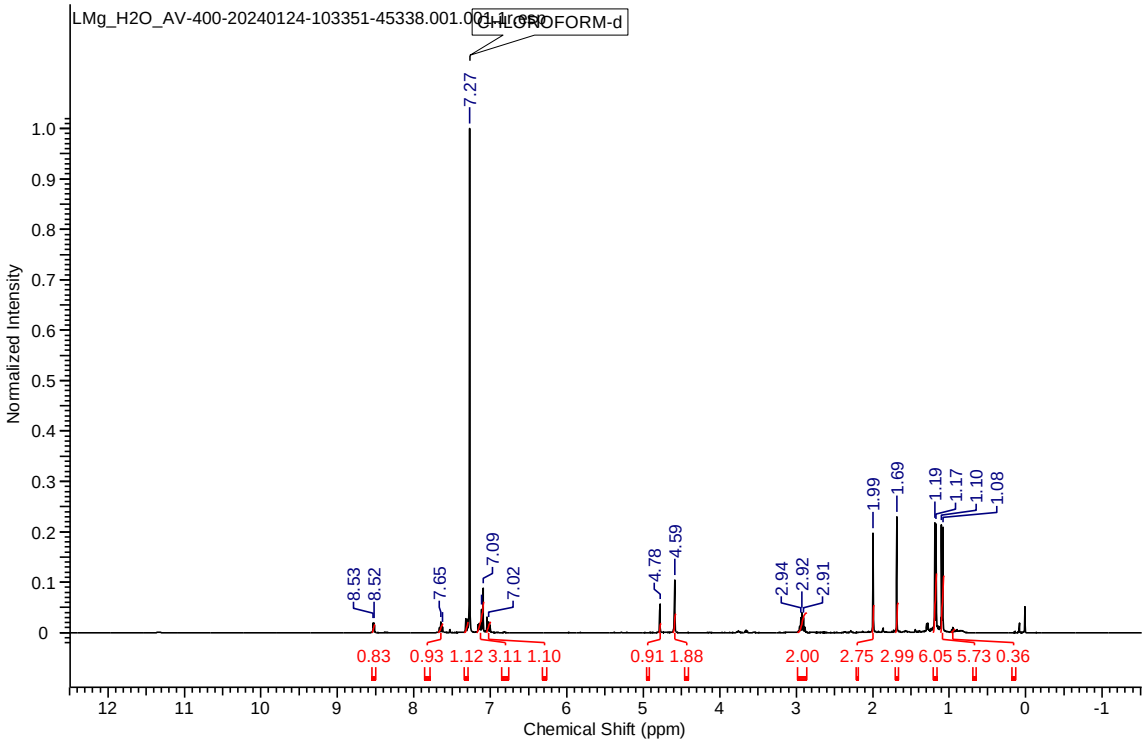

Figure A23. The ^{1}H NMR of **3.3**

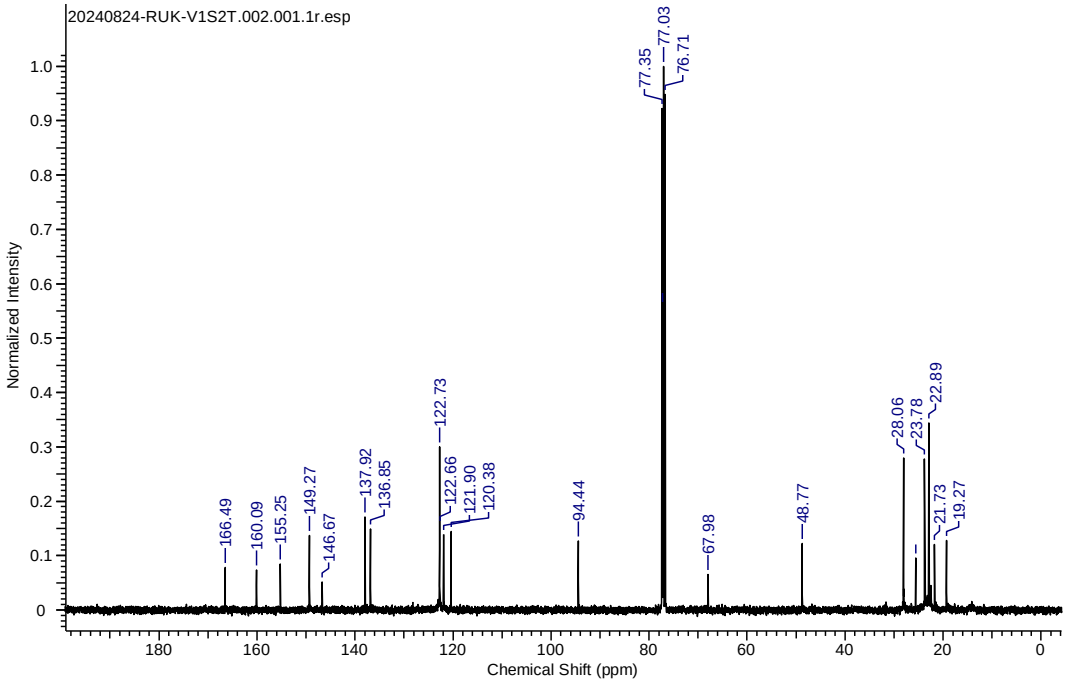

Figure A24. The ^{13}C NMR of **3.3**

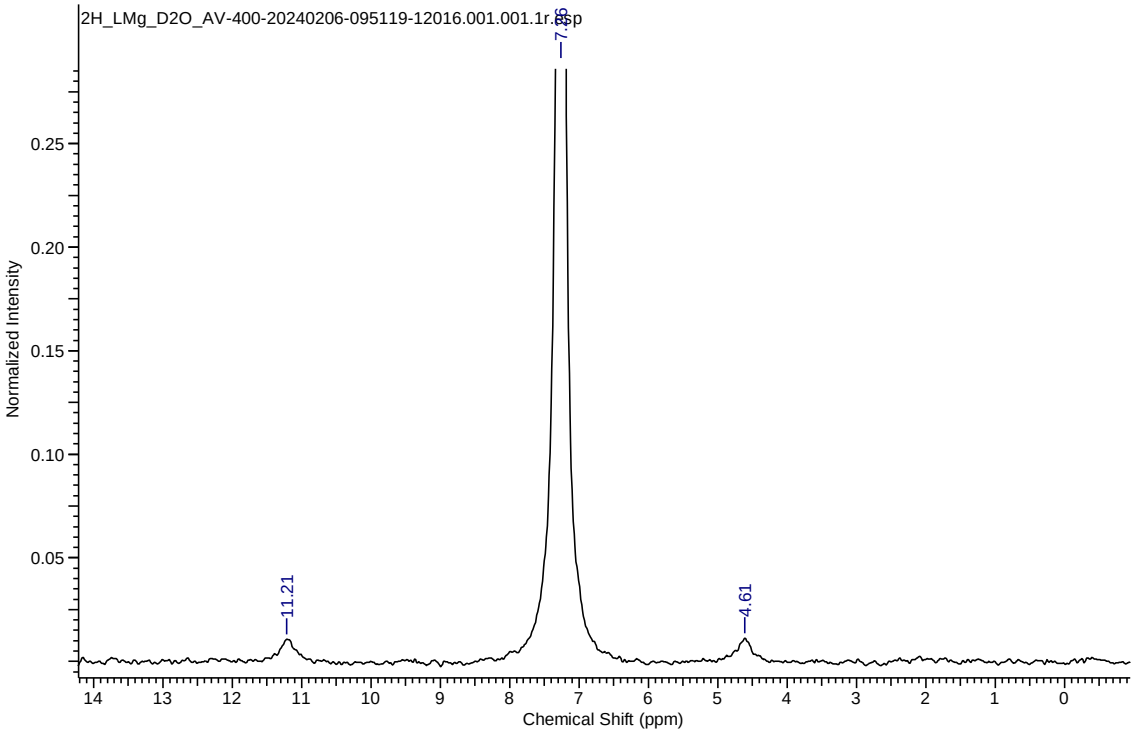

Figure A25. The ^{2}H NMR of **3.4**

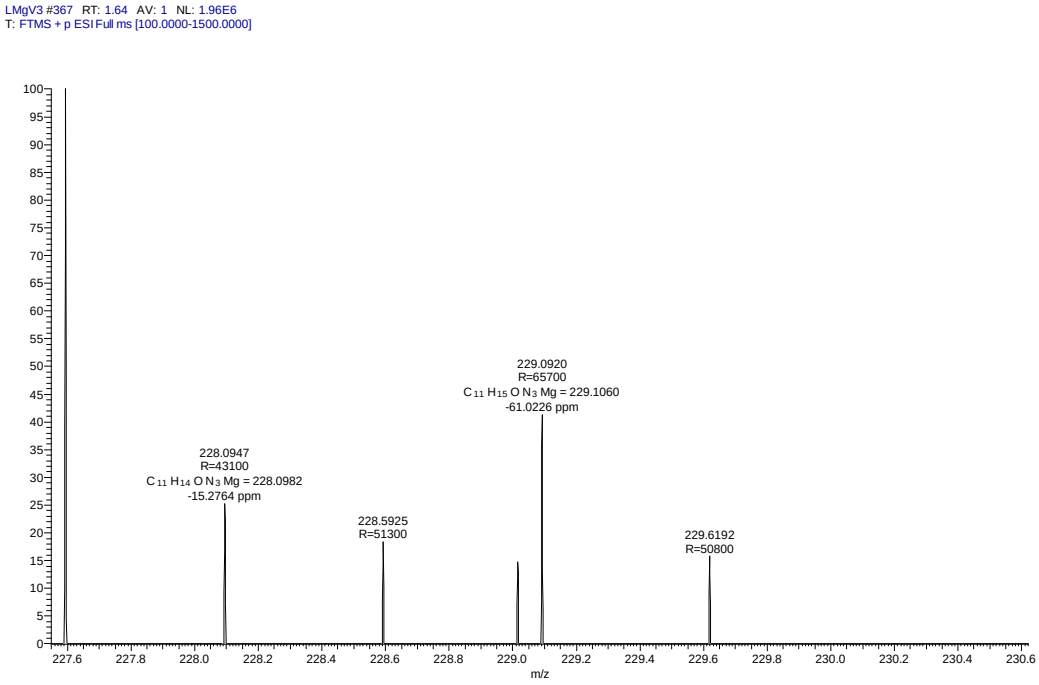

Figure A26. The HRMS of **3.3**

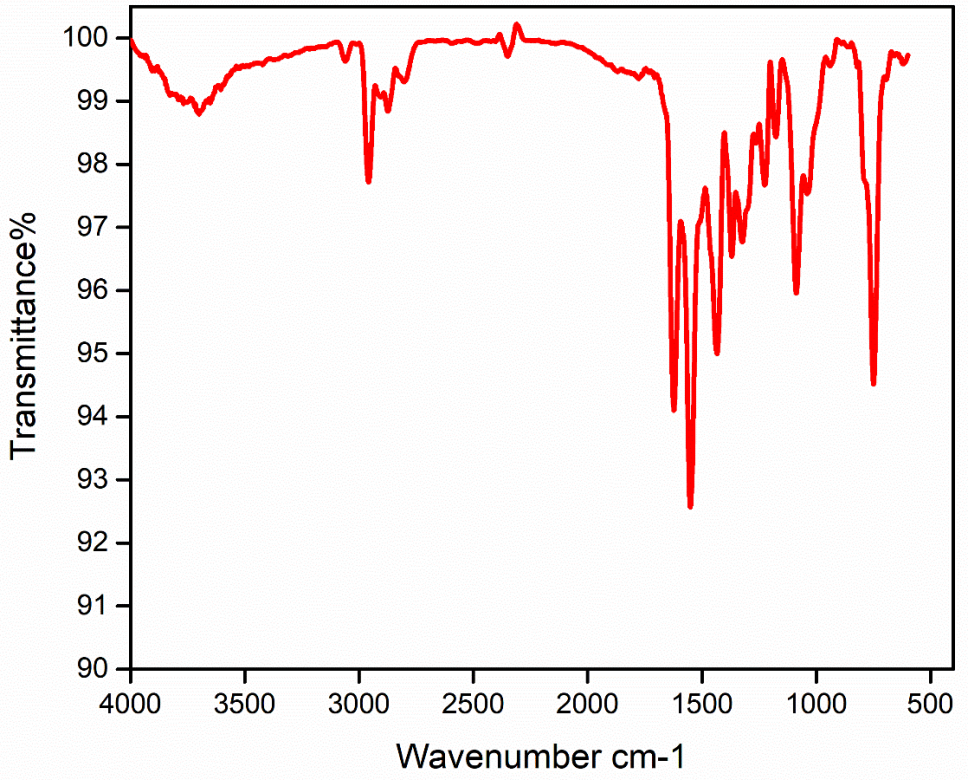

Figure A27. IR (ATR mode) of **3.3**.

6.3.4 Synthesis and characterization of compound 3.5: K-selectride (potassium tri-sec-butylborohydride) (0.5 ml, 0.55 mmol, 1.0 M in THF) was slowly added to a stirred solution

of 1 (0.300 g, 0.50 mmol) in THF (15 ml) at –78 °C over a period of 15 min, the solution color was changed from magenta to yellow after the addition. The solution was warmed to room temperature and stirred for 5 h. All volatiles were removed under reduced pressure and extracted with mixture of THF (5 ml) and hexane (5 ml). The solvent was reduced to 3-5 mL, and stored at –4 °C in a freezer to obtain the colorless crystals of **3.5** in a week suitable for X-ray analysis. The yield of three was very less due to other impurities present in the flask. Because of less yield we were not able to record all other characterizations other than SCXRD.

6.3.5 Synthesis and characterization of compound 3.6: lithiated trimethylsilyl diazomethane $LiC(SiMe_3)N_2$ (1.45 mL, 0.87 mmol, 0.6 M in hexane) was added drop by drop to the toluene solution of **2** (300 mg, 0.58 mmol) at – 70 °C. The reaction was then allowed to warm to room temperature and stirred overnight. The colour of the reaction changed from deep red to orange during the course of the reaction. The volatiles were removed under high vacuum and the residue was extracted using hexane (10 ml) and toluene (5 ml) mixture. The solvent was reduced till saturation and kept at – 36 °C to obtain the extremely air- and moisture-sensitive yellow color crystals of **3.6** suitable for X-ray analysis. Yield: 0.15 g (76 %). Due to the solubility issue, we could not record the NMR of **3.6** despite several attempts in toluene-d_8, THF-d_8. While the compound is stable in solid-state inside a glove-box, it readily decomposes in solution to free ligand in 10-15 minutes.

6.3.6 Crystal Structure Detail of 3.1-3.3 and 3.5, 3.6

Crystal data of compound 3.1: $C_{31}H_{46}N_3O_2MgBr$, M = 596.93, CCDC: 2378739, colorless, block, 0.18 x 0.16 x 0.12 mm^3, monoclinic, space group '*P2₁/c'*, *a = 9.3717(7)Å*, *b = 17.4965(14)Å*, *c = 18.6975(12)Å*, α = 90°, β = 102.637(2)°, γ = 90°, Volume = 2991.6(4)$Å^3$, Z = 4, *T* = 100(2) K, D_{calc} (g cm^{-3}) = 1.325, *F*(*000*) = 1264, μ (mm^{-1}) = 1.427, 236659 reflections collected, 7772 unique reflections (R_{int}= 0.0279), 7044 observed ($I > 2\sigma$ (I)) reflections, multi-scan absorption correction, T_{min} = 0.773, T_{max} = 0.843, 349 refined parameters, *S* = 1.026, *R*1 = 0.0279, *wR*2 = 0.0707 (all data *R* = 0.0330, *wR*2 = 0.0743), maximum and minimum residual electron densities; $\Delta\rho_{max}$ = 1.010, $\Delta\rho_{min}$= -0.383 ($eÅ^{-3}$).

Crystal data of compound 3.2 : $C_{35}H_{53}N_3MgO_3$**,** M = 589.51, CCDC: 2378740, Red, Plate, 0.21 × 0.16 × 0.13 mm^3, monoclinic, space group 'P*2₁/n'*, *a = 12.3574(10)Å*, *b =*

18.9989(16)Å, c = 15.1393(11)Å, α = 90°, β = 110.007(2)°, γ = 90°, Volume = 3339.9(5)Å^3, Z = 4, *T* = 100(2) K, D_{calc} (g cm^{-3}) = 1.172, *F*(*000*) =1283, μ (mm^{-1}) = 0.091, 87901 reflections collected, 9310 unique reflections (R_{int}= 0.0628), 5968 observed ($I > 2\sigma$ (*I*)) reflections, multi-scan absorption correction, T_{min} = 0.983, T_{max} = 0.988, 412 refined parameters, *S* = 0.959, *R*1 = 0.0628, *wR*2 = 0.1377 (all data *R* = 0.1209, *wR*2 = 0.1688), maximum and minimum residual electron densities; $\Delta\rho_{max}$ = 0.508, $\Delta\rho_{min}$= -0.580(eÅ^{-3}).

Crystal data of compound 3.3: $C_{50}H_{70}N_6Mg_2O_2$**,** M = 481.97, CCDC: 2408476, color less, block, 0.28 × 0.24 × 0.22 mm^3, triclinic, space group 'P-1*'*, *a = 11.3385(6)Å, b = 15.5115(9)Å, c = 15.5132(9))Å*, α = 80.677(2)°, β = 87.084(2)°, γ = 83.992(2)°, Volume = 2676.0(6)Å^3, Z = 2, *T* = 100(2) K, D_{calc} (g cm^{-3}) = 1.144, *F*(*000*) = 1004, μ (mm^{-1}) = 0.090, 141706 reflections collected, 12778 unique reflections (R_{int}= 0.0553), 10145 observed ($I > 2\sigma$ (*I*)) reflections, multi-scan absorption correction, T_{min} = 0.975, T_{max} = 0.980, 612 refined parameters, *S* = 1.061, *R*1 = 0.0553, *wR*2 = 0.1277 (all data *R* = 0.0734, *wR*2 = 0.1372), maximum and minimum residual electron densities; $\Delta\rho_{max}$ = 0.537, $\Delta\rho_{min}$= -0.382 (eÅ^{-3}).

Crystal data of compound 3.5: $C_{30}H_{39}N_3MgO$**,** M = 481.97, CCDC: 2378746, red, block, 0.26 × 0.22 × 0.20 mm^3, monoclinic, space group 'C*2/c'*, *a = 18.4046(12)Å, b = 18.0672(13)Å, c = 16.9266(11)Å*, α =90°, β =99.464(2)°, γ = 90°, Volume = 5551.8(6)Å^3, Z = 8, *T* = 100(2) K, D_{calc} (g cm^{-3}) = 1.153, *F*(*000*) = 2080, μ (mm^{-1}) = 0.090, 92466 reflections collected, 6903 unique reflections (R_{int}= 0.0694), 4650 observed ($I > 2\sigma$ (*I*)) reflections, multi-scan absorption correction, T_{min} = 0.977, T_{max} = 0.982, 326 refined parameters, *S* = 1.044, *R*1 = 0.0694, *wR*2 = 0.1422 (all data *R* = 0.1133, *wR*2 = 0.1645), maximum and minimum residual electron densities; $\Delta\rho_{max}$ = 1.18, $\Delta\rho_{min}$= -0.336 (eÅ^{-3}).

Crystal data of compound 3.6: $C_{27}H_{39}MgN_5Si$, M = 486.03, colorless, block, 0.18 × 0.15 × 0.12 mm^3, monoclinic, space group 'C*2/c'*, *a = 19.8967(13)Å, b = 16.7007(10)Å, c = 17.6900(11)Å*, α =90°, β = 105.673(2)°, γ = 90°, Volume = 5659.6(6)Å^3, Z = 8, *T* = 100(2) K, D_{calc} (g cm^{-3}) = 1.141, *F*(*000*) = 2096, μ (mm^{-1}) = 0.128, 72446 reflections collected, 6078 unique reflections (R_{int}= 0.0506), 4225 observed ($I > 2\sigma$ (*I*)) reflections, multi-scan absorption correction, T_{min} = 0.1120, T_{max} = 0.1502, 316 refined parameters, *S* = 1.046, *R*1 = 0.0506, *wR*2

= 0.1004 (all data R = 0.0900, $wR2$ = 0.1187), maximum and minimum residual electron densities; $\Delta\rho_{max}$ = 0.260, $\Delta\rho_{min}$= -0.328 (eÅ^{-3}).

6.4: Chapter 4 experimental details

6.4.1 Synthesis and characterization of compound 4.1 and 4.2: The toluene solution of aryl alkynes RC≡CH (0.42 mmol, 5 ml toluene) was dropwise added to the stirred toluene solution of **3.2** (0.200 g, 0.38mmol) at –70 °C. There was no colour change at low temperature. The reaction mixture was then allowed to warm at room temperature and stirred overnight. The color of the reaction mixture changed from red to pale brown. All the volatiles were removed under high vacuum and the solid was extracted into toluene (6 ml) and filtered using frit over celite. The solution was reduced to super saturation and kept at –36 °C to get suitable colourless crystals of **4.1** (R = Ph), and **4.2** (R = 4-fluorophenyl). Yield: 0.150 g (81 %) for **4.1** and 0.140 g (76 %) for **4.2**. We are unable to record the HRMS data of **4.1** and **4.2** due to less stability.

4.1: ^{1}H NMR (400 MHz, C_6D_6, 298K): δ = 9.74 (br. s., 1 H, Py), 7.34 (d, J=7.3 Hz, 2 H, Py), 6.96 - 7.06 (m, 5 H, Ph_{PhCCH}), 6.74 - 6.87 (m, 3 H, Ph_{dipp}), 6.50 (br. s., 1 H, Py), 4.77 (s, 1 H, CH), 4.15 (s, 2 H, CH_2), 3.19 - 3.31 (m, 2 H, CH_{dipp}), 1.78 (s, 3 H, CH_3), 1.71 (s, 3 H, CH_3), 1.39 (d, J=6.9 Hz, 6 H, $CH_{3(dipp)}$), 1.16 ppm (d, J=6.9 Hz, 6 H, $CH_{3(dipp)}$) ppm.

^{13}C NMR (101 MHz, $CDCl_3$, 298K) δ = 165.8 (s) 160.4 (s) 141.8 (s) 137.5 (s) 137.1 (s) 131.7 (s) 128.9 (s) 127.9 (s) 127.7 (s) 127.4 (s) 125.3 (s) 124.2 (s) 122.9 (s) 121.5 (s) 120.9 (s) 94.1 (s) 68.3 (s) 53.5 (s) 28.2 (s) 24.9 (s) 21.0 (s) ppm.

4.2: ^{1}H NMR (400 MHz, C_6D_6, 298K): δ = 9.81 (br. s., 1 H, Py), 7.27 (br. s., 4 H, Ph_{PhCC}), 7.02 (br. s., 1 H, Py), 6.96 (br. s., 1 H,Ph_{dipp}), 6.79 (br. s., 2 H, Ph_{dipp}), 6.50 (br. s., 1 H, Py), 4.91 (s, 1 H, CH), 4.30 (br. s., 2 H, CH_2), 3.39 (m, 2 H, CH_{dipp}), 1.84 (s, 3 H, CH_3), 1.50 (d, J=6.5 Hz, 6 H, $CH_{3(dipp)}$), 1.30 (d, J=6.8 Hz, 6 H, $CH_{3(dipp)}$), 1.23 ppm (br. s., 3 H, CH_3) ppm.

^{13}C NMR (101 MHz, C_6D_6, 298K) δ = 167.3 (s) 165.9 (s) 160.3 (s) 149.9 (s) 141.8 (s) 137.1 (s) 133.1 (s) 128.9 (s) 127.9 (s) 127.6 (s) 127.4 (s) 125.3 (s) 122.8 (s) 121.5 (s) 120.9 (s) 114.3 (s) 94.1 (s) 68.4 (s) 53.5 (s) 28.2 (s) 24.9 (s) 24.4 (s) 24.0 (s) 22.9 (s) 21.0 (s) ppm.

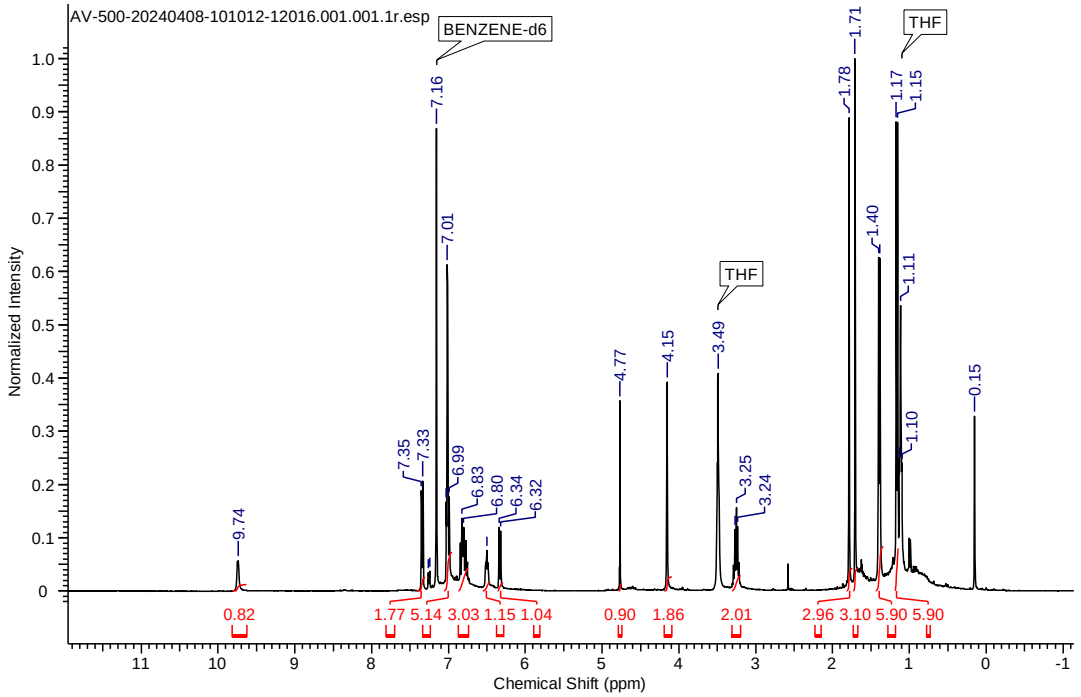

Figure A28. The ^{1}H NMR of **4.1**

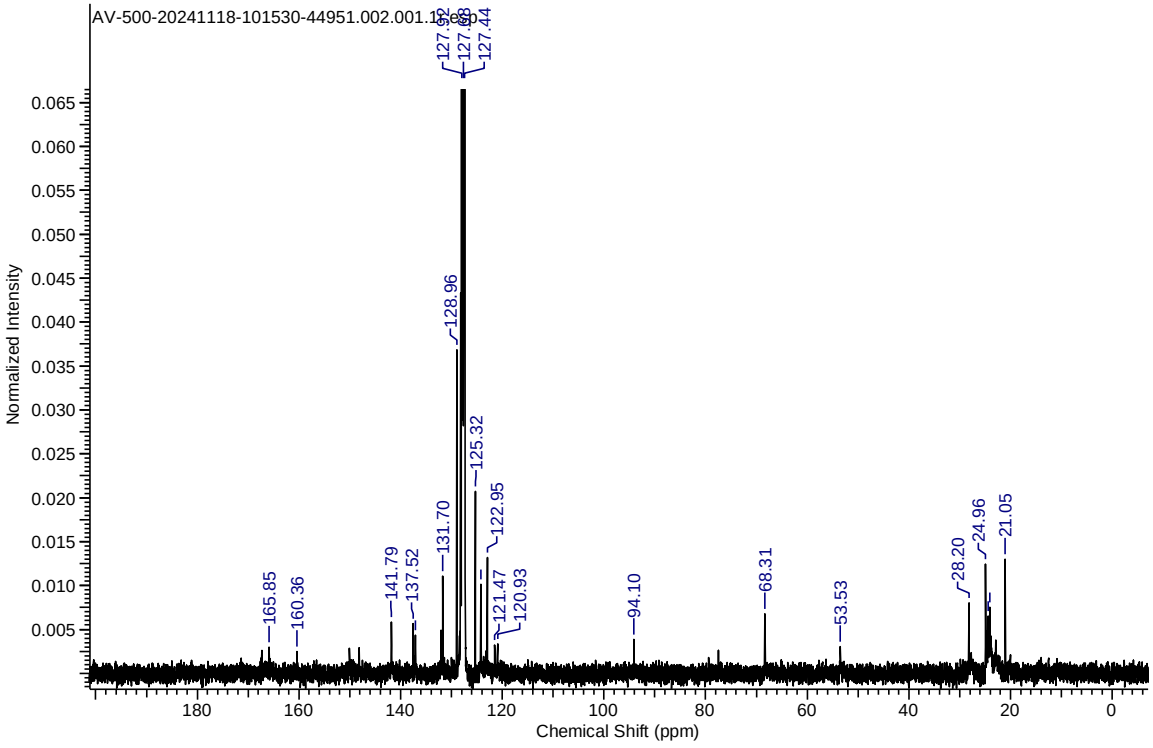

Figure A29. The ^{13}C NMR of **4.1**

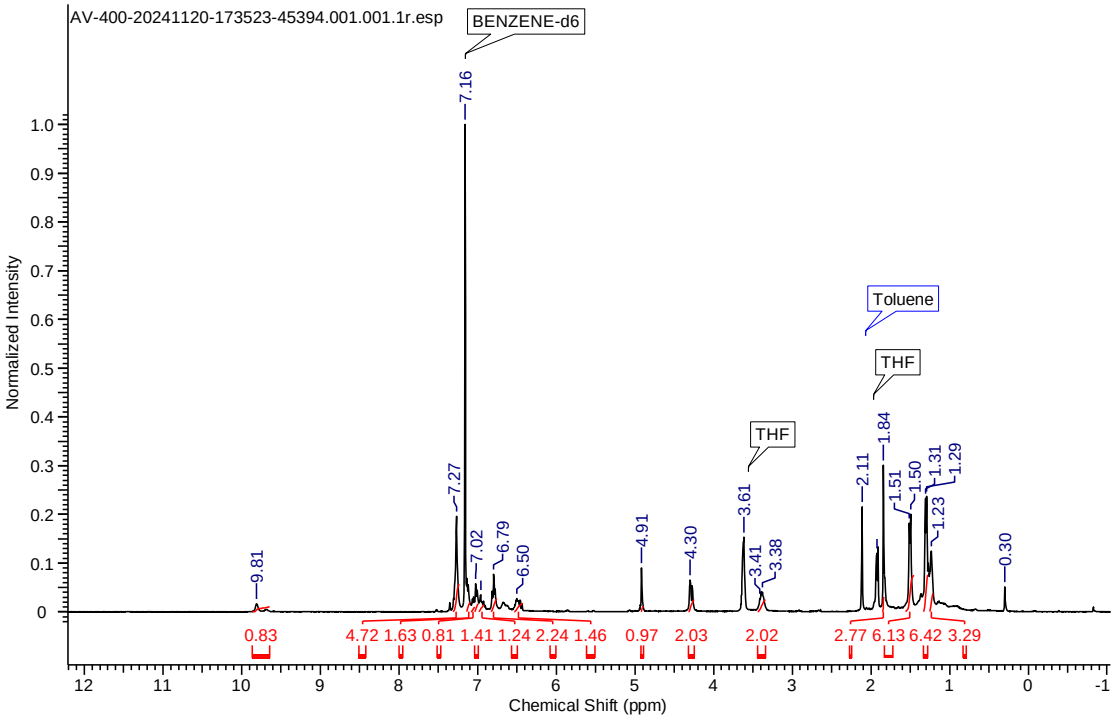

Figure A30. The ^{1}H NMR of **4.2**

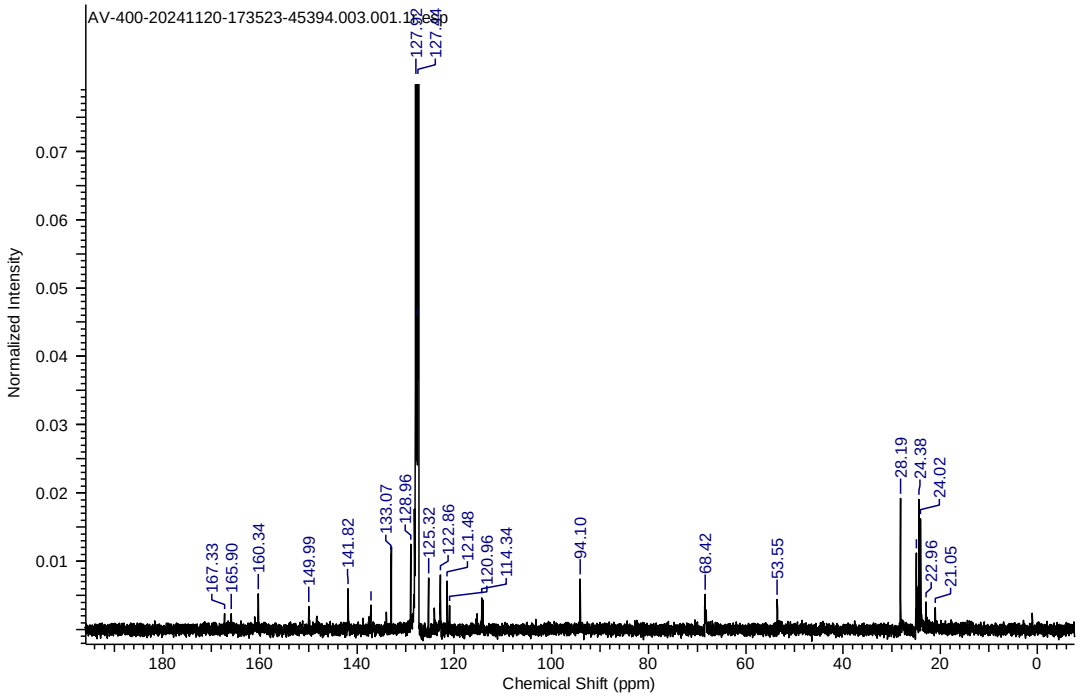

Figure A31. The ^{13}C NMR of **4.2**

6.4.2 Synthesis and characterization of compound 4.3: Trimethylsilyl diazomethane (1.45 mL, 0.87 mmol, 0.6 M in hexane) was added drop by drop to the THF solution of **3.2** (300 mg, 0.58 mmol) at – 70 °C. The reaction was then allowed to warm to room temperature and stirred

overnight. The color of the reaction changes from deep red to magenta during the course of the reaction. The volatiles were removed under high vacuum and the residue was extracted using hexane (10 ml) and THF (5 ml) mixture. The solvent was reduced till saturation and kept at –36 °C to obtain the extremely air- and moisture-sensitive red colored crystals of **4.3** suitable for X-ray analysis. Yield: 0.15 g (76 %). Due to the solubility issue, we could not record the NMR of **4.3** despite several attempts in toluene-d_8, THF-d_8. While the compound is stable in solid-state inside a glove-box, it readily decomposes in solution to free ligand in 10-15 minutes. IR (cm^{-1}): 2955, 2865, 2129, 1625, 1590, 1549, 1432, 1377, 1361, 1332, 1303, 1248, 1225, 1181, 1123, 1100, 1032, 992, 833, 789, 746, 615 cm^{-1}.

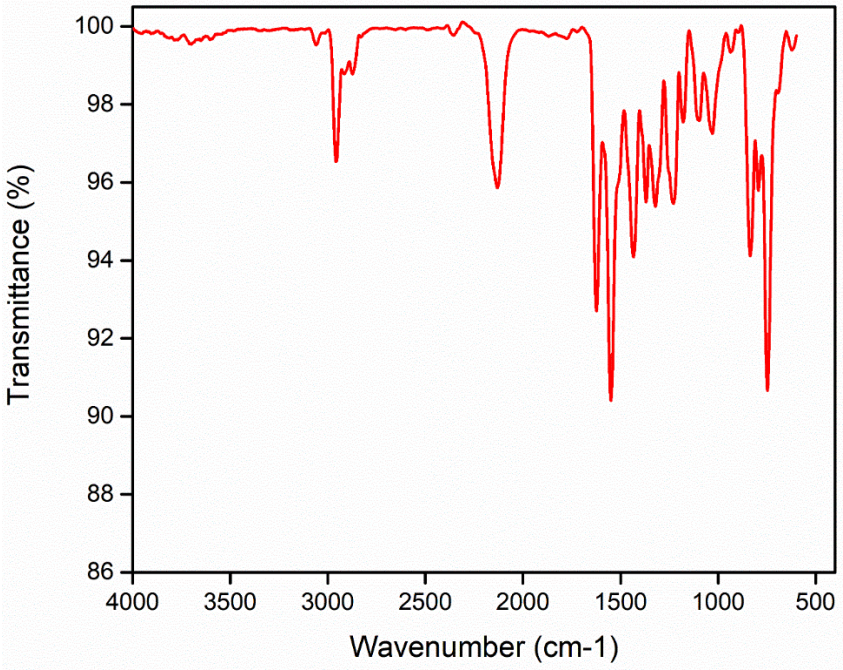

Figure A32. The IR (ATR mode) of **4.3**

6.4.3 Synthesis and characterization of compound 4.4: A Schlenk tube having a magnetic needle was charged with 4-iodotoluene (30 mg, 0.137 mmol), magnesium alkynylide complex **4.1** (82 mg, 0.171 mmol) and catalyst $Pd(PPh_3)Cl_2$ (5 mg, 6.8µg) in a glove box under Ar atmosphere and thf was added to the reaction mixture. The reaction was stirred overnight at

room temperature. The conversion was monitored using TLC. The volatiles were removed under high vacuum and the solid was obtained. The C-C coupled product **4.4** purified *via* column chromatography using hexane/ethyl acetate as elutes. Yield: 0.028 g (80 %).

^{1}H NMR (CHLOROFORM-d ,400MHz): δ = 7.52 - 7.57 (m, 3 H), 7.43 - 7.47 (m, *J*=8.0 Hz, 2 H), 7.33 - 7.38 (m, 4 H), 7.16 - 7.19 (m, *J*=7.9 Hz, 2 H), 2.39 (s, 3 H) ppm.

^{13}C NMR (101 MHz, CHLOROFORM-*d*) δ = 138.4 (s) 132.5 (s) 131.6 (s) 131.5 (s) 129.2 (s) 129.1 (s) 128.5 (s) 128.3 (s) 128.1 (s) 123.5 (s) 120.2 (s) 89.6 (s) 88.7 (s) 77.4 (s) 77. (s) 76.7 (s) 21.5 (s) ppm.

^{13}C NMR DEPT-135(101 MHz, CHLOROFORM-*d*) δ = 132.53 (s) 131.58 (s) 131.53 (s) 129.24 (s) 129.15 (s) 128.47 (s) 128.34 (s) 128.09 (s) 21.53 (s) ppm.

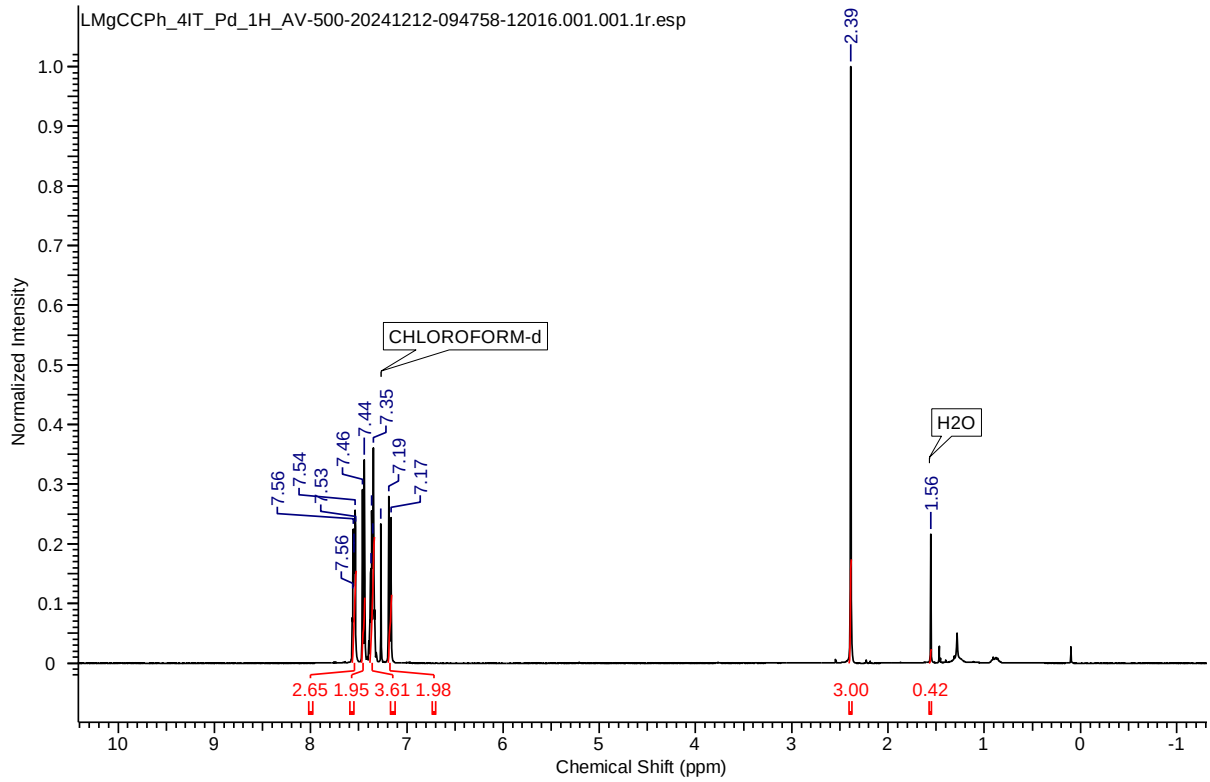

Figure A33. The ^{1}H NMR of **4.4**

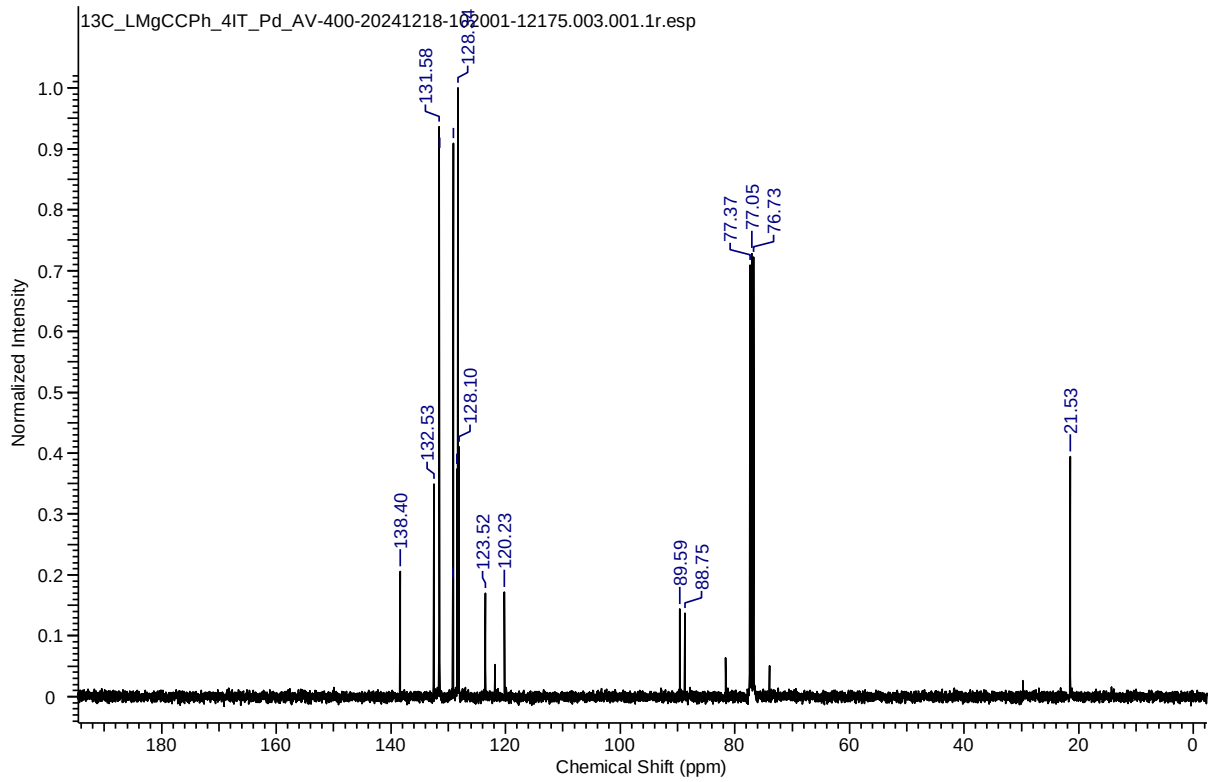

Figure A34. The ^{13}C NMR of **4.4**

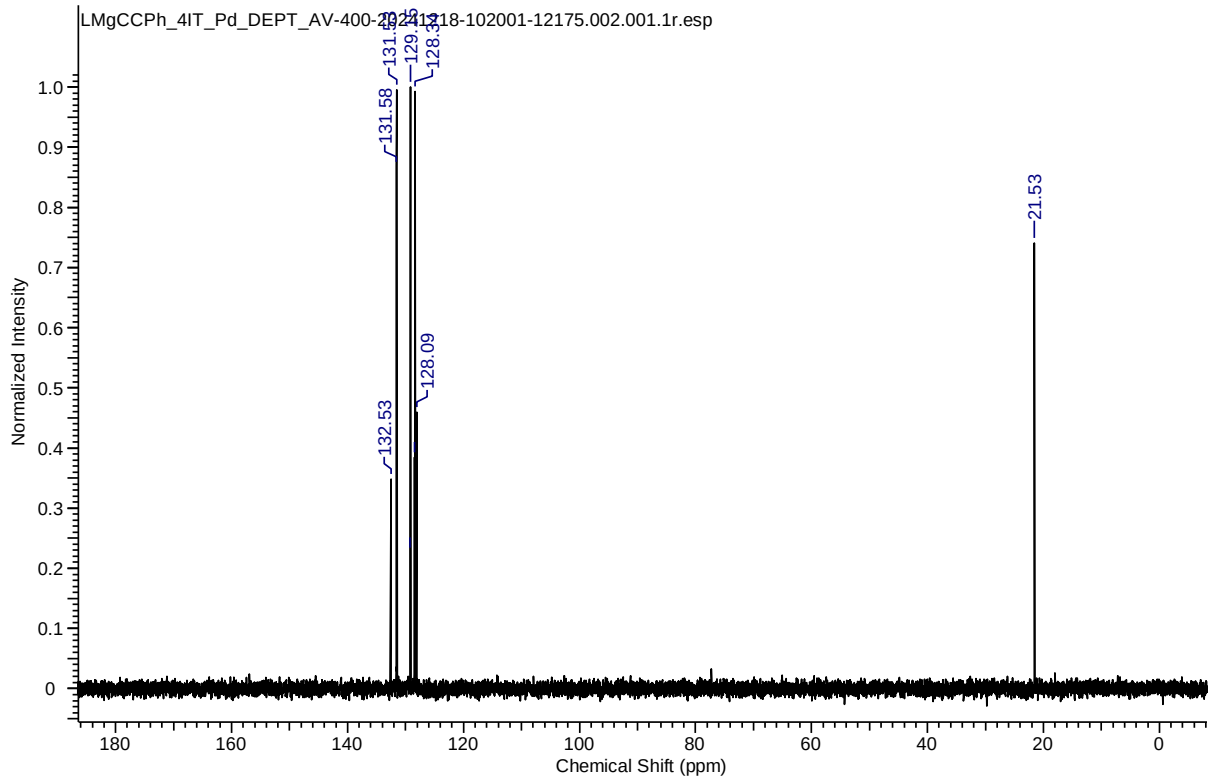

Figure A35. The ^{13}C DEPT-135 NMR of **4.4**

6.4.4: Crystal details for compounds 4.1-4.3

Crystal data of compound 4.1: $C_{35}H_{43}N_3MgO$**,** M = 638.17, CCDC: 2408477, colorless, 0.31 × 0.26 × 0.18 mm^3, monoclinic, space group '$P2_1/c$', *a = 16.348(13)Å, b = 19.198(15)Å, c = 11.982(9)Å,* α =90°, β =96.579(18)°, γ = 90°, Volume = 3736(5)Å^3, Z = 4, *T* = 100(2) K, D_{calc} (g cm^{-3}) = 1.135, *F*(*000*) = 1376, μ (mm^{-1}) = 0.083, 50772 reflections collected, 6965 unique reflections (R_{int}= 0.1187), 3552 observed ($I > 2\sigma(I)$) reflections, multi-scan absorption correction, T_{min} = 0.975, T_{max} = 0.985, 460 refined parameters, *S* = 1.068, *R*1 = 0.1187, *wR*2 = 0.2660 (all data *R* = 0.2105, *wR*2 = 0.3277), maximum and minimum residual electron densities; $\Delta\rho_{max}$ = 0.443, $\Delta\rho_{min}$= -0.377 (eÅ^{-3}).

Crystal data of compound 4.2: $C_{30}H_{39}N_3MgO$**,** M = 608.07, CCDC: 2408478, colorless, plate, 0.23 × 0.18 × 0.12 mm^3, triclinic, space group 'P-1', *a = 8.754(2)Å, b = 12.999(4)Å, c = 16.179(5)Å,* α =70.704(9)°, β = 80.148(8)°, γ = 79.983(8)°, Volume = 1898.3(8)Å^3, Z = 1, *T* = 100(2) K, D_{calc} (g cm^{-3}) = 1.189, *F*(*000*) = 650.0, μ (mm^{-1}) = 0.092, 32277 reflections collected, 6698 unique reflections (R_{int}= 0.0849), 4195 observed ($I > 2\sigma(I)$) reflections, multi-scan absorption correction, T_{min} = 0.980, T_{max} = 0.989, 484 refined parameters, *S* = 1.040, *R*1 = 0.0849, *wR*2 = 0.1742 (all data *R* = 0.1396, *wR*2 = 0.2009), maximum and minimum residual electron densities; $\Delta\rho_{max}$ = 0.958, $\Delta\rho_{min}$= -0.403 (eÅ^{-3}).

Crystal data of compound 4.3: $C_{27}H_{39}N_5MgSi$**,** M = 486.03, CCDC: 2378742, plate, red, 0.22 × 0.18 × 0.12 mm^3, monoclinic, space group 'C 2/c, *a = 12.2445(10)Å, b = 20.9010(16)Å, c = 22.9953(16)Å,* α = 90°, β = 94.428(2)°, γ = 90°, Volume = 5867.4(8)Å^3, Z = 8, *T* = 100(2) K, D_{calc} (g cm^{-3}) = 1.100, *F*(*000*) = 2096 μ (mm^{-1}) = 0.124, 160532 reflections collected, 7523 unique reflections (R_{int}= 0.0537), 6820 observed ($I > 2\sigma(I)$) reflections, multi-scan absorption correction, T_{min} = 0.1082, T_{max} = 0.1592, 316 refined parameters, *S* = 1.078, *R*1 = 0.0537, *wR*2 = 0.1274 (all data *R* = 0.0671, *wR*2 = 0.1364), maximum and minimum residual electron densities; $\Delta\rho_{max}$ = 0.419, $\Delta\rho_{min}$= -0.361 (eÅ^{-3}).

6.5: Chapter 5 experimental details:

6.5.1 Synthesis and characterization of compound 5.1: 1.05 equivalent of $AlH_3.NMe_2Et$ (0.103 g, 0.6 mmol) and **LH** (0.2 g, 0.57 mmol) were dissolved in 10 ml of Et_2O in separate

Schlenk flasks. Under cooling condition, $AlH_3.NMe_2Et$ solution in Et_2O was cannulated to the ligand solution in Et_2O. Warmed the reaction mixture to room temperature and stirred it for 4 h. Slowly the colour changed from yellow to purple. After 4 hrs, purple solution was cannulated and concentrated. The crystals of compound **5.1** was obtained at – 4 °C after 2 days.

Yield: 0.130 g (60 %)

^{1}H NMR (400 MHz, 298 K, $CDCl_3$): δ = 8.73 (d, J = 5.5 Hz, 1 H), 7.88 (t, J = 8.5 Hz, 1 H), 7.40 (t, J = 6.4 Hz, 2 H), 7.24 (m, 2 H), 7.13 (m, 1 H), 5.21 (s, 1 H), 4.96 (s, 1 H), 4.81 (s, 1 H), 3.52 (m, 1 H), 2.78 (m, 1 H), 2.30 (s, 3 H), 1.76 (s, 3 H), 1.37 (d, J = 6.6 Hz, 3 H), 1.25 (d, J = 6.5 Hz, 3 H), 1.08 (d, J = 6.5 Hz, 3 H), 1.01 ppm (d, J = 6.5 Hz, 3 H) ppm

^{13}C{^{1}H} NMR (125 MHz, 298 K, CDCl3): δ =170 (s), 167.1 (s), 155.6 (s), 146 (s),140 (s), 126.3 (s), 124.3 (s), 121.5 (s), 98.6 (s), 51.6 (s), 28.6 (s), 28 (s), 26 (s), 25 (s), 24.7 (s), 24.6 (s), 24.3 (s), 24 (s) ppm.

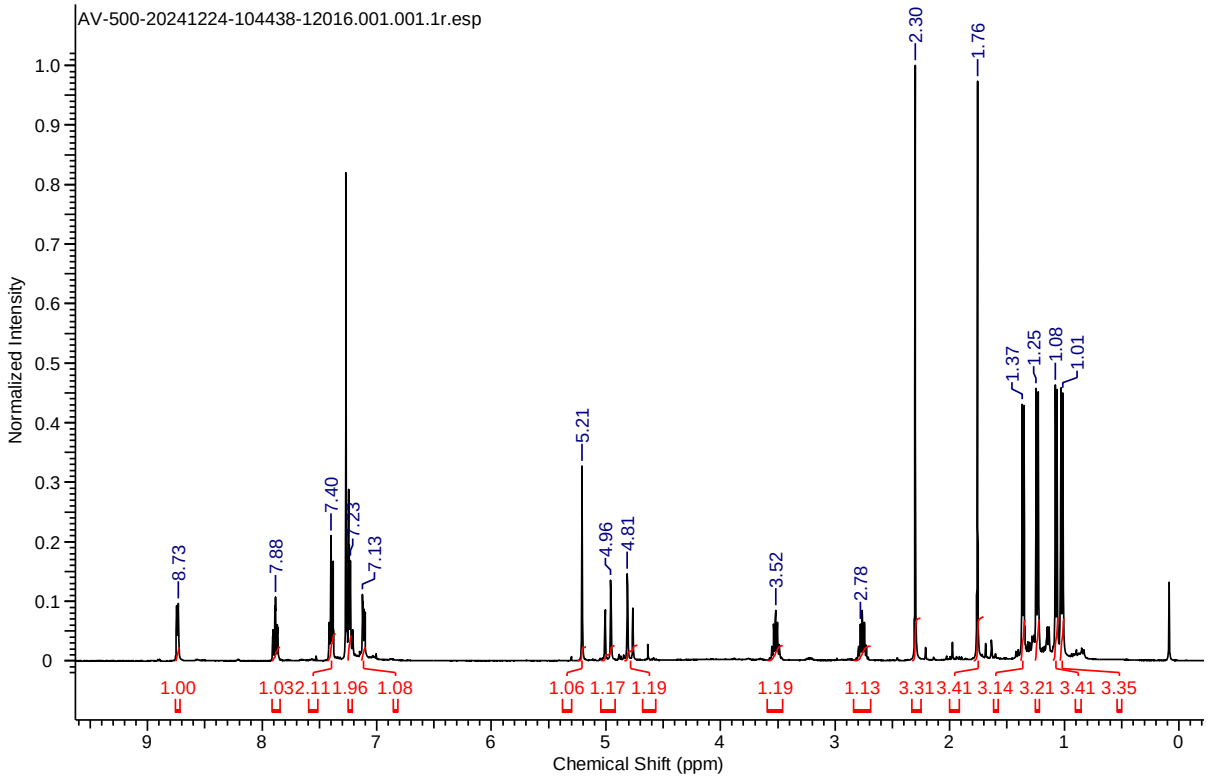

Figure A36. The ^{1}H NMR of **5.1**

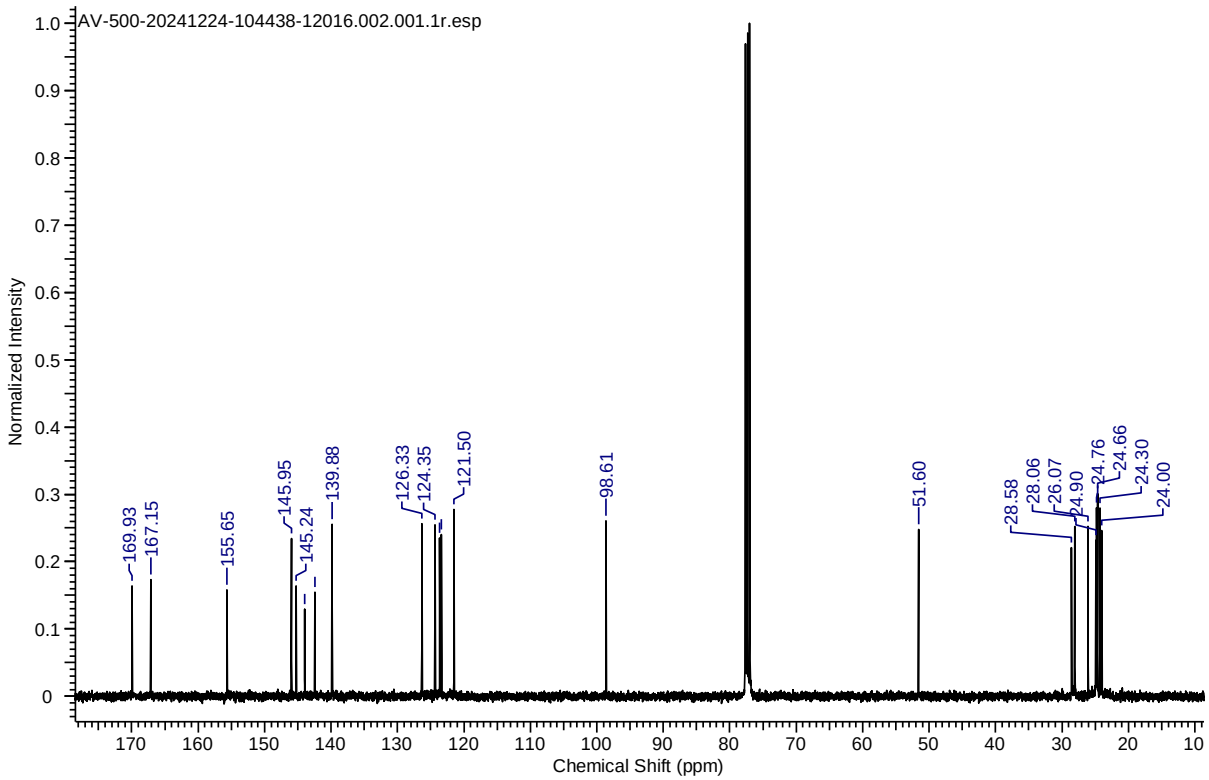

Figure A37. ^{13}C NMR spectrum of **5.1**

6.5.2 Synthesis and characterization of compound 5.2: 1.05 equivalent of AlH3.NMe2Et (0.103 g, 0.6 mmol) and LH (0.2 g, 0.57 mmol) were dissolved in 10 ml of toluene in separate Schlenk flasks. Under cooling condition, AlH3.NMe2Et solution in was cannulated to the ligand solution in toluene. Warmed the reaction mixture to room temperature and run it for 6 h. Slowly the colour changed from yellow to purple. After 6 hrs, the purple solution was cannulated and concentrated. The crystals of compound **5.2** suitable for SCXRD was obtained at – 36 °C within 24 h. Due to less stability in d-solvents we were unable to get a clean ^{13}C NMR and HRMS data.

Yield: 0.18 g (42 %)

^{1}H NMR (400 MHz, C_6D_6, 298 K): δ = 8.57 (d, J = 5.5 Hz, 2 H), 7.28 - 7.34 (m, 3 H), 7.21-7.26 (m, 2 H), 7.19 (d, J = 1.8 Hz, 1 H), 6.73 - 6.80 (m, 2 H), 6.40 (t, J = 4 Hz, 2 H), 6.23 (d, J = 7.9 Hz, 2 H), 5.10 (s, 2 H), 4.26 (d, J = 19.4 Hz, 2 H), 3.99 - 4.07 (m, 3 H), 3.93 (d, J = 19.5 Hz, 2 H), 3.68 - 3.79 (m, 2 H), 3.18 - 3.29 (m, 2 H), 1.78 (d, J = 6.6 Hz, 6 H), 1.73 - 1.75 (d, J = 6.6 Hz, 6 H), 1.70 (s, 7 H), 1.66 (d, J = 6.6 Hz, 2 H), 1.32 (d, J = 2.5 Hz, 6 H), 1.30 (d, J = 2.5 Hz, 6 H), 1.24 (d, J = 6.9 Hz, 3 H), 1.14 (d, J = 7.0 Hz, 6 H) ppm.

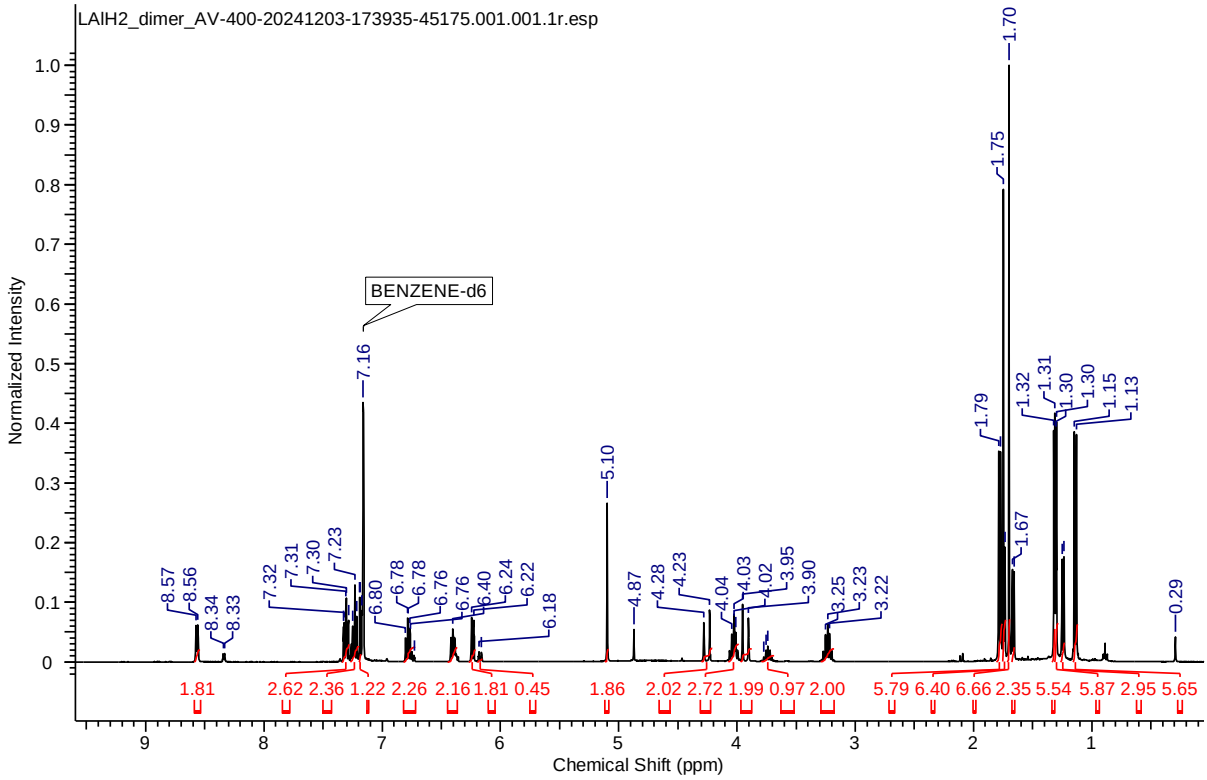

Figure A38. The ^{1}H NMR of **5.2**

6.5.3 Synthesis and characterization of compound 5.3: 1.2 equivalent of BnK (0.089 g, 0.686 mmol) and LH (0.2 g, 0.57 mmol) were dissolved in 20 ml of toluene under cooling condition. Warmed the reaction mixture to room temperature and stirred for 6 h. To this AlCl3 (0.092 g, 0.686 mmol) solution in toluene was added under cooling condition. Run the reaction for overnight. Carried out frit filtration and reduced the resulting toluene solution to yield compound **5.3** in 83% yield. The crystals were grown at – 4 °C.

^{1}H NMR (400 MHz, 298 K, $CDCl_3$): δ = 8.90 (d, J = 5.5 Hz, 1 H), 7.5 (t, J = 8.5 Hz,1 H), 7.40 (t, J = 6.4 Hz, 1 H), 7.33 (d, J = 7.9 Hz, 1 H), 7.24-7.20 (m, 1 H), 7.15 (d, J = 7.0 Hz 2 H), 5.30 (s, 1 H), 4.88 (s, 2 H), 3.15 - 3.28 (m, 2 H), 2.30 (s, 3 H), 1.77 (s, 3 H), 1.27 (d, J = 6.8 Hz, 6 H), 1.14 ppm (d, J = 6.9 Hz, 6 H) ppm.

^{13}C NMR (101 MHz, $CDCl_3$, 298 K): δ = 171.1 (s) 167.4 (s) 152.8 (s) 146.9 (s) 143.9 (s) 142.9(s) 139 (s) 126.4 (s) 123.6 (s) 123.6 (s) 121.3 (s) 97.8 (s) 76.7 (s) 50.1 (s) 28.2 (s) 25.3 (s) 24.7 (s) 24.5 (s) 24.5 (s) ppm.

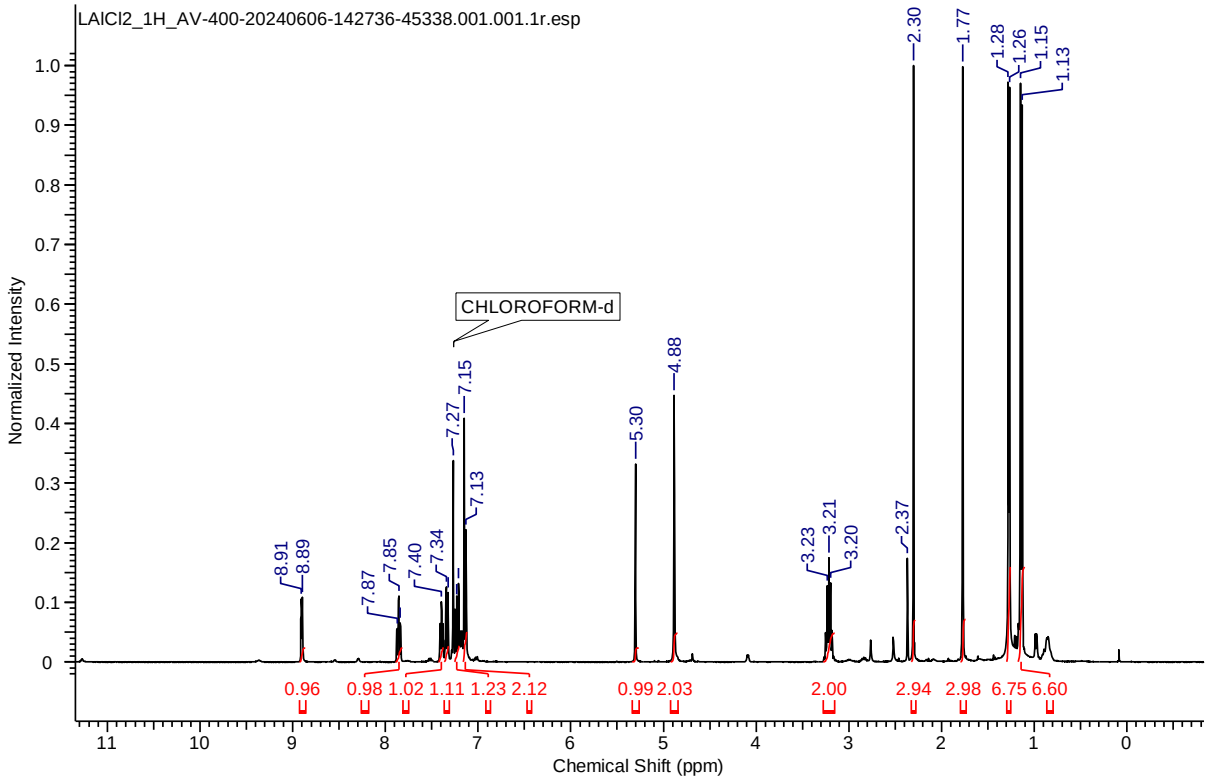

Figure A39. ^{1}H NMR spectrum of **5.3**

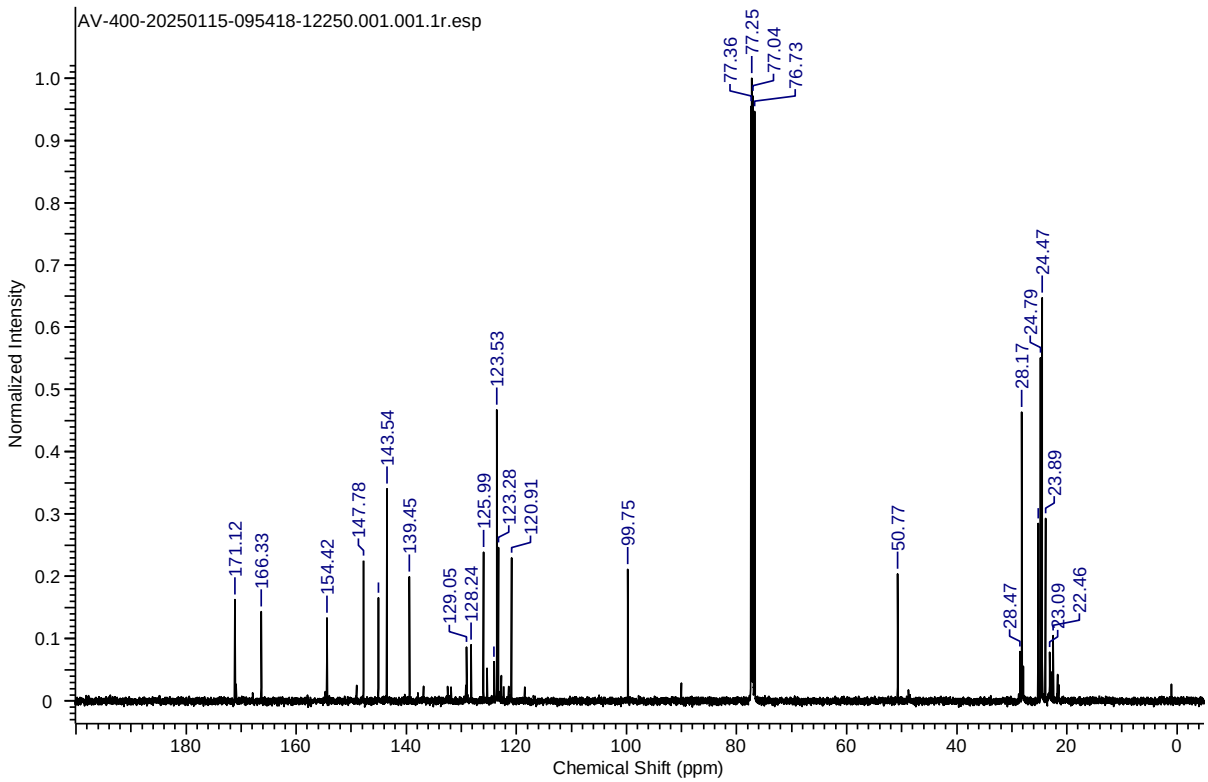

Figure A40. ^{13}C NMR spectrum of **5.3**

6.5.4 Synthesis and characterization of compound 5.4: 1.2 equivalent of BnK (0.089 g, 0.686 mmol) and LH (0.2 g, 0.57 mmol) were dissolved in 20 ml of toluene under cooling condition. Warmed the reaction mixture to room temperature and stirred for 6 h. To this $GaCl_3$ (0.120 g, 0.686 mmol) solution in toluene was added under cooling condition. Run the reaction for overnight. Carried out frit filtration and reduced the resulting toluene solution to yield compound **5.4** in 81 %. The crystals were grown at – 4 °C.

^{1}H NMR (400 MHz, 298 K, CDCl3) δ = 8.88 (d, J = 5.5 Hz, 1 H), 7.83 (t, J = 8.5 Hz, 1 H), 7.39 (t, J = 6.5 Hz 1 H), 7.32 (d, J = 7.9 Hz 1 H), 7.25 (d, J = 5.5 Hz, 1 H), 7.14 (d, J = 7.0 Hz, 2 H), 5.15 (s, 1 H), 4.89 (s, 2 H), 3.22 (m, 2 H), 2.31 (s, 3 H), 1.78 (s, 3 H), 1.27 (d, J = 6.8 Hz, 6 H), 1.16 ppm (d, J = 6.9 Hz, 6 H) ppm**.**

^{13}C NMR (101 MHz, $CDCl_3$, 298 K): δ = 171.1 (s) 167.4 (s) 152.9 (s) 147.0 (s) 143.9 (s) 143.0 (s) 139.0 (s) 129.1 (s) 128.2 (s) 126.4 (s) 123.6 (s) 123.6 (s) 121.3 (s) 97.8 (s) 77.4 (s) 77.3 (s) 77.1 (s) 76.7 (s) 50.1 (s) 28.2 (s) 25.3 (s) 24.8 (s) 24.5 (s) 24.5 (s) ppm.

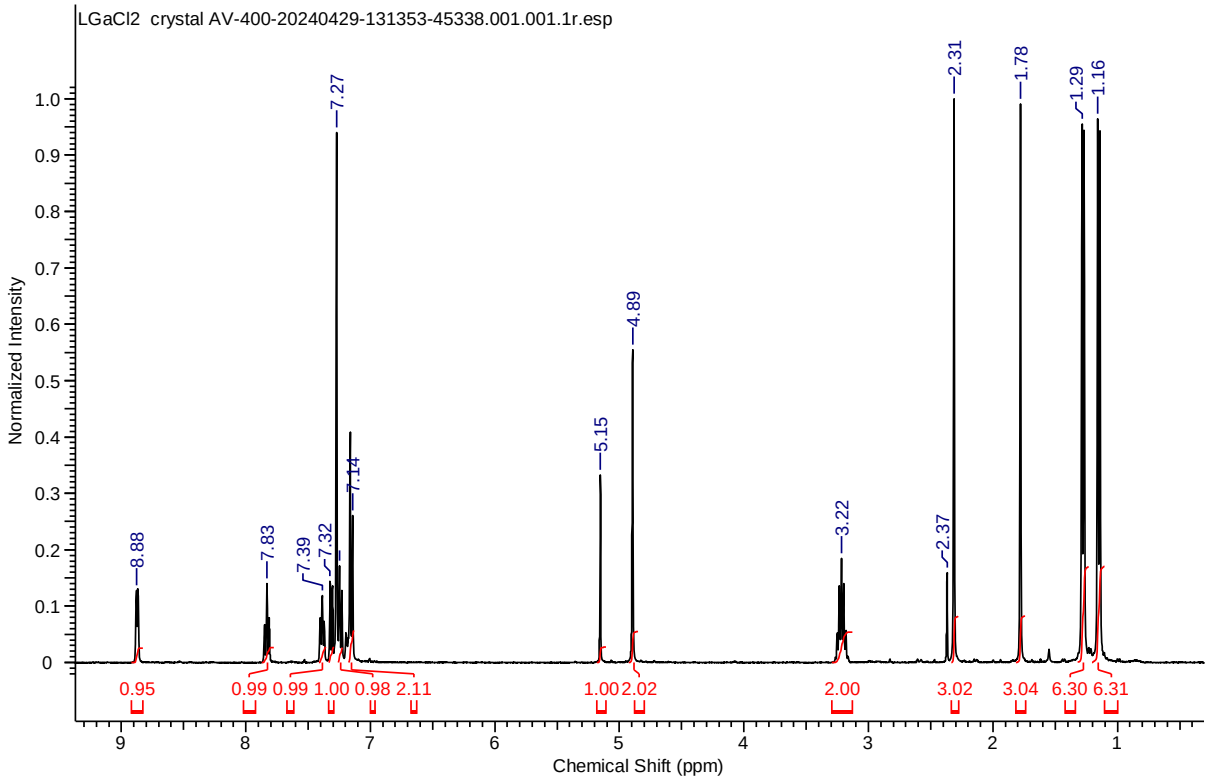

Figure A41. ^{1}H NMR spectrum of **5.4**

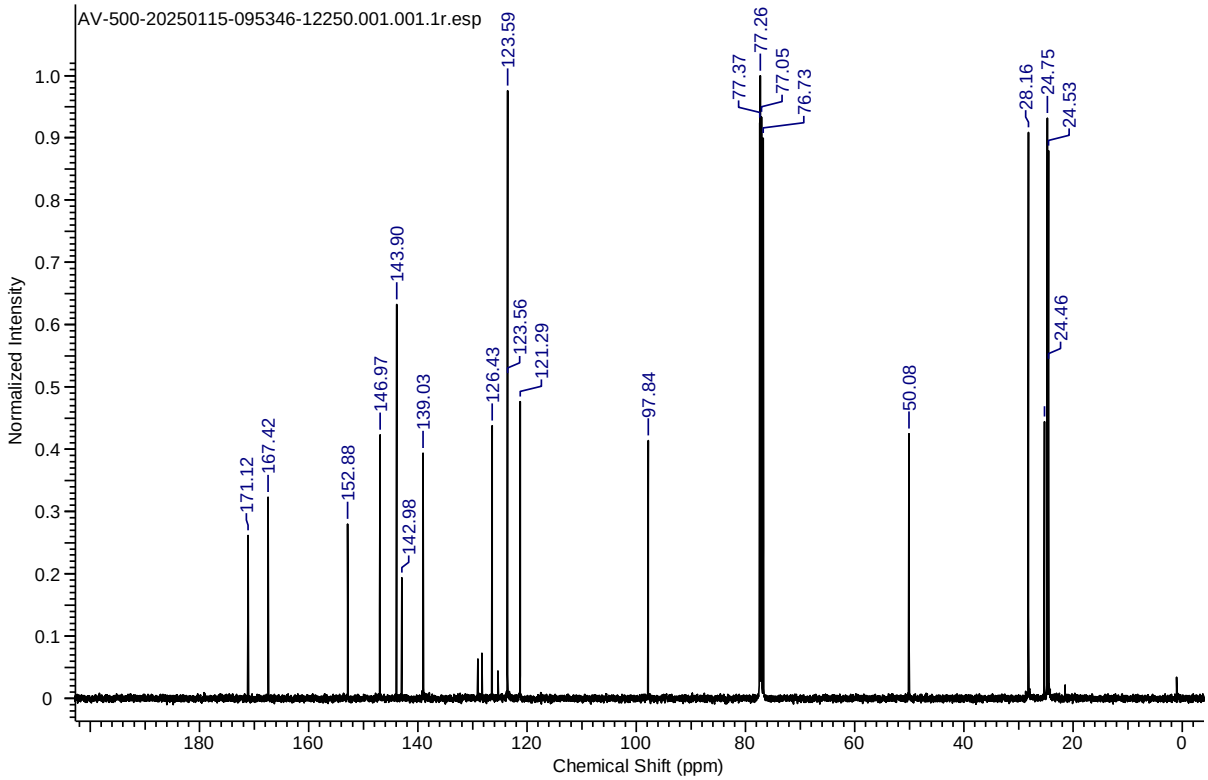

Figure A42. ^{13}C NMR spectrum of **5.4**

6.5.5: Crystal details for compounds 5.1, 5.2 and 5.4

Crystal data of compound 5.1: $C_{23}H_{32}AlN_3$**,** M =377.49, colorless, 0.22 × 0.26 × 0.31 mm^3, monoclinic, space group '$P2_1/c$', *a = 8.8203(3)Å, b = 14.9167(6)Å, c = 16.1642(7)Å,* α =90°, β = 92.5120(10)°, γ = 90°, Volume = 2124.68(14)Å^3, Z = 4, *T* = 100(2) K, D_{calc} (g cm^{-3}) = 1.180, *F*(*000*) = 816, μ (mm^{-1}) = 0.108, 147188 reflections collected, 8222 unique reflections (R_{int}= 0.414), 6255 observed ($I > 2\sigma$ (I)) reflections, multi-scan absorption correction, T_{min} = 0.1143, T_{max} = 0.1620, 258 refined parameters, *S* = 1.067, *R*1 = 0.0414, *wR*2 = 0.0986 (all data *R* = 0.0681, *wR*2 = 0.1110), maximum and minimum residual electron densities; $\Delta\rho_{max}$ = 0.371, $\Delta\rho_{min}$= -0.286 (eÅ^{-3}).

Crystal data of compound 5.2: $C_{46}H_{64}Al_2N_6$ M = 754.98, colorless, plate, 0.23 × 0.16 × 0.11 mm^3, triclinic, space group '*P-1*', *a = 13.7933(7)Å, b = 19.0774(10)Å, c = 21.4366(12)Å,* α = 101.952(2)°, β = 105.336(2)°, γ = 102.573(2)°, Volume = 5095.3(5)Å^3, Z = 2, *T* = 100(2) K, D_{calc} (g cm^{-3}) = 1.163, *F*(*000*) = 1928, μ (mm^{-1}) = 0.100, 388723 reflections collected, 37425 unique reflections (R_{int}= 0.0503), 31186 observed ($I > 2\sigma$ (I)) reflections, multi-scan absorption correction, T_{min} = 0.1133, T_{max} = 0.1597, 1205 refined parameters, *S* = 1.309, *R*1 =

0.0503, *wR*2 = 0.1647 (all data *R* = 0.0647, *wR*2 = 0.1755), maximum and minimum residual electron densities; $\Delta\rho_{max}$ = 0.661, $\Delta\rho_{min}$= -0.864 (eÅ^{-3}).

Crystal data of compound 5.4: $C_{23}H_{30}GaN_3Cl_2$ M = 486.03, plate, colorless, 0.22 × 0.18 × 0.12 mm^3, monoclinic, space group '$P2_1/c$', *a* = *13.9451(19)Å*, *b* = *15.735(2)Å*, *c* = *26.963(4)Å*, α = 90°, β = 104.4(6)°, γ = 90°, Volume = 5732.3(19)Å^3, Z = 4, *T* = 111(2) K, D_{calc} (g cm^{-3}) = 1.359, *F*(*000*) = 2456 μ (mm^{-1}) = 1.172, 84273 reflections collected, 12649 unique reflections (R_{int}= 0.1596), 7178 observed ($I > 2\sigma(I)$) reflections, multi-scan absorption correction, T_{min} = 0.0939 , T_{max} = 0.1507, 663 refined parameters, *S* = 1.078, *R*1 = 0.1596, *wR*2 = 0.3656 (all data *R* = 0.2439, *wR*2 = 0.3875), maximum and minimum residual electron densities; $\Delta\rho_{max}$ = 0.407, $\Delta\rho_{min}$= -0.341 (eÅ^{-3}).

6.6 References

1. S. Pahar, V. S. V. S. N. Swamy, T. Das, R. G. Gonnade, K. Vanka and S. S. Sen, Access to diverse germylenes and a six-membered dialane with a flexible beta-diketiminate. *Chem. Commun.*, 2020, **56**, 11871–11874.
2. Bruker (2006). APEX2, SAINT and SADABS. Bruker AXS Inc. Madison, Wisconsin, USA.
3. G. M. Sheldrick, Short History of SHELX. *Acta Crystallogr*, 2008, ***A64***, 112-122.
4. L. J. Farrugia, ORTEP-3 for Windows - a version of ORTEP-III with a Graphical User Interface (GUI). *J. Appl. Cryst.* 1997, **30**, 565–565.
5. M. Frisch, G. Trucks, H. Schlegel, G. Scuseria, M. Robb, J. Cheeseman, G. Scalmani, V. Barone, B. Mennucci and G. Petersson, *Gaussian 09, Version D. 01 Software for Calculation*; Gaussian. Inc.: Wallingford, CT, USA, 2013.
6. J. P. Perdew, K. Burke and M. Ernzerhof, Generalized Gradient Approximation Made Simple. *Phys. Rev. Lett.* 1996, **77**, 3865– 3868.
7. F. Weigend and R. Ahlrichs Balanced Basis Sets of Split Valence, Triple Zeta Valence and Quadruple Zeta Valence Quality for H to Rn: Design and Assessment of Accuracy. *Phys. Chem. Chem. Phys.* 2005, **7**, 3297– 3305.
8. T. Lu and F. Chen, Multiwfn: A Multifunctional Wavefunction Analyzer. *J. Comput. Chem.* 2012, **33**, 580−592.
9. W. Humphrey, A. Dalke and K. Schulten, VMD: Visual Molecular Dynamics. *J. Mol. Graphics* 1996, **14 (1)**, 33−38.

10. T. Ziegler and A. Rauk, On the Calculation of Bonding Energies by the Hartree Fock Slater Method: I. The Transition State Method. *Theoretica Chimica Acta* 1977, **46**, 1−10.
11. M. P. Mitoraj, A. Michalak and T. Ziegler, A Combined Charge and Energy Decomposition Scheme for Bond Analysis. *Chem. Theory Comput.* 2009, **5 (4)**, 96220.
12. M. P. Mitoraj and A. Michalak, Multiple Boron−Boron Bonds in Neutral Molecules: An Insight from the Extended Transition State Method and the Natural Orbitals for Chemical Valence Scheme. *Inorg. Chem.* 2011, ***50,*** 2168.

ABSTRACT

Name of the Student: Vishal Kumar Sharma **Registration No.:** 10CC19A26042

Faculty of Study: Chemical Sciences **Year of Submission:** 2025

AcSIR academic centre/CSIR Lab: CSIR-NCL **Name of the Supervisor:** Dr. Sakya S. Sen

Title of the thesis: Tridentate NacNac Ligand Supported Main-Group and Transition Metal compounds: Pendent Picolyl Powers Peculiar Chemistry

---

This thesis covers the basics of ligand design in organometallics and the importance of a ligand in stabilization of a metal center. Here, we have discussed monoanionic nacnac ligand and its advancements in transition metals and main group chemistry. The introduction of modified tridentate nacnac ligand having picolyl prydine arm as an extra donor site to provide stabilization. ***Chapter 2*** discusses the synthesis and characterization of a tridentate nacnac ligand-stabilized T-shaped Ni(I) metalloradical, including its radical trapping using TEMPO as a trapping agent. The reactivity of the complex toward small molecule activation is also investigated. Structural and bonding arrangements of all complexes were elucidated through single-crystal X-ray diffraction (XRD) analysis. DFT studies further corroborate the presence of a single unpaired electron localized on the nickel centre, confirming its metalloradical nature. ***Chapter 3*** contains the synthesis of monomeric magnesium bromide complex and dearomatized magnesium complex using Grignard reagent and dibutylmagnesium respectively. Among them dearomatized magnesium complex has been utilised to activate O–H bond of water, which was confirmed by deuterium-labelling experiments. The synthesis of magnesium hydride is also attempted eventually leading to inter molecular pyridine reduction. ***Chapter 4*** covers the utilization of dearomatized magnesium complex towards C–H bond of terminal alkynes and diazoalkane. The magnesium alkynylide complexes of magnesium was structurally characterized using single crystal XRD and NMR spectroscopy. The magnesium alkynylide complexes were further explored towards the C–C cross coupling using Pd as a catalyst. ***Chapter 5*** details the synthesis of tridentate nacnac ligand-supported aluminium and gallium halides using a novel synthetic protocol that had not been previously achieved using other bases. The solvent effect on the stability of tridentate nacnac-stabilized aluminium hydride was investigated, leading to the successful isolation of a monomeric aluminium hydride complex. Density Functional Theory (DFT) calculations were performed to elucidate the reaction mechanism and confirm the formation of the final aluminium hydride dimer through the identified intermediate species.

List of all publication(s) in SCI Journal(s) (published & accepted) with complete bibliographic details

1. **Vishal Sharma,** Soumya Ranjan Dash, Kumar Vanka, Rajesh G. Gonnade and Sakya S. Sen*, Magnesium–Ligand Cooperation in Breaking the O–H and C–H Bonds of Water and Diazoalkane, *Organometallics,* https://doi.org/10.1021/acs.organomet.5c0003 (2025).
2. Sanjukta Pahar†, **Vishal Sharma**†, K. Vipin Raj, Mayur P. Sangole, Christy P. George, Kirandeep Singh, Kumar Vanka, Rajesh G. Gonnade And Sakya S. Sen, Tridentate NacNac Tames T-Shaped Nickel(I) Radical, *Chem. Eur. J.*, 30, e202303957(2024) († : Equal contribution).

Other Publications

3. Rohit Kumar, **Vishal Sharma**, Subhrashis Banerjee, Kumar Vanka and Sakya S. Sen*, Controlled reduction of isocyanates to formamides using monomeric magnesium, *Chem. Commun.*, 59, 2255 - 2258 (2023).

4. Rohit Kumar, Sayan Dutta, **Vishal Sharma**, Praval P. Singh, Rajesh G. Gonnade*, Debasis Koley* and Sakya S. Sen*, Monomeric Magnesium Catalyzed Alkene and Alkyne Hydroboration, *Chem. Eur. J.*, 28, e202201896 - (1-8) (2022).

5. Sanjukta Pahar, **Vishal Sharma**, Biplab mahata, Christy P. George, Himanshu Sharma, Kumar Vanka and Sakya S. Sen*, Tridentate NacNac Stabilized Tin and Nickel Complexes: Access to a Monomeric Nickel Hydride and Its Catalytic Application, *Inorg. Chem.*, 61, 17370 - 17377 (2022).

6. Rohit Kumar, **Vishal Sharma**, Shailja Jain, Himanshu Sharma, Kumar Vanka and Sakya S. Sen*, A Well-Defined Calcium Compound Catalyzes Trimerization of Arylisocyanates into 1,3,5-Triarylisocyanurates, *ChemCatChem.*, 14, e202101788 - (1-6) (2022).

7. Sanjukta Pahar, **Vishal Sharma,** Srinu Tothadi and Sakya S. Sen*, Pyridylpyrrolido ligand in Ge(II) and Sn(II) chemistry: Synthesis, reactivity and catalytic application, *Dalton Trans.*, 50, 16678 - 16684 (2021).

8. Milan Kumar Bisai, **Vishal Sharma,** Rajesh G. Gonnade* and Sakya S. Sen*, Reactivities of Silaimines with Boranes: From Cooperative B-H Bond Activation to Donor Stabilized Silyl Cation, *Organometallics.*, 40, 2133 - 2138 (2021).

List of papers with abstract presented (oral/poster) at national/international conferences/seminars with complete details

1. Delivered a talk in 2nd ICMGSC meet at IISER Thiruvananthapuram (Feb, 2025) on "Magnesium-ligand cooperation in O−H and C−H bond cleavage of water, alkyne and diazoalkane".
2. Delivered a talk in NCL-RF Annual Student Conference at CSIR-National Chemical Laboratory, Pune, India, (November 2024) on "Magnesium-ligand cooperation in O−H and C−H bond cleavage of water, alkyne and diazoalkane".
3. Presented Poster at 30th ICOMC Jaypee palace Agra, India, (July, 2024) on "C-H and O-H Bond Activation by Magnesium via Metal Ligand Cooperation (MLC)".
4. Presented Digital Poster at RSC Linkedin Conference (March, 2024) on "Tridentate NacNac Tames T-Shaped Nickel(I) Radical".
5. Presented Poster at ICMGSC, IISER Thiruvananthapuram (Feb, 2023) on "A Tridentate NacNac Stabilized Tin and Nickel Complexes: Access to a Monomeric Nickel Hydride and its Catalytic Application".
6. Presented Poster at Science Day, CSIR-NCL Pune, India (Feb, 2023) on "Synthesis and Reactivity of T-Shaped Nickel Radical".
7. Presented Digital Poster at RSC twitter Conference (Feb, 2023) on "Tridentate NacNac Tames T-Shaped Nickel(I) Radical".
8. Presented Poster at MTIC-XIX, BHU Banaras, India (Dec, 2022) on "Tridentate NacNac Tames T-Shaped Nickel(I) Radical".
9. Presented Digital Poster at LatinXChem Twitter Conference (Sep, 2021) on "Synthesis and Reactivity of Silaimines".
10. Presented Poster at Science Day, CSIR-NCL Pune, India (Feb, 2021) on "Synthesis and Reactivity of Silaimines".

About the Author

Mr. Vishal Kumar Sharma son of Shanti Lal Sharma and Sushila Sharma, was born in Chittorgarh district, Rajasthan, India, in 1996. He completed his B.Sc. from University College of Science, Mohan Lal Sukhadia University, Udaipur, Rajasthan. He obtained his master's degree from National Institute of Technology, Jamshedpur, Jharkhand. After qualifying CSIR-National Eligibility Test (NET-JRF) examination, he moved to Catalysis and Inorganic Chemistry Division, CSIR-National Chemical Laboratory, Pune, India to pursue her Ph.D. degree under the guidance of Dr. Sakya Singha Sen. His research area lies on "*Tridentate NacNac Ligand Supported Main-Group and Transition Metal compounds: Pendent Picolyl Powers Peculiar Chemistry*."

Education and Research Experience

Ph.D.: From August 2019 to till date, working under the supervision of Dr. Sakya Singha Sen at CSIR- National Chemical Laboratory. I will be completing my doctoral work by May 2025.

CSIR-JRF: Qualified in chemical sciences, 2018 with all India rank 65.

M.Sc.: (2016-2018) National Institute of Technology, Jamshedpur, Jharkhand, India.

B.Sc.: (2014-2016) University College of Science, Mohan Lal Sukhadia University, Udaipur, Rajasthan, India.

List of Scientific Contributions

1. ***Vishal Sharma,*** *Soumya Ranjan Dash, Kumar Vanka, Rajesh G. Gonnade and Sakya S. Sen*,* Magnesium–Ligand Cooperation in Breaking the O–H and C–H Bonds of Water and Diazoalkane, *Organometallics, https://doi.org/10.1021/acs.organomet.5c0003 (2025).*

2. *Sanjukta Pahar*[†], ***Vishal Sharma***[†], *K. Vipin Raj, Mayur P. Sangole, Christy P. George, Kirandeep Singh, Kumar Vanka, Rajesh G. Gonnade and Sakya S. Sen,* Tridentate NacNac Tames T-Shaped Nickel(I) Radical, *Chem. Eur. J.*, 30, e202303957(2024) († : Equal contribution).

3. *Rohit Kumar, **Vishal Sharma**, Subhrashis Banerjee, Kumar Vanka and Sakya S. Sen*,* Controlled reduction of isocyanates to formamides using monomeric magnesium, *Chem. Commun.*, 59, 2255 - 2258 (2023).

4. *Rohit Kumar, Sayan Dutta, **Vishal Sharma**, Praval P. Singh, Rajesh G. Gonnade*, Debasis Koley* and Sakya S. Sen*,* Monomeric Magnesium Catalyzed Alkene and Alkyne Hydroboration, *Chem. Eur. J.*, 28, e202201896 - (1-8) (2022).

5. *Sanjukta Pahar, **Vishal Sharma**, Biplab mahata, Christy P. George, Himanshu Sharma, Kumar Vanka and Sakya S. Sen*,* Tridentate NacNac Stabilized Tin and Nickel Complexes: Access to a Monomeric Nickel Hydride and Its Catalytic Application, *Inorg. Chem.*, 61, 17370 - 17377 (2022).

6. *Rohit Kumar, **Vishal Sharma**, Shailja Jain, Himanshu Sharma, Kumar Vanka and Sakya S. Sen*,* A Well-Defined Calcium Compound Catalyzes Trimerization of Arylisocyanates into 1,3,5-Triarylisocyanurates, *ChemCatChem.*, 14, e202101788 - (1-6) (2022).

7. *Sanjukta Pahar, **Vishal Sharma**, Srinu Tothadi and Sakya S. Sen*,* Pyridylpyrrolido ligand in Ge(II) and Sn(II) chemistry: Synthesis, reactivity and catalytic application, *Dalton Trans.*, 50, 16678 - 16684 (2021).

8. *Milan Kumar Bisai, **Vishal Sharma**, Rajesh G. Gonnade* and Sakya S. Sen*,* Reactivities of Silaimines with Boranes: From Cooperative B-H Bond Activation to Donor Stabilized Silyl Cation, *Organometallics.*, 40, 2133 - 2138 (2021).

Symposia Attended

National conferences: 2 (Poster)

1 (Oral presentation)

International conferences: 3 (Poster presentation)

3 (Poster presentation: Virtual mode)

1 (Oral presentation)

Chemistry–A European Journal
Research Article
doi.org/10.1002/chem.202303957
Chemistry Europe
European Chemical Societies Publishing
www.chemeurj.org

Tridentate NacNac Tames T-Shaped Nickel(I) Radical

Sanjukta Pahar[+],[a, b] Vishal Sharma[+],[a, b] K. Vipin Raj,[b, c] Mayur P. Sangole,[b, c] Christy P. George,[b, c] Kirandeep Singh,[b, c] Kumar Vanka,[b, c] Rajesh G. Gonnade,[b, c] and Sakya S. Sen*[a, b]

Dedicated to Professor Ramaswamy Murugavel on the occasion of his 60th birthday

The reaction of a nickel(II) chloride complex containing a tridentate β-diketiminato ligand with a picolyl group [2,6-iPr$_2$-C$_6$H$_3$NC(Me)CHC(Me)NH(CH$_2$py)]Ni(II)Cl (**1**)] with KSi(SiMe$_3$)$_3$ conveniently afforded a nickel(I) radical with a T-shaped geometry (**2**). The compound's metalloradical nature was confirmed through electron paramagnetic resonance (EPR) studies and its reaction with TEMPO, resulting in the formation of a highly unusual three-membered nickeloxaziridine complex (**3**). When reacted with disulfide and diselenide, the S–S and Se–Se bonds were cleaved, and a coupled product was formed through carbon atom of the pyridine-imine group. The nickel(I) radical activates dihydrogen at room temperature and atmospheric pressure to give the monomeric nickel hydride.

Introduction

Transition metal complexes with partially filled d shells have garnered considerable attention due to their unique reactivity and electronic structure.[1a,b] The presence of three-coordinate nickel complexes, in particular, has intrigued researchers because they are rare,[2] and have biological relevance because they resemble the proximal nickel site of acetylcoenzyme A synthase.[1c,d] These complexes typically adopt a trigonal planar (D_{3h}) geometry to minimize steric repulsion among the ligands. However, the exploration of T-shaped complexes is of particular interest as the enforced T-shaped geometry suggests direct access to one of the d-orbitals, specifically d_{z2} or d_{x2-y2}, depending on its orientation, pointing towards the available coordination site. Enforcing a strictly T-shaped coordination mode presents challenges, as three-coordinate complexes tend to favor trigonal-planar coordination geometries due to reduced inter-ligand steric repulsion.[1] In the late 2000s, Caulton and his team conducted ground-breaking studies, uncovering remarkable chemistry involving a T-shaped Co(I) complex supported by a PNP pincer ligand.[3] Strictly T-shaped nickel(I) radicals are rare (Scheme 1).[4] Gade and his colleagues also published seminal work in this area, isolating a T-shaped iron complex.[5] To isolate the metalloradicals, it is crucial to prepare a structurally rigid support ligand. Recent studies on T-shaped first-row transition metal complexes have capitalized on pincer ligands, which offer significant advantages. The prearranged, meridional coordination mode of these ligands supports the active center, while the substituents on the peripheral donor atoms effectively shield the coordination sphere.[6]

The utility of nacnac ligand system in main-group or transition metal chemistry is enormous and as expected, the ligand has been studied in nickel chemistry, which dated back to 1968.[7] Recently, Holland and his colleagues reported a three-coordinate β-diketiminate-nickel(I) complex with a carbonyl ligand, but its structure does not strictly adhere to the T-shape.[8a] The same holds true for Limberg's β-diketiminate-

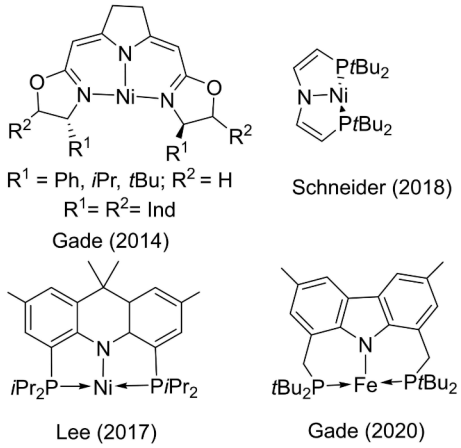

Scheme 1. Selected examples of T-shaped Ni and Fe radicals.

[a] *Dr. S. Pahar,[+] V. Sharma,[+] Dr. S. S. Sen*
Inorganic Chemistry and Catalysis Division
CSIR-National Chemical Laboratory
Dr. Homi Bhabha Road, Pashan, Pune 411008 (India)
E-mail: ss.sen@ncl.res.in
Homepage: http://academic.ncl.res.in/ss.sen

[b] *Dr. S. Pahar,[+] V. Sharma,[+] Dr. K. V. Raj, M. P. Sangole, C. P. George, Dr. K. Singh, Dr. K. Vanka, Dr. R. G. Gonnade, Dr. S. S. Sen*
Academy of Scientific and Innovative Research (AcSIR), Ghaziabad-201002 (India)

[c] *Dr. K. V. Raj, M. P. Sangole, C. P. George, Dr. K. Singh, Dr. K. Vanka, Dr. R. G. Gonnade*
Physical and Materials Chemistry Division
CSIR-National Chemical Laboratory
Dr. Homi Bhabha Road, Pashan, Pune 411008 (India)

[+] *The first two authors contributed equally for the manuscript*

Supporting information for this article is available on the WWW under https://doi.org/10.1002/chem.202303957

© 2023 Wiley-VCH GmbH

nickel(I) dinitrogen complex.[8b] More recently, our research group and others have utilized a modified nacnac ligand, wherein one of the N-aryl moieties is replaced with a methyl-pyridine sidearm. We and others have reported the synthesis of a range of complexes, encompassing main-group, transition metal, and lanthanide species, employing this tridentate nacnac ligand [2,6-*i*Pr$_2$-C$_6$H$_3$NC(Me)CHC(Me)NH(CH$_2$py)].[9] Through our investigations, we have demonstrated that this ligand successfully stabilizes a monomeric Ni(II) hydride species by virtue of the additional donation from the coordinating picolyl moiety.[10] In this study, we present the preparation of the first T-shaped Ni(I) radical using a non-pincer ligand (**2**). The presence of the metal-centered radical was confirmed through the isolation of the TEMPO adduct (**3**). Remarkably, **2** undergoes unusual C–C bond formation via coupling upon reaction with Ph_2S_2 and Ph_2Se_2. The activation of dihydrogen is also observed resulting in the previously reported monomeric nickel hydride.[10]

Results and Discussion

Typically T-shaped nickel(I) and iron(I) radical species have been obtained by reducing the corresponding halides.[4,5] Very recently, we have employed KSi(SiMe$_3$)$_3$ not only to introduce the hypersilyl moiety to any main-group species, but as a reducing agent.[11] The same was reported by Power and coworkers for the formation of Bi–Bi bond from bismuth halides.[12] Our initial plan was to introduce the hypersilyl moiety to Ni, but when compound **1** was reacted with KSi(SiMe$_3$)$_3$, it smoothly yielded a T-shaped Ni(I) radical (**2**) in high yield (Scheme 2).

The red crystals of **2** are stable in the glove-box for almost 30 days without any decomposition whereas some of the Ni(I) radicals are unstable even in the glove-box.[13a] The molecular structure of complex **2** is shown in Figure 1. The solid-state structure shows that the central nickel atom has adopted the T-shaped geometry with the L–Ni–L angles of 173.41, 85.91, and 98.94°, similar to those reported by Lee and coworkers.[4] Paramagnetic species **2** is NMR inactive which negates the anticipation of dimer formation in solution state as well. The molecular ion peak was detected with the highest relative intensity at m/z 406.1783. The cyclic voltammogram of compound **2** shows a reversible redox behavior with redox peak at −1.35/−1.32 V ($Ni^{I}\rightarrow Ni^{0}/Ni^{0}\rightarrow Ni^{I}$) and Quasi reversible peak at −1.94/−1.86 V ($Ni^{II}\rightarrow Ni^{I}/Ni^{I}\rightarrow Ni^{II}$) vs Fc/Fc+ (Fc = [(η-C$_5H_5$)$_2$Fe]), (Figure S12, in the ESI).[14] Further to confirm the presence of radical on nickel, we have treated **2** with TEMPO (2,2,6,6-tetramethylpiperidine-1-oxyl radical), which led to the formation of diamagnetic nickel-oxaziridine derivative, **3** with N–Ni–O three-membered ring in η^2-coordination mode (Scheme 2). The formation of the three-membered ring occurs with concomitant cleavage of the Ni–N$_{pyridyl}$ bond. Yellow colored single crystals of **3** suitable for X-ray diffraction studies were grown from the saturated solution of hexane/toluene at −30 °C in a freezer. The molecular structure of **3** is shown in Figure 2 along with the important bond lengths and angles in the legends. The Ni–N$_{TEMPO}$ and Ni–O bond distances are 1.960(5) and 1.830(4) Å respectively, which is comparable to the related Ni-TEMPO complexes.[13] The ^{1}H and ^{13}C NMR spectra in CDCl$_3$ show the expected number of resonances and multiplicity for a diamagnetic complex presenting the TEMPO-bonded Ni center.

To confirm the radical nature of **2**, we have also performed the EPR experiment in the solid state at 298 K. The Ni center in the complex features a T-shaped geometry with s = 1/2. Interestingly, X-band EPR spectra showed a rhombic/quasi-rhombic signal[15] with $g_x = 2.205$, $g_y = 2.142$, and $g_z = 2.115$, which is in well agreement with such Ni(I) (s = 1/2 spin state) T-shaped complexes.[4] The simulated spectrum merged with the experimental spectrum is given below in Figure 3.

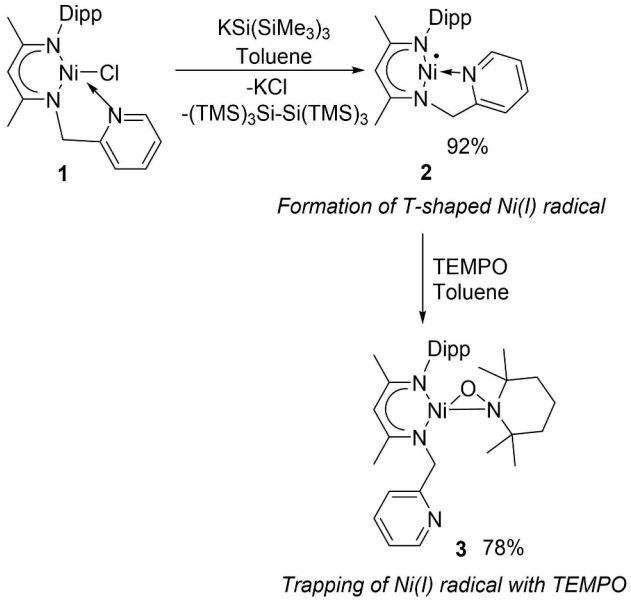

Scheme 2. Facile formation of T-shaped Ni(I) radical using a non-pincer ligand and its reaction with TEMPO.

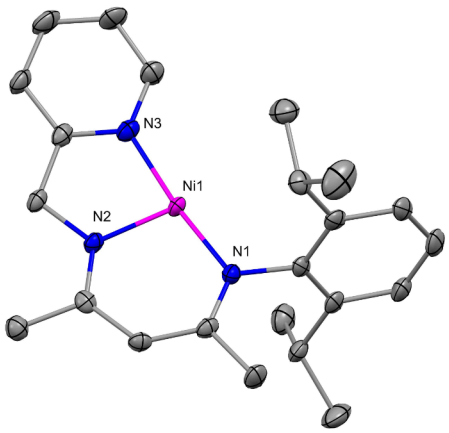

Figure 1. The molecular structure of **2** with anisotropic displacement parameters depicted at the 50% probability level. Hydrogen atoms are not shown for clarity. Selected bond lengths (Å) and bond angles (°): Ni1–N1 1.866(3), Ni1–N2 1.902(3), Ni1–N3 1.910(3); N1–Ni1–N2 98.94(13), N1–Ni1–N3 173.41(13), N2–Ni1–N3 85.91(14). CCDC: 2271416.

15213765, 2024, 12, Downloaded from https://chemistry-europe.onlinelibrary.wiley.com/doi/10.1002/chem.202303957. By Csir-National Chemical, Wiley Online Library on [21/01/2025]. See the Terms and Conditions (https://onlinelibrary.wiley.com/terms-and-conditions) on Wiley Online Library for rules of use; OA articles are governed by the applicable Creative Commons License

© 2023 Wiley-VCH GmbH

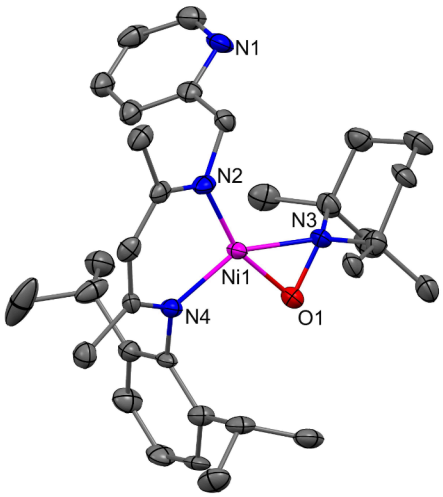

Figure 2. The molecular structure of **3** with anisotropic displacement parameters depicted at the 50% probability level. Hydrogen atoms are not shown for clarity. Selected bond lengths (Å) and bond angles (°): Ni1–O1 1.830(4), Ni1–N4 1.878(5), Ni1–N2 1.878(5), Ni1–N3 1.960(5), O1–N3 1.403(6); O1–Ni1–N4 102.73(19), O1–Ni1–N2 160.9(2), N4–Ni1–N2 95.8(2), O1–Ni1–N3 43.30(18), N4–Ni1–N3 145.9(2), N2–Ni1–N3 117.8(2), N3–O1–Ni1 73.3(3). CCDC: 2271420.

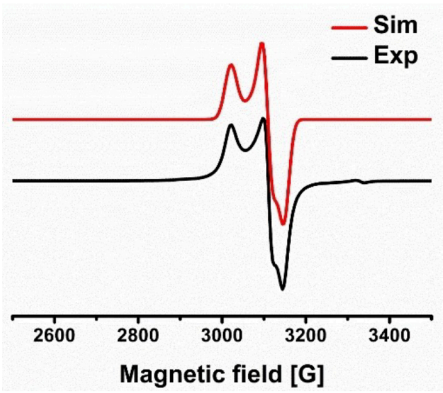

Figure 3. Experimental (black line) and simulated (red line) X-band EPR spectrum of **2** in toluene at 100 K. [Simulation parameters: $g_x = 2.205$, $g_y = 2.142$, $g_z = 2.115$, $w_x = 28$, $w_y = 22$, $w_z = 24$].

To understand the magnetic behaviour of compound **2** SQUID measurement was performed and showed a weak antiferromagnetic interaction. The calculated effective magnetic moment using $2.828\sqrt{\chi_M T} = \mu_{eff}$ gives value nearly 6 BM (Bohr Magneton), which further confirms the affluence of a single electron on the nickel center.

To gain insight into the electronic structure of **2**, density functional theory calculations were conducted at the PBE-D3/TZVP level of theory. The spin density plot of **2** (see Figure 4) reveals that the majority of the unpaired electron spin is localized around the vacant coordination site of the nickel center, providing evidence for the observed metallo radical character of the nickel. Analysis of the Kohn-Sham frontier orbitals indicates that the SOMO primarily resides on nickel's $d_{x2\text{-}y2}$ orbital,[16,17] with significant contributions from the nitrogen atoms, while the LUMO is localized on the pyridine ring

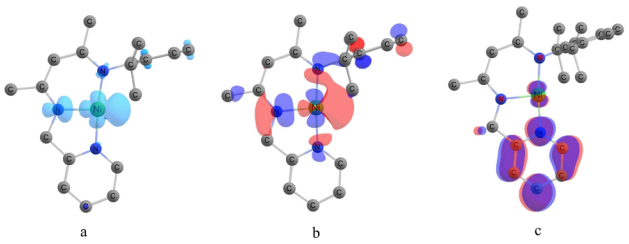

Figure 4. (a) The spin density plot, (b) the SOMO, and (c) the LUMO of **2**. The isovalue of the spin density plot is 0.004, while for the SOMO and LUMO, the isovalue is 0.04.

(see Figure 4). Additionally, we have also plotted the spin density, SOMO, and LUMO of **2** at the B3LYP-D3/def2-TZVP level of theory (see Figure S14 in the SI), and they match the results obtained at the PBE-D3/TZVP level of theory.

With the Ni(I) complex in hand, we have performed the reaction between diphenyldichalcogenides and compound **2**. The addition of 0.5 equivalents of diphenyl disulfide (Ph_2S_2) to a toluene solution of **2** resulted in the cleavage of the S–S bond homolytically and led to the construction of the Ni–S bond in **4**. The addition of one equivalent of Ph_2S_2 led to the formation of **4** along with C–C coupled product (**6**) formed via coupling of the imine carbons (Scheme 3). A precedent for such C–C coupling has been reported by Wolczanski and coworkers, who described C–C bond formation via coupling of the imine carbons.[9c] The solid state structures of **4** and **6** are shown in Figure 5 and 7, respectively. The molecular structure of **4** shows a diamagnetic Ni center with a Ni–S bond length of 2.2330(3) Å, whereas the dimeric product **6** shows the Ni–S and C–C bond lengths 2.207(18) and 1.572(13) Å, respectively. Likewise, the reactivity with Ph_2Se_2 resulted in the formation of monomer **5** along with the formation of the C–C coupled dimeric product **7** at the $-CH_2$ position of the picolyl group (Scheme 3). Both **5** and **7** were crystalized in the same reaction flask at −30 °C (Figure 6 (for molecular structure of **5**) and (Figure 8 (for molecular structure of **7**)). The Ni–Se bond length of compounds **5** and **7** are 2.3446(4) and 2.342(14) Å, respectively. The C–C bond length of C–C coupled product **7** is 1.580(11) Å. The Ni–S and Ni–Se bond lengths are in good agreement with the previously reported Ni–E (E = S, Se) bonds by Roesky and coworkers i.e. 2.2030(12) and 2.3582(4) Å respectively.[18] In the

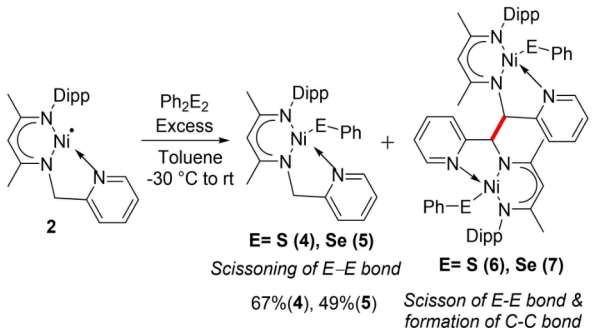

Scheme 3. Activation of dichalcogenides.

© 2023 Wiley-VCH GmbH

15213765, 2024, 12, Downloaded from https://chemistry-europe.onlinelibrary.wiley.com/doi/10.1002/chem.202303957. By Csir-National Chemical, Wiley Online Library on [21/01/2025]. See the Terms and Conditions (https://onlinelibrary.wiley.com/terms-and-conditions) on Wiley Online Library for rules of use; OA articles are governed by the applicable Creative Commons License

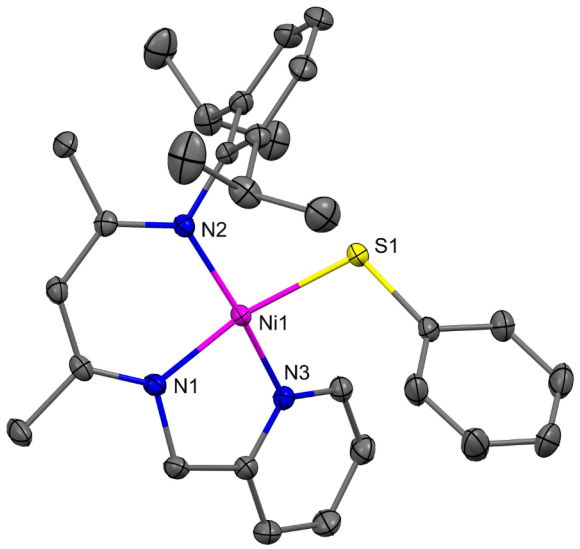

Figure 5. The molecular structure of **4** with anisotropic displacement parameters depicted at the 50% probability level. Hydrogen atoms are not shown for clarity. Selected bond lengths (Å) and bond angles (°): Ni1–N1 1.8789(9), Ni1–N2 1.8923(9), Ni1–N3 1.9063(10), Ni1–S1 2.2330(3); N1–Ni1–N2 94.39(4), N1–Ni1–N3 83.81(4), N2–Ni1–N3 163.60(4), N1–Ni1–S1 164.36(3), N2–Ni1–S1 93.04(3), N3–Ni1–S1 92.83(3), C1–S1–Ni1 106.76(4). CCDC: 2271418.

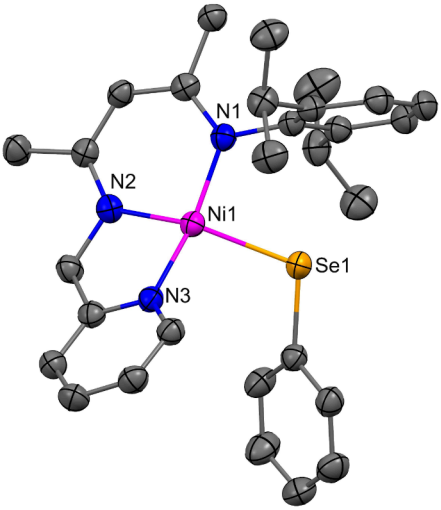

Figure 6. The molecular structure of **5** with anisotropic displacement parameters depicted at the 50% probability level. Hydrogen atoms are not shown for clarity. Selected bond lengths (Å) and bond angles (°): Ni1–N1 1.8758(18), Ni1–N2 1.8910(18), Ni1–N3 1.9043(19), Se1–C1 1.916(2), Se1–Ni1 2.3446(4); C1–Se1–Ni1 105.72(7), N1–Ni1–N2 94.47(8), N1–Ni1–N3 84.00(8), N2–Ni1–N3 162.99(8), N1–Ni1–Se1 162.13(6), N2–Ni1–Se1 93.11(6), N3–Ni1–Se1 93.32(6). CCDC: 2271417.

past decade, there has been a growing focus among chemists on the activation of molecular hydrogen. Precious metals have been explored over the years as a means to activate H_2, while the first row earth abundant Ni complexes are emerging due to their environmental friendly and cost-effective properties courtesy to the pioneering works by the groups of Peters, Driess, Rodríguez and others.[19,20]

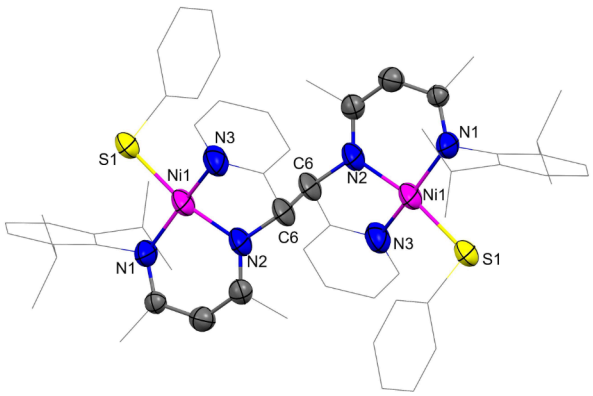

Figure 7. The molecular structure of **6** with anisotropic displacement parameters depicted at the 50% probability level. Hydrogen atoms are not shown for clarity. Selected bond lengths (Å) and bond angles (°): Ni1–N1 1.910(6), Ni1–N2 1.876(5), Ni1–N3 1.922(5), Ni1–S1 2.207(18), C6–C6 1.572(13); N2–Ni1–N1 94.6(18), N2–Ni1–N3 82.7(2), N1–Ni1–N3 165.2(2), N2–Ni1–S1 167.6(16), N1–Ni1–S1 92.11(14), N3–Ni1–S1 93.3(17).CCDC: 2271467.

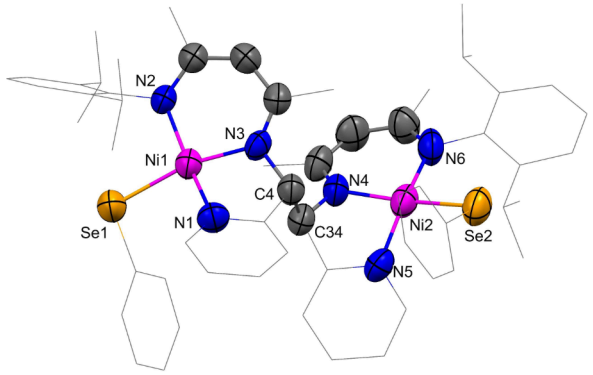

Figure 8. The molecular structure of **7** with anisotropic displacement parameters depicted at the 50% probability level. Hydrogen atoms are not shown for clarity.Selected bond lengths (Å) and bond angles (°): Ni1–N1 1.932(6), Ni1–N2 1.921(6), Ni1–N3 1.886(6), Ni1–Se1 2.342(14), C4–C34 1.580(11), Ni2–N4 1.893(6), Ni2–N5 1.895(7), Ni2–N6 1.915(7), Se2–Ni2 2.3570(15); N3–Ni1–N1 83.2(3), N3–Ni1–N2 95.3(3), N2–Ni1–N1 162.5(3), N1–Ni1–Se1 92.9(2), N2–Ni1–Se1 93.6(19), N4–Ni2–N5 83.5(3), N4–Ni2–N6 94.3(3), N5–Ni2–N6 162.5(3), N4–Ni2–Se2 160.0(2), N5–Ni2–Se2 93.0(2), N6–Ni2–Se2 94.7(2). CCDC: 2271463.

The bubbling of hydrogen gas to the toluene solution of compound **2** resulted in an immediate color change from red to orangish yellow. Inspection of the ^{1}H NMR indicates the rupture of the H–H σ-bond and the formation of monomeric nickel(II) hydride **8** (Scheme 4). The formation of compound **8** was

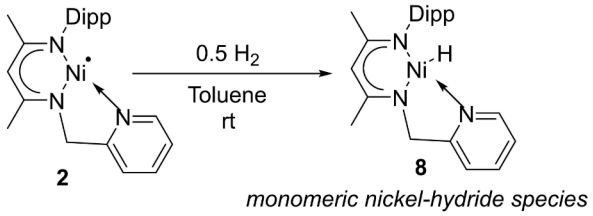

Scheme 4. Dihydrogen activation by Ni(I) radical at ambient temperature and pressure.

© 2023 Wiley-VCH GmbH

15213765, 2024, 12, Downloaded from https://chemistry-europe.onlinelibrary.wiley.com/doi/10.1002/chem.202303957. By Csir-National Chemical, Wiley Online Library on [21/01/2025]. See the Terms and Conditions (https://onlinelibrary.wiley.com/terms-and-conditions) on Wiley Online Library for rules of use; OA articles are governed by the applicable Creative Commons License

confirmed through a comparison of spectroscopic data and unit cell values with previously reported literature.[10]

Conclusions

In summary, a T-shaped thermally stable nickel(I) radical (**2**) was synthesized by combining a nickel(II) chloride complex [2,6-*i*Pr$_2$-C$_6$H$_3$NC(Me)CHC(Me)NH(CH$_2$py)]Ni(II)Cl (**1**)] and KSi(SiMe$_3$)$_3$. The presence of the radical center on Ni was verified by the formation of an unusual three-membered nickeloxaziridine complex (**3**) upon reaction with TEMPO as well as from the rhombic/quasi-rhombic signal in X-band EPR spectrum. DFT studies confirmed a T-shaped nickel(I) center with a half-filled d_{x2-y2} orbital as the SOMO. Homolytic cleavage of σ-bonds of dihydrogen, disulphide and diselenide by **2** at ambient conditions was investigated. The activation of dihydrogen by **2** produces a monomeric nickel hydride (**8**) and underscores the effectiveness of utilizing a metalloradicals in dihydrogen activation.

Supporting Information

Please see Supporting Information for the synthesis and characterization for **2**–**8**, and structural data for **2**–**7**. Deposition Numbers 2271416 (**2**), 2271420 (**3**), 2271418 (**4**), 2271417 (**5**) 2271467 (**6**) and 2271463 (**7**) contain the supplementary crystallographic data for this paper. These data are provided free of charge by the joint Cambridge Crystallographic Data Centre and Fachinformationszentrum Karlsruhe Access Structures service. Additional references cited within the Supporting Information.[21–36]

Acknowledgements

S.S.S is thankful for SJF Grant SB/SJF/2021-22/06, GOI for providing financial assistance. SP thanks DST, India for the INSPIRE Fellowship (IF160314). VS and MPS thank CSIR, India for their research fellowships. We thank Mr. Bappaditya Goswami from IISER-Kolkata for EPR measurements. The support and the resources provided by 'PARAM Brahma Facility' under the National Supercomputing Mission, Government of India at the IISER Pune are gratefully acknowledged. We are also thankful to CSIR-FIRST scheme (MLP102826) for financial support.

Conflict of Interests

The authors declare no conflict of interest.

Data Availability Statement

The data that support the findings of this study are available in the supplementary material of this article.

Keywords: Nickel · Hydrogen Activation · Metalloradical · C–C Bond Formation · Tridentate nacnac

[1] a) S. Alvarez, *Coord. Chem. Rev.* **1999**, 193–195, 13–41; b) C. C. Cummins, *Prog. Inorg. Chem.* **1998**, *47*, 685–836; c) Structural review: C. L. Drennan, T. I. Doukov, S. W. Ragsdale, *J. Biol. Inorg. Chem.* **2004**, *9*, 511–515; d) Mechanistic review: E. L. Hegg, *Acc. Chem. Res.* **2004**, *37*, 775–783.
[2] For selected reference: a) G. A. Dawson, Q. Lin, M. C. Neary, T. Diao, *J. Am. Chem. Soc.* **2023**, *145*, 20551–20561; b) C. L. Wagner, G. Herrera, Q. Lin, C. T. Hu, T. Diao, *J. Am. Chem. Soc.* **2021**, *143*, 5295–5300; c) A. Bismuto, P. Müller, P. Finkelstein, N. Trapp, G. Jeschke, B. Morandi, *J. Am. Chem. Soc.* **2021**, *143*, 10642–10648.
[3] a) M. J. Ingleson, H. Fan, M. Pink, J. Tomaszewski, K. G. Caulton, *J. Am. Chem. Soc.* **2006**, *128*, 1804–1805; b) M. J. Ingleson, M. Pink, K. G. Caulton, *J. Am. Chem. Soc.* **2006**, *128*, 4248–4249; c) M. J. Ingleson, M. Pink, H. Fan, K. G. Caulton, *J. Am. Chem. Soc.* **2008**, *130*, 4262–4276.
[4] a) C. Yoo, Y. Lee, *Angew. Chem. Int. Ed.* **2017**, *56*, 9502–9506; *Angew. Chem.* **2017**, *129*, 9630–9634; b) F. Schneck, J. Ahrens, M. Finger, A. C. Stuckl, C. Wurtele, D. Schwarzer, S. Schneider, *Nat. Commun.* **2018**, *9*, 1161 (1-8); c) C. Rettenmeier, H. Wadepohl, L. H. Gade, *Chem. Eur. J.* **2014**, *20*, 9657–9665.
[5] J. C. Ott, H. Wadepohl, L. H. Gade, *Angew. Chem. Int. Ed.* **2020**, *59*, 9448–9452; *Angew. Chem.* **2020**, *132*, 9535–9539.
[6] a) J. C. Ott, D. Bürgy, H. Guan, L. H. Gade, *Acc. Chem. Res.* **2022**, *55*, 857–868; b) C.-Y. Lin, P. P. Power, *Chem. Soc. Rev.* **2017**, *46*, 5347–5399.
[7] a) J. E. Parks, R. H. Holm, *Inorg. Chem.* **1968**, *7*, 1408–1416; b) D. Mindiola, *Angew. Chem. Int. Ed.* **2009**, *48*, 6198–6200; *Angew. Chem.* **2009**, *121*, 6314–6316.
[8] a) N. A. Eckert, A. Dinescu, T. R. Cundari, P. L. Holland, *Inorg. Chem.* **2005**, *44*, 7702–7704; b) S. Pfirrmann, C. Limberg, C. Herwig, R. Stößer, B. A. Ziemer, *Angew. Chem. Int. Ed.* **2009**, *48*, 3357–3361; *Angew. Chem.* **2009**, *121*, 3407–3411.
[9] a) S. Yadav, R. Dixit, M. K. Bisai, K. Vanka, S. S. Sen, *Organometallics* **2018**, *37*, 4576–4584; b) S. Pahar, V. S. V. S. N. Swamy, T. Das, R. G. Gonnade, K. Vanka, S. S. Sen, *Chem. Commun.* **2020**, *56*, 11871–11874; c) W. D. Morris, P. T. Wolczanski, J. Sutter, K. Meyer, T. R. Cundari, E. B. Lobkovsky, *Inorg. Chem.* **2014**, *53*, 7467–7484; d) X. Xu, Y. Chen, G. Zou, J. Sun, *Dalton Trans.* **2010**, *39*, 3952–3958.
[10] S. Pahar, V. Sharma, B. Mahata, C. P. George, H. Sharma, K. Vanka, S. S. Sen, *Inorg. Chem.* **2022**, *61*, 17370–17377.
[11] a) S. Pahar, V. Sharma, S. Tothadi, S. S. Sen, *Dalton Trans.* **2021**, *50*, 16678–16684; b) M. K. Bisai, V. S. V. S. N. Swamy, T. Das, K. Vanka, R. G. Gonnade, S. S. Sen, *Inorg. Chem.* **2019**, *58*, 10536–10542; c) M. K. Bisai, V. Sharma, R. G. Gonnade, S. S. Sen, *Organometallics* **2021**, *40*, 2133–2138; d) M. K. Bisai, T. Das, K. Vanka, R. G. Gonnade, S. S. Sen, *Angew. Chem. Int. Ed.* **2021**, *60*, 20706–20710; *Angew. Chem. Int. Ed.* **2021**, *133*, 20874–20878; e) M. K. Bisai, V. S. Ajithkumar, R. G. Gonnade, S. S. Sen, *Organometallics* **2021**, *40*, 2651–2657; f) M. K. Bisai, V. S. Ajithkumar, K. V. Raj, K. Vanka, R. G. Gonnade, S. S. Sen, *Chem. Commun.* **2023**, *59*, 1669–1672; g) K. Gour, M. K. Bisai, S. S. Sen, *Eur. J. Inorg. Chem.* **2022**, e202200071 (1-14).
[12] R. Wolf, J. Fischer, R. C. Fischer, J. C. Fettinger, P. P. Power, *Eur. J. Inorg. Chem.* **2008**, 2515–2521.
[13] a) S. Pelties, D. Herrmann, B. de Bruin, F. Hartl, R. Wolf, *Chem. Commun.* **2014**, *50*, 7014–7016; b) U. Chakraborty, F. Urban, B. Mühldorf, C. Rebreyend, B. de Bruin, N. van Velzen, S. Harder, R. Wolf, *Organometallics* **2016**, *35*, 1624–1631; c) D. Isrow, B. Captain, *Inorg. Chem.* **2011**, *50*, 5864–5866.
[14] J. B. Diccianni, J. Katigbak, C. Hu, T. Diao, *J. Am. Chem. Soc.* **2019**, *141*, 1788–1796.
[15] a) P. Zimmermann, A. F. R. Kilpatrick, D. Ar, S. Demeshko, B. Cula, C. Limberg, *Chem. Commun.* **2021**, *57*, 875–878; b) D. Herebian, E. Bothe, E. Bill, T. Weyhermüller, K. Wieghardt, *J. Am. Chem. Soc.* **2001**, *123*, 10012–10023.
[16] M. J. Ingleson, B. C. Fullmer, D. T. Buschhorn, H. Fan, M. Pink, J. C. Huffman, K. G. Caulton, *Inorg. Chem.* **2008**, *47*, 407–409.
[17] C. Yoo, S. Oh, J. Kima, Y. Lee, *Chem. Sci.* **2014**, *5*, 3853–3858.
[18] C. Zovko, F. Krätschmer, S. Schmidt, T. P. Seifert, M. T. Gamer, P. W. Roesky, *ChemPlusChem* **2022**, *87*, e2022002.
[19] a) W. H. Harman, J. C. Peters, *J. Am. Chem. Soc.* **2012**, *134*, 5080–5082; b) Y. Wang, A. Kostenko, S. Yao, M. Driess, *J. Am. Chem. Soc.* **2017**, *139*, 13499–13506; c) Y. Cai, S. Jiang, T. Rajeshkumar, L. Maron, X. Xu, *J. Am. Chem. Soc.* **2022**, *144*, 16647–16655.

© 2023 Wiley-VCH GmbH

15213765, 2024, 12, Downloaded from https://chemistry-europe.onlinelibrary.wiley.com/doi/10.1002/chem.202303957. By Csir-National Chemical, Wiley Online Library on [21/01/2025]. See the Terms and Conditions (https://onlinelibrary.wiley.com/terms-and-conditions) on Wiley Online Library for rules of use; OA articles are governed by the applicable Creative Commons License

[20] a) G. Zeng, S. Sakaki, *Inorg. Chem.* **2013**, *52*, 2844–2853; b) P. Ríos, J. Borge, F. Fernández de Córdova, G. Sciortino, A. Lledós, A. Rodríguez, *Chem. Sci.* **2021**, *12*, 2540–2548; c) K. Boonpalit, C. Uthayopas, P. Surawatanawong, *Organometallics* **2022**, *41*, 259–269.
[21] Bruker (**2006**). APEX2, SAINT and SADABS. Bruker AXS Inc. Madison, Wisconsin, USA.
[22] G. M. Sheldrick, *Acta Crystallogr.* **2008**, *A64*, 112–122.
[23] G. M. Sheldrick, *Acta Crystallogr.* **2015**, *C71*, 3–8.
[24] L. J. Farrugia, *J. Appl. Crystallogr.* **1997**, *30*, 565.
[25] X. Wang, Y. Fu, D. Tranca, K. Jiang, J. Zhu, J. Zhang, S. Han, C. Ke, C. Lu, X. Zhuang, *ACS Appl. Energ. Mater.* **2021**, *4*, 2891–2898.
[26] TURBOMOLE V7.5 **2020**, a development of University of Karlsruhe and Forschungszentrum Karlsruhe GmbH, 1989–2007, TURBOMOLE GmbH, since 2007; available from https://www.turbomole.org.
[27] J. P. Perdew, K. Burke, M. Ernzerhof, *Phys. Rev. Lett.* **1996**, *77*, 3865–3868.
[28] S. Grimme, J. Antony, S. Ehrlich, H. Krieg, *J. Chem. Phys.* **2010**, *132*, 154104 (1-19).
[29] A. Schäfer, C. Huber, R. Ahlrichs, *J. Chem. Phys.* **1994**, *100*, 5829–5835.
[30] K. Eichkorn, O. Treutler, H. Öhm, M. Häser, R. Ahlrichs, *Phys. Lett.* **1995**, *240*, 283–289.
[31] M. Sierka, A. Hogekamp, R. Ahlrichs, *J. Chem. Phys.* **2003**, *118*, 9136–9148.
[32] A. Klamt, G. Schüürmann, *J. Chem. Soc.-Perkin Trans.* **1993**, 799–805.
[33] M. J. Frisch, G. W. Trucks, H. B. Schlegel, G. E. Scuseria, M. A. Robb, J. R. Cheeseman, G. Scalmani, V. Barone, B. Mennucci, G. A. Petersson, H. Nakatsuji, M. Caricato, X. Li, H. P. Hratchian, A. F. Izmaylov, J. Bloino, G. Zheng, J. L. Sonnenberg, M. Hada, M. Ehara, K. Toyota, R. Fukuda, J. Hasegawa, M. Ishida, T. Nakajima, Y. Honda, O. Kitao, H. Nakai, T. Vreven, J. A. Montgomery Jr, J. E. Peralta, F. Ogliaro, M. Bearpark, J. J. Heyd, E. Brothers, K. N. Kudin, V. N. Staroverov, R. Kobayashi, J. Normand, K. Raghavachari, A. Rendell, J. C. Burant, S. S. Iyengar, J. Tomasi, M. Cossi, N. Rega, J. M. Millam, M. Klene, J. E. Knox, J. B. Cross, V. Bakken, C. Adamo, J. Jaramillo, R. Gomperts, R. E. Stratmann, O. Yazyev, A. J. Austin, R. Cammi, C. Pomelli, J. W. Ochterski, R. L. Martin, K. Morokuma, V. G. Zakrzewski, G. A. Voth, P. Salvador, J. J. Dannenberg, S. Dapprich, A. D. Daniels, O. Farkas, J. B. Foresman, J. V. Ortiz, J. Cioslowski and D. J. Fox, Gaussian 09; Revision D.01, Gaussian, Inc, Wallingford, CT, **2013**.
[34] A. D. Becke, *J. Chem. Phys.* **1993**, *98*, 5648–5652.
[35] F. Weigend, R. Ahlrichs, *Phys. Chem. Chem. Phys.* **2005**, *7*, 3297–3305.
[36] S. Miertuš, E. Scrocco, J. Tomasi, *Chem. Phys.* **1981**, *55*, 117–129.

Manuscript received: December 4, 2023
Accepted manuscript online: December 5, 2023
Version of record online: January 10, 2024

15213765, 2024, 12, Downloaded from https://chemistry-europe.onlinelibrary.wiley.com/doi/10.1002/chem.202303957. By Csir-National Chemical, Wiley Online Library on [21/01/2025]. See the Terms and Conditions (https://onlinelibrary.wiley.com/terms-and-conditions) on Wiley Online Library for rules of use; OA articles are governed by the applicable Creative Commons License

© 2023 Wiley-VCH GmbH

ORGANOMETALLICS

pubs.acs.org/Organometallics Article

Magnesium−Ligand Cooperation in Breaking the O−H and C−H Bonds of Water and Diazoalkane

Vishal Sharma, Soumya Ranjan Dash, Kumar Vanka, Rajesh G. Gonnade, and Sakya S. Sen*

Cite This: https://doi.org/10.1021/acs.organomet.5c00031 Read Online

ACCESS | Metrics & More | Article Recommendations | Supporting Information

ABSTRACT: In our previous paper, we reported that the reaction of a tridentate nacnac ligand with a pendant picolyl group, with KHMDS and MgI_2, resulted in the formation of a homoleptic hexacoordinate magnesium compound. Here, we show that the analogous reaction of the ligand with CH_3MgBr led to a heteroleptic magnesium bromide species (**1**). Attempts to generate the magnesium hydride species from **1** led to the dearomatization of the pyridine ring, and the resulting product was a magnesium hydroxide (**3**) presumably generated due to an adventitious amount of water. The reaction of the ligand with nBu_2Mg afforded a unique dearomatized magnesium species (**2**) in high yield. Theoretical calculations reveal the presence of a nonbonding orbital on the magnesium, susceptible to nucleophilic attack. Indeed, the reaction of **2** with H_2O/D_2O cleaves the O−H/D bond via magnesium−ligand cooperation and generates a magnesium hydroxide (**4** and **5**). In addition, **2** reacts with Me_3SiCHN_2 and cleaves the C−H bond to generate another unusual, well-defined magnesium compound with a bridging isocyanide moiety (**6**) via migration of the $SiMe_3$ group from the carbon to the nitrogen atom. The latter can be described as a dimer of magnesium isocyanamide. DFT calculations were performed to understand the electronic structures of the synthesized molecules.

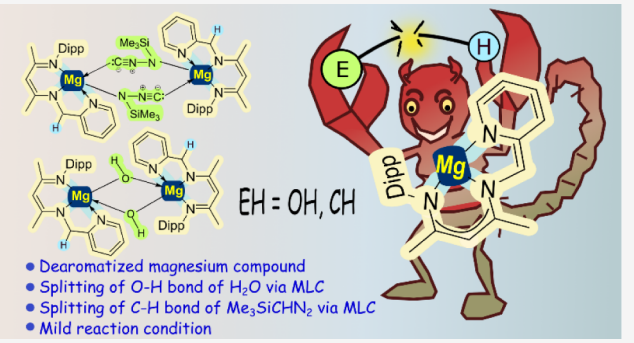

INTRODUCTION

The design of compounds that advantageously make use of metal−ligand cooperativity as a tool to facilitate the bond-breaking or bond-making steps has become increasingly popular. However, the exploitation of cooperativity in small molecule activation and homogeneous catalysis has traditionally been limited to transition metals; the transfer of such design principles to s-block element-based catalysis is, in comparison, underdeveloped. Remarkable exceptions are Milstein's catalytic hydrogenations and Harder's alkene hydroamination with magnesium.[1−3]

Very recently, we have been working on a tridentate nacnac ligand with a pendant picolyl group and have prepared a series of compounds, including germanium, tin, aluminum, a monomeric nickel hydride, and a T-shaped nickel radical.[4−6] When we used the same ligand to synthesize alkaline earth metal compounds using KHMDS and MgI_2 or CaI_2, the reactions resulted in homoleptic alkaline earth metal compounds.[7] Here, we have modified the magnesium precursors and prepared a heteroleptic magnesium bromide (**1**) and a dearomatized magnesium compound (**2**). The latter is a new entry to dearomatized magnesium complexes (Scheme 1).[1−3,8] **2** was later used for the heterolytic cleavage of O−H/D and C−H bonds through magnesium−ligand cooperation.

Scheme 1. Selected Examples of Previously Reported Dearomatized Magnesium Compounds

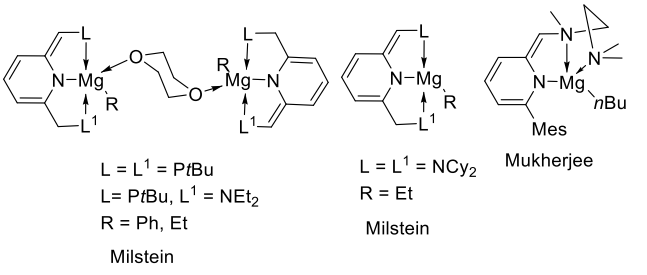

RESULTS AND DISCUSSION

The reaction of the ligand with CH_3MgBr smoothly afforded heteroleptic magnesium bromide (**1**). Surprisingly, the analogous reaction with nBu_2Mg resulted in an immediate

Received: January 24, 2025
Revised: March 10, 2025
Accepted: March 13, 2025

Downloaded via NATL CHEMICAL LABORATORY on March 25, 2025 at 10:38:05 (UTC).
See https://pubs.acs.org/sharingguidelines for options on how to legitimately share published articles.

ACS Publications © XXXX American Chemical Society

color change from yellow to dark magenta and the formation of a dearomatized magnesium compound (**2**) via deprotonation from the picolyl backbone (Scheme 2). Both compounds

Scheme 2. Synthesis of Heteroleptic Magnesium Bromide (1) and a Magnesium Species with a Dearomatized Picolyl Moiety (2); pyridine ligand has Changed from L Type to X Type Ligand

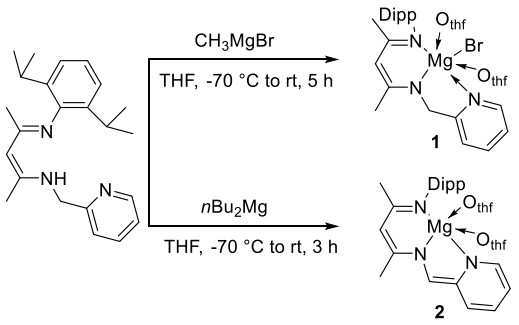

have been structurally characterized. The colorless crystals of **1** were obtained in THF at −4 °C after 2 days. The molecular structure of **1** is shown in Figure 1. The bond length of Mg1−

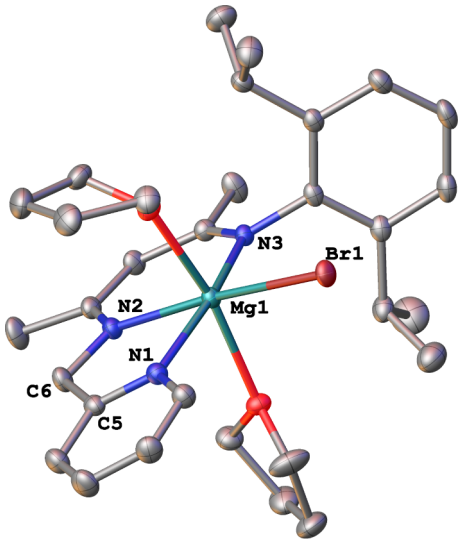

Figure 1. Molecular structure of **1** with anisotropic displacement parameters depicted at the 50% probability level. Hydrogen atoms are not shown for the sake of clarity. Selected bond lengths (Å) and bond angles (°): Br1−Mg1 2.5712(5), Mg1−N3 2.1470(12), Mg1−N2 2.1061(12), Mg1−N1 2.2340(13), C5−C6 1.504(2); N3−Mg1−N2 89.48(5), N1−Mg1−N3 166.76(5), N1−Mg1−N2 77.66(5).

N1 = 2.234(13) Å is longer than those of the other two Mg−N bonds (2.147(12) Å and 2.106(12) Å), confirming the coordination bond with the pyridine nitrogen. The molecular ion peak was detected with the highest relative intensity at m/z 452.1495. The crystals suitable for SC-XRD of **2** were obtained in THF/hexane at −36 °C within a week. The molecular structure of **2** is shown in Figure 2. The magnesium atom is five-coordinate and adopts a distorted TBP geometry. As expected, the bond length of Mg1−N2 = 2.106(18) Å is considerably shorter than that of Mg1−N1 = 2.234(13) Å in **1**, suggesting the covalent nature of the Mg−N bond along with Mg1−N1 = 2.08(18) Å and Mg1−N3= 2.09(18) Å. The bond length between C5−C6 = 1.3764(3) Å in **2** is shorter than that

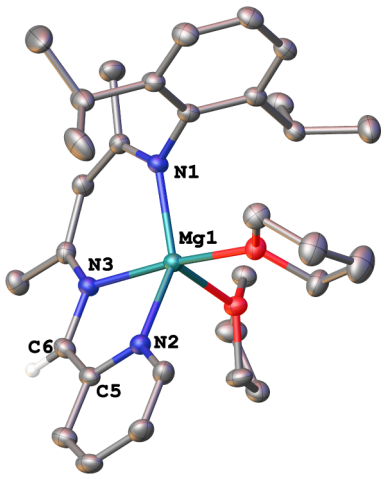

Figure 2. Molecular structure of **2** with anisotropic displacement parameters is depicted at the 50% probability level. Hydrogen atoms are not shown for clarity. Selected bond lengths (Å) and bond angles (°): Mg1−N1 2.0811(18), Mg1−N2 2.1073(18), Mg1−N3 2.0914(18), C5−C6 1.374(3); N1−Mg1−N3 89.07(7), N1−Mg1−N2 146.11(7), N2−Mg1−N3 80.00(7).

of **1** (C5−C6 = 1.504(2) Å), which supports that deprotonation takes place from the picolyl moiety, resulting in double bond formation and dearomatized structure. The ^{1}H NMR of **2** shows peaks at 5.04 ppm for the methine CH of the side arm, along with 5.42, 6.16, 6.39, and 6.82 ppm for the pyridine, confirming the dearomatized structure. The molecular ion peak was detected with the highest relative intensity at m/z = 372.2401.

Frontier orbital analysis revealed that the HOMO and LUMO of **2** (without the THF moieties) are delocalized on the backbone β-diketiminate methyl pyridinato ligand (excluding the Dipp moiety), whereas the MO corresponding to the vacant nonbonding (LP*) orbital of Mg, the site for the attack of incoming nucleophiles, was obtained at LUMO+1 (Figure 3). The MEP reveals a significant positive potential (+80.0 kcal/mol) localized at the magnesium center, which lies within the plane of the Mg-bound β-diketiminate methyl pyridinato ligand. Notably, two additional regions of positive potential are observed above and below this plane, with values

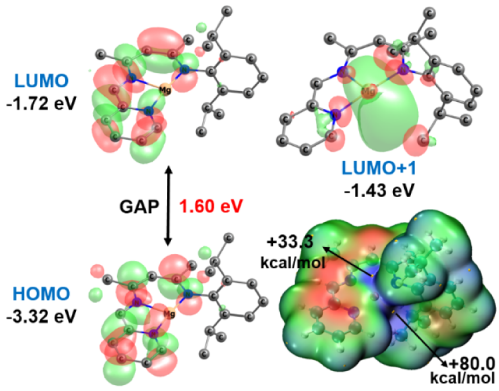

Figure 3. Frontier orbitals of compound **2** (without the THF moieties) along with molecular electrostatic potential (MEP) plot (RGB color scale, isovalue = 0.001 au). In the MEP, blue highlights the positive/electron deficient region, and red shows the electron rich region.

https://doi.org/10.1021/acs.organomet.5c00031
Organometallics XXXX, XXX, XXX−XXX

of +34.4 and +33.3 kcal/mol, respectively. Although the classification of these positive potentials as sigma-holes or pi-holes is debatable,[9] it is notable that these positive potentials govern the directionality of incoming nucleophiles, as evident in the crystal structures of **1** and **2**.

Reactivity of 1: Attempt for Magnesium Hydride. Preparation of magnesium hydride is an attractive target, as examples of discrete, stable, and isolatable Mg−H species remain relatively rare.[8,10−14] Our attempts to make magnesium hydride species from **1** remained unsuccessful. The reaction of **1** with the K-selectride led to the reduction of the pyridine ring and the formation of **3**. We assume the magnesium hydride was formed in the first step, which subsequently reduces the pyridine ring.[15−17] The adventitious amount of water present in the reaction mixture reacts with the magnesium center and affords a four-membered Mg_2NO ring (**3**) (Scheme 3).

Scheme 3. Attempt to Prepare Magnesium Hydride from 1 Led to Donor−Acceptor Stabilized Monomeric Magnesium Hydroxide (3)

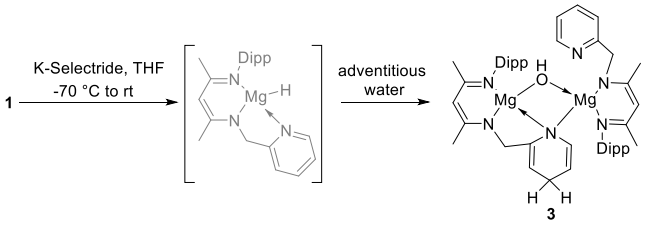

Though we were able to obtain a few crystals of **3**, it was always obtained as yellow oily deposits containing significant amounts of impurities, which do not permit for a full spectroscopic characterization. The molecular structure of **3** is shown in Figure 4, which shows a four-membered ring and a dearomatized pyridine ring. The nitrogen−magnesium bond distances, Mg1−N6 2.230(15) Å and Mg2−N6 2.1972(15) Å, exhibit a notable difference. This suggests that the Mg1−N6 interaction is predominantly coordinate in nature, whereas the Mg2−N6 bond displays characteristics of a covalent bond.

Reactions with H_2O and D_2O. With dearomatized magnesium compound (**2**) in hand, we have performed the reaction of **2** with H_2O at −70 °C in THF (Scheme 4),

Scheme 4. Splitting of the O−H and O−D Bonds of Water and D_2O by a Magnesium Species (2)

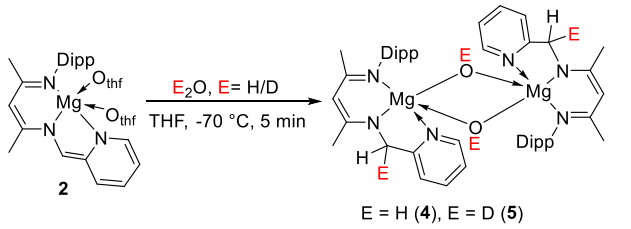

resulting in an immediate color change from magenta to reddish orange. The orange crystals of **4** were obtained from the THF solution at −36 °C. To confirm the deprotonation of water by **2**, the same reaction was repeated with D_2O in THF (Scheme 4), and ^2H NMR was recorded. The ^2H NMR

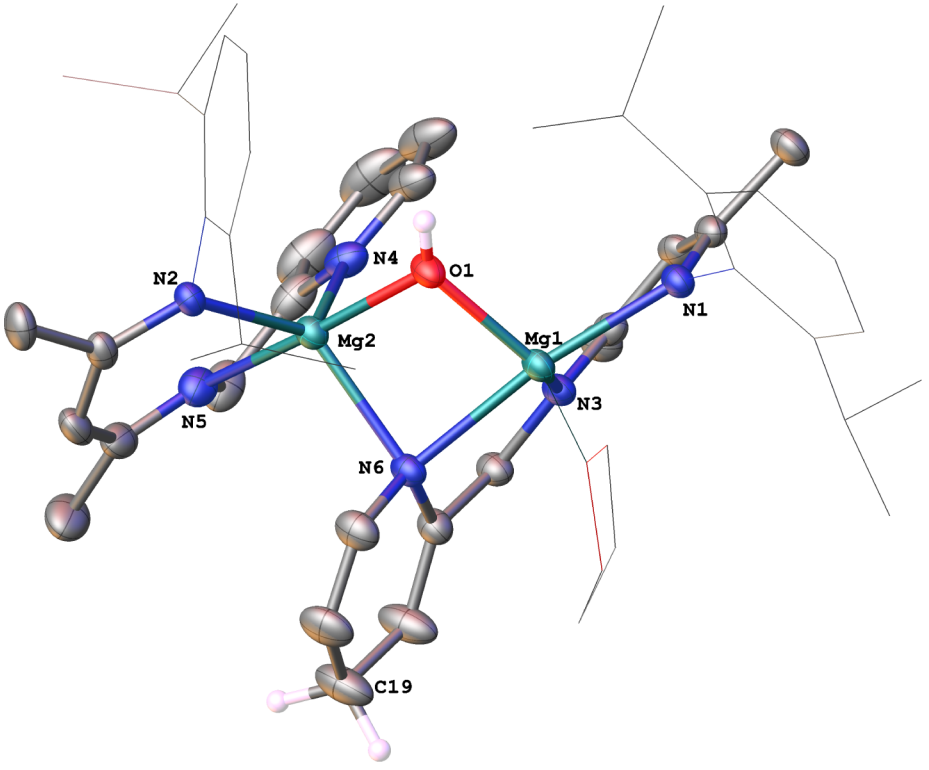

Figure 4. Molecular structure of **3** with anisotropic displacement parameters is depicted at the 50% probability level. Hydrogen atoms (except on the pyridine ring) are not shown for clarity. Selected bond lengths (Å) and bond angles (°): Mg1−N1 2.128(15), Mg1−N3 2.079(15), Mg1−N6 2.230(15), Mg1−O1 1.951(14), Mg2−O1 1.972(14), Mg2−N4 2.182(16), Mg2−N5 2.082(16), Mg2−N2 2.119(15), Mg2−N6 2.197(16); N1−Mg1−N6 165.38(6), N6−Mg1−N3 78.63(6), Mg1−O1−Mg2 39.51(4), Mg1−N6−Mg2 46.27(4), O1−Mg2−N6 83.15(6).

https://doi.org/10.1021/acs.organomet.5c00031
Organometallics XXXX, XXX, XXX−XXX

spectrum of **5** shows peaks at 4.61 and 11.21 ppm, corresponding to CD (methylene side arm) and OD, respectively, for **5**.

While well-defined magnesium hydroxide compounds are known thanks to the works of Parkin, Bochmann, Roesky, Stalke, and others,[18−20] they were prepared either serendipitously or by hydrolysis of Mg−amide or Mg−Me bonds. No magnesium hydroxide was prepared via MLC so far. The single-crystal X-ray structure of **4** is shown in Figure 5, which

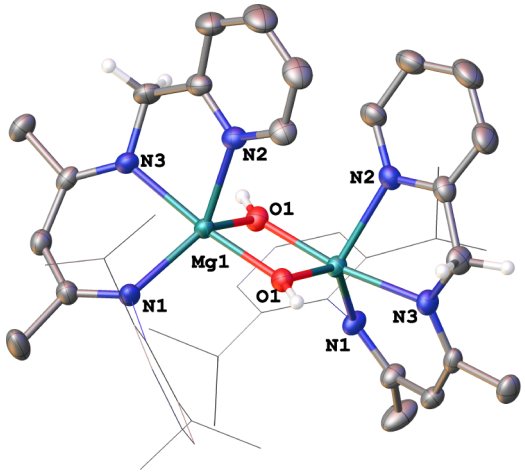

Figure 5. Molecular structure of **4** with anisotropic displacement parameters is depicted at the 50% probability level. Hydrogen atoms are not shown for clarity. Selected bond lengths (Å) and bond angles (°): Mg1−N1 2.128(2), Mg1−N2 2.142(2), Mg1−N3 2.090(2), Mg1−O1 1.9813(17), C12−C13 1.503(3); N1−Mg1−N2 126.22(8), N1−Mg1−N3 85.52(8), N2−Mg1−N3 76.30(8), O1−Mg1−N1 98.48(8), O1−Mg1−N2 95.06(8), O1−Mg1−N3 171.19(18).

reveals a centrosymmetric dimer. The two nitrogen−magnesium bonds are similar, Mg1−N1 2.128(2) Å and Mg1−N3 2.090(2) Å, while the Mg1−N2 bond is considerably longer at 2.192(2) Å, reflecting the conversion from a covalent bond to a dative bond. Similarly, the C−C bond length at the backbone increases to 1.503(3) Å, confirming the formation of a single bond after protonation by water.

Furthermore, DFT calculations revealed that the binding of the water molecule at the Mg center (**2**) is thermodynamically favorable by 7.6 kcal/mol (ΔG). The cleavage of the O−H bond of the water molecule was found to be readily feasible, requiring only a +5.8 kcal/mol kinetic barrier via metal−ligand cooperation (Figure 6). The cleavage of the O−H bond leads to monomeric magnesium hydroxide (ΔG = −17.1 kcal/mol), which, upon dimerization, forms a highly exergonic compound **4** (ΔG = −44.6 kcal/mol) (Figure 6).

Cleavage of the C−H Bond of Diazoalkane. Subsequently, we envisage to extend this study to the cleavage of the C−H bond of Me_3SiCHN_2, which has not been studied by MLC so far, and developing compounds based on other abundant s-block metals to perform this task is highly desirable. Very recently, Maron and Xu reported the synthesis of a zinc diazoalkyl complex, which was obtained from the C−H bond cleavage of Me_3SiCHN_2 by a zinc hydride.[21] We have reported the same using a saturated five-membered NHC.[22] The addition of 1 equiv of Me_3SiCHN_2 to the THF solution of **2** led to an immediate color change to orange, which is characteristic of the protonation of the dearomatized picolyl backbone. **6** was obtained through the C−H bond cleavage of

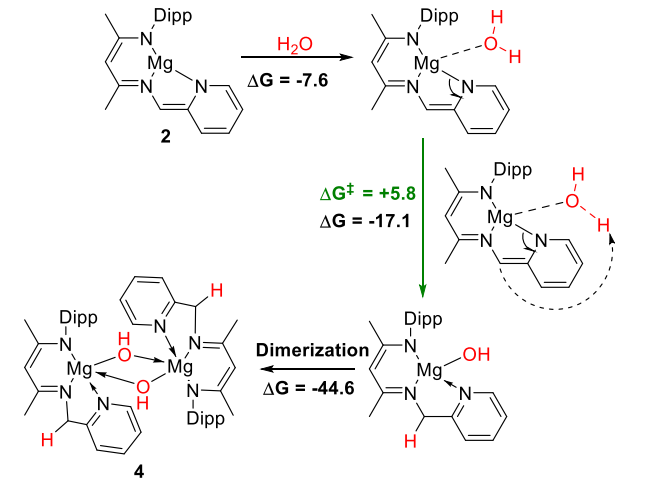

Figure 6. Pathway for the activation of water molecule leading to the formation of **4**, computed at the PBE-D3/def2TZVP level of theory.

Me_3SiCHN_2 via MLC, with the concomitant migration of the $SiMe_3$ group from the carbon to the nitrogen atom (Scheme 5).[23−25]

Scheme 5. Splitting of the C−HBond of Me_3SiCHN_2 by Magnesium Species (2)

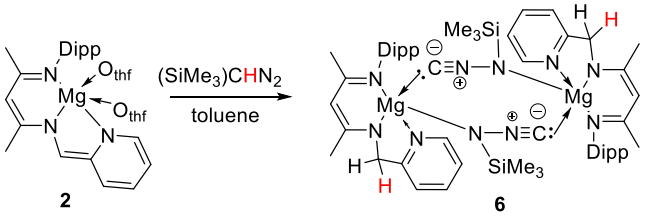

Figure 7 depicts the molecular structure of **6**, which is a centrosymmetric dimer. There are three Mg−N covalent

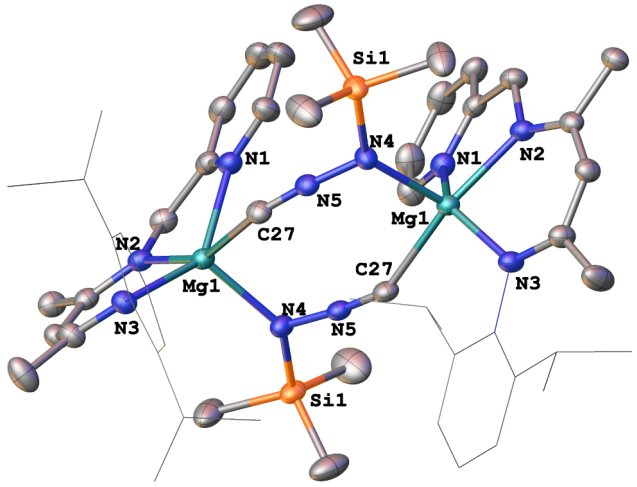

Figure 7. Molecular structure of **6** with anisotropic displacement parameters is depicted at the 50% probability level. Hydrogen atoms are not shown for clarity. Selected bond lengths (Å) and bond angles (°): Mg1−N3 2.0992(13), Mg1−N2 2.0864(13), Mg1−N1 2.2497(15), Mg1−N4 2.1130(13), Mg1−C27 2.2482(17), N5−C27 1.163(2), N4−N5 1.3415(15); N1−Mg1−N2 85.57(5), N2−Mg1−N4 104.18(5), N3−Mg1−N4 116.28(5), N3−Mg1−C27 97.01(8), N2−Mg1−C27 157.08(6), N1−Mg1−N3 140.13(5).

https://doi.org/10.1021/acs.organomet.5c00031
Organometallics XXXX, XXX, XXX−XXX

bonds of more or less the same lengths: 2.0992(13), 2.0864(13), and 2.1130(13) Å, while the Mg−N1 bond length is substantially longer (2.2497(15) Å). The Mg−C bond length of 2.2482(16) Å is slightly shorter than the magnesium-*tert*-butyl isonitrile adduct, $\{Mg[CH(SiMe_3)_2](\mu\text{-}Br)(CNtBu)\}_2$ (2.12 Å), as reported by Lappert.[26] The N5−C27 bond length of 1.163(19) Å indicates the formation of C≡N triple bond and is in good agreement with the C≡N bond lengths reported by Jones and coworkers in $\{[HC(C(Me)N\text{-}2,6\text{-}iPr_2C_6H_3)_2]Mg[\mu\text{-}CN)]\}_3$.[27]

The formation of compound **6** is unique, and so we studied its electronic structure. From Wiberg bond index (WBI) analysis of **6**, it was observed that the Mg−C (WBI = 0.146) and Mg−N (WBI = 0.072) bonds at the bridging site have very low covalent character (Figure 8). These findings are also

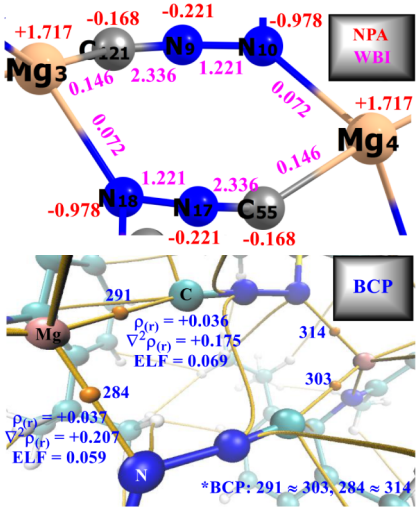

Figure 8. WBI, NPA, and BCP analysis of **6** (only the bridging site is shown for clarity).

corroborated by bond critical point (BCP) analysis, where both the electron density (ρ_r) and the Laplacian of electron density ($\nabla^2\rho_r$) were found to be positive and associated with a very low electron localization function (ELF) value. Notably, a high contribution from electrostatic interactions (58%) was obtained from the energy decomposition analysis (EDA) of **6**, considering a monomeric unit of Mg−N(SiMe$_3$)NC. The contribution from orbital interaction was found to be only about 28%, whereas the contribution from dispersion interaction was 13%. This suggests that electrostatic interactions are the driving force for the formation of **6**.

Natural bond orbital (NBO) analysis also could not locate any bonding NBO corresponding to the bridging Mg−N or Mg−C, although it revealed that both of these interactions are facilitated by electron density transfer from the lone pair of N and C to the nonbonding vacant orbital (LP*) of Mg (Figure 9). Interestingly, the charge transfer interaction between C and Mg was found to be much stronger in comparison to the N−Mg interaction. The charge transfer from C to Mg, considering the fragmentation via two units of Mg−N(SiMe3)NC, was also observed through an extended transition state-natural orbital for chemical valence (ETS-NOCV) analysis.

CONCLUSIONS

In summary, a dearomatized magnesium compound (**2**) supported by a tridentate nacnac ligand was readily synthesized

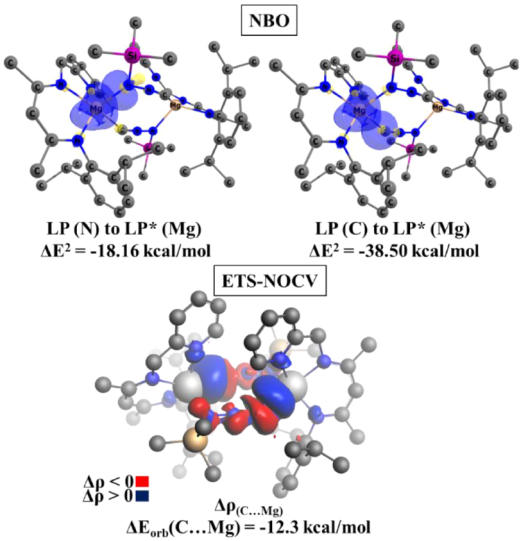

Figure 9. NBO and ETS-NOCV analysis of **6**. For the ETS-NOCV plot, the red region represents the outflow of electron density (charge depletion), and the blue region represents the inflow of electron density (charge accumulation).

and crystallographically characterized, and its electronic structure was studied through DFT calculations. It has been experimentally revealed for the first time that the O−H bond of H_2O and the C−H bond of Me_3SiCHN_2 can be cleaved by magnesium−ligand cooperation involving an aromatization-dearomatization pathway, previously unknown for alkaline earth metals. We are now engaged in cleaving other C−H bonds using **2**, and those results will be published in due course.

ASSOCIATED CONTENT

Supporting Information

The Supporting Information is available free of charge at https://pubs.acs.org/doi/10.1021/acs.organomet.5c00031.

Complete synthesis, spectroscopic and structural details of compounds **1**−**6**, and details of theoretical calculations (PDF)

Cartesian coordinates for the calculated structures (XYZ)

Accession Codes

Deposition Numbers 2378739, 2378740, 2378742, 2378746, and 2408476 contain the supplementary crystallographic data for this paper. These data can be obtained free of charge via the joint Cambridge Crystallographic Data Centre (CCDC) and Fachinformationszentrum Karlsruhe Access Structures service.

AUTHOR INFORMATION

Corresponding Author

Sakya S. Sen − *Inorganic Chemistry and Catalysis Division, CSIR-National Chemical Laboratory, Pune 411008, India; Academy of Scientific and Innovative Research (AcSIR), Ghaziabad 201002, India;* orcid.org/0000-0002-4955-5408; Email: ss.sen@ncl.res.in

Authors

Vishal Sharma − *Inorganic Chemistry and Catalysis Division, CSIR-National Chemical Laboratory, Pune 411008, India;*

https://doi.org/10.1021/acs.organomet.5c00031
Organometallics XXXX, XXX, XXX−XXX

Academy of Scientific and Innovative Research (AcSIR), Ghaziabad 201002, India

Soumya Ranjan Dash − *Academy of Scientific and Innovative Research (AcSIR), Ghaziabad 201002, India; Physical and Materials Chemistry Division, CSIR-National Chemical Laboratory, Pune 411008, India;* orcid.org/0000-0001-7267-6104

Kumar Vanka − *Academy of Scientific and Innovative Research (AcSIR), Ghaziabad 201002, India; Physical and Materials Chemistry Division, CSIR-National Chemical Laboratory, Pune 411008, India;* orcid.org/0000-0001-7301-7573

Rajesh G. Gonnade − *Academy of Scientific and Innovative Research (AcSIR), Ghaziabad 201002, India; Physical and Materials Chemistry Division, CSIR-National Chemical Laboratory, Pune 411008, India;* orcid.org/0000-0002-2841-0197

Complete contact information is available at: https://pubs.acs.org/10.1021/acs.organomet.5c00031

Notes

The authors declare no competing financial interest.

■ ACKNOWLEDGMENTS

We are thankful to the Focused Basic Research (FBR) grant from CSIR, India (FBR060307). V.S. thanks CSIR, India, for a research fellowship.

■ DEDICATION

This paper is dedicated to Prof. Samaresh Bhattacharya on the occasion of his 65th birthday.

■ REFERENCES

(1) Liang, Y.; Das, U. K.; Luo, J.; Posner-Diskin, Y.; Avram, L.; Milstein, D. Magnesium Pincer Complexes and Their Applications in Catalytic Semihydrogenation of Alkynes and Hydrogenation of Alkenes: Evidence for Metal−Ligand Cooperation. *J. Am. Chem. Soc.* **2022**, *144* (41), 19115−19126.

(2) Liang, Y.; Luo, J.; Diskin-Posner, Y.; Milstein, D. Designing New Magnesium Pincer Complexes for Catalytic Hydrogenation of Imines and N -Heteroarenes: H $_2$ and N−H Activation by Metal−Ligand Cooperation as Key Steps. *J. Am. Chem. Soc.* **2023**, *145* (16), 9164−9175.

(3) Freitag, B.; Fischer, C. A.; Penafiel, J.; Ballmann, G.; Elsen, H.; Färber, C.; Piesik, D. F.; Harder, S. Bora-amidinate as a Cooperative Ligand in group 2 Metal Catalysis. *Dalton Trans.* **2017**, *46*, 11192−11200.

(4) Pahar, S.; Swamy, V. S. V. S. N.; Das, T.; Gonnade, R. G.; Vanka, K.; Sen, S. S. Access to diverse germylenes and a six-membered dialane with a flexible beta-diketiminate. *Chem. Commun.* **2020**, *56*, 11871−11874.

(5) Pahar, S.; Sharma, V.; Mahata, B.; George, C. P.; Sharma, H.; Vanka, K.; Sen, S. S. Tridentate NacNac Stabilized Tin and Nickel Complexes: Access to a Monomeric Nickel Hydride and Its Catalytic Application. *Inorg. Chem.* **2022**, *61*, 17370−17377.

(6) Pahar, S.; Sharma, V.; Vipin Raj, K.; Sangole, V.; P, M.; George, C. P.; Singh, K.; Vanka, K.; Gonnade, R. G.; Sen, S. S. Tridentate NacNac Tames T-Shaped Nickel(I) Radical. *Chem. -Eur. J.* **2024**, *30* (12), No. e202303957.

(7) Yadav, S.; Dixit, R.; Bisai, M. K.; Vanka, K.; Sen, S. S. Alkaline Earth Metal Compounds of Methylpyridinato beta-diketiminate Ligands and their Catalytic Application in Hydroboration of Aldehydes and Ketones. *Organometallics* **2018**, *37*, 4576−4584.

(8) Mandal, C.; Sarkar, S.; Panda, S.; Mallick, D.; Mukherjee, D. Synthesis and reactivity of a heteroleptic magnesium hydride on a dearomatized picolyl-based NNN-chelator. *Dalton Trans.* **2024**, *53*, 17343−17350.

(9) Grabowski, S. J. Magnesium Bonds: From Divalent Mg Centres to Trigonal and Tetrahedral Coordination. *ChemistrySelect* **2018**, *3*, 3147−3154.

(10) Rauch, M.; Ruccolo, S.; Parkin, G. Synthesis, Structure, and Reactivity of a Terminal Magnesium Hydride Compound with a Carbatrane Motif, [Tism Pr i Benz]MgH: A Multifunctional Catalyst for Hydrosilylation and Hydroboration. *J. Am. Chem. Soc.* **2017**, *139* (38), 13264−13267.

(11) Schnitzler, S.; Spaniol, T. P.; Maron, L.; Okuda, J. Formation and Reactivity of a Molecular Magnesium Hydride with a Terminal Mg−H Bond. *Chem. -Eur. J.* **2015**, *21* (32), 11330−11334.

(12) Arrowsmith, M.; Maitland, B.; Kociok-Köhn, G.; Stasch, A.; Jones, C.; Hill, M. S. Mononuclear three-coordinate magnesium complexes of a highly sterically encumbered *β*-diketiminate ligand. *Inorg. Chem.* **2014**, *53*, 10543−10552.

(13) Bakewell, C. Magnesium hydrides bearing sterically demanding amidinate ligands: Synthesis, reactivity and catalytic application. *Dalton Trans.* **2020**, *49*, 11354−11360.

(14) Bonyhady, S. J.; Green, S. P.; Jones, C.; Nembenna, S.; Stasch, A. A Dimeric Magnesium(I) Compound as a Facile Two-Center/Two-Electron Reductant. *Angew. Chem., Int. Ed.* **2009**, *48*, 2973−2977.

(15) (a) Arrowsmith, M.; Hill, M. S.; Hadlington, T.; Kociok-Köhn, G.; Weetman, C. Magnesium-Catalyzed Hydroboration of Pyridines. *Organometallics* **2011**, *30*, 5556−5559. (b) Hill, M. S.; Kociok-Köhn, G.; MacDougall, D. J.; Mahon, M. F.; Weetman, C. Magnesium hydrides and the dearomatisation of pyridine and quinoline derivatives. *Dalton Trans.* **2011**, *40*, 12500−12509. (c) Weetman, C.; Mahon, M. F.; Hill, M. S. Magnesium-catalysed hydroboration of pyridines: Kinetic analysis and poly-pyridine dearomatisation. *Polyhedron* **2016**, *103*, 115−120. (d) Hill, M. S.; Kociok-Köhn, G.; MacDougall, D. J.; Mahon, M. F.; Weetman, C. Kinetically Directed Reactivity of Magnesium Dihydropyridides with Organoisocyanates. *Organometallics* **2015**, *34*, 2590−2599.

(16) Liu, X.; Li, B.; Hua, X.; Cui, D. 1, 2-Hydroboration of pyridines by organomagnesium. *Org. Lett.* **2020**, *22*, 4960−4965.

(17) Intemann, J.; Lutz, M.; Harder, S. Multinuclear magnesium hydride clusters: Selective reduction and catalytic hydroboration of pyridines. *Organometallics* **2014**, *33*, 5722−5729.

(18) Ghosh, P.; Parkin, G. Synthesis and Structure of a Magnesium Hydroxide Complex Supported by Tris(pyrazolyl)hydroborato Ligation, $\{[Tp^{Ar,Me}]Mg(\mu\text{-}OH)\}_2$ (Ar = p-Bu^{t}C$_6$H$_4$). *Inorg. Chem.* **1996**, *35*, 1429−1430.

(19) Sánchez-Barba, L. F.; Hughes, D. L.; Humphrey, S. M.; Bochmann, M. Ligand Transfer Reactions of Mixed-Metal Lanthanide/Magnesium Allyl Complexes with *β*-Diketimines: Synthesis, Structures, and Ring-Opening Polymerization Catalysis. *Organometallics* **2006**, *25*, 1012−1020.

(20) Nembenna, S.; Singh, S.; Sen, S. S.; Roesky, H. W.; Ott, H.; Stalke, D. *β*-Diketiminate Stabilized Magnesium Hydroxide, Heterobimetallic, and Halide Complexes: Synthesis and X-ray Structural Studies. *ZAAC* **2011**, *637*, 201−205.

(21) Jiang, S.; Cai, Y.; Rajeshkumar, T.; Rosal, I. D.; Maron, L.; Xu, X. Synthesis and Reactivity of a Zinc Diazoalkyl Complex: [3 + 2] Cycloaddition Reaction with Carbon Monoxide. *Angew. Chem., Int. Ed.* **2023**, *62* (34), No. e202307244.

(22) Balayan, K.; Sharma, H.; Vanka, K.; Gonnade, R. G.; Sen, S. S. Uncovering diverse reactivity of NHCs with diazoalkane: C−H activation, C‡C bond formation, and access to N-heterocyclic methylenehydrazine. *Chem. Sci.* **2024**, *15*, 18387−18394.

(23) Evans, W. J.; Montalvo, E.; Champagne, T. M.; Ziller, J. W.; DiPasquale, A. G.; Rheingold, A. L. Organolanthanide-Based Synthesis of 1,2,3-Triazoles from Nitriles and Diazo Compounds. *J. Am. Chem. Soc.* **2008**, *130*, 16−17.

(24) Jana, A.; Objartel, I.; Roesky, H. W.; Stalke, D. Dehydrogenation of LGeH by a Lewis N-Heterocyclic Carbene Borane Pair under the Formation of L′Ge and its Reactions with B(C$_6$F$_5$)$_3$ and

Trimethylsilyl Diazomethane: An Unprecedented Rearrangement of a Diazocompound to an Isonitrile. *Inorg. Chem.* **2009**, *48*, 7645−7649.
(25) Ren, W.; Gu, D. An Azobenzenyl Anion Radical Complex of Magnesium: Synthesis, Structure, and Reactivity Studies. *Inorg. Chem.* **2016**, *55*, 11962−11970.
(26) Caro, C. F.; Hitchcock, P. B.; Lappert, M. F.; Layh, M. Neutral Isonitrile Adducts of Alkali and Alkaline Earth Metals. *Chem. Commun.* **1998**, 1297−1298.
(27) Ma, M.; Stasch, A.; Jones, C. Magnesium(I) Dimers as Reagents for the Reductive Coupling of Isonitriles and Nitriles. *Chem. - Eur. J.* **2012**, *18*, 10669−10676.

https://doi.org/10.1021/acs.organomet.5c00031
Organometallics XXXX, XXX, XXX−XXX